DEVELOPMENT OF INSTRUMENTS FOR ASTRONOMICAL SITE CHARACTERIZATION AND THEIR APPLICATION

(Corrected Copy)

A Thesis
Submitted for the Degree of

Doctor of Philosophy (Technology)

Submitted by

TARUN KUMAR SHARMA

Department of Applied Optics & Photonics
University College of Technology
University of Calcutta

DEVELOPMENT OF INSTRUMENTS FOR ASTRONOMICAL SITE CHARACTERIZATION AND THEIR APPLICATION

(Corrected Copy)

A Thesis
Submitted for the Degree of

Doctor of Philosophy (Technology)

Submitted by

TARUN KUMAR SHARMA

Department of Applied Optics & Photonics
University College of Technology
University of Calcutta

Dedicated to

My Family

Acknowledgements

It is my great pleasure to thank Prof. Padmakar Singh Parihar and Dr. Ravinder Kumar Banyal for their valuable guidance throughout this work. They gave me a lot of encouragement and confidence in perusing this thesis.

I would like to thank all the Directors of Indian Institute of Astrophysics, the Dean and all the Chairs of Board of Graduate Studies (B.G.S during 2009 - 2016) for giving me the opportunity to work in this institute and providing all the facilities required to carry out my research work. I also thank all the academic and administrative sections of the institute for letting me attend various conferences during my tenure. I thank all the members of the NLOT site survey team for their help in the procurement of the various components required for the development of various instruments under this project.

I am thankful to all the professors of Department of Applied Optics and Photonics, Calcutta University, Prof. A. K. Chakraborty, Prof. L. N. Hazra; Prof. A. Ghosh; Dr. Kallol Bhattacharya; Dr. Samir Kumar Sarkar; Prof. A. Basu Ray and Dr. (Mrs.) Mina Ray; Mr. N. Chakraborthy and Mr. S. Bagchi. Due to above professionals, I have learned various aspects of optics and their applications.

I am also grateful to IIA faculty members who introduced me to Astronomy and astronomical instrumentation. I would like to convey my thanks and regards to Assoc Prof. S. Annapurni, Assoc Prof. U. S. Kamath, Prof. S. K. Saha, Prof. K. E. Rangarajan, Assoc Prof. Arun Mangalam, Assoc Prof. Gajendra Pandey, Assoc Prof. Sivarani, Assoc Prof. A. Satyanarayana, Assoc Prof. R. Ramesh, Dr. J. P. Lancelot, Prof. A. K. Saxena. I am thankful to Assoc Prof. Muthu Mariappan, In-charge of VBO for his constant motivation during the stay at Kavalur. Thanks to Dr. J. P. Lancelot and Prof. A. K. Saxena for explaining various facilities at the Photonics Division within IIA

Campus.

I would like to thank Er. Madan Mohan Kemkar for helping me in the design of mechanical structure of various instruments, and also in reviewing the completed instrument designs. I would also like to thank Mr. Timmaiah N., Mr. Periyanayagam and Mr. Sagayanathan K. for helping in the fabrication of various parts, and test set-ups for different instruments.

I am thankful to IAO Engineer-in-charge Angchuk Dorje for making my stay comfortable during my visits to IAO Hanle. Er. Jorphail Sonam, Er. Mahay Tashi Tsering, and Er. Dorjai Tsewang has helped a lot in the installation and maintenance of various instruments. I am also thankful to IAO technicians Dorjay Phuntsok, Phuntsok Dorjay and Pamber Tashi for their efforts while installing the different instruments. Urgain Stanzin and Dadul has done a wonderful job of operating these instruments.

I thank all my seniors Dr. Girijesh Gupta, Dr. Veeresh Singh, Dr. Krishna Prasad, Dr. Bharath Kumar, Dr. G. Uday Kumar, Dr. S. Ramya, Mr. A. B. Sudhakar Reddy, Dr. Ananth C. Pradhan, Dr. Tapan Mishra, Dr. Sajal kumar Dhara, Ms. Anantha Chanumolu, Dr. Sasikumar Raja, Mr. Arun Surya for providing useful information at regular times. I enjoyed the company of my classmates Mr. Kishore Poolapalli, Mr. Narsi Reddy Anugu, Mr. Jyotirmoy Paul, Ms. Soumi Paul and Ms. Amita Mohanty. I also enjoyed the company of my friends at PG Hall, Calcutta and Bhaskra Hostel, Bangalore.

Tarun Kumar Sharma

Abstract

Before setting up any large observational facility, selection of a suitable site is an important task. It requires a variety of site survey instruments, which helps to carry out a detailed comparative study of candidate sites and choose the best one. There are a number of parameters used, to judge the suitability of a site for installation of a large telescope. Few of these parameters are meteorological in nature like Winds speed, Temperature, Ground-level humidity, Precipitable water vapor, etc. and can be easily obtained by installing commercially available weather stations. Whereas, several other key parameters can only be derived by making use of specifically designed site survey devices and these parameters are Cloud cover, overall atmospheric seeing, Turbulence profiles, Atmospheric transparency, Sky brightness, etc. Most of these site survey instruments are indigenously developed devices and cannot be procured commercially.

In order to search a few potential sites for the India's future large telescope project: - National Large Optical Telescope (NLOT), we have initiated a site survey program and started indigenously developing various site characterization instruments. Under this Ph.D. thesis, we have developed two innovative instruments. The first one is an automated extinction monitor, a device which measure atmospheric transparency very precisely. Other device is a scanning cloud monitor, uses IR sensor to measure excess radiation reflected from the cloud. In addition to above two works, the effort has also been made to develop a sturdy telescope for the MASS-DIMM instrument.

Automated Extinction Monitor (AEM) is a unique device for measurement of the atmospheric extinction and sky brightness in automatic mode, it can also detect the presence of thin clouds. There are hardly any observatories around the globe which have got such a dedicated instrument for the continuous measurement of

atmospheric transparency. AEM is a small equatorial mount telescope with provision to change the polar angle depending upon the latitude of the place. We make use of a telephoto lens as main telescope optics, which gives the advantage of wide field and short focal length. The wide field allows the instrument to observe several hundred stars in a single frame, which in turn increases the measuring accuracy of the instrument. Short focal length also helps in reducing the overall size of the instrument. A Peltier cooled large format but very compact CCD with inbuilt shutter from Apogee is used as an imager. The telescope control hardware is developed around a high end microcontroller having capability to work in networked environment. All the software required, to control the telescope, control of CCD and data analysis have been developed under Linux platform. We have developed a fully automatic instrument, which does not require any operator. AEM is protected by a motorized enclosure, which has been designed and fabricated in-house. Instrument was installed at IAO Hanle in November 2012, and several improvements has been made in the instrument, and the instrument is in continuous operation. So far we have collected more than 150 nights data, and out of that about 92 nights data has been analyzed and reported in this thesis. Extinction measured using AEM as well as 2m HCT telescope matches very well. Device is also very sensitive to measure very small changes in the sky transparency over the night. AEM can also very precisely measure sky brightness which again very well matches with HCT data. As a trail run, we looked at the possibility of using part of the spare time of AEM in variability study of bright variable stars.

The information related to the clarity of sky can be either obtained by making use of a device like All Sky CCD Camera or else by using NIR sensors. The CCD-based detectors are found to be not very sensitive during night time and any automatic algorithm to investigate images for clarity of sky at nights are subjected to large errors. Whereas, manual handling of a large amount of imagery data collected over

longer run from different sites is indeed a cumbersome task. To avoid this problem, a scanning cloud monitor which uses an array of thermopile sensor can be a better choice and has been developed under the present thesis. All Sky Scanning Cloud Monitor is a unique instrument for determining the cloud coverage of the sky. Instrument operates on the principle of detection of IR radiations reflected form the clouds. The detecting element (sensor) is a thermopile based sensor with an internal thermistor for ambient temperature compensation. This type of sensor has a small finite field which can cover only a small portion of the sky. To overcome this difficulty we have used an array of the sensors mounted on a circular arc. This arc along with sensors is rotated in azimuth to cover the whole 360 degrees of the sky. The mechanical design and fabrication, sensor electronics, instrument controller and the data acquisition system have been designed and developed in-house. The software required to operate instrument as well as for data acquisition and analysis has also been developed. This instrument was installed at IAO Hanle in December 2015. Altogether we have collected data for 65 nights in three months of instrument operation. The data has been analyzed and also percentage cloud cover is computed. From distribution, we get that nearly 70% of the time sky is clear (cloud cover less than 10%). Whereas, fully cloud time is not more than 3%. Remaining time which is about 27% of total time is found be partially clear. We also cross-checked these finding with CONCAM all-sky data and confirmed that our scanning cloud monitor provides reliable results.

A MASS-DIMM (Multi-Aperture Scintillation Sensor-Differential Image Motion Monitor) has been acquired from TMT Project USA, which gives turbulence profile of the atmosphere. One of the prime requirement of this instrument is that it needs very stable telescope which can work in open and windy condition. We are developing a very stable telescope which can operate in windy conditions without degrading the image quality. For doing this, we have explored all aspects of the telescope design

and have chosen the approach which is best suited for our requirement. The telescope is an Alt-Az (Altitude-Azimuth) mount telescope. To minimize the cross section area and hence dynamic wind loading on the telescope, a carbon fiber truss based 16-inch f/8 Ritchey-Chretien OTA from TPO USA is used. Another measure taken is to make use of Direct Drive Technology, which removes any intermediate reduction system (gear, timer belts, friction drive, etc.), this makes the telescope electromechanically stiff and very responsive. We have also explored the possibility of designing the motor in-house, and an initial prototype has been made. An effort has also been made to develop the drive electronics for the direct drive motor. At present, the telescope design and analysis has been completed, and it is going through manufacturing/assembling phase.

List of Publications

Papers Published in Refereed Journals:

1. **T. K. Sharma**, and P. S. Parihar. “Network Based Data Acquisition and Logging System using PIC Microcontroller" International Journal of Engineering (IJE), Volume (8) : Issue (2) : 2014, 22-29.

2. **T. K. Sharma**, and P. S. Parihar “Computer based Non-Contact Temperature measurement system" Journal of Instrument Society of India, Volume (45) : Issue (2) : 2015, 121-23.

Papers Published in Conference Proceedings:

1. **T. K. Sharma**, P. S. Parihar, and P. M. M. Kemkar“All sky scanning cloud monitor for NLOT site survey" - Journal of Physics: Conference Series **595** (2015) 012032. doi:10.1088/1742-6596/595/1/012032

2. P. S. Parihar, **T. K. Sharma**, A. Surendram, P. M. M. Kemkar, Dadul, Urgain Stanzin, and G. C. Anupama. “Characterization of sites for Indian Large Optical Telescope Project" - Journal of Physics: Conference Series **595** (2015) 012025. doi:10.1088/1742-6596/595/1/012025

Table of Contents

List of Figures

Page

List of Tables

CHAPTER 1

INTRODUCTION

During last two decades, several large observing facilities which host large optical-NIR telescope of the size eight meter and above have been created by different countries. Further, driven by the need to explore deeper, clearer and fainter, several mega projects aiming to have 25-40m size optical-NIR telescopes such as TMT (Thirty Meter Telescope) and E-ELT (European-Extremely Large Telescope) are in the process of becoming a reality. Setting up such a large observatory is no longer possible for a single group or a country, but it is slowly becoming a collective effort in which more than one country and groups are involved. Looking at the huge investment required to set up such observatories, astronomers started looking at sites which can give the best scientific return on the money spent. Driven by this new philosophy, they started choosing the best sites anywhere on the globe. Once such a site is selected then the next sensible and cost effective way is to install other large telescopes at the same place, which helps to reduce the cost involved in creating the new infrastructure as well as the operation of the observatory over several decades.

Decades-long efforts have resulted in the identification of few best sites around the globe, and few example of these are Hawaii, Canary Island, Paranal Chile, etc. These are the places where several countries have put their telescopes of 8m size and above, in addition to several smaller telescopes.

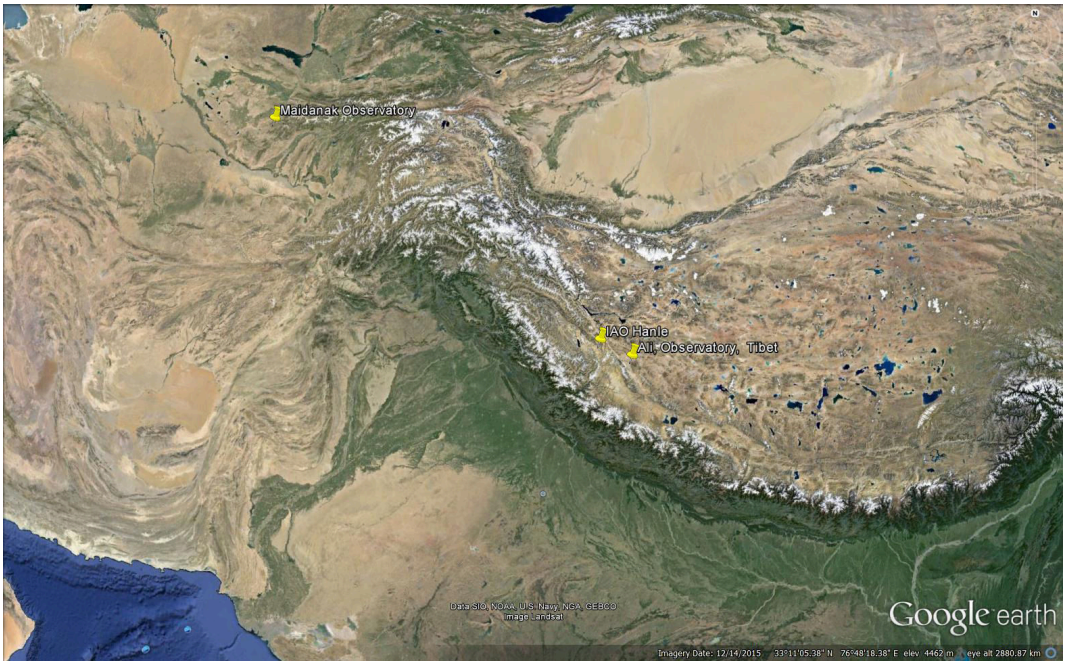

Fig. 1.1: Three promising sites on Himalaya, found to be equally good like sites in Hawaii or Chile. In near future this whole region may be populated with several large telescopes, serving need of Asian countries.

It appears that there are several sites in Himalayan region which can be equally good like other best sites. However, these sites have not been fully explored and hence unknown to most of the Astronomical Community of the world. The preliminary site survey carried out by the former Soviet Union and Uzbek astronomers on Mount Maidanak in Uzbekistan (Il'Yasov et al., 1999; Kornilov et al., 2009), Indian astronomers in Ladakh region (Cowsik et al., 2002b; Prabhu, 2014) and Chinese astronomers in western Tibet (Yao et al., 2012; Ye et al., 2016) shows that Himalayan region can be equally good place for Optical and NIR astronomy and deserve to host large observing facilities. This region offers a large number of cloud free clear nights, atmosphere free from dust and pollen, very low humidity and

temperature, and is located very far from the city lights. Also, this part of Himalaya is less affected by the two monsoons. Indian astronomers have chosen Hanle Ladakh (78°57′51″E, 32°46′46″N, 4517m) and installed a 2m size telescope as a precursor for future large telescope. Whereas, Ali in western Tibet (80°01′36″E, 32°19′32″N, 5100m) has been chosen by the Chinese Astronomers for their future near-infrared optical facility. Mount Maidanak (66°53′47″E, 38°40′22″N, 2593m) is known to be one of the best sites for several decades and there is a group of small telescopes installed and being used. Figure 1.1 shows the Google Earth image of all three sites. The Indian and Chinese sites are very close-by (about 150km apart), and are expected to have almost similar observing conditions, except atmospheric seeing which may vary substantially from place to place. Both Indian and Chinese groups would like to develop their respective sites as a center for modern optical-NIR astronomy with regional cooperation from neighboring countries. Like Chile, these two sites may be populated with several mid to large size telescopes, serving the need of Asian countries like, India, China, Thailand, Taiwan, Iran, Indonesia, Malaysia, and countries part of the former Soviet Union. In these countries, astronomy research is slowly getting momentum and they already have several 1-4 meter size telescopes. The rise in their economic strength makes these countries capable of supporting the needed investment to establish large observing facilities, which otherwise was not possible 20-25 years back.

During the mid 90's several sites in India were explored for India's future Optical-NIR telescope and finally it was found that the best site within the country can be found in the Himalayan region. The Changthang region of Ladakh on Tibetan plateau is a high-altitude, arid and cold region. This place is far from any artificial light pollution, having low atmospheric aerosols, little affected by monsoon and has got clear sky all through the year. It provides an excellent opportunity for developing astronomical facilities at a variety of wavelengths, and an initiative has already been

taken to establish astronomical facility over there. As a pathfinder to the large telescope, one moderate size Optical telescope was installed during 2000 at one of the peaks called Mt. Saraswati in Hanle. Since then, slowly all the required infrastructure is being created. With more than a decade-long observing experience with 2m size telescope it has been found that Hanle region thus has the required characteristics of a good astronomical site and could be a natural candidate site for any future large aperture optical-infrared telescope (Cowsik et al., 2002a). However, setting up 8-10 meter size telescope requires huge amount of investment and the manpower, therefore, a thorough understanding and characterization of the intended sites is necessary.

1.1 Best astronomical sites in the world

Astronomical observatories are usually located at high altitude and far from the urban population. One of the prerequisites for any good site is that it should have a large number of clear nights, preferably distributed to all through the year. The impact of cloud cover on the science capability of the facility is quite clear. Sites with a low fraction of clear nights are less productive than sites with the high fraction of photometric and usable nights. Observatory should be also located at the place which is free from significant light pollution at the time of construction. Additionally, it should have less prospects for habitation, which ultimately lead to the light pollution.

Another parameter which plays a very important role in deciding whether the site is suitable to host a big observatory or not is the atmospheric seeing. The impact of good natural seeing on the scientific productivity of any observatory cannot be overstated. Resolution-critical problems, such as strong-lensing, crowded field photometry, and velocity dispersion in the galactic nucleus are strongly seeing dependent, and the depth of all sky-limited observations depend on seeing to

somewhere between the first and second power. There are host of new exciting science cases getting benefited with the Adaptive Optics system, which boost the spatial resolution of the telescope to the extent of diffraction limit. The effective AO corrections are highly sensitive to the native seeing through the size of the isoplanatic angle and length of the coherence time.

The ground-based infrared observations till mid-IR is slowly becoming more effective technique to probe a large number of science problems. The near and mid-IR atmospheric windows are set by the absorption spectrum of water and CO2. Sites with high precipitable water vapor are found to have narrower and less stable observing windows, as well as high thermal-IR background. Therefore, the best sites, where both optical and IR observation can be effectively carried out should be a cold site having extremely low precipitable water vapor, preferably less than 2 mm.

Other parameters which also contribute in making any site suitable for astronomical observatory are minimal change in diurnal and seasonal temperatures, low wind speed and gust, easy approachability, the high mechanical integrity of soil and low seismicity. Since big observatories are expected to host a number of large telescopes, which requires huge investment, therefore, it is expected that the chosen site should have stable weather patterns over extended period say years or even decades.

Most world-class astronomical observatories are located close to coastal mountain ranges and islands. Chile is one of the few places on Earth with mountains that meet the stringent requirements of astronomical observatories. There are a number sites in Chile, which either already host an observatory or proposed for futures large telescopes such as E-ELT, GMT etc. These sites may be divided into two classes: moderate elevation, primarily coastal sites, and high elevation inland sites. Las Campanas, La Silla, Cerro Tololo and Paranal are all examples of moderate elevation sites in coastal ranges. Whereas, the ALMA site Chajnantor in the middle of the

Atacama desert is the best example of the high altitude sites in the Chile.

On the Island of Hawaii, Mauna Kea is considered the highest (4200m from sea level) island mountain in the world. The place was first identified by Gerard Kuiper to be used for ground-based infrared astronomical observation. However, it was John Jefferies, a professor at university of Hawaii, who succeeded in getting NASA grant to install a relatively large size (2.2m) telescope, which saw the first light in 1970. After recognizing the importance of the Mauna Kea site for both optical and NIR observations, a number of other observing facilities such as CFHT, UKIRT, SUBARU and the Keck telescopes have been installed by different astronomical groups. Mauna Kea is also considered to be one of the preferred site for forthcoming TMT project.

Roque de Los Muchachos Observatory (ORM), in La Palma, Canary Islands, Spain, is another place which hosts a large number of telescopes ranging from few tens of inches to 10m size, mostly from Europe. The site infrastructure is managed by the Instituto de Astrofisica de Canarias, which includes providing the access road, utilities, high-speed data links and the mountain-top residential facilities for observers. Altitude of ORM is moderate (2300m), however, parameters which characterizes any site such as seeing, sky brightness, number of clears nights are as good as other best sites in the world.

In addition to coastal and sites in Islands, continental places such as Maidanak in Uzbekistan, Hanle in India and Ali in China, can be considered equally good sites in Asia. These are very high altitude, thinly populated, extremely cold and dry desert sites, best suited for Optical, IR and Submillimeter astronomy. Some activities are already undertaken to characterize these sites for creating future large observing infrastructure, however, more efforts are needed to draw any conclusion.

Table 3 provide all relevant parameters, which can be used to judge the relative observing quality of the worlds few best sites.

Table 1.1: Site parameters for few best observatories around the world.

Parameter	IAO	Mauna Kea	La Silla	La Palma (ORM)	Aromazones (E-ELT)
Altitude(m)	4467	4200	2400	2250	3064
Median Seeing(arc-sec)	1.2	0.5	0.76	0.55	0.41
Extinction in V Band (mag)	0.120	0.119	0.164	0.137	0.162
Sky Brightness in V Band (mag)	21.28	21.5	21.7	21.9	21.9
Usable Nights(%)	81	72	-	72	89
PWV (mm)	1.5	1.9	4.0	4.14	-
Isoplanatic Angle(arc-sec)	-	2.69	1.26	2.33	2.04
Coherence Time(ms)	-	5.1	-	6.0	4.6
Average Night Temperature(C)	-1.0	2.3	-	7.3	7.5
Median Night wind speed(m/s)	4.0	5.7	-	8.2	7.2

1.2 Overview of astronomical site survey instruments

There are a number of parameters which needs to be carefully studied before choosing any astronomical site for the purpose of installing a large telescope. Few of these parameters are meteorological in nature and can be easily obtained by installing commercially available weather stations. Whereas, there are several other key parameters which can only be derived by making use of specifically designed site survey devices. Broadly, all these parameters can be classified in following categories:-

1. **Meteorological parameters:-** Winds speed, temperature, ground-level humidity, precipitable water vapor, etc. are the meteorological parameters, which can be easily obtained using weather stations. Nowadays, these weather stations are used so extensively, and also, instruments are standardized to such an extent that the data obtained at two different observatories can be directly compared. Use of automatic weather stations to get meteorological information is usually the first step toward more rigorous site survey activities needed for any new observing facility. Knowledge of the distribution of wind speed helps to choose right kind of telescope and dome structures, design the best telescope controls which can up to some extent reject wind disturbances. Aerosols and water vapor contents

are also important parameters as they absorb and scatter the light coming from stars and hence decide transparency and brightness of the sky. Precipitable water vapor affects the observation towards the longer wavelengths. Meteorological parameters also help to get some idea about availability of useful observing time for an observatory. Downtime of an observatory can be considered as a time when observation is not possible due to snow, rain, ice, cloud coverage and high wind speed.

2. **Parameters related to image quality:-** The standard practice is that once a large number of sites are explored by making use of meteorological data coming from ground and satellite based sources, then next task is to select a few candidate sites and conduct more intensive exploration using dedicated site survey instruments. The parameters, which can affect the quality of the image are atmospheric seeing, turbulence profile, isoplanatic angle, turbulence time constant, etc.. The atmospheric transparency and sky brightness may not degrade the image quality but may affect measurement accuracy. Knowledge of these parameters is of particular importance in the case of modern telescopes, which uses techniques such as adaptive optics. Additionally, these parameters are also required for the design of new telescopes and instruments.

3. **Parameters related to telescope construction:-** Soil properties of the site, ground level wind velocity, are the parameters required to be studied before the telescope installation. Seismicity of a site can also be an important parameter, if the telescope is intended to use adaptive optics or the interferometry.

Most of the parameters mentioned above which characterize any site are required to be collected for the longer duration to establish the statistics, and see seasonal and day to day variations. Apart from the above mentioned parameters accessibility of a site, available infrastructure, local or remote operation of telescopes, electrical power

and availability of manpower can also play a significant role in the selection of a site.

For determining all these parameters for a particular site, different instruments are used. Some of them are:-

1. Seeing monitors: - Differential Image Motion Monitor (DIMM), Multi-aperture scintillation Sensors (MASS).
2. Atmospheric turbulence profiles Cn2 (h, t): - Microthermal measuring instruments, Generalized Scidar(GS), Single Stars Scidar (SS).
3. Extinction and sky brightness monitors.
4. Automatic Weather Station (AWS), All Sky Camera(ASC).
5. Satellite images for high altitude dust monitoring.

1.3 National Large Optical Telescope Project

In the 70's Indian astronomers carried out night-time astronomical observations using one meter and smaller optical telescopes. Subsequently, IIA lead a national initiative of building the 2.34m Vainu Bappu Telescope indigenously, which got commissioned in 1984. During this period, the gap between the optical telescopes used by Indian astronomers compared to that available elsewhere in the world was not large, the largest operational telescope during that time was the 5 m Hale telescope at the Palomar Observatory. During the last two decades, when the world has gone ahead in building and observing using 10-11m class telescopes, astronomers in India are limited to carry out observation using their 2m class optical telescopes which is still ongoing. Recently installed 3.6m Devasthal Optical Telescope (DOT), which saw the first light on March 22, 2015, will be the largest telescope in India. Even when the 3.6m DOT telescope becomes operational to its full capacity, the gap between Indian

astronomers having access to 3m size telescope and the rest of the world having access to 10-11m class telescopes is more than three times.

Recently, India has become one of partner at the 10% level to the Thirty Meter Telescope (TMT) project, which will be the world's second largest telescope, after the E-ELT. Hence, in about a decade from now, astronomers from India will be able to do cutting edge science owing to their access to one of the most powerful telescopes of the time. However, the telescope like TMT, where Indian contribution is just 10%, would not be enough to cater the need of growing astronomical community of India. Furthermore, TMT is intended to be primarily used to carry out very specialized science by making use of specially designed back-end instruments. Whereas, smaller Indian telescopes of 2-3m class will be best suited to regular observations by few individual groups. Therefore, there is a need from Indian astronomers to have 10m class telescope equipped with state-of-art back-end instruments and carry out the science which is only possible by this size telescopes. Furthermore, it is strongly felt that Indian astronomers will not be able to make efficient use of the TMT without having access to a mid-size 10m telescope, which will help to generate a large number of science cases for the TMT.

The idea of building a large optical telescope of 6m and above in India has been recurring over and over since 1984 or so, but no real progress has been made except the identification of few potential sites for the future telescope. In recent years with resurrected interest, astronomers at IIA Bangalore have started working towards the realization of India's 10m telescope project named NLOT(National Large Optical Telescope). The activities linked to developing the conceptual design of the NLOT, prototyping NLOT subsystems like segment support, actuators, edge sensor, etc. have already started. A group of engineers led by IIA scientists have also started exploring, which technology developed for TMT can be utilized in NLOT as it is and which one require modifications/changes. In addition to above, it was also decided to carry out

a comprehensive site survey in and around Hanle and ensure that this is indeed the best place which can host India's large optical-NIR telescope.

1.4 Review of past site characterization works

A national project headed by Arvind Bhatnagar was initiated to search for sites in Ladakh region. The survey carried out during 1984-1989 near Nimmu (4100m above MSL) on Leh-Kargil road northwest of Leh found this place suitable for astronomy, except relatively less number of clear nights. Few years later, under separate initiative to identify suitable sites for large Optical-NIR Observatory, Indian Institute of Astrophysics (IIA) started surveying Himalayan and trans-Himalayan region. Six potential sites all above 4000m from mean sea level were identified by making use of available topographical maps, weather data, and satellite imagery. Based on preliminary survey carried out at six places, Digpa-ratsa Ri, Hanle, Ladakh was chosen for further detailed study. Digpa ratsa Ri, which was later renamed as Mt. Saraswati is located in Hanle Valley, which is nearly 260km from Leh, the biggest township in the Ladakh region of India. The mountain peak is 4517m above sea level at longitude of 78°57′51″E and latitude 32°46′46″N. Once observatory site was narrowed down to Mt. Saraswati, then continuous monitoring of the weather by making use of automated weather station (AWS) and cloud coverage by visual monitoring started in 1995. A DIMM seeing monitor was also developed in-house and used in campaign mode during 1998-1999 for about 50 nights. In April 1995 a sun-spectrophotometer was installed to measure the precipitable water vapor, which was followed by the installation of 220 GHz radiometer for continuous operation in December 1999 (Ananthasubramanian et al., 2004). Analysis of the meteorological parameters acquired from AWS, cloud coverage from visual monitoring, precipitable water from sun-spectrophotometer and 220Ghz radiometer and seeing measurements

from DIMM indicated Hanle to be a world-class astronomical site for the national large optical telescope (Cowsik et al., 2002a; Bhatt et al., 2000; Prabhu, 2014). Following the identification and characterization of the Hanle site, a committee chaired by Dr. K. Kasturirangan suggested the development of the site in two steps: (1) create a needed infrastructure required for any observatory which include the capability of remote operation of the whole observatory through dedicated satellite link and install a moderate size optical-NIR telescope, and (2) development of the large infrared optical telescope by utilizing this infrastructure and experience gained.

Hanle is a high-altitude, arid and cold place. This place is far from any artificial light pollution having low atmospheric aerosols, not much affected by monsoon and has got clear sky throughout the year. This site provides an excellent opportunity for developing astronomical facilities at a variety of wavelengths and an the initiative has already been taken to establish an astronomical facility over there. Following recommendation of Kasturirangan committee, as pathfinder to a large telescope, a 2m size Optical-NIR telescope was installed in September 2000 on Mt. Saraswati. More than a decade-long observing experience with HCT telescope has shown that Hanle region thus has the essential characteristics of an excellent astronomical site and could be a natural candidate site for any future large aperture Indian optical-infrared telescope.

1.5 Candidate sites for NLOT

IAO Hanle is in operation since 2003, and with regular observation, it is found to be one of the best astronomical sites in the country. IAO Hanle already has a good infrastructure and skilled manpower, which has got experience in working at high altitude cold climatic conditions. This makes IAO Hanle the first choice for installation of the country's future large telescope. Below, we mention few parameters

which makes the IAO an excellent siteCowsik et al. (2002a):-

1. IAO Hanle provides a large number of usable nights throughout the year. About 53% of nights are photometric and 75% of nights are spectroscopic.

2. A DIMM seeing monitor was installed and operated at IAO. Regular observations over the years show a median seeing in the range of 0.9-1.1 arc-second.

3. IAO Hanle has got a very dark sky. Observations made using 2m HCT telescope show the sky brightness of 21.3 mag/$arcsec^2$ in V band. Also the whole Ladakh region is very thinly populated and hence the future light pollution threat is almost nill.

4. The UBVRI extinctions recorded using HCT over time shows that Hanle sky is very transparent and stable. There is not much seasonal as well as long-term variation in the sky transparency. The very low U band extinction (0.36 mag) can be exploited to extend observations to the near UV.

5. The average air temperature at Hanle varies from -15 to +10 Degrees in a year. The average difference between day and night time temperature is less than 4 degrees.

6. IAO Hanle has got low mean relative humidity (RH) less than 40%for all the year except the month of July to September, at this time RH is about 50%

7. Precipitable water vapor (PWV) is lowest during the winter months of November, December and January (1 mm) and it is maximum during July and August (6 mm) when the surface temperatures are at the yearly high. The low values of PWV, consistent with other high altitude observatories make this site ideally suited for infra-red observations.

8. The median night-time wind speed is 2.2 m/s.

9. Snowfall is only a few days in a year.

10. The total rainfall in a year is less than 7 cm.

Tall mountain ranges surround the Mt. Saraswati, which is located at the center of Hanle valley. Looking at the local topology, it appears that most likely Mt. Saraswati where currently 2m size telescope is installed may not be exposed to laminar flow and hence can be subjected to poor seeing. With an expectation that seeing may be better in the neighboring mountain peaks, it was decided to explore few other mountain peaks close to the base camp of IAO Hanle. A field trip was undertaken in October 2007 to check the suitability of these sites regarding altitude, accessibility and horizon clearance. Three sites were selected, which are located within a 30Km radius of the Hanle and are easily approachable. These sites are:-

1. Kalak Tartar (KTT) (5486m)

2. Raindong (5055m)

3. Quin-Tso (5060m)

In the first round of scrutiny, the Quin-Tso was rejected mainly due to its distance from the base camp and also being close to two large lakes (not suitable for NIR observation). Remaining two sites Raindong and KTT were chosen for further exploration. Being very close to IAO, these sites are expected to have almost similar site conditions except the ground layer seeing which may strongly depend on local topology and may substantially vary from place to place. As a first step, in the year 2007-2008 two AWS were installed on these two peaks and weather data mainly wind speed and direction, relative humidity, soil and ambient ground temperatures have been acquired. Simultaneously collected wind data from three different places is

useful to understand the wind flow pattern. So far no attempts have been made to measure seeing on these two mountain tops. The idea is to carry out extensive site survey at IAO Hanle using varieties of instrument giving all sort of information about this place. Whereas, a collection of meteorological data, measuring the atmospheric seeing and turbulence profile are planned to be carried at KTT and Raindong. Figure 1.2 shows a Google map image of the IAO Hanle, KTT and Raindong sites.

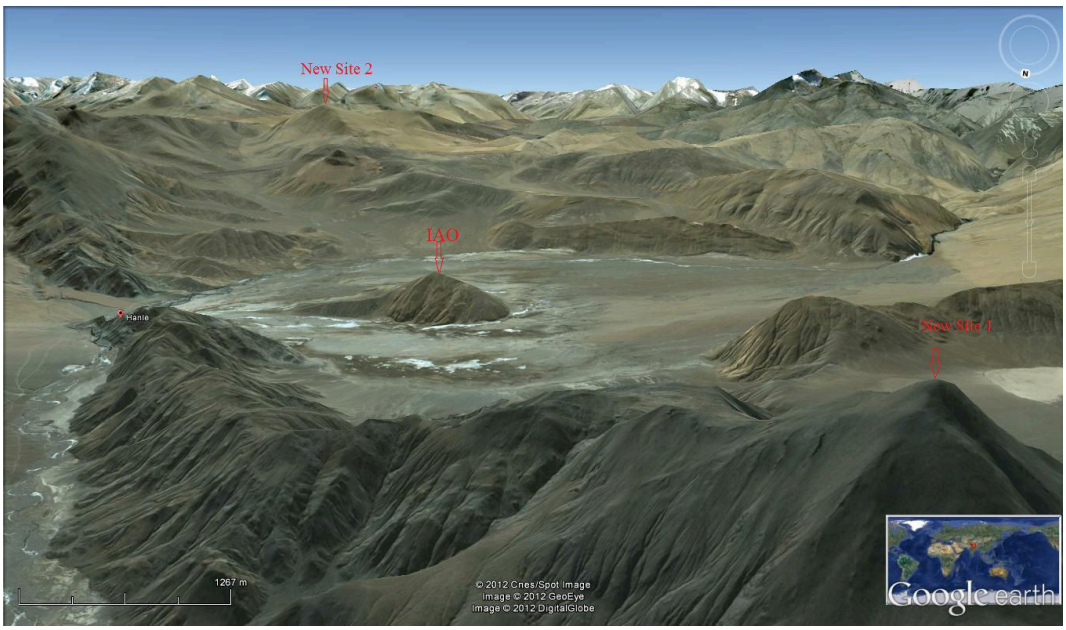

Fig. 1.2: Proposed sites for NLOT project. Site 1 (Lower right corner) is Raindong site, and Site 2 (Upper left) is KTT site. IAO Hanle can also be seen in center of the picture.

1.6 Need for developing new site survey instruments

Meteorological parameters can be easily obtained using automatic weather stations. Whereas, parameters like cloud cover, overall atmospheric seeing, turbulence profiles, isoplanatic angle, turbulence time constant, atmospheric transparency, sky brightness, etc. requires use of specially designed instruments. Most of these instruments are indigenously developed devices and cannot be procured by a commercial supplier. These devices are designed specifically to suit the requirements of the particular site

as well as desired science outcome. Therefore, we decided to design and develop few very important site survey instruments under this thesis. The idea was not to just replicate some of the survey devices, but to come up with very new instruments suitable for surveying any astronomical site. We chose to develop three instruments, an Automated Extinction Monitor(AEM), All Sky Scanning Cloud Monitor(ASSCM) and the Direct Drive based Telescope for MASS-DIMM instrument. The first two devices are indeed very innovative and extremely useful for reliable measurement of cloud cover and the sky transparency. Whereas, the third one is a telescope driven by the direct drive motors, expected to perform well without getting affected by a windy environment.

1.6.1 Automated Extinction Monitor(AEM)

The cloud coverage is primarily used to judge the quality of night, whether it is photometric or spectroscopic. Cloud free sky is usually assumed to be photometric, whereas, the partially cloudy sky is considered as spectroscopic. However, in practice, it has been noticed that atmospheric transparency can vary even during cloud-free nights, which is linked with changes in atmospheric aerosol and absorption by water molecules. By doing photometric observations of stars, atmospheric extinction can be precisely measured. In most observatories around the world, these measurements are taken by the bigger telescopes along with the science observation. This method of ascertaining sky transparency has two disadvantages. First, it results in an inefficient use of a larger telescope, if extinction measurements are taken separately. Second, this method fails to provide long-term continuous statistics required for thoroughly characterizing the local sky condition. The best way to generate an accurate statistics of photometric nights over a longer run is to have a dedicated device working in monitoring mode, but capable of measuring atmospheric extinction and sky

brightness with an accuracy usually achieved by large telescope. Driven by this requirement, we decided to develop Automated Extinction Monitor (AEM).

AEM is a standalone automated instrument designed to measure any small variation in the atmospheric transparency in one of the optical band. The same device can also measure the sky brightness with a better precision than any large telescope. We use a telephoto lens, a specially designed equatorial telescope mount, and a thermo-electrically cooled CCD camera. The instrument is developed in such a way that manual intervention required during its operation is almost negligible. AEM was installed at IAO Hanle in 2014 and since then it is in regular use.

1.6.2 All Sky Scanning Cloud Monitor

A CCD camera based all-sky monitor is an inexpensive tool, however, the appearance of clouds in the optical wavelength images is very deceptive due to its strong dependency on apparent sky brightness, which in turn depend on phases of the Moon, local light pollution and other atmospheric variables. Automated software tools developed to derive a quantitative information of cloudiness from all-sky images, usually fails to extract cloud information reliably, and results are often found to be inconsistent with other methods. Therefore, we decided to develop an instrument free from the shortcomings mentioned above, which can provide very reliable cloud cover statistics.

Our cloud monitor uses thermopile sensors which measure sky brightness temperature. Since there is a significant contrast between the temperature of clear sky and sky covered with cloud, therefore, we found this method to be more precise and reliable in detecting the cloud. The device uses an array of thermopile sensors mounted on a curved plate which is rotated in azimuth in steps. Device has gone through tedious laboratory as well as on-sky calibration, and tests and found to meet

the expected performance. Scanning cloud monitor has been installed at IAO Hanle in December 2015.

1.6.3 Direct drive based telescope for MASS-DIMM instrument

MASS-DIMM (Multi-Aperture Scintillation Sensor-Differential Image Motion Monitor) is a very useful site survey instrument which gives turbulence profile of the atmosphere. From TMT Project USA, a MASS-DIMM device has been acquired. One of the prime requirements of this instrument was that it needed a very stable telescope. Therefore, we decided to develop a very stable telescope which can work in windy conditions without degrading the image quality.

Our MASS-DIMM telescope can work in both Alt/Az and equatorial mode. Cross section area of the telescope is kept minimum by making use of lightweight carbon fiber truss in place of a tube. The direct drive technology is used, in which torquer motors are directly coupled with the telescope load axes. A customize controller and Drive developed in-house can control the telescope. A GPS is used for providing the accurate time information critical for ALT/AZ telescope operation. The telescope is completed, and preliminary factory testing has been carried out. Shortly it is expected to be installed at IAO Hanle along with MASS-DIMM instrument. Attempts have also been made to design, model and develop a prototype 3-phase axial flux direct drive motor suitable for astronomical telescopes of moderate size.

1.7 Thesis overview

Thesis is organized as follows:-

Chapter 2:- Concept of atmospheric extinction, techniques to measure extinction, AEM hardware, control system, instrument software and tracking, pointing and image

quality performance of the instrument is described.

Chapter 3:- This chapter present the results obtained from analysis of the data gathered by the AEM instrument. Results related to extinction, sky brightness and detection of thin clouds are presented. We also briefly describe our effort to explore the possibility of using AEM for stellar variability study.

Chapter 4:- Techniques to monitor clouds, operating principle of scanning cloud monitor and theory of non-contact temperature measurement are presented. Instrument electronics, software, calibration procedure and results are described.

Chapter 5:- This chapter describes the MASS-DIMM instrument and the design requirements of the telescope for MASS-DIMM instrument. Results of the mechanical analysis of the telescope and the wind load analysis of the OTA truss are also presented. Finally, we present preliminary results of testing of the direct drive motor using custom made drive.

Chapter 6:- Design of the direct drive axial flux motor, and microcontroller based controller and drive are described in this chapter. The results of the motor operation using drive are also presented.

Chapter 7:- This chapter presents the conclusion of the work carried out.

CHAPTER 2

AUTOMATED EXTINCTION MONITOR

Transparency of local sky is one of the key parameters for a site, as it defines the quality of the photometric observations. For precise flux calibration, extinction measurements must be made with great care and the observed data must be corrected for extinction. The study of the atmospheric extinction also allows to better characterize an observing site, and many such studies are conducted around the world to monitor the extinction (Tug, 1977; Sterken and Jerzykiewicz, 1977; Rufener, 1986; Lockwood and Thompson, 1986; Angione and de Vaucouleurs, 1986; Burki, 1995). The time variability of atmospheric extinction can range from few seconds to few days and months. The primary source of variable extinction appears to be the process of dust settling at night, the formation of new particles by homogeneous or ion induced nucleation, shrinking or swelling of the aerosol due to water vapor variations and diurnal change in ozone concentration. Also, cloud processing

enhances the growth of aerosol particles which in turn scatters more light (Reimann et al., 1992; Weber and McMurry, 1996). For a potentially good astronomical site, a large number of photometric nights and a stable sky transparency is highly desirable. Usually, clear nights are assumed to be photometric nights, and it is expected that the atmospheric extinction would be stable all through the night. However, observational data shows that sky transparency can vary even during clear nights. For any astronomical site, the best estimate of photometric nights come from extinction measurements carried out on a regular basis with a dedicated instrument monitoring the extinction for a span of several years.

In most observatories extinction measurement is carried out along with science observations. These measurements are less frequent and usually undertaken in the night which is expected to be photometric. There are several studies on atmospheric extinction using extinction data accumulated over several years, sometimes even over decades from such observations (Sterken and Manfroid, 1992; Reimann et al., 1992; Metlov, 2004; B. Kumar et. al., 2000; C. S. Stalin et. al., 2008; Buton, 2013). The primary goal of these studies is to explore the long-term effect, if any, due to the volcanic eruption, solar activity cycles, any meteorological changes as well as the man-made pollution. In most cases the data collected for extinction study is found to be very heterogeneous and comes from different telescopes as well as detector systems. Furthermore, extinction variations over shorter time interval have not been well studied. Therefore, a device like our extinction monitor can provide very accurate extinction estimates, thus saving precious large telescope time. There are very few dedicated observations carried out on the regular basis to record extinction (Burki, 1995; Garcia-Gil et al., 2010). There has been a plan to built a robotic extinction monitor for ESO, but so far to our knowledge, there is no such monitoring device developed (S. Stefan, et. al., 2000). The only device which is being effectively used to explore extinction and thin clouds is CFHT SkyProbe (Steinbring et al., 2009). This

system uses a small SBIG camera coupled with 50 mm lens (FoV 5 x 7 degrees), mounted on CFHT telescope as a piggyback.

Our motivation to develop the automated extinction monitor comes from small robotic telescopes developed for variability study like ASAS (Pojmanski, 1997), ROTSE (Akerlof, 2000) or projects to search for extra-solar planets like HATNET (Bakos, 2004) or Super-WASP (D. L. Pollacco et. al., 2006). All these projects make use of commercially available small telephoto lens and thermoelectrically cooled CCD cameras fixed on simple equatorial mount. We carefully analyzed ASAS-3 images as well as photometric data and found that this simple device could indeed provide very accurate photometry of hundreds of stars in the FoV. This photometric data can either be used to study the variability of stars or can also be effectively used to determine atmospheric extinction. After this study, we decided to design and develop an inexpensive extinction monitor which can provide very accurate statistics of atmospheric extinction and its variation at different time scales.

2.1 Atmospheric extinction

The intensity of starlight gets reduced while passing through the Earth's atmosphere due to scattering and absorption by air molecules and aerosols (dust particles, raindrops, ice crystals, etc.). Since the distance which light traverse through atmosphere depends on the position of an object in the sky, the larger the distance of object from the zenith, more the extinction will be. There are three primary sources of atmospheric extinction and these are:-

1. Extinction due to Rayleigh scattering,
2. Extinction due to absorption by Ozone, and
3. Extinction due to scattering by Aerosols.

2.1.1 Extinction due to Rayleigh scattering

Rayleigh scattering is an elastic scattering of the optical radiation by atmospheric molecules. In this type of scattering the physical size of the scatterer, i.e., the atmospheric molecule is much smaller than the wavelength of light. Rayleigh scattering is well understood theoretically as well experimentally. According to Hayes and Latham (1975) the extinction due to Rayleigh scattering at any given wavelength λ can be expressed as

$$k_{ray}(\lambda, h) = 9.4977 \times 10^{-3} \times \frac{1}{\lambda^4} \times C^2 \times exp(\frac{-h}{7.966}) \tag{2.1}$$

Where the molecular gas scale height is taken as 7.966 Km and C is given as

$$C = 0.23465 + \frac{107}{146 - \frac{1}{\lambda^2}} + \frac{0.93161}{41 - \frac{1}{\lambda^2}} \tag{2.2}$$

2.1.2 Extinction due to absorption by Ozone

The absorption of optical radiation by molecules in the atmosphere is primarily associated with individual optical absorption transitions between the allowed quantized energy levels of the molecule i.e. rotational, vibrational, or electronic energy states. The transitions between vibrational levels occur in the near-IR (2 to 20 μm wavelength), and electronic transitions generally occur in the UV-visible region (0.3 to 0.7 μm). In the optical region, the absorption is dominated by ozone. Ozone is mainly located in the lower portion of the Stratosphere (approximately 13-40 km above Earth's surface), and its thickness varies seasonally as well as geographically. The expression for the extinction due to ozone is given below.

$$k_{oz}(\lambda) = 0.69375 \times 1210 \times exp[-131(\lambda - 0.26)] + 0.055 \times exp[-188(\lambda - 0.5)^2] \tag{2.3}$$

Extinction due to ozone plays very prominent role toward shorter wavelength and it does not depend on the altitude of the site.

2.1.3 Extinction due to scattering by Aerosols

Extinction by aerosols and fine particulates in the atmosphere is due to Mie scattering which is similar to the Rayleigh scattering, except the size of the scatterer is of the same order of magnitude as the wavelength of the incident light. Below is the expression for atmospheric extinction due to aerosol:-

$$k_{Aro}(\lambda, h) = A_0 \times \lambda^{-\alpha} \times exp(\frac{-h}{H_A}) \tag{2.4}$$

Where H_A is the density scale height of water vapor aerosols, found to be about 1.5km. The A_0 is the total optical thickness of atmospheric aerosols at 1 micron, which depends on the total content of particles and on their efficiency for scattering and absorption, and usually taken as 0.087 (Mohan et al., 1999; Bessell, 1990). The α is a parameter which depends on the size as well as the shape of aerosol grains and usually taken as 0.8.

The total extinction at any given wavelength for a given site (constant altitude) is, therefore, a linear combination of these three contributions and can be expressed as

$$k_\lambda = k_{ray}(\lambda, h) + k_{oz}(\lambda) + k_{Aro}(\lambda, h) \tag{2.5}$$

From extensive observations and detailed atmospheric modeling, it has been found that while the first two component shows relatively slow variation, the last one plays a principal role in atmospheric extinction variation. It is a matter of common experience shared by observational astronomers that even in clear nights and good

weather conditions which are usually qualified as photometric nights, the atmospheric extinction is found to be variable over a night.

2.2 Variable atmospheric extinction

The atmospheric extinction coefficient is an important parameter for an observing site. Stability of this parameter indicates the photometric quality of the observing site. Hence, it is important to monitor the extinction coefficient over a longer duration to detect any short term and long term variation that could point towards degrading or the improving observing condition. The time scale for variations in extinction can vary from few hours to several years when only photometric quality nights are considered (Burki, 1995). Primary reasons for variable extinction over different time scale are changes in atmospheric water vapor contents, changes in aerosol concentration, volcanic activity, the motion of the air masses due to the global atmospheric circulation, etc. These variations are well studied and documented by various groups (Reimann et al., 1992; Sterken and Manfroid, 1992; Poretti and Zerbi, 1993a; Burki, 1995). Air pollution also plays a major role in variable extinction. Also, the photometric observation can be used to study the atmospheric pollution.

2.2.1 Short term variations

Short term variation usually refers to the inter-night and intra-night variation in extinction. Even during clear nights qualified as photometric, the extinction can evolve. The main process which is responsible for nightly drift in atmospheric extinction is the shrinking and swelling of aerosols due to change in the moisture content of the local atmosphere. Dust settling during the night also plays an important role in extinction variation. Dust and aerosols are injected and transported

in the atmosphere by the wind and their distribution depend on a variety of parameters.

2.2.2 Long term variations

Long-term variation refers to the seasonal variation in extinction. These variations are caused by seasonal variation of the aerosol and water vapor contents in the atmosphere. Long-term extinction variation is also affected by volcanic activity. A volcanic eruption can induce long-term perturbation of normal distribution of Stratospheric aerosols. Volcanic eruption causes the large amount of SO_2 to be injected into the atmosphere which is very efficient absorber when it is converted to sulfuric acid by a photochemical effect in the presence of water vapor. Considerable increase in the visual extinction was found after the eruption of El Chichon in 1982 which lasted for about 1000 days (Burki, 1995). Similarly, aerosol extinction due to Pinatubo and Nevado del Ruiz volcanic eruption has been documented by McCormick and Veiga (McCormick and Veiga, 1992).

2.3 Extinction and sky brightness measurements at IAO Hanle using HCT

The 2m HCT telescope is operational since May 2003. As part of science observations, time to time extinction and sky brightness measurements have been carried out. Multiband imaging data on 58 nights collected during 2003-2008, have been reduced and analyzed by Stalin et.al. (2008) (C. S. Stalin et. al., 2008). The average values along with the standard deviation in the distribution for all five Johnson standard photometric bands are given in the Table 2.1. The observed extinction in U, B and V very well matches with theoretical values derived with the certain assumption made

on scale heights. Whereas, extinction values in R and I photometric bands are found to be higher than computed values. On an average, extinction during the summer months is slightly greater than that during the winter months. This might be due to an increase of dust in the atmosphere during the summer months. No clear evidence of a correlation between extinction in all bands and the average nighttime wind speed is found.

Whereas, night sky brightness was estimated using 210 HFOSC images obtained on 47 nights and covering the declining phase of solar activity cycle-23. The zenith corrected values of the moonless night sky brightness in $mag/arcsec^2$ is given in the Table 2.1. These values of sky brightness indicate that IAO is a dark site for optical observations. Except for the I band, the sky brightness in other bands at IAO are similar to those of other dark sites in the world. The little bright nature of the sky in I band at IAO, might be due to the presence of strong OH rotation-vibrational Meinel bands in the red region of the optical spectrum. Sky brightness obtained over first four years period shows no substantial evidence of any changes. Similarly, comparison with monthly averaged 2800 MHz solar flux shows no clear dependency of sky brightness on solar activity.

Table 2.1: Atmospheric extinction and Sky brightness at IAO Hanle in various photometric bands, measured using HCT telescope.

Band	Extinction	Sky Brightness ($mag/arcsec^2$)
U	0.36±0.007	22.14±0.32
B	0.21±0.004	22.42±0.30
V	0.12±0.004	21.28±0.20
R	0.09±0.004	20.54±0.37
I	0.05±0.003	18.86±0.35

Data presented in table 2.1 indicates that the IAO Hanle has all the required characteristics regarding the extinction and the sky brightness. This makes Hanle the primary choice for the future large aperture telescope (NLOT).

2.4 Atmospheric Extinction:- Definition

The amount of light lost when it passes through the atmosphere of Earth can be found by using the radiation transfer equation. If object is not very far away from zenith, then we can approximate the atmosphere by plane parallel stratified layers in which all quantities like pressure, temperature and absorption coefficient depends on the height only.

Radiation transfer equation can be written as

$$\frac{dI_\lambda}{dS} = -\alpha_\lambda I_\lambda + \epsilon_\lambda \tag{2.6}$$

where α_λ is extinction per unit wavelength, and ϵ_λ is the source function. Since there is no source of light in case of atmosphere, hence source function will be zero and the Equation 2.6 can be written as

$$\frac{dI_\lambda}{I_\lambda} = -\alpha_\lambda dS \tag{2.7}$$

If we integrate the Equation 2.7 we can get the flux coming from the object. Let $I_{\lambda 0}$ is the intensity outside the earth's atmosphere and I_λ is the intensity near the earth's surface, then we get

$$ln(\frac{I_\lambda}{I_{\lambda 0}}) = -\int_0^S \alpha_\lambda dS \tag{2.8}$$

Here optical depth is defined as

$$\tau_\lambda = -\int_0^S \alpha_\lambda dS \tag{2.9}$$

Putting optical depth into Equation 2.8 we get

$$\frac{I_\lambda}{I_{\lambda 0}} = e^{-\tau_\lambda} \tag{2.10}$$

Now the flux can be converted into the magnitude by taking log and multiplying by -2.5

$$m_\lambda - m_{\lambda 0} = -2.5 \times log(e^{-\tau_\lambda}) = -1.086\tau_\lambda \tag{2.11}$$

$$m_\lambda = m_{\lambda 0} + k_\lambda \tag{2.12}$$

Equation 2.12 is true only when the object is at zenith or very near to the zenith. For objects located far from zenith the above equation can be written as (Bouguer's equation):-

$$m_\lambda = m_{\lambda 0} + k_\lambda \sec Z \tag{2.13}$$

$$m_\lambda = m_{\lambda 0} + k_\lambda X \tag{2.14}$$

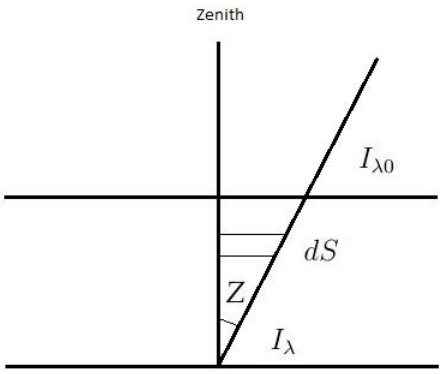

Fig. 2.1: Atmospheric extinction in plane parallel case.

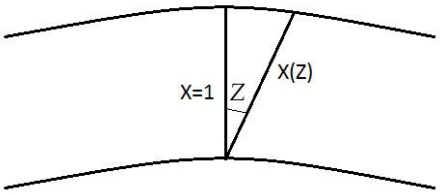

Fig. 2.2: Atmospheric extinction considering curved atmosphere.

Where X= sec Z, is the airmass.

In above derivation, it has been assumed that atmosphere is made of plane parallel stratified layers as shown in Figure 2.1, and the effect of the curvature of the atmosphere has not been considered. At large zenith distance, we have to take care of curvature of earth's atmosphere as shown in Figure 2.2.

Hence for zenith distance (z $\geq$ 60°), airmass can be expressed as

$$X = \sec Z - 0.0018167(\sec Z - 1) - 0.002878(\sec Z - 1)^2 - 0.0008083(\sec Z - 1)^3 \quad (2.15)$$

To determine the atmospheric extinction, objects are observed at different zenith angles and their apparent magnitude is plotted against airmass and a straight line is fit into it. The slope of the line gives the extinction coefficient as shown in Figure 2.3.

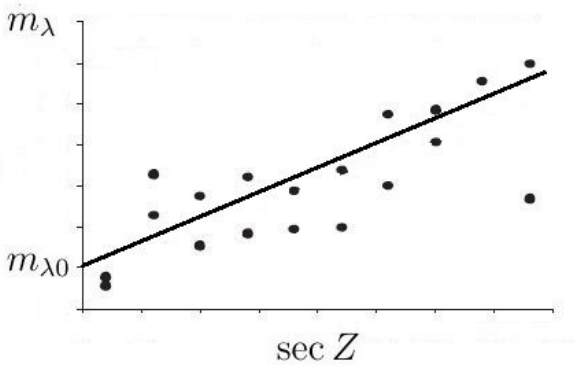

Fig. 2.3: Atmospheric Extinction Coefficient.

2.5 Techniques for measuring extinction

There are different methods introduced to measure atmospheric extinction (Poretti and Zerbi, 1993a; Arne and Ronald, 1990). The most widely used method is to observe any

standard stellar field over varying airmass. This method is time-consuming and can easily take 3-4 Hours of very precious telescope time. In another method, A-type stars which have got nearly zero photometric color but known standard magnitudes are observed at variable airmass and then extinction is derived. This method is relatively faster than the first method as extinction can be derived in less than an hour. Whereas, there is another method which can give instantaneous extinction measurement. All these three techniques are briefly described in subsequent sections.

2.5.1 Standard stellar field observation over varying airmass

This method of extinction measurement relies on continuously tracking of object and grabbing images at varying airmass. A stellar field can be selected which has got a large number of nonvariable stars. The instrumental magnitude is plotted against airmass, and the slope of the straight line fit gives the extinction. The average extinction can be determined from several such extinction plots generated for different stars. This method does not require a prior knowledge of the standard magnitude of the objects. It is free from inaccuracies caused by instrumental instabilities since these parameters do not change over the timescale of a night. This method provides a reliable estimate of extinction in the night when atmospheric transparency is stable. However, this technique requires minimum 3 hours of telescope time.

2.5.2 Observing A-type stars at different airmass

In this method, A-type standard stars which have got nearly zero photometric colors, but located at different zenith angles are observed. Following the Equation 2.16, when (V-v) is plotted against airmass then we again expect a straight line. Where V and v are standard and instrumental magnitude respectively. The slope of this straight line

is nothing but extra atmospheric extinction in V band. A similar derivation can be adopted for other photometric bands, provided these bands closely match with the standard photometric system such as Johnson and Cousins. The term ζ_v which is zero point, is linked with photometric transformation and knowledge of this term is not required for measurement of extinction. What is needed is observing a large number of A-type stars distributed all over zenith angles. In the same time, these stars should be observed as fast as possible, so that any change in atmospheric transparency during observation should not affect the extinction measurement.

$$V - v = \zeta_v - k_v sec Z \tag{2.16}$$

One of the variants of this method is to make use of photometric transformation coefficients and then one need not to observe only A-type stars. Any star at varying zenith distance can provide reliable extinction measurement, provided transformation coefficients have not changed.

2.5.3 Instantaneous determination of extinction

This method basically rely on the fact that if extra-atmospheric instrumental magnitude v_0 of a non-variable star is measured by using some ground based system then it is possible to measure instantaneous extinction coefficient $k_v(t)$, by using the formula given below:

$$k_v(t) = \frac{v_t - v_0}{sec Z} \tag{2.17}$$

Where v_t is instrumental magnitude measured by the same telescope-detector-filter system. The biggest advantage of this method is the real-time measurement and forecasting of the extinction. However, the main difficulty in the

application of this method is the reliable measurement of the v_0. One such method for accurate measurement of v_0 is described in detail by Poretti and Zerbi (1993b). Added difficulty is that the instrumental conditions (detector temperature, dark current stability, filter characteristics, detector gain, etc.) should be stable over a long time.

2.6 AEM hardware

AEM is a small yoke mounted equatorial telescope dedicated for atmospheric extinction and sky brightness measurement. Figure 2.4 shows a Solid model drawing of the instrument. A telephoto lens is used as optics, and a large format commercial camera is used as a detector. Stepper motors are used for driving both the RA and DEC axis of the instrument. Optical incremental encoders are used for providing the position feedback. Limit switches are installed on both the axis to restrict the movement. The instrument also has a polar alignment mechanism, which is used to change the polar angle depending upon the Latitude of the place.

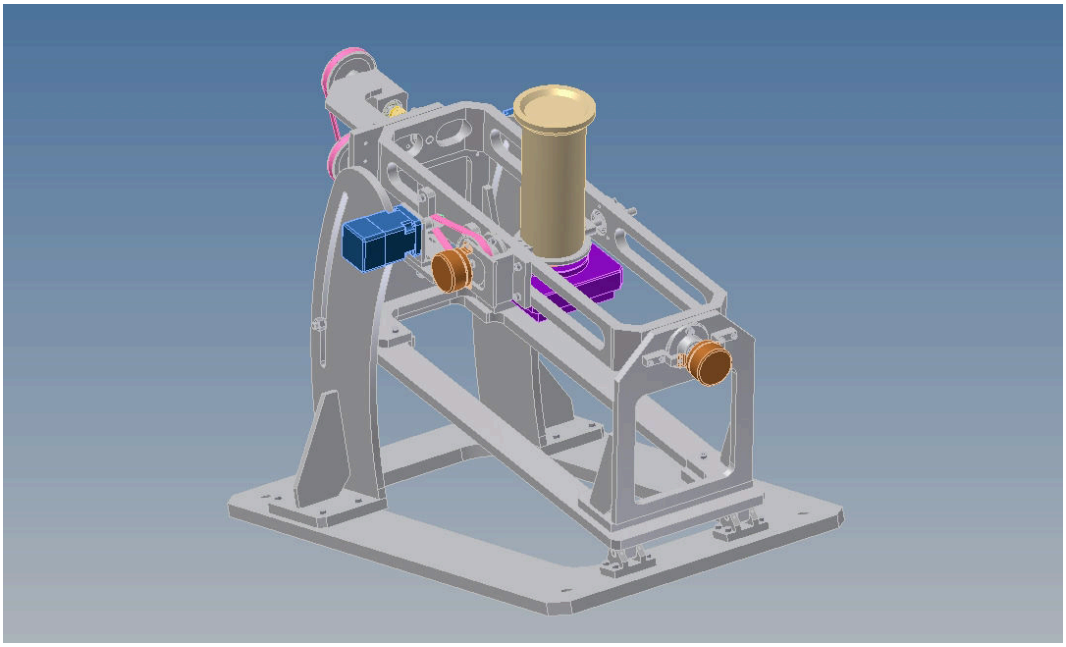

Fig. 2.4: Solid model drawing of the AEM instrument.

2.6.1 Design requirements

Initial concept design of the instrument was prepared locally by ourselves. The primary requirement for AEM are listed below:

1. The mount of the telescope should be equatorial.
2. AF-S Nikon 300mm f/4D IF-ED Telephoto lens is the main optics of the instrument. An interface unit must be designed, which connects both the CCD camera and the lens to the instrument. This interface should also provide focus adjustments.
3. Depending on the latitude of the place, there must be a provision to align the equatorial axis with the polar axis. The adjustment range should be between 12° to 36°.
4. Since IAO Hanle is subjected to high wind speeds, the cross-section area of the instrument should be optimized.
5. The RA axis being the main tracking axis, it must be driven by a combination of high reduction anti-backlash gear and timer belt-pulley. Dec axis can be driven by timer belt-pulley with medium reduction.
6. All-sky pointing accuracy better than 2′, as the FoV of the instrument is quite large.
7. Open loop tracking performance of less than an arc-second in one minute.
8. The maximum angular travel distance of both axes is about 180 degree (i.e. from east to the west horizon and north to south), but there should be unobstructed 360° movement if the limits fail.
9. Hall effect based limit switches should be placed on both the axis for North, South, East and West limits.

10. Rotary hollow shaft encoders should be placed on both the axis. Index pulse of the encoder will also act as the home pulse for the telescope.

11. There must be a provision to balance both the RA and DEC axis of the instrument.

12. A sliding roof type of enclosure to protect the device from rain and dust, when it is not in use.

2.6.2 Major components

Below we describe the important components used in the instrument.

Fig. 2.5: AF-S Nikon 300mm f/4D IF-ED telephoto lens.

2.6.2.1 Optics *Nikon: - AF-S Nikon 300mm f/4D IF-ED*

AF-S Nikon 300mm f/4D IF-ED Telephoto lens shown in Figure 2.5 is used as optics of the instrument. Use of telephoto lens provides two advantages. First, for a given focal length the size of telephoto lens is the smallest. This helps in keeping the size of the instrument small. Second, a telephoto lens has a large field of view, this enables to observe a large number of stars simultaneously, which increases the extinction measurement accuracy. Also, these are commercial products, readily available and cost-effective. Table 2.2 lists some of the specifications of the lens.

Table 2.2: Telephoto lens specifications.

Parameter	Value
Focal Length	300 mm
F ratio	F/4
Maximum Aperture	75 mm
FOV (with U32 CCD)	2.82 $\times$ 1.9 degree
Lens Construction (Groups/Elements)	6/10
Dimensions (from the camera's lens mounting flange)	$\approx$90 $\times$ 222.5 mm
Weight	$\approx$1.440 kg
Plate scale (with U32 CCD)	4.67″/pixel

2.6.2.2 Detector *ALTA U32*

The detector used with the instrument is an Alta U32 CCD from Apogee. The Alta U32 has a 3.2-megapixel (2184 x 1472) full frame sensor with high quantum efficiency. Apogee U32 uses the monochrome Kodak KAF-3200E/ME CCD chip. We have chosen this CCD because it has got a very low thermal count (0.05 e^-/pixel/sec), low readout noise (8 e^- RMS at 1 MHz) and very high quantum efficiency (86% at 610nm). The CCD camera is shown in Figure 2.6. The camera is supplied with open source Linux driver, which has been used for developing the customized software for the AEM instrument. Table 2.3 lists important parameters of the U32 camera.

Fig. 2.6: Alta U32 CCD camera from Apogee.

Table 2.3: U32 CCD Camera specifications.

Parameter	Value
CCD	Kodak KAF-3200E/ME
Array size	2184 × 1472
Pixel size	6.8 × 6.8 micron
Imaging area	14.8×10.0 mm (148.7 mm^2)
Linear full well capacity	55000 e^-
QE(400 nm)	53 %
Peak QE(610 nm)	86 %
Anti-blooming	None
PC interface	USB 2.0
System noise	8 e^- RMS at 1 MHz and 2 counts at 7 MHz
Pixel binning	1×1 to 8 × 1472 on-chip
Exposure time	30 milliseconds to 183 minutes (2.56 μs increments)
Dark current	0.05 e^-/pixel/sec (at -25°C)
Temperature stability	±0.1°C
Shutter	Vincent 25 mm
Back Focal Distance	0.69″ (17.50 mm).

Fig. 2.7: MXE-1010 embedded computer from Adlink.

2.6.2.3 Control computer *MXE-1010*

An embedded computer-controller MXE-1010 shown in Figure 2.7 from Adlink[1] is used as a control computer for the instrument. It is a very rugged computer which can work in very harsh environment ranging from -20 to 70 °C. The computer has an Intel Atom N270 processor, 2GB DDR2 RAM, 32GB Solid State Drive(SSD), two serial RS232 ports, and three Ethernet ports. This Control computer runs the Instrument

[1] http://www.adlinktech.com/index.php

Control Software and is responsible for fully automated operation of the instrument. Control computer performs high-level tasks like accepting the user inputs, various calculation required for pointing the telescope, handling CCD camera etc.

2.6.2.4 Stepper motor *SloSyn M061-LE02*

Stepper motors M061-LE02 from Slo-Syn are used for driving the RA and DEC axis of the instrument. Figure 2.8(a) shows the image of the motor. These are the main specifications of the motor:-

1. Standard frame size (NEMA 23).
2. 200 steps per revolution (1.8° step angle).
3. Rated current is 1 Amp and maximum holding torque is 0.42 Nm.
4. Windings can be connected in series and parallel configuration for changing the maximum current.

These motors are operated in microstepping mode to achieve smooth movements required for tracking and pointing of instrument. A microstepping stepper motor driver board described in Section 2.7.2 has been developed to operate these motors.

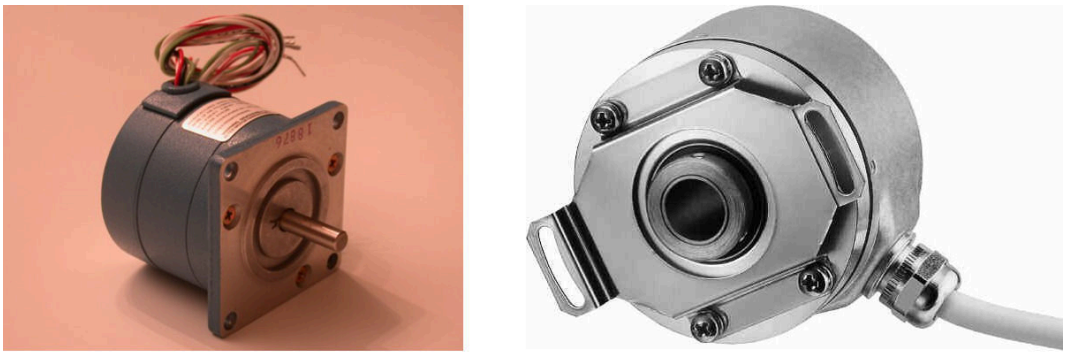

(a) (b)

Fig. 2.8: (a) M061-LE02 Stepper motor from Slo-Syn, and (b) RI-58 incremental encoders from Hengstler.

2.6.2.5 Encoder *Hengstler RI-58*

Incremental encoders RI-58 from Hengstler shown in Figure 2.8(b) are used to get the position information of the RA and Dec axes of the telescope. An incremental encoder generates two pulses which are in phase quadrature. These pulses are used by the Encoder Processor and Multiplexer board to generate information like position and the speed of the different axes. Section 2.7.3 explains the Encoder Processor and Multiplexer board. These are the technical specifications of the encoder:-

1. The resolution is 10000 pulses per revolution.
2. Mounting is hollow shaft type.
3. Different outputs are Phase A, Phase B, index pulse and one alarm output. The alarm output goes high when something is not working properly inside the encoder.
4. Operates on a five-volt power supply.
5. Environmental protection is IP64 certified.

2.6.2.6 Limit switch *Hamlin 55100-3H*

Hall effect based proximity sensors are used as a limit switch for sensing overrun of the drive on each axis. The Dec axis has got limit switches in North and South, which restrict telescope motion within the safe limit. Similarly, RA axis has got East and West switches. Sensor has a 3- wire interface and operates on 5V supply. The sensors get activated when a magnet is brought near the sensor body. The sensors are mounted on the stationary parts of the instrument in RA and DEC axes. The sensing magnets are mounted on the RA axis frame and on the counterweight disc in case of Dec axis respectively.

2.6.3 Telescope mount and drive

AEM being a small instrument, the mount was decided to be Equatorial. The initial concept design was prepared by ourselves, which was later modified by an external designer to meet the various requirements. Solid Model drawing of the instrument is shown in Figure 2.4, and the Instrument installed at IAO Hanle is shown in Figure 2.9. Various sub-systems of the telescope mount are described below:-

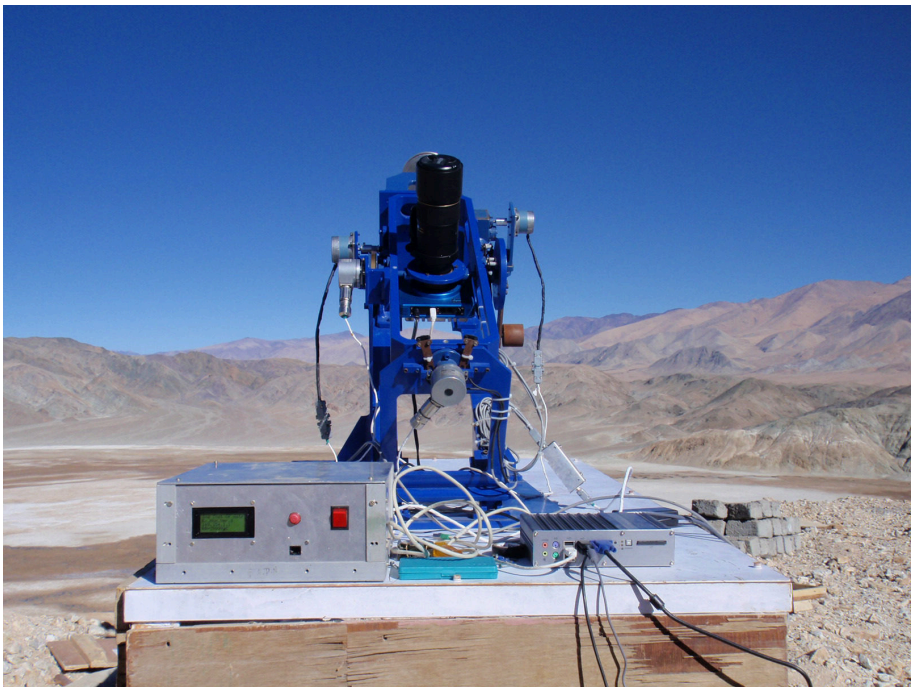

Fig. 2.9: Automated Extinction Monitor installed at IAO Hanle. Control computer and telescope controller kept on table can also be seen.

2.6.3.1 Polar alignment mechanism

The equatorial telescope requires it's RA axis to be aligned with the rotation axis of the Earth to track the objects. If the telescope is installed at one place, this is a one-time adjustment. In this case, also the telescope structure is designed for a particular location, and the RA axis is fixed at an angle equal to the latitude of the place. A site survey instrument may also have to be installed at various sites. This requires some

alignment mechanism in the instrument itself. The latitude of the Bangalore is 12° 58′18″ North and that of the IAO Hanle is 32° 46′46″ North. AEM has a mechanism which allows the polar angle to be changed from 10° to 36°. The mechanism consists of fixing the south end of the instrument about a pivot and moving the north end along an arc. The south end of the instrument is pivoted using bearings and is free to rotate. The North end is free to move up and down along two supporting plates. Once aligned, the north end is fixed at its position by tightening the bolts.

2.6.3.2 RA axis drive

RA axis of the instrument is driven by a drive mechanism consisting of a stepper motor, a gear box, and timer belt pulley. Stepper motor drives the gear box with reduction of 100. The motor shaft is coupled with the gear box input shaft using a flexible coupling to overcome any misalignment. The gear box, in turn, drives the timer belt pulley system, which gives a reduction ratio of 10. A 10 teeth pulley is mounted on the gearbox output shaft and is connected to the bigger pulley with 100 teeth using a timer belt. The bigger pulley is mounted on the telescope RA axis. The stepper motor itself is operated in microstepping mode, and requires 3200 (200 full steps $\times$ 16 microstepping) pulses to complete one revolution. Hence, the total number of micro-steps required for completing the one rotation of the RA axis can be calculated as:-

$$10 \times 100 \times 200 \times 16 = 3200000 \quad \text{microsteps} \tag{2.18}$$

The angle moved by the telescope RA axis for each micro-step is calculated as

$$\frac{\text{Arc-seconds in} \quad 360^\circ}{3200000} \tag{2.19}$$

$$\frac{1296000}{3200000} = 0.405'' \tag{2.20}$$

This means the RA axis can move as little as 0.405″. The equatorial telescope requires the RA axis to be moved at constant rate of 15″/sec in order to track the objects. Step-rate required for tracking can be calculated as

$$\frac{\text{Arc-seconds in one second}}{\text{Step-angle in Arc-second}} \tag{2.21}$$

$$\frac{15}{0.405} = 37.037 \tag{2.22}$$

This means 37.037 micro-steps are taken by the motor every second in order to track the objects. This constant frequency pulse output is generated by the Stepper Motor Driver Controller Board and is fed to the stepper motor driver board.

2.6.3.3 Dec axis drive

Equatorial telescopes require tracking only in RA axis; DEC axis needs to be moved only while pointing. Keeping this in mind, initially, only a small reduction of 5 was used between the motor and the DEC axis. However, it was soon realized that for better pointing accuracy the Dec axis also requires a large reduction gear. Therefore in December 2015, we modified the DEC drive to uses a small PIC gear with a reduction of 500. The output shaft of the gearbox is connected to the DEC axis with a timing belt pulley system having a reduction of 5. The motor is driven in micro-stepping mode and requires 3200 micro-steps to complete one revolution. The total number of micro-steps required by the DEC axis to complete one rotation can be calculated as

$$5 \times 500 \times 200 \times 16 = 8000000 \quad \text{microsteps} \tag{2.23}$$

Angle moved by the DEC axis for each micro-step of the motor shaft can be calculated as:-

$$\frac{\text{Arc-seconds in} \quad 360^\circ}{8000000} \tag{2.24}$$

$$\frac{1296000}{8000000} = 0.162'' \tag{2.25}$$

The use of large reduction on both the axes has significantly improved the pointing accuracy of the instrument, and allows the instrument to do regular science observations along with the extinction measurements.

2.6.3.4 Encoder mounting

Incremental encoders are mounted directly on both the RA and DEC axes of the instrument for precise position information. We have chosen to mount the encoder on the driving axis itself to remove any error, which may arise because of errors in the gear mechanism. RA axis drive has a provision to connect one more encoder to the gearbox input shaft, which can be used for speed feedback of the RA axis. This functionality has not been implemented.

Although the encoder generates 10000 pulses per revolution, the Encoder Processor and Multiplexer board interpolate this number by 4 bringing the number of pulses to 40000. Each encoder pulse now corresponds to 32.4″ of the sky.

2.6.3.5 CCD-Telescope-Lens Adapter

A CCD-Telescope-lens adapter shown in Figure 2.10 was designed and fabricated in-house to mount both the CCD and the optics on the instrument. A telephoto lens has a standard C-mount for camera interface. The CCD has two mounting mechanisms. One method consists of mounting the CCD using the mounting holes provided on the front side of the CCD but it can also be mounted using the threads present right above the shutter as shown in Figure 2.6. The adapter which we have designed has got C type mount on the front side to get interfaced with Nikon telephoto lens and the threads on the back side for mounting the CCD camera. The adapter also has a provision to adjust the distance between the CCD and lens which helps to get CCD chip on the focal plane of the lens. Once the correct focus is achieved, a threaded locking ring is used to freeze the separation between CCD and the lens system. The adapter has got a mounting flange which interfaces CCD + Lens system with AEM mount.

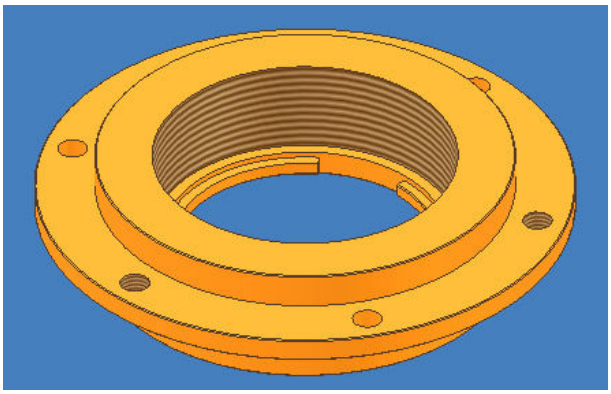

Fig. 2.10: Solid model drawing of the CCD-Telephoto Lens interface.

2.6.3.6 Mount balancing system

An imbalanced telescope will result in excessive wear and tear in the gear system used to drive it. It will also result in increased power consumption in the electronic drive circuitry used for operating the motor. The imbalanced telescope can also

introduce extra tracking and pointing errors. A single balancing mechanism is incorporated in the telescope which balances both the RA and DEC axis of the instrument. The mechanism consists of a circular disc mounted on the DEC axis. The disk has several tapped holes around its periphery. Weights are mounted on this disk in such a way that both the RA and DEC axis gets balanced.

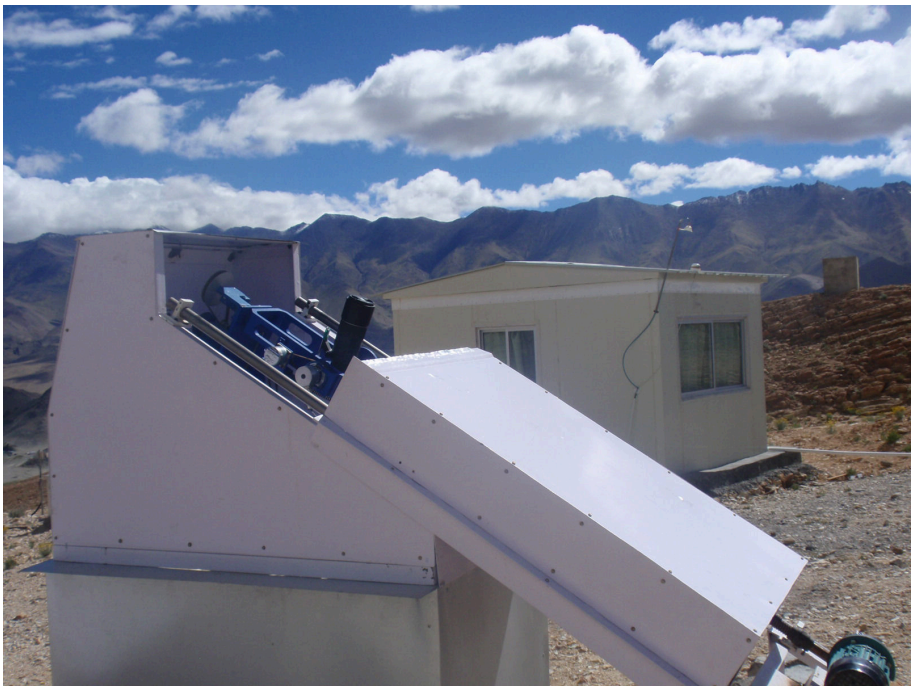

Fig. 2.11: AEM housed inside a sliding roof enclosure.

2.6.4 Instrument enclosure

A small sliding roof type of enclosure was designed and fabricated in-house for the instrument as shown in Figure 2.11. Since the IAO Hanle is subjected to very high wind speed, most often during the day time, therefore, the enclosure volume and cross section area, both are optimized. The instrument is placed inside the box structure, and whenever it is required the roof is opened and closed by issuing a command from the AEM controller. At present, the enclosure operation is manual and not linked to weather station. Which means, operator is required to manually

start the instrument. From this point onwards, the instrument operates on its own. The sliding roof of the enclosure is operated using lead-screw mechanism. Here motor powers the lead-screw and roof moves over two guide rods, which are located on both sides of the enclosure. The mechanical limit switches are located in the fully opened and the fully closed positions of the enclosure. These limit switches automatically cut off the power, once the enclosure is fully opened or closed and, this way, prevents any damage to the instrument as well as the enclosure driving mechanism. The enclosure also has a storage area just below the instrument, where the control computer and the other electronics are placed.

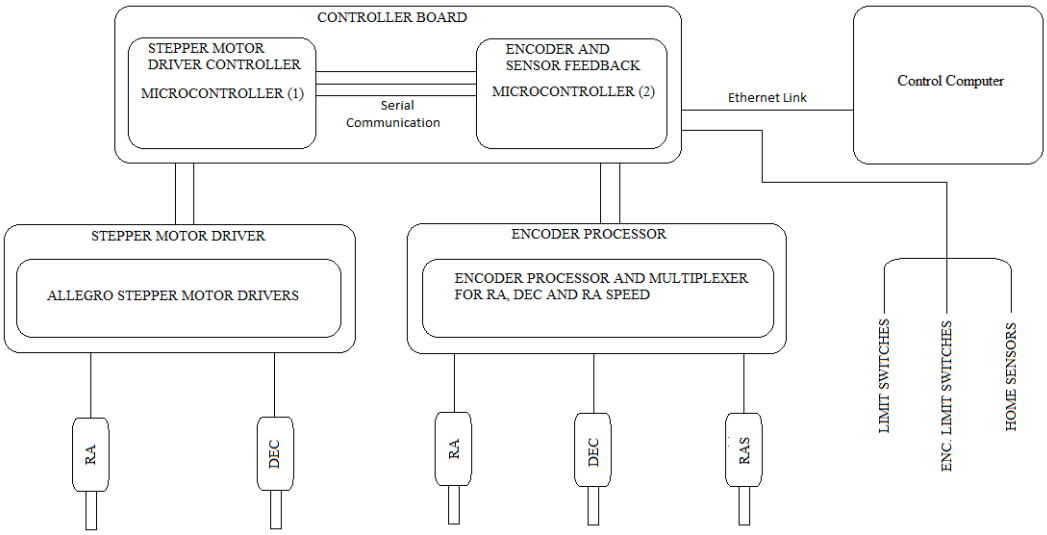

Fig. 2.12: Block Diagram of the Telescope Control System.

2.7 Telescope control system

Although the AEM is a small instrument, it has all the features required for fully automatic operation. A very robust, fully automatic network-based control system has been designed, developed and tested . A block diagram of the whole control system is shown in Figure 2.12, and installed controller is shown in Figure 2.13. The

telescope control system is the low-level hardware which directly interacts with the control components like motor, encoders, limit switches, etc. An embedded computer is used to control the instrument. All high-level calculations are performed by this computer, and only final commands and related data are sent to the control system via Ethernet. Telescope control system accepts these commands and performs the task accordingly.

Fig. 2.13: Telescope Control System placed beside AEM, IP address of the instrument can also be seen on the LCD display.

Whole telescope control hardware can be divided into three parts. These are: - Controller Board, Stepper Motor Driver Board, and Encoder Processor and Multiplexer Board. All these boards are mounted inside the telescope control system shown in Figure 2.13. These parts are described below.

2.7.1 Controller board

The controller board is developed using PIC18F97J60 microcontroller from Microchip. There are two such microcontrollers on the controller board. These are important features of the PIC18F97J60, which makes it suitable for our application:-

1. This microcontroller chip has got a total of nine 8-bit input-output ports (70 pins), any of them can be configured as input or output depending upon the application.

2. This chip has got an inbuilt Ethernet controller, which eliminated the need for an external Ethernet controller and associated complex programming.

3. The internal flash memory of the chip is 132 KB, which is required for writing the various functions related to the telescope operation. Although we have also provided an external memory, which can be used for data storage.

4. An internal ram of 4 Kbyte.

5. Total five external interrupts, some of which are used for handset interface.

6. Two Serial ports (USART) and two MSSP (master synchronous serial port).

7. Sixteen 10 bit analog to digital converters are also provided, which can be used to read the output of different sensors.

8. 3.3V operation for low power consumption.

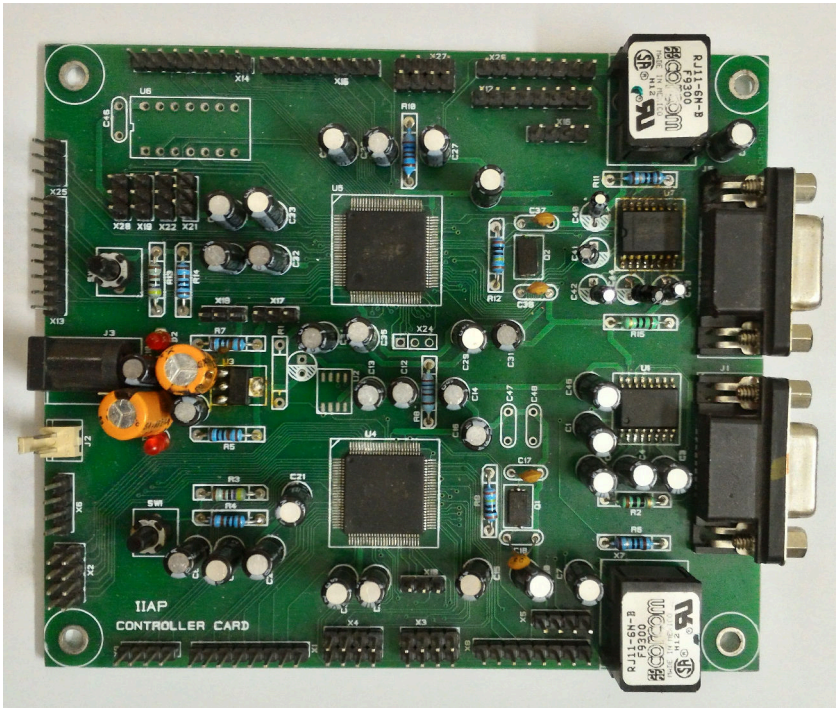

Fig. 2.14: Controller board PCB with all the components mounted.

Circuit description

A detailed schematic diagram of the controller board is given in the Appendix A. Figure 2.14 shows the finished PCB for the Controller board with all the components mounted. As mentioned earlier, the board has got two separate microcontroller units. These are called *Encoder and Sensor Feedback Controller*, and *Stepper Motor Driver Controller*. These two controllers communicate with each other using serial RS232 communication. Below we describe the tasks handled by these two controllers.

2.7.1.1 Encoder and sensor feedback controller

The encoder and Sensor Feedback controller establishes the Ethernet link between the Control computer and the AEM instrument. It accepts the commands coming from the Control computer. Depending upon the type of command, this controller can either pass the command to the Stepper Motor Driver Controller or can execute the command

itself. These are the few tasks handled by this controller:-

1. The controller gives the instrument the ability to work in a networked environment by providing Ethernet connectivity. Although the instrument is installed at IAO Hanle, it can be remotely operated from CREST Campus (Hosakote) of IIA.

2. It accepts the motion related commands from the Control computer, and passes it to the Stepper Motor Driver Controller.

3. This controller also accepts the output coming from the Encoder Processor and Multiplexer board. It can select any of the two encoders (RA and DEC encoder), and read the absolute position information.

4. Since all encoders are multiplexed to reduce the number of input lines; two selection lines are provided to select any encoder.

5. The controller also accepts the outputs from four different limit switches.

6. A 25 MHz crystal oscillator is used as a clock source for the microcontroller. Ethernet functionality requires the 41.67 MHz clock for its operation. An internal PLL converts the 25 MHz to 41.67 MHz.

7. A 4 line character LCD is also handled by it. Information like IP address of the instrument, commands coming from the control computer and the status of command execution, position of the telescope, etc. are displayed on the LCD.

2.7.1.2 Stepper motor driver controller

These are the important tasks handled by the stepper motor driver controller:-

1. The microcontroller generates the control signals required for operating the Stepper Motor Driver. The different signals are pulse, direction, micro-step

select, enable and sleep. These signals are generated in two sets, one for each axis (RA and DEC).

2. It also generates the motion profiles for the stepper motors. Motion profile includes tracking, acceleration, constant speed movement and de-acceleration. These profiles are required for smooth operation of each axis.

3. It accepts the output of limit switches, and the home pulse coming from the encoders.

2.7.2 Stepper motor driver board

The stepper Motor Driver Controller generates the signals required for motor operation. However, it can not drive the motor on its own. Therefore, a Stepper Motor Driver board was designed and developed to drive the motors. The driver circuit is based on A3984 IC from Allegro. Figure 2.15 shows the completed PCB board for the Stepper Motor Driver. Circuit schematic for the driver board is shown in Appendix B and the control signals required to operate the motor are described in Appendix D. This driver accepts the digital signals like step, direction, microstep select, enable and sleep from the Main controller board. The driver internally takes care of the phase sequencing, thus not loading the controller board with extra calculation.

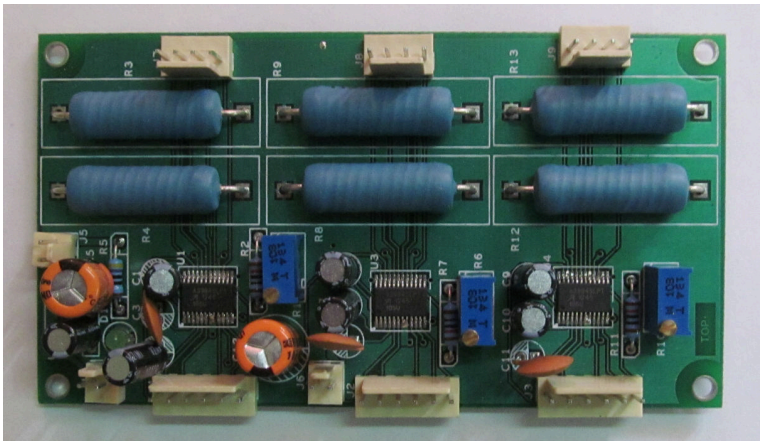

Fig. 2.15: Stepper motor driver PCB board.

Below we mention some of the important features of the driver:-

1. Board can simultaneously drive 3 stepper motors as 3 driver circuitry are placed on a single board.
2. It can operate any bipolar stepper motor in full, half, quarter and sixteen step modes. Also, these modes can be selected digitally using control pins.
3. Automatically take care of the phase sequences.
4. Internal low voltage and thermal shutdown circuitry.
5. Can operate on 3.3 volt supply (low power consumption).
6. Any motor up to the maximum current rating of the 2 Amps can be operated.
7. The maximum current can be set using an external potentiometer.

2.7.3 Encoder processor and multiplexer board

An incremental encoder RI-58 is used on both the RA and DEC axis of the instrument. Incremental encoders generate the quadrature output signal, where two outputs are

90° shifted. Another output is the index pulse, which is generated once for every revolution to indicate the home position. These outputs can be used to generate the absolute position information, once homing of the encoder is completed. We have designed a dedicated Encoder Processor and Multiplexer board. The board converts the quadrature output of the encoder to absolute output. It also interpolates the encoder output by 4 times, thereby converting the 10000 pulses to 40000 pulses per revolution. This board can handle 3 incremental encoders simultaneously. Figure 2.16 shows the completed PCB board.

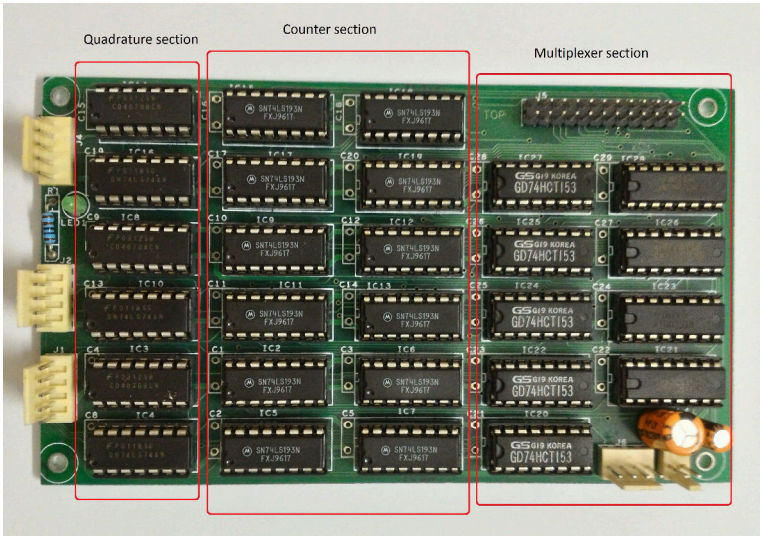

Fig. 2.16: Encoder processor and multiplexer PCB board. Three sections of the board are quadrature section, counter section and the multiplexer section.

Circuit Description

The detailed circuit schematic of this board is shown in Appendix C. There are three sections of the complete board as shown in Figure 2.16. These are: - Quadrature section, Counter section, and Multiplexer section. The Quadrature section of the board consists of D flip-flop and NOR-gates. It accepts the encoder A and B pulses and converts it to the count UP and count DOWN pulse. This section also generates two lower order bits, thereby increasing the encoder resolution by 4 times. There are three quadrature circuits in this section, one for each encoder.

Count UP and count DOWN pulses from the quadrature section are supplied to the counter section of the board. This section consists of the four binary counter IC's 74HC193. These counters are connected in series, meaning the output of first is connected to the input of second and so on. This way the counter section can count up to a maximum of a 16-bit number. The reset input of the counter section is connected to the index or home output of the encoder. This allows having a reference for the start of counting. Once encoder passes through the index mark, all the counters reset, and starts counting from zero. This section has 3 counter circuits, one for each encoder.

The absolute position information provided by the each encoder is 16-bit (40000 counts for one revolution) wide, this means 3 encoders will have a total of 48 lines. This will require a large number of I/O pins on the reading electronics. To limit the output lines from the encoder board, we have multiplexed the output of three encoders. A 74HC153 dual 4 to 1 multiplexer IC based circuitry is designed. This section accepts the 16-bit wide output of 3 encoders and provides one of the encoder output depending upon the logic present on the selection lines.

2.8 AEM Software

An intelligent software has been written for fully-automatic operation of the AEM instrument. The software can be divided into two parts. The first one is the embedded software which is a low-level software and run in the microcontrollers. The second code is a high-level software or Instrument Control Software, executes inside the Control Computer. Both these software's are described below.

2.8.1 Embedded software

This is a low-level software, which directly interacts with the control hardware like motors, encoders, and limit switches. Since there are two microcontrollers on the Controller Board, two separate codes are written. The first code is for the Stepper Motor Driver Controller. This code provides different functionalities like homing, pointing and tracking of the telescope axes. The code also interprets the signal received from the limit and the home switches (index output of the Encoder) and then an appropriate action is taken. It also accepts the commands coming from Communication Controller. The second part of the embedded code is for Encoder and Communication Controller. This part of the code provides the Ethernet-based communication link between the instrument and the control computer. It also interfaces the encoders to the instrument. This code receives commands from the control computer and depending on action required it either executes itself or pass it to the Stepper Motor Driver Controller via serial RS232 link. Table 2.4 lists the set of commands which are implemented in the Embedded code. These commands may or may not have accompanying data depending upon the nature of the command. Depending on the needed operations, one or a sequence of commands are issued by the control computer.

Table 2.4: List of Embedded commands provided in the controller board.

Command	Operation
INIT	Initialize the AEM instrument
H_RA	Home RA axis
H_DE	Home DEC axis
PRAE	Point RA axis EAST
PRAW	Point RA axis WEST
PDEN	Point DEC axis NORTH
PDES	Point DEC axis SOUTH
ORAE	Offset RA axis EAST
ORAW	Offset RA axis EAST
ODEN	Offset DEC axis NORTH
ODES	Offset DEC axis SOUTH
OENC	Open Instrument enclosure
CENC	Close Instrument enclosure
PARK	Park AEM instrument RA and DEC axis
STOP	Stop tracking in RA axis
RSUM	Resume tracking in RA axis
G_RA	Get RA axis encoder count
G_DE	Get DEC axis encoder count
RSTM	Reset the microcontrollers
GSTS	Get the status of limits, homing and tracking
CRAS	Change speed of RA axis

Since microcontrollers have limited memory, only basic functions related to the instrument operation are implemented in the Embedded Software. All calculation intensive tasks are handled by the High level software. MPLAB IDE from Microchip has been used for developing these codes. Programming language used is embedded C. TCP/IP stack and C18 compiler tools along with MPLAB IDE have been used for easy development of the code in C language. The compiled code (Hex code) is loaded to the microcontroller using the MPLAB ICD3 programmer.

2.8.2 Instrument control software

This software runs on the control computer and makes the automatic operation of the AEM instrument possible. The software takes care of all high-level calculations and

sends only the commands and the accompanying data to the instrument. This part of software controls the operation of the CCD, telescope controller and instrument enclosure. C/C++ programming language is used for developing the software. Open source library provided by the Apogee is used to control the CCD. The software takes command input from the user and operates the instrument accordingly. The user input is provided in the form of two different files (.txt files). These are: - Data file (Scheduler file) and the Configuration file.

Data File (Scheduler File)

All the required information for the scheduled observation is given through this file. Following are the various parameters which the user can provide:-

1. Name of the Object.
2. Type of observations (Bias, Dark or Object).
3. Whether coordinate data is in decimal or in Hour, Minute and seconds (HMS format) (1: - In decimal, 0: - in HMS format).
4. RA of the Object.
5. DEC of the Object.
6. Exposure time in seconds.
7. Pause time between two exposures in seconds.
8. Number of frames to be taken.
9. Total time spend.
10. Object data is modified or not (generated by the software).
11. Finish flag for the object (generated by the software).

Configuration File

This file requires following data to be provided by the user:-

1. Latitude of the site.
2. Longitude of the site.
3. Directory for saving the images captured by the CCD.
4. On the start of instrument whether RA homing is required or not (1: - Homing required, 0: - Homing not required).
5. On the start of instrument whether DEC homing is required or not (1: - Homing required, 0: - Homing not required).
6. Whether RA pointing is required or not (1: - Pointing required, 0: - Pointing not required).
7. Whether DEC homing is required or not (1: - Pointing required, 0: - Pointing not required).
8. Whether Imaging is required or not (1: - Imaging required, 0: - Imaging not required).
9. Whether coefficients related to the pointing model of the instrument.

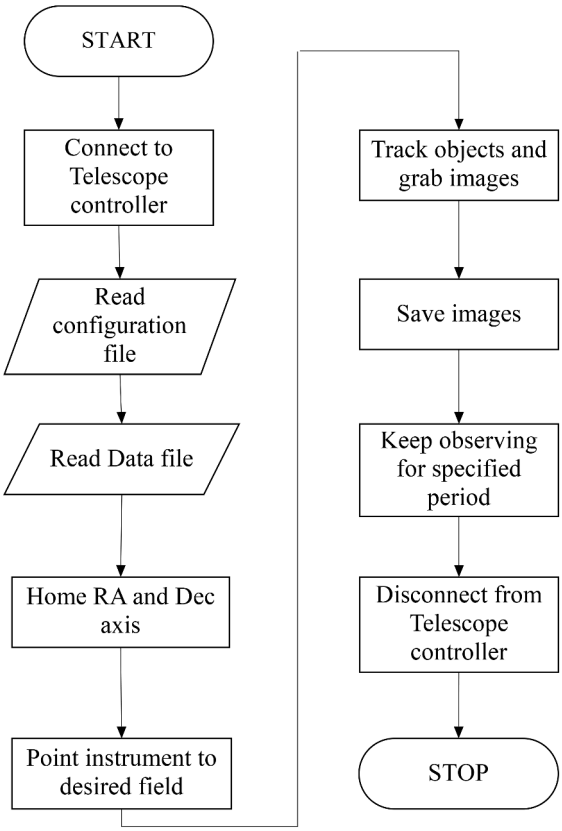

Fig. 2.17: Flowchart of the high level software of the instrument.

Considering the fact that the device will be all the time operated in the automated mode, we have not introduced any GUI. The code run on the Linux terminal window, and it displays various commands issued by instrument, command response, instrument status, etc. Images captured by the CCD are saved in FITS format along with a header, which contains observation-related information. Table 2.5 lists some of the parameters saved in the fits header. The program also generates a step by step log of the instrument operation with the time stamp, which can be very useful for troubleshooting if the instrument malfunctions. Figure 2.17 shows the flow chart of the software operation.

Table 2.5: List of parameters saved in the image header.

Parameter
Date of Observation
Observation Site
Latitude of site
Longitude of site
Name of Telescope
Name of CCD
No. of pixels in Horizontal direction
No. of pixels in vertical direction
CCD chip temperature
Frame exposure time
Readout noise of CCD
Gain of CCD Indian standard time
Universal time
Local Sidereal Time
Julian Date
Airmass
Name of Object
Object RA
Object DEC
RA encoder value
DEC encoder value
Telescope Hour Angle
Telescope Declination

2.9 Telescope performance

2.9.1 Pointing

Since the FoV of the AEM is very large (2.8 x 1.9 Degree), therefore, we do not require very high pointing accuracy, which is usually needed in case of large telescopes with smaller FoV. However, for the purpose of easiness of reducing the data using image reduction tools, it is good to have smaller pointing error and for AEM we aimed to have pointing error less than 2 arc-minutes. We have also implemented a pointing model which corrects any systematic repeatable pointing error. Initially, the pointing

in the RA axis was found to be good, whereas the Dec axis was subjected to large non-repeatable pointing error hence, can not be corrected by pointing model. Then after we modified the Dec axis drive unit, the telescope started giving the satisfactory pointing performance. The telescope pointing has been checked in two ways. In the first approach, on a given night instrument is pointed to a large number of stars distributed all over sky then pointing error is computed. In this approach, we get all sky pointing accuracy for a particular night. If the device is mechanically stable, then we expect same pointing performance in subsequent nights too. In another approach, the pointing error is computed from images of a stellar field which was repeatedly observed over more than 15 nights and plot of the pointing error is shown in Figure 2.18. The RMS pointing error is found to be about 52.7″ and all the points lie within a circle whose radii is 90″.

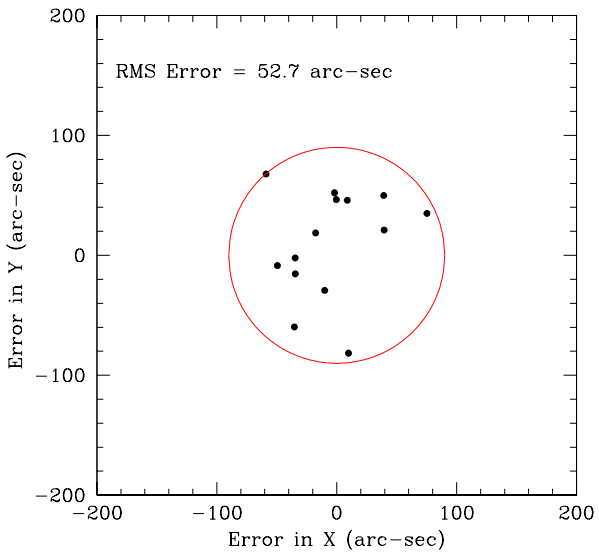

Fig. 2.18: Plot of the pointing error determined by repeatedly observing a stellar field over 15 nights. The radius of the circle is 90″.

2.9.2 Tracking

Since there is no provision for the guiding, the AEM was expected to have a decent tracking performance and we aimed for less than an arc-second over one minute of exposure. The above specification is driven by the need to have the longest exposure of about 120 seconds which will degrade images by half a pixel (one pixel is 4.67″). For extinction observation, we have repeated the observation of any stellar field over very long duration (8-10 hours), so these images can also be used to check the tracking performance of the telescope.

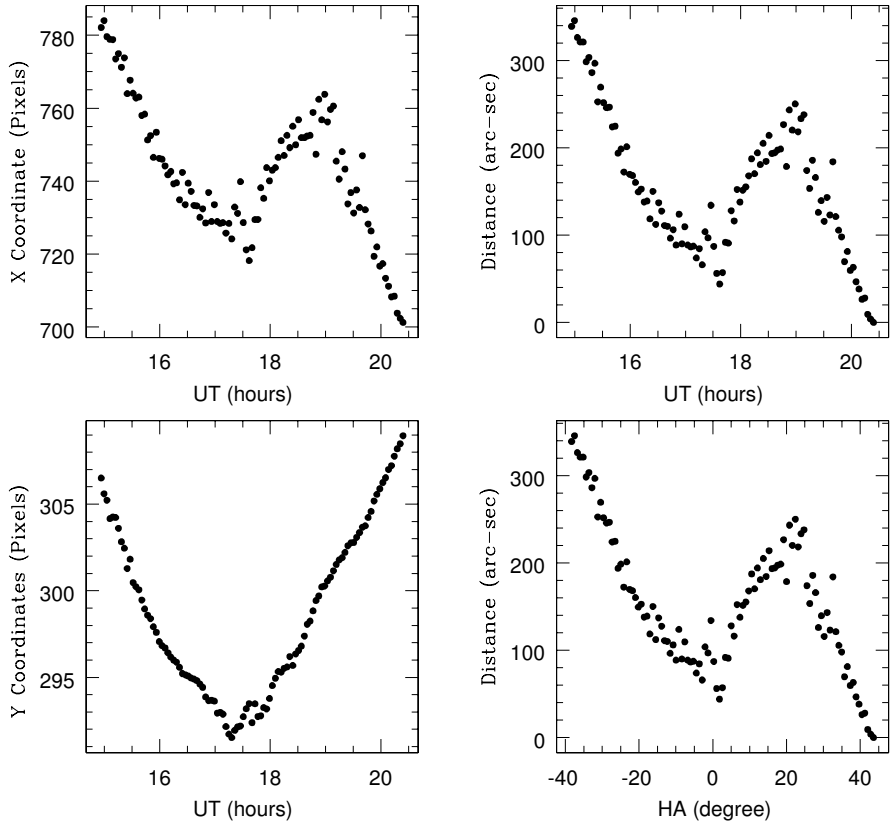

Fig. 2.19: Plots showing the tracking performance of the AEM in RA (X coordinate) and DEC axis (Y coordinate).

We determine the position of a star on CCD images and its X-Y position has been plotted against time as shown in Figure 2.19. The plot of X & Y position versus UT

shows how good the tracking performance is in X (RA axis) and Y (Dec axis). It appears that the tracking error in Dec, though it is much smaller than RA, is probably due to polar miss-alignments of the telescope which need to be further improved. Whereas, the error in RA axis is very large and primarily subjected to driving mechanism. The worst tracking error is as poor as 2.3″ and the best performance is about 0.2″ over a minute of time. The source of the tracking error appears mainly mechanical in nature and is due to the periodic error in the combination of worm gearbox and the timer belt-pulley based drive of RA axis. We hope to improve the tracking performance by better tuning the tracking rate of RA axis, training and correcting periodic error introduced by the gear train and further improving the polar alignment.

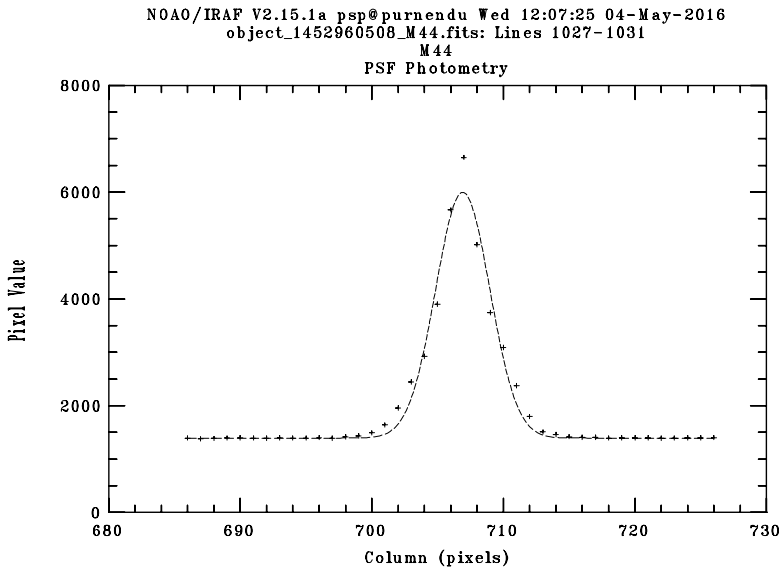

Fig. 2.20: The radial plot of a star in an AEM image obtained by giving 60 second exposure time.

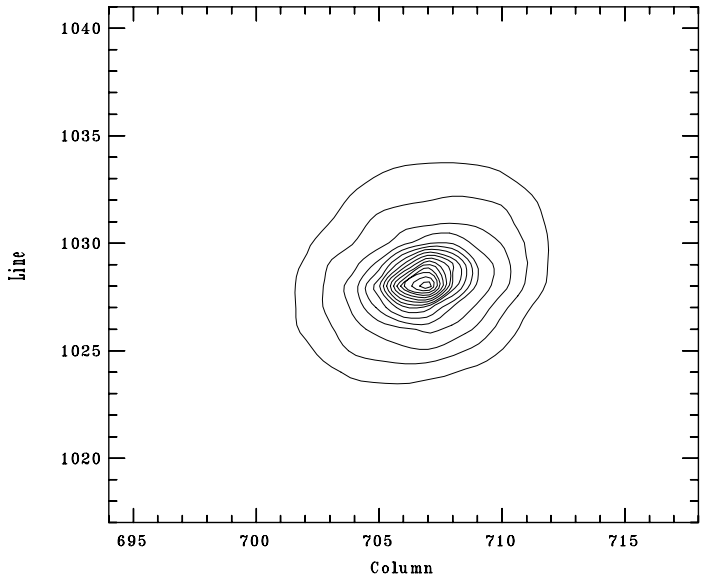

Fig. 2.21: The contour plot of a star in an AEM image obtained by giving 60 second exposure time.

2.9.3 Image quality

The FoV of the system is quite large 2.8 x 1.9 Degree, however, the image quality over the entire field of view is found to be good and uniform. Figure 2.20 and Figure 2.21 shows the radial plot and the contour plot for a star in image captured by AEM for 60 second exposure time. The diffraction limited image for the 75mm aperture telephoto lens is 1.84″, and the seeing at the site varies from 1-2 arc-second. Therefore, FWHM of the star in our field is expected to be about 2.1-2.7 arc-second and at the best focus, the whole starlight will get confined to within one pixel. This would make photometric measurement inaccurate, and that's why during observation the telephoto lens is slightly defocused.

CHAPTER 3

AEM RESULTS

3.1 Observation details

After preliminary testing at IIA Bangalore and VBO Kavalur sometime in July 2012, AEM was transported to IAO Hanle and kept onto a table in open environment (as shown in Figure 2.9 in Chapter 2). The instrument was once again tested for pointing, tracking as well as other performances. During November-December 2012, trail observation for the extinction was also carried out. In this very first test run, it was realized that we needed to have a permanent enclosure as well as improvement to the Dec axis drive. After about one and half year later in July 2014, the upgraded AEM housed inside a motorized computer controlled enclosure started working. Nearly about 50 nights of data was collected during July 2014 to April 2015, then again some problem in the AEM hardware was noticed, and AEM observation was discontinued for some time. It took some time to replace the

controller board as well as one of the encoders which stopped working. To improve pointing accuracy in the Dec axis an additional gear system with 500:1 reduction was added. Then after since December 2015, the AEM has been in regular use. So far we have collected more than 150 nights data, and out of that about 92 nights data has been analyzed and reported in this thesis. Sky brightness measurement required observation of the known fields, which in turn needs better pointing accuracy. Since initial instrument pointing was very poor, we could not make the observation for the sky brightness. Regular observation of sky brightness started from December 2015 only.

3.2 Data reduction

Images captured by the AEM needs to be processed before they can be used for the photometry or some other image analysis work. Captured images need to be corrected for bias, dark and flat field corrections before any data analysis can take place. We briefly describe these steps in the subsections below.

3.2.1 Bias correction

The bias images are the CCD frames taken with zero second exposure when the shutter is in closed position. The pixel values that are found in the bias image are due to a negative offset voltage applied by the control electronics. In the case of large CCD read-out noise, it is advised to collect a large number of bias frames and combine them by taking median value for each pixel. Subtracting the median combined bias image rather than average pixel image from the observation image removes the pixel-to-pixel structure introduced by read-out electronics to an image. Analysis of the bias frames captured over the period of nearly three-month shows that bias value

is not very stable. Bias value changes nearly 40 counts despite having very stable CCD temperature which is set at -40 °C and varied by ±0.15 °C from this temperature set point. We have noticed intra-night changes in the bias level by few counts. Figure 3.1 show a master bias frame generated for one of the night. Figure 3.2 shows the distribution of CCD temperature and median pixel counts for the bias frames.

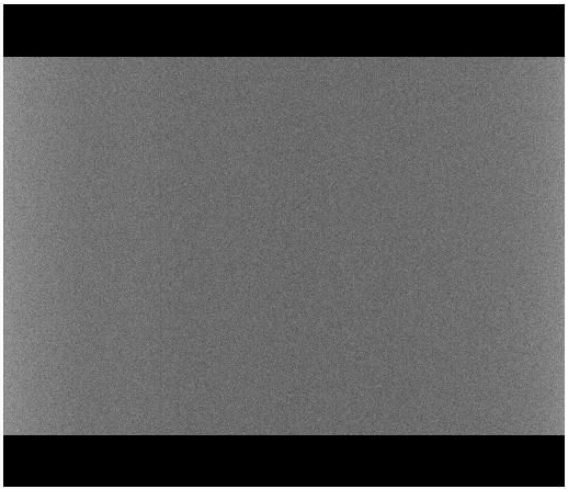

Fig. 3.1: Master bias frame after combining 20 frames obtained in a single night.

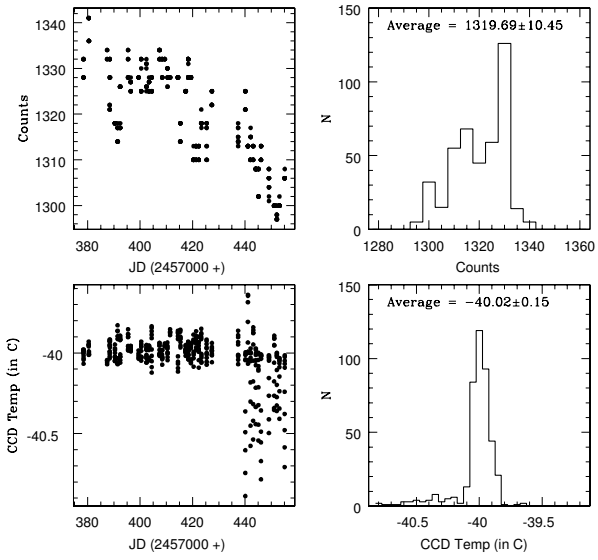

Fig. 3.2: Plots showing the distribution of median bias values and the CCD temperature.

3.2.2 Dark correction

The number of electrons recorded by each pixel on a CCD chip may have an additional component, which is not related to the incident light from the source. The extra component is usually due to thermally generated electrons inside the CCD pixels. The generation of the thermal electron depends exponentially on the ambient temperature and can be a significant contributor to the noise. These thermally generated electrons affect the CCD operation in two ways. First, it reduces the dynamic range of the CCD. Secondly, it introduces a temperature dependent noise. Solution to this problem lies in operating the CCD at a very low temperature and keeping this temperature constant for all the observation to remove any temporal variation in noise. In the case of large-format Astronomical CCD camera, the CCD chip is cooled by the liquid Nitrogen, down to -110 °C resulting in a very little dark current. Whereas, in the case of less expensive small-format CCD camera, cooling is done by a thermo-electric device (like Peltier cooler). This type of cooling allows CCD chip to be cooled 40-60 °C below the ambient temperature. The CCD camera used in AEM is Peltier cooled and having some contribution from the dark current (0.05 e^-/pixel/sec (at -25°C)).

To remove the effect of dark current from the object image, we need to acquire a separate dark frame which has only the dark current signal. This is accomplished by taking an exposure of the same duration as the object frame to be processed, but keeping the CCD shutter closed. This ensures that no light reaches the CCD, so that the only recorded signal is the dark current. It is extremely important that the dark current frames should be of the same duration as the object image, and it must also be taken at the same CCD temperature. Like bias frames, the typical procedure for using dark frames is to acquire several (6-10 are usually sufficient) dark frames with the same exposure time and temperature and average them to construct a master dark

frame. The master dark frame is subtracted from the object frames, and this procedure is called the dark correction. Figure 3.3 shows various plots for CCD pixel counts and CCD temperature for the dark frames.

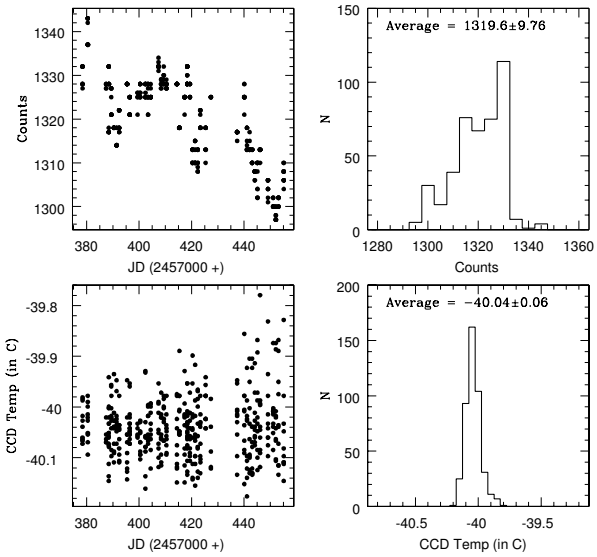

Fig. 3.3: Plots showing the distribution of median dark values and the CCD temperature.

Likewise the bias frames, the median dark value obtained over three months period is analyzed, and it shows similar behavior. After studying the variation of the dark frames, we realized that for very accurate sky brightness measurements we need to take dark frames before and after observing standard stellar fields, and then use the average dark values for the correction.

3.2.3 Flat correction

The last correction applied to a CCD image is flat-fielding. This correction accounts for the fact that the sensitivity of all the pixels is neither same nor constant over the time. The pixel sensitivity has two components; these are spatial and the temporal variation. The telescope optics may not transmit light uniformly across the entire field of view. This may be due to the vignetting, the presence of dust on the CCD chip, the dust on

CCD window as well as on the filters, etc. In addition to this, the QE of individual pixels varies across the CCD causing a variation in sensitivity. To correct for these effects, one must acquire flat-field images. Capturing flat-field images require a source of uniform illumination, either a diffuse screen illuminated by a light source in the dome itself, or the twilight sky. Flat field frames grabbed with a dome diffusing screen are known as 'Dome Flats'and those taken using the twilight sky as the illumination source are known as 'Sky Flats'. It is well-known fact that the twilight sky flats are better than dome flats and do not require any additional arrangement. For the AEM, we decided to go with sky flats. The exposure time of flat field images is set to such value so that a significant signal level is recorded. Several flats are taken to allow for the construction of a master flat. These flat frames should be corrected for the bias as well as for the dark, as described before. In the next step, the master flat is normalized with respect to the median count of the master flat frame. The flat field correction is done by dividing the image to be corrected with the normalized master flat frame. Figure 3.4 shows the image of the master flat (sky flat) for the AEM. Figure 3.5 shows the column plot for the Master Flat.

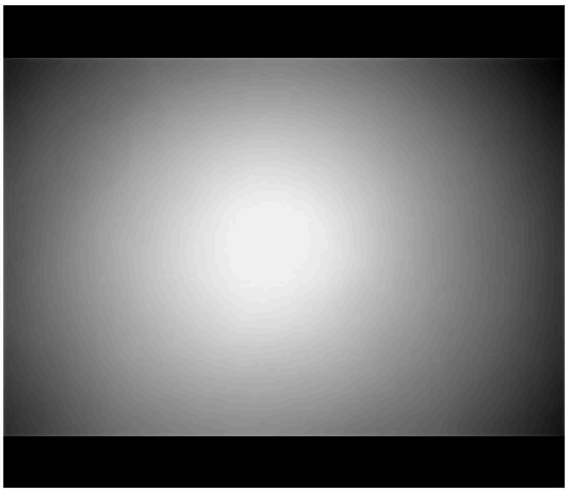

Fig. 3.4: Image of the Master Flat frame.

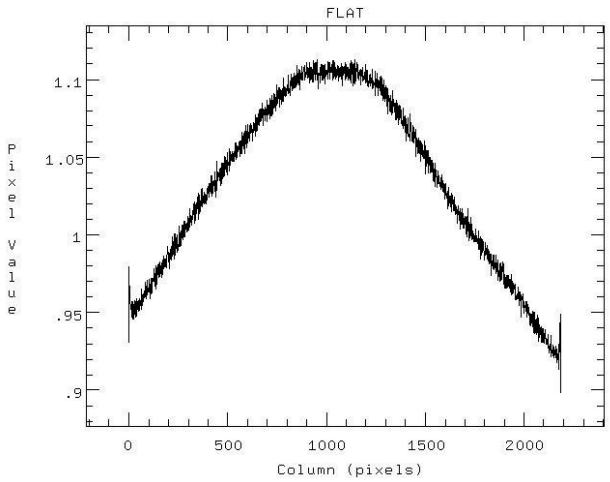

Fig. 3.5: Column plot for the Master Flat frame.

When we corrected object frames for the flat, then expectation was that it would leave a very uniform background. Contrary to our expectations we notice that flat correction is non-uniformly changing the background and also photometry carried out by flat corrected frames was not so accurate. Therefore, we decided not do the flat fielding and carried out photometry without flat fielding.

3.2.4 Identification of stars and photometry

Once the object frames are corrected for bias, dark and flat, they are ready to be used for the photometric analysis. Each object frame will have a large number of stars, cosmic rays, hot pixels and sometimes also the diffuse objects like faint galaxies, comet, nebulae, etc. As far as the extinction measurement is concerned, we are only interested in stars, and hence, they need to be distinguished from other objects. At present, we have used DAOPHOT package available inside IRAF to identify large number of stars in the first reference frame. The parameters used in daofind task like standard deviation of the background, FWHM of the stellar profile, detection threshold, etc. are dynamically determined. Then after photometry is done using DAOPHOT phot task. Phot task sets numerical apertures for stars and sky, once again

refine the stellar coordinates, determines sky and then does photometry for different aperture starting from one pixel to 15-pixel radii. After a lot of trial and error, we found that the aperture of 10-pixel radii is good enough to include 99.99% light coming from stars in varying atmospheric seeing as well as images subjected to telescope tracking errors. Telescope tracking is found to be good, and frame to frame drift is well within the centering box of the phot task. Therefore, we have written an IRAF CL script which does photometry of all the frames by computing coordinate for subsequent frames. The final product of the scripting is a file which contains photometric data of a large number of stars along with other details like Julian Date, UT, Airmass, etc.

3.3 Determination of extinction

We have used two different methods to determine the atmospheric extinction coefficient. The first method is a very classical method in which single star or a group of stars are observed over varying airmass, and the slope of the linear regression fit between magnitude and airmass is nothing but extinction coefficient. Whereas in another method, we try to identify nonvariables and their extra-atmospheric magnitudes. Then after extinction is computed by knowing the instantaneous magnitude and the computed airmass. We briefly describe these methods in sections below.

3.3.1 Extinction measurement by observing stellar field over varying airmass

Typically, one or more stars are observed over varying air-mass and then their magnitudes are determined and plotted against air-mass. The slope of the linear fit to

the data provides the extinction measurement. After the sunset once sky becomes dark, the AEM shutter opens, the telescope initializes, and seeks for the home. Once homing is completed the telescope points to a predetermined field in the eastern sky about 30 degrees above the horizon. The same field is repeatedly observed till object reaches to 30 degrees from the west horizon. The field is observed over both side of the meridian and covers almost $\pm$ 4 Hour angle. In between dark and bias frames are also periodically collected. After bias, dark and flat field corrections as described in previous sections, stars brighter than 11th magnitude are identified and aperture photometry with numerical aperture usually 10 pixels is carried out. In practice extinction can be computed from a single star, however, use of 10-20 stars distributed all over the field gives a more precise extinction measurement. Figure 3.6 shows extinction plots for the single star (Left) as well as multiple stars (Right).

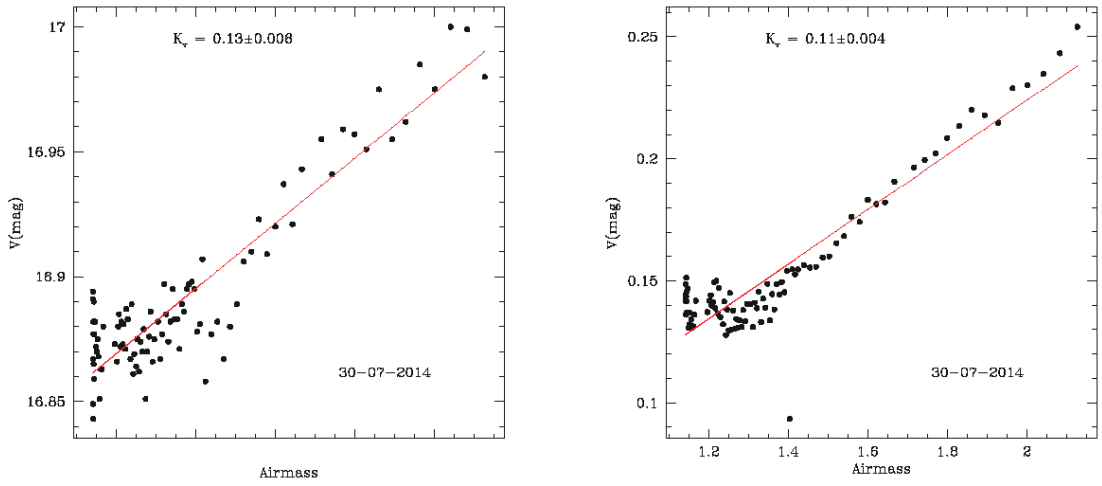

Fig. 3.6: Extinction plot generated using single star (left), and multiple stars (right).

In the case of using multiple stars for the extinction measurement, we have adopted two different methods. In the first technique linear regression is fitted separately to data of every single star and then zero-point is subtracted. After that, an average magnitude for every frame is computed and plotted against air-mass. The

linear fit to this data gives a slope which is the average extinction considering magnitude of all the stars. Since the field of view of the AEM is quite large, at higher zenith angle, an airmass within FOV can be very different for different stars and computing extinction based on airmass of the center of FoV for all the stars can introduce systemic errors. To circumvent this difficulty, we compute air-mass for every star separately and then determine extinction from all the stars to finally get the average extinction value. Till 2.5 air-mass, we do not find much difference between the extinction values derived using above two techniques. Therefore, extinction values for all the observed nights were obtained using the first techniques only. We find that in a typical stable night, our extinction measurement can be as precise as few milli-mag.

3.3.2 Instantaneous measurement of extinction

In the previous chapter, we have briefly described the techniques used to determine the atmospheric extinction in real time. Despite being a very useful method, this technique has hardly been used to measure extinction. Since this technique requires stable photometric measuring device, this technique was found to be not suitable for PMT or photodiode based photometers. However, now that CCD gives very stable performance, therefore, it is relatively simple to adopt this technique. Since we repeatedly monitor any extinction field for about 15 nights, it gives us an opportunity to check how well instantaneous measurements are possible. For this we went through the procedure described in the details in Section 2.5.3 and identified 10 stars which shows minimum SD and hence found to be non-variable and best suited for extinction measurements. Once such stars are identified then, we choose 5-6 nights in which the sky was found to be stable and very accurate measurement of extinction was possible using the technique described earlier. Then the extinction corrected

instrumental magnitude (v_0) was determined for all 10 stars and once again ensured that their time series plots show no systematic variation. After that the average v_0 was determined for each star and used in Equation 2.17 to determine extinction k(t) which is instantaneous extinction and may vary over the time. Similar extinction value is derived from remaining 9 stars and finally, an average extinction value is computed, which is very accurate. Various extinction plots generated using this technique are shown in Appendix D.

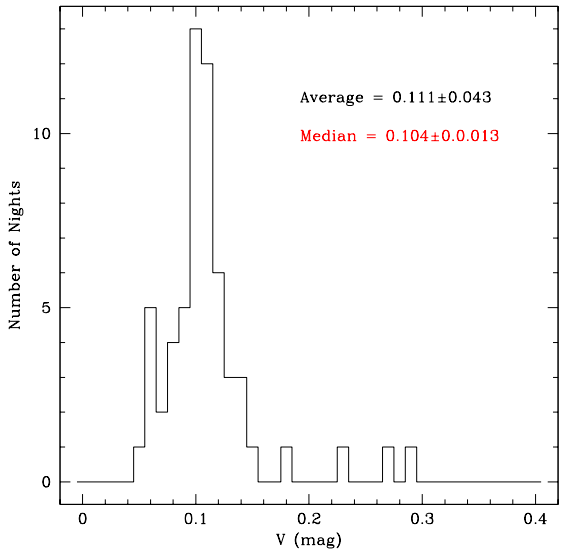

Fig. 3.7: Histogram plot of V band extinction measured using AEM during 2014-16.

3.4 Extinction results

3.4.1 Distribution of extinction

Very few extinction measurement comes from November-December 2012 observing run, most of the extinction data comes from 2014-2016 observations. Due to various reasons as mentioned at the beginning of the chapter, AEM extinction observation is not spread over all seasons. We have acquired data for about 150 nights in which

nearly 92 nights were found to be visually clear and hence in classical definition can be considered as photometric nights. Out of 92 clear nights, reliable estimates of extinction is possible on about 59 nights only. On the remaining nights either the sky transparency was found to be unstable or there was the presence of thin cloud/haze, which is very hard to detect by conventional methods. The statistical analysis of 59 nights extinction data shows that extinction in V band can be as small as 0.05 mag and 0.3 mag on the upper side. Whereas, average and median extinction value comes out to be 0.111 ± 0.043 and 0.104 ± 0.013 respectively. Figure 3.7 shows the histogram plot of 59 nights extinction data. From the plot, the distribution appears to be Gaussian. However, more data is needed to draw any conclusion. The measured extinction value matches very well with the theoretical prediction of 0.0943 mag.

3.4.2 Comparison with HCT data

We have also compared extinction values determined using AEM and 2m size HCT telescope, which is located at the same place and both measurements show nearly identical results. Despite our best effort, we could not get extinction measurement done on same night by both HCT and AEM. Therefore, we could compare only average observed extinction values. The average of HCT extinction from 58 different nights is reported to be 0.12 mag (C. S. Stalin et. al., 2008), whereas our average value is 0.111 mag. These two values matches very well, however, the small difference can be interpreted due to different seasonal coverage. We do not have much data coming from summer seasons which is expected to be having slightly higher extinction value.

3.4.3 Correlation with weather parameters

Extinction varies over various time scales, from few minutes to months and years. There is no clear understanding of what causes these variations, more specifically the

variations which happens within night as well intra-night. In the past, there were few attempts to relate extinction coefficient with meteorological parameters such as temperature, humidity, wind speed etc. We have also attempted to explore it and check if any such correlation exists. We collected weather data like ground temperature, RH, wind speed and atmospheric pressure from HCT telescope weather station. The nightly average values were computed for data collected between evening 8 PM to morning 5 AM. This is the period in which extinction monitor was found to be operating. We also collected extinction measurements carried out using HCT for 32 nights. Then after nightly extinction values are plotted against average weather parameters as shown in Figure 3.8, here red circle represents the HCT data and the solid black dot represents the AEM data. Correlation coefficients are computed and listed in the table 3.1.

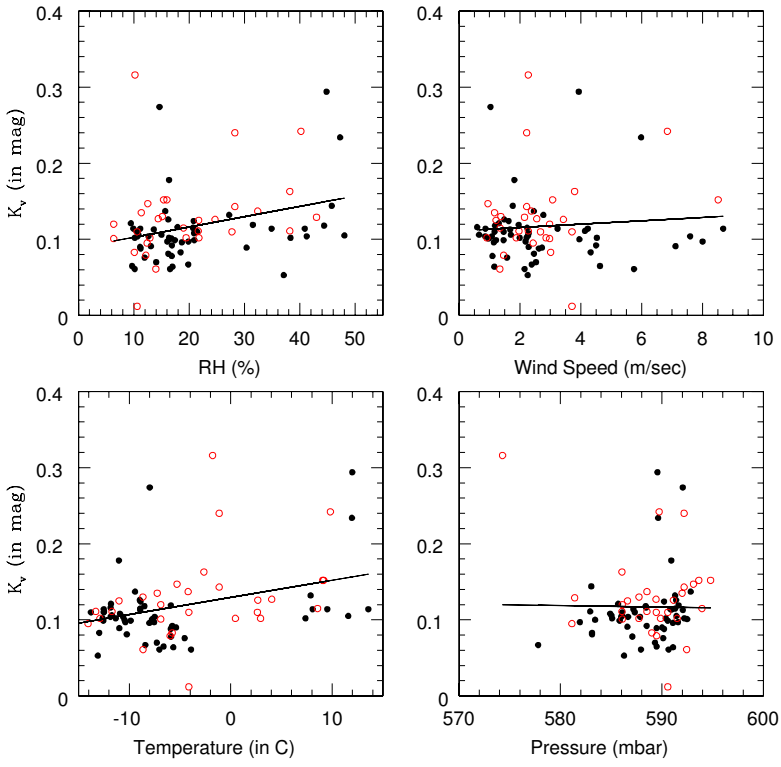

Fig. 3.8: Plots between atmospheric extinction(Red circle data is from HCT and solid Black dot data is from AEM) value and various average meteorological parameters obtained from HCT weather station.

From the plots as well as from correlation coefficients it appears that atmospheric extinction coefficient is weakly related to changes in the RH and ground temperature, in the sense that higher RH and ground temperature can give increased extinction. That means one can expect increased atmospheric extinction in the July-August months which are hottest months at IAO Hanle and also affected by Monsoon making the environment more humid. To establish a reliable relation between extinction and weather parameters, more data distributed uniformly all over the year is needed. We do not find any correlation between extinction and wind speed as well as pressure. Stalin et. al. (2008) also reported similar finding between their extinction values and the wind speed.

Table 3.1: Extinction and weather parameters correlation coefficients.

Parameter	RMS	Corr. Coefficients
RH	0.046	0.299
Temperature	0.046	0.345
Wind Speed	0.048	0.080
Pressure	0.049	-0.014

3.4.4 Nights showing variable sky transparency

Using AEM and the procedure as described in the Section 3.3.2 we can determine instantaneous extinction, which is one of the powerful tools to study the behavior of sky transparency over a shorter period, like extinction variation within a night. For this study, we have determined instantaneous extinction values for total 15 nights in January 2016. Figure 3.9 shows few example of intra-night extinction variability. From these plots, it is evident that very minute variation in the sky transparency can be recorded because our measurement accuracy is as better as 0.5 millimagnitude. Our study which is limited to 15 nights shows that none of these nights can be designated as a perfect photometric night because atmospheric extinction varies by 0.01 to 0.02

mag (equivalent to 1-2% change in atmospheric transparency) and even more in few nights. Though every night shows different behavior, however, it appears that one common trend apparent in all these nights is that atmospheric extinction is high in the early evening and then it slowly improves. In the beginning, we thought that this could be a reflection of improper computation of air-mass or departure from the plane parallel atmospheric model. However, if this is the case then we expect symmetry in the plot when extinction is plotted against hour angle, which does not exist at all. Other reason could be a change in the seeing which can modulate the flux received within fixed numerical aperture. This possibility also get discarded because the use of largest aperture which can encompass full stellar light for any variable seeing give similar results.

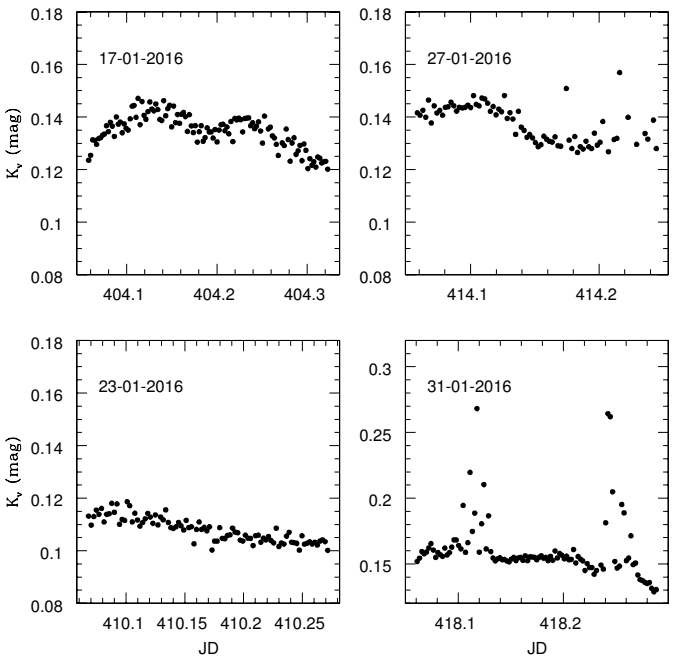

Fig. 3.9: Plot of instantaneous extinction values against time.

3.5 Detection of thin clouds by AEM

The presence of thick cloud is very easy to detect by using all-sky night camera. Wheres, very thin cloud for example high altitude cirrus cloud is difficult to distinguish from dark sky background. Similarly, at poor sites extinction produced by aerosol may change very erratically over the course of night, which in turn changes sky transparency. Ability to measure atmospheric extinction with high precision enables AEM to detect the presence of thin clouds which otherwise remains unnoticed by other means of monitoring. One of the best diagnostics of the presence of variable extinction can be a scatter around the best fit line in the extinction plot. During nights when sky transparency is stable, we find the scatter to be very small and extinction measurement to be very accurate. However, there are also cases, where we find large scatter in the extinction measurements which most likely indicate the presence of cirrus clouds in the sky or highly variable seeing during the night. If we choose sufficiently large aperture, then the effect of variable seeing can be eliminated. The cirrus cloud extended over the large region can temporally change atmospheric extinction. One such example is shown in the Figure 3.10. A very extended cirrus cloud passed through the local atmosphere on the night of August 1, 2014, and created an extinction jump of 0.3 mag. It took almost an hour for the cloud to pass and the sky to become stable again.

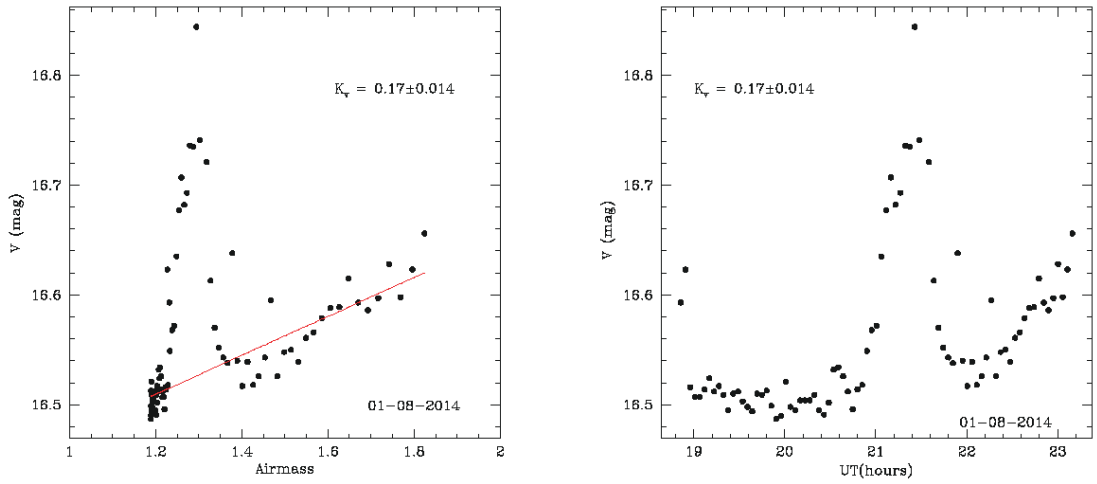

Fig. 3.10: Magnitude Vs. Airmass (Left), and Magnitude Vs. Time (Right) clearly indicates the presence of thin cloud.

3.6 Measurement of sky brightness

In addition to measuring extinction and detecting thin clouds, the AEM can also be used to measure sky brightness very precisely. In order to measure the sky brightness, AEM is pointed to a relatively less crowded field, away from Milky-way and Zodiac light and having at least few standard stars in the FoV. The chosen field is observed when it is closer to Zenith with long exposure as permitted by AEM tracking performance. Large number of stars within the field are identified, and their standard V magnitudes are extracted. The instrumental magnitude of these stars and the sky around it are determined using aperture photometry. We choose the largest circular aperture for the star which includes 99.99 % Stellar flux. Whereas, the sky is computed again around the star from an annular region of 10-pixel width and inner radii much larger than chosen for stars usually, 40 pixels. Following the procedure described by C. S. Stalin et. al. (2008) sky brightness is estimated . Airglow is airmass dependent and is expected to be large at low sky elevations. The sky brightness is

therefore corrected for the airglow, following the method described in Patat (2003). Sky brightness is expressed as:

$$V_{sk} = -2.5 \times log\frac{C_{sk}}{C_s} + 2.5 \times log(A) + K_v X + V \tag{3.1}$$

Where V_{sk} is the sky brightness, C_{sk} and C_s are the flux of the sky and stars in terms of the counts, A is aperture in arc-second, K_v is extinction in V band, X is airmass and V is standard magnitude of the star.

The effect of the airglow is corrected as follows

$$V'_{sk} = V_{sk} + \triangle m \tag{3.2}$$

where

$$\triangle\, m = 2.5 \times log[(1-f) + fX] + K_v(X-1) \tag{3.3}$$

and

$$X = [1 - 0.96 \times sin^2(Z)]^{0.5} \tag{3.4}$$

Where Z is zenith angle, K_v is extinction and f is a factor determined by Patat (2003).

Table 3.2: Average sky brightness with and without correcting for airglow.

Date	Airmass	Average Sky Brightness	Airglow Corrected Sky Brightness
14-12-2015	1.18	21.43±0.045	21.59±0.045
16-12-2015	1.03	21.43±0.048	21.47±0.048
18-12-2015	1.04	21.37±0.043	21.41±0.043
09-01-2016	1.14	21.65±0.067	21.79±0.067
12-01-2016	1.22	21.66±0.056	21.85±0.056
13-01-2016	1.16	21.70±0.057	21.85±0.057
15-01-2016	1.16	21.67±0.056	21.82±0.056
16-01-2016	1.16	21.68±0.056	21.82±0.056

At present measurement for the sky brightness is not as frequent as we have for extinction. Furthermore, sky brightness measurement is carried out during the darker period (absence of Moon) and also requires observation of standard field as well as careful reduction of the data. Therefore, at present, we have quite a few sky brightness measurement results. In each frame, we have chosen about 10 stars, and there are total five sky frames for a single stellar field. Table 3.2 lists the Sky brightness measurement carried out in eight nights during the month of December 2015 and January 2016. Since our observations are very close to zenith, therefore, we report sky measurements both with and without airglow correction. The average and median V-band sky-brightness value obtained from AEM observations turns out to be 21.57 $\pm$ 0.14 and 21.70 $\pm$ 0.18 $mag/arcsec^2$ respectively. Whereas, using HCT data collected over 2003-2007 on 47 nights, C. S. Stalin et. al. (2008) reports average sky brightness in V as 21.54 $\pm$ 0.37, which is slightly different from our values. We find the darkness of the local sky slightly better than one reported by the previous study. However, at present our sample size is smaller, and we hope that in near future we will have even better temporal coverage than the previous study and provide much more accurate measurements of sky brightness.

Fig. 3.11: AEM image of the field close to M42 which has been monitored during January 12-31, 2016.

3.7 Use of AEM for variability studies

AEM being a fully automated instrument, carries observation very efficiently. It was realized after few months of regular observation that extinction and sky brightness requires nearly 50-60 % device time. In remaining time device can be used to monitor some interesting variables stars. Even in most of the cases both extinction and variability study can be carried by using the same set of data. In the sense that few stars in the same FoV, which are nonvariables can be used for extinction measurement and variables for scientific study. To explore the potential of the instrument for the variability study a field near Orion Nebula Cluster which harbors a large number of pre-main sequence stars was monitored during January 12 to 31, 2016. Figure 3.11 shows an image of the field captured by AEM. On each night more than 8-10 hour long observation which comprises more than 130 object frames of 60 sec exposure, dark as well as bias frames were acquired.

The differential photometry was performed using the technique of ensemble photometry (Gilliland and Brown, 1988; Everett and Howell, 2001; Parihar et al., 2009). In ensemble photometry, the differential magnitude is computed with respect to the average magnitude of a large number of non-variable reference stars. The advantage of this technique is that, in the averaging process, the uncertainties of the ensemble stars magnitudes due to statistical fluctuations as well as short-term small incoherent variations will cancel each other. The uncertainty in the magnitude of the artificial comparison, therefore, will be smaller than the uncertainty in the magnitude of a single star and this, in turn, will produce less noisy light curves. While computing the average ensemble magnitude, we first determined the average flux of all ensemble stars and, then the ensemble magnitude was computed from the average flux. This way of computing ensemble magnitude gives more weight to the bright stars which are expected to have a smaller error related to photon noise. The whole procedure

described above is iterative and start with a large number of bright stars distributed all over the frame. While constructing the ensemble, the program excludes those ensemble stars whose standard deviation is larger than the threshold sigma value which is about 0.02 mag. In differential photometry, selection of an optimum aperture which gives best results is crucial. Although a larger aperture increases the signal strength, however, at the same time, it increases the contribution of the noise due to the background fluctuations and CCD readout. It is well known that signal-to-noise ratio is a function of the size of aperture and is found to be maximum with an aperture radius of one FWHM of the stellar profile (B.Howell, 1989). Since an average FWHM of the stars in AEM images varied between 2-3 pixels and sometimes we have also noticed the effect of the tracking error, therefore, to be safe we have chosen aperture size 5 pixels for all the frames and stars. The final output of the data reduction is a file which contains differential time-series magnitudes with other useful information for all stars in the field including the ensemble stars.

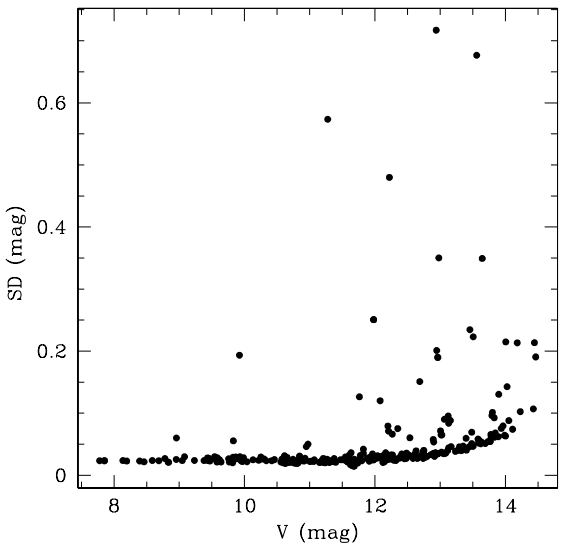

Fig. 3.12: Plot of the standard deviation versus V magnitude for all 350 stars in the field. Stars showing higher standard deviations are possible variables.

In the next step, variables need to be distinguished from nonvariables. We have

computed standard deviation (SD) of ensemble differential magnitudes and plotted it against the standard magnitude of the stars as shown in the Figure 3.12. Nonvariables are found to have lower SD and follow a standard trend in which SD slowly increases as stars become fainter. Whereas, variables are expected to have larger SD and stellar objects whose SD is 3 times SD of nonvariables in the particular magnitude bands are identified as variables. In the next step time series plots are generated for all these stars as shown in Figure 3.13, and from these plots, it was assured that larger SD is indeed linked with the variability. We have identified more than 30 variables in our fields and by exploring the literature it turns out that more than half of these variables are new discovery made by our AEM instruments. Further, follow-up study of these variables are required. However, they are most likely expected to be variables belonging to the pre-main sequence of stellar evolution and mostly Herbig A type and low-mass T Tauries objects.

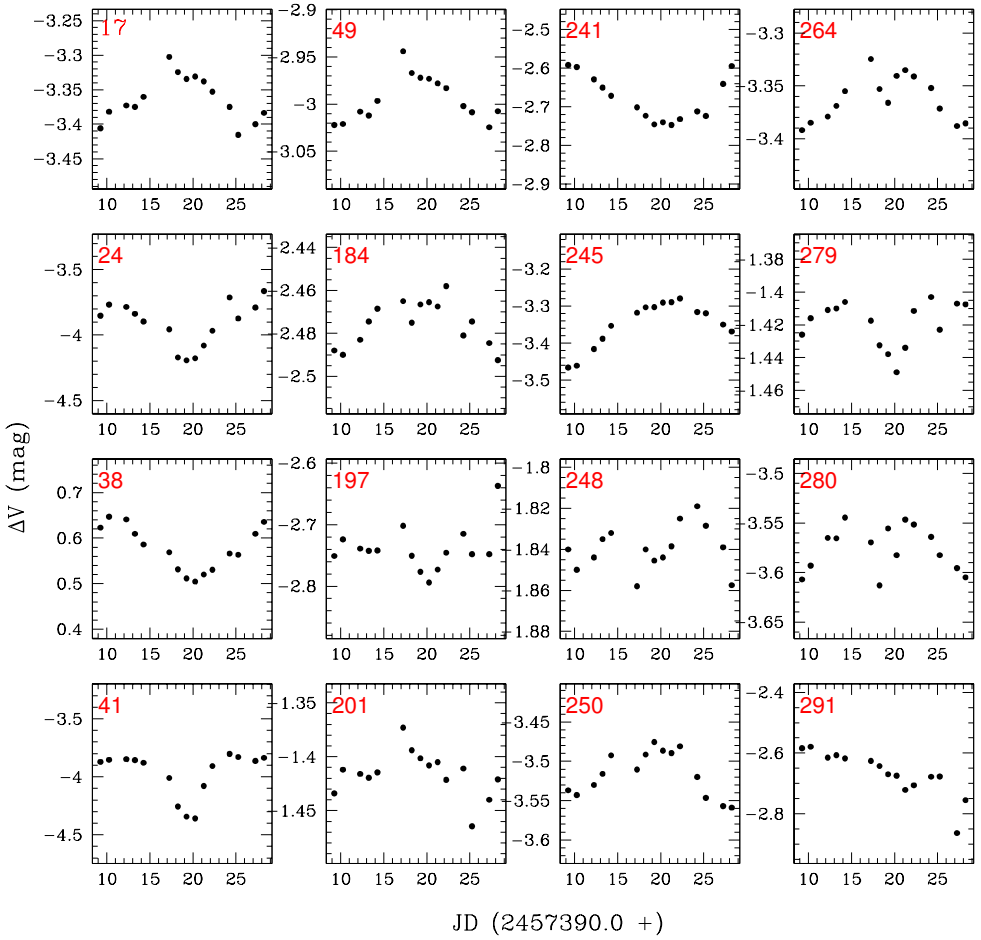

Fig. 3.13: Few example light curves of variable stars detected by AEM in Orion Nebula.

3.8 Discussion

From the reduction and analysis of the data collected using AEM we can conclude that indeed such an inexpensive device can very effectively be used to study transparency of the local atmosphere. It can also very precisely measure sky brightness. Both of these parameters need to be monitored before and after setting up any observatory. We have shown that very precise measurement of extinction and sky brightness is possible with our device. Additionally being a dedicated monitor, such device can collect a complete data sets, required to study the cause of variability, which is so far poorly understood.

The very large plate/pixel scale (21.71 $arcsec^2$/pixel) of AEM make sky brightness measurements much more accurate. Each pixel of AEM cover nearly 260 times larger sky portion than HCT telescope and hence 260 times more signal coming from the sky. One of the important findings of the AEM is that a clear sky, which will otherwise be characterized as photometric night may found to have variable sky transparency and hence may not be photometric at all. Such nights may be about 15-20$\%$ of the total clear nights and hence any statistics for photometric night generated based on visual inspection of the clarity of the sky needs to be taken with great precautions.

Any science which requires photometric measurement needs additional telescope time to determine extinction for that night. Usually, extinction is measured using the same large telescope and hence a good fraction of precious telescope time is spent in extinction measurement. We have shown from this work that having a simple device like AEM (maybe with additional filters set), atmospheric extinction can be measured with the same precision, what one can expect from a large telescope. And this way by making use of a device like AEM, one can save very precious large telescope time which could otherwise be used for scientific observations. Additionally, a byproduct of such a device can be variability study of a large number of interesting fields. Using such a small device with robust reduction technique, it is possible to carry out accurate differential photometry of stellar object up to 14 mag in V band. The large FoV allows to simultaneously observe hundreds of stars every night.

CHAPTER 4

ALL SKY SCANNING CLOUD MONITOR

Availability of a large number of clear nights is one of the prime requirement for any observatory, and this parameter needs to be reliably determined before setting-up a new observatory. For any existing observatory, monitoring of clouds in real time helps to fully automate the telescope system. Furthermore, in the case of semi-automatic or manual operation of a telescope, the observer can select a right target located in the clear portion of the sky by looking at cloud cover maps and hence make effective use of partially clear nights. All these objectives can be met if the observatory operates a very reliable automated all-sky cloud monitor, which regularly broadcasts local sky condition. There are several ways to monitor sky for cloudiness, and these methods are briefly described in the section below.

4.1 Techniques to monitor clouds

4.1.1 Manual observation

The oldest method of monitoring the sky condition is visual observation. In this method usually an observer checks the sky condition periodically (at an interval of half an hour or one hour) and records this in a log book. The results obtained by this method can be very subjective and depend on upon many factors like eye adaptation of the observer, fatigue, etc. During the moonless period, it is also hard to detect cloud patches with respect to dark background sky. The results obtained by visual observation on the clarity of sky is less accurate, specifically at night time and also it is a very cumbersome job to carry out over a longer period.

4.1.2 CCD based all sky camera

A CCD camera with a fish-eye lens to capture the whole sky in optical wavelength is a great improvement over the manual observation method. Several such devices usually called All-Sky Night Camera have been used by different groups (T. E.Pickering, 2006; W. Skidmore et. al., 2011). A CCD camera-based all-sky monitor (working in visible wavelengths range) is an inexpensive tool, which also overcome the shortcomings of the manual visual observation. However, this method has also got few shortcomings. The appearance of clouds in the optical images is very deceptive due to its strong dependency on the apparent optical sky brightness which in turn depends on the phase of the Moon, local light pollution, and other atmospheric variables. Automated software tools developed to extract a quantitative information of cloudiness from all-sky images usually fail to extract cloud information reliably and results are often found to be inconsistent with other methods (L. Shamir and R. J. Nemiroff, 2005).

4.1.3 All sky IR imager

The infrared radiation coming from clouds can be divided into two parts. One part of the radiation is due to the clouds own temperature, while another part is the radiation emitted by the Earth's surface which is reflected back by the clouds. The primary wavelength range of these radiations lie in $8-14\mu$m. In this wavelength band, the clear sky appears cold and clouds appear warm. The effect of variable sky brightness due to Moon becomes minimal, and hence, a mid-IR sensor provides the greatest cloud/sky discrimination. A mid-IR imaging camera is best suited for this purpose. However, it is too expensive, primarily because of the cost of the infrared detector and the need of special arrangement for cooling the detector. Only a few such camera are in use for cloud monitoring (M. Suganuma et. al., 2007; J. Sebag et. al., 2010).

4.1.4 Use of IR sensor for cloud detection

In an attempt to provide an inexpensive cloud detector working in the mid-IR range, Ashley & Jurcevic (1991) developed a cloud detector based on pyroelectric infrared element (M. C. B. Ashley and J. S. Jurcevic, 1991). However, this instrument required a continuous mechanical chopping between the sky and the comparison source. The chopping was required because of the use of the pyroelectric infrared element, which responds to infrared signal but returns to the DC level within few seconds. The sensor also required the use of a mirror, which is not suitable for long-term operation due to deterioration from dust. Subsequently Clay et.al. (1998), used infrared thermopile based sensor for cloud detection (R. W. Clay et. al., 1998). This device does not require any mechanical chopping between sky and the comparison source. Since the sensor had an inbuilt Infrared lens, it even does not require any external optical component. A thermopile is a very inexpensive infrared sensor, most suitable for cloud monitoring without requiring any cooling and requires simple detector electronics. Both cloud

monitors mentioned here uses single detector with a limited field of view and can only detect clouds present in a certain direction.

Fig. 4.1: CONCAM all sky camera installed at IAO Hanle along with StellaCam (black unit).

4.2 Monitoring IAO sky using CONCAM

CONCAM stands for **CON**tinuous **CAM**era, designed and built by Robert Nemiroff and his team at the Michigan Technical University. The aim of this project was to monitor the night sky around the globe using a set of cameras installed at different observatories around the world. It is a well designed and built, self-contained instrument. CONCAM consists of a fish-eye lens that projects the night sky onto a SBIG CCD camera. The camera works during nighttime and takes images every couple of minutes. These images are corrected for bias and flat, before being displayed. In 2004-05, one CONCAM camera system was installed at IAO Hanle as shown in Figure 4.1. Then after it has been in regular use with very little downtime. Reduced images are automatically transferred to CREST campus of IIA, Bangalore as well as archived. With over ten years of operation more than a million all-sky night

images are collected. These all sky CONCAM images are periodically displayed on the Institute website under **IAO Sky Condition(Live):Nightsky**[1] link.

Although CONCAM is very helpful in accessing the sky condition in real time and optimizing the nightly observation, however, it could not meet more ambitious goal to automatically generate extinction map by doing photometry of the bright stars distributed all over the sky.

4.3 Motivation for developing Scanning Cloud Monitor

The IAO Hanle all sky CONCAM device which is working since 2005 has produced millions of all-sky images. For the purpose of surveying IAO site for proposed National Large Optical Telescope (NLOT), we put an effort to analyze this very valuable archived imagery data to generate reliable statistics of availability of clear nights at Hanle. Because there are millions of images which can not be handled manually to get information about sky condition, so we started developing a software tool which can automatically extract cloud information from these CCD images. After a year of efforts, we realized that this task was indeed daunting and it is not easy to develop an automated software tool which can handles all-sky images obtained at variable phases of the Moon and Environmental condition. At the same time, we realized similar effort carried out by other groups and the similar problem faced by them, and so far there is no standardized software which can be used to generate statistics on the clarity of the sky. With this experience, we decided to develop a device which can overcome this problem and can work as a monitor and provide reliable data on number of available clear nights at IAO Hanle.

[1] `http://crest.iiap.res.in/iaonightcam.html`

4.4 Operating principle of the Scanning Cloud Monitor

The scanning cloud monitor instrument works on the principle of measurement of sky temperature using a mid-IR sensor. The temperature of the clear sky is lower than the temperature of the sky filled with clouds, as clouds primarily act like a screen which reflect back the IR radiation emitted by warmer earth surface. That means presence of the cloud produces an enhanced IR signal compared to the clear sky. Therefore, if we measure IR radiation which in turn can be used to measure brightness temperature of the sky, then one can detect the presence of clouds very reliably. Since excess IR emission is associated with ground temperature which is usually 0-20 °C, so the peak earth emission falls at 10 μm and the sensor having higher sensitivity in the range 8 to 14 μm is well suited for measuring IR radiation expected from clouds (R. Sloan and J. H. Shaw and D. Williams, 1955). There are a number of sensors available to measure IR radiation; however, we find a thermopile sensor most suited to us because it has got higher sensitivity and stability as well as it is inexpensive detector commercially available. A thermopile sensor consists of a large number of thermocouples connected in series connection. These sensors work on the principle of Seebeck effect and converts the thermal energy to electrical energy in the form of the voltage output. The sensor has two junctions, and these junctions are called measuring junction and the reference junctions. A thermopile sensor generates a voltage proportional to the temperature difference between the two junctions, which implies that thermopile can be used only for differential temperature measurement. Absolute temperature measurement requires the output of the thermopile sensor be corrected for changes in the reference junction temperature. This correction is called the ambient temperature compensation.

TPS334L5.5 Thermopile sensor

Figure 4.2 shows a TPS334L5.5 thermopile sensor from Perkin Elmer used for

measuring the sky temperature. It comes as a complete unit in a TO5 package. Measurement junction of the sensor is at the focus of the IR lens (built into sensor unit), which gives it a field of view of 7°. The lens also acts as a filter and has a flat passband from 2 to 22 μm. The reference junction of the sensor is in contact with the sensor body and a thermistor. The thermistor is used for measurement of the reference junction temperature, and implementation of the ambient temperature compensation scheme. The sensor has a sensing area of 0.7×0.7 mm^2, high sensitivity of 55 V/W, and a small noise voltage of 35 $nv/\sqrt{Hz}$.

Fig. 4.2: TPS334L5.5 Thermopile sensor from Perkin Elmer.

4.5 Theory of non-contact temperature measurement

The thermopile sensor generates a voltage output which is a function of the power of incident infrared radiation. Since every object emits radiation with a power depending upon its temperature, the signal generated by the thermopile sensor can be used to measure the object temperature. This method of non-contact temperature measurement is called pyrometry (Schilz, 2001).

Total radiation power P emitted by an object at temperature T can be expressed by the Stefan−Boltzmann law as

$$P = \sigma.\varepsilon.T^4 \tag{4.1}$$

Where σ is the Stefan−Boltzmann constant and ε is the emissivity of the object.

The value of the emissivity for common substances lies in the range of 0.85 to 0.95. Equation 4.1 can be used for measurement of temperature using thermopile sensor. We can modify Equation 4.1 and introduce the terms related to the geometry of the sensor and ambient temperature. Ambient temperature is required to be included because thermopile itself emits radiation depending upon its own temperature. Now we can write a new equation, which relates the net power $P^{'}$ received by the sensor from the object with the temperature T_{obj} and the ambient temperature T_a. The total radiation power received by the sensor can be written as

$$P^{'} = K^{'}.(\varepsilon_{obj}T_{obj}^4 - \varepsilon_a T_a^4) \tag{4.2}$$

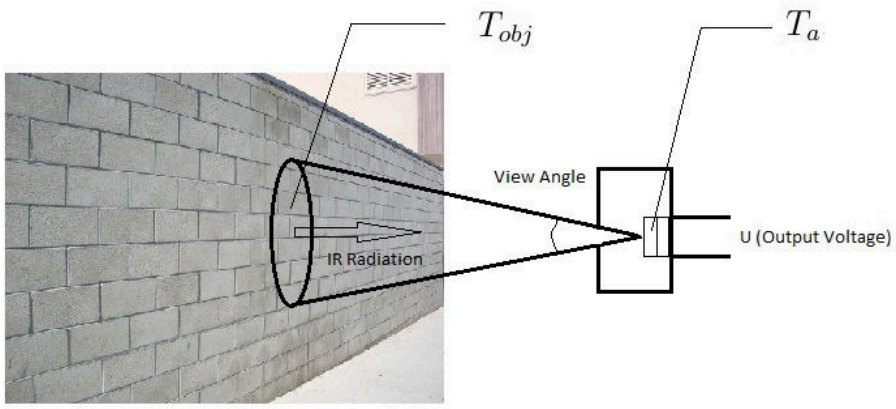

Fig. 4.3: Definition of the Field of View (FOV) or the view angle for the thermopile sensor.

Where $K^{'}$ is called the instrument factor, and includes the view angle ϕ of the instrument (Smith, 1990) as shown in Figure 4.3. ϕ is the angular measure of the cone through which sensor receives the radiations. It is expressed as

$$K^{'} = K.\sin^2(\phi/2) \tag{4.3}$$

Now the total received radiation power can be written as

$$P^{'} = K.(\varepsilon_{obj}T_{obj}^{4} - \varepsilon_{a}T_{a}^{4}).\sin^{2}(\phi/2) \tag{4.4}$$

The voltage generated by thermopile sensor is proportional to the incident radiation power on the sensor. The proportionality constant S is called the sensitivity of the instrument. Output voltage of the thermopile can be expressed as

$$U = S.P^{'} \tag{4.5}$$

$$U = S.K.(\varepsilon_{obj}T_{obj}^{4} - \varepsilon_{a}T_{a}^{4}).\sin^{2}(\phi/2) \tag{4.6}$$

Equation 4.6 is the most basic equation which gives us a relation between the output voltage of the thermopile, temperature of an object and the ambient temperature. Equation 4.6 is valid only if the sensor sees all the wavelengths and that too with the same sensitivity, which is not the case with practical sensors. A practical sensor never sees all the wavelengths, and T^4 law will not apply. The nature of the exact relationship between the object temperature and the voltage will depend on many factors like object temperature range and the spectral characteristics of the instrument etc. The relationship will also change with the addition of any lens, mirror or filter in the path of the object and the sensor. A deviation constant δ can be introduced to make the temperature dependence a $T^{4-\delta}$ law. Now the equation can be written as

$$U = S.K.(\varepsilon_{obj}T_{obj}^{4-\delta} - \varepsilon_{a}T_{a}^{4-\delta}).\sin^{2}(\phi/2) \tag{4.7}$$

Equation 4.7 forms the basis of temperature measurement using thermopile sensors. It relates the output voltage of the thermopile sensor to the object

temperature, ambient temperature or the reference junction temperature and view angle of the instrument.

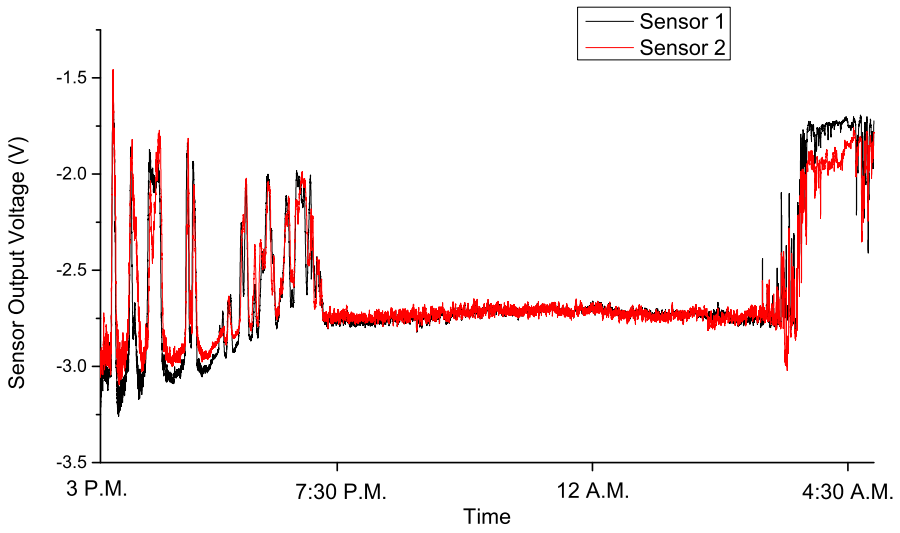

Fig. 4.4: Voltage output of two thermopile sensors looking at same part of the sky.

4.6 Experiments with a single sensor

Before proceeding to develop a full scanning cloud monitoring instruments, we decided to conduct a test to check the sensitivity of the thermopile sensor to sky as well as the cloud. For this experiment, a basic electronics board was developed and the analog output voltage of the sensor was recorded using a NI-6008 data acquisition device. To ensure that there is no false signal generated by a single sensor, we used two sensors pointed to same part of the sky and hence expected to measure similar voltage output. The output of the thermopile sensor and the thermistor were recorded for a duration of one month to cover all the possible sky conditions like the fully clear sky, fully cloudy sky, thin clouds, etc. A Webcam was also installed in the vicinity of the sensor board pointing in the same direction as the sensors. The sensor output was recorded every second, whereas Webcam images were captured at an

interval of one minute to keep the data size small. The data recorded from thermopile sensors and Webcam were analyzed. We found that both the sensor were giving similar voltage outputs for clear sky and cloud patches passing through FoV of the sensors. Figure 4.4 shows the sensor response for one night of observation (3 P.M. to 4:30 A.M.). Initial data shows the moving patches of clouds, sky becomes clear at about 7:15 P.M.. The sky remains clear until 3 A.M. in the morning, after which it becomes fully cloudy. Both sensors respond in similar fashion to the clear and cloudy sky, although there is little offset between two sensors output voltages. In the same time, images captured by Webcam were used to confirm that sensor was able to distinguish clear and cloudy sky. From this exercise we found that indeed thermopile sensor has indeed enough sensitivity for cloud detection and can further be used in our proposed all-sky scanning cloud monitor.

4.7 Instrument structure

The cloud monitors developed by Ashley & Jurcevic(1991) and Clay et. al.(1998) both uses a single detector element. These cloud monitors could cover only a small portion of the sky, and sees only in a certain direction with a small field of view. Clay et. al. made efforts to use a single sensor and scan the whole sky. In this system, an infrared Fresnel lens was used giving the sensor a field of view of 3°. The sensor unit was mounted on a Gimbal to point the sensor in the different portions of the sky. This setup required 30 minutes of time to complete one scan of the sky. During such a long scanning time, there can be a significant change in the position of the clouds in the sky. Hence, the generated cloud map may not be very accurate, if the clouds are moving at high speed. Inspired by Clay et. al. work, we decided to develop a scanning cloud monitor which can generate a cloud map in very short duration of time. At the same time, the device should have enhanced temperature resolution as well as stability.

Fig. 4.5: Laboratory picture of the first version of the cloud monitor instrument.

Figure 4.5 shows the laboratory picture of the first version of the cloud monitor instrument. The TPS334L5.5 Thermopile sensor has a field of view of 7°, which means single sensor can cover only a small portion of the sky. 12 sensor units are mounted on the circular arc, which covers 84 ° of the sky in altitude, starting from zenith. This scanning unit rotates around azimuth in steps of 7° to cover the whole sky. The scanning unit is rotated by a stepper motor and timer belt−pulley based drive. All electronic boards like data acquisition and logging board, SD card module, stepper motor driver and optical isolation boards are mounted inside the lower box structure of the instrument. A Hall effect based home and limit switch is also provided to determine the initial position of the scanning unit. The completed instrument was installed at IAO Hanle and was tested for a month. During this test we noticed few shortcomings of the instrument which are briefly described below:

1. IAO Hanle is subjected to very high wind. The scanning unit of the present instrument structure was driven by a simple combination of a small stepper

motor and a timer belt-pulley. This drive mechanism was not able to overcome the wind induced torque, and the scanning unit was moving due to the wind resulting in inaccurate sky maps.

2. All the electronics of the instrument was kept inside the hexagonal structure, and there was a possibility of water going inside and damaging the electronic boards.

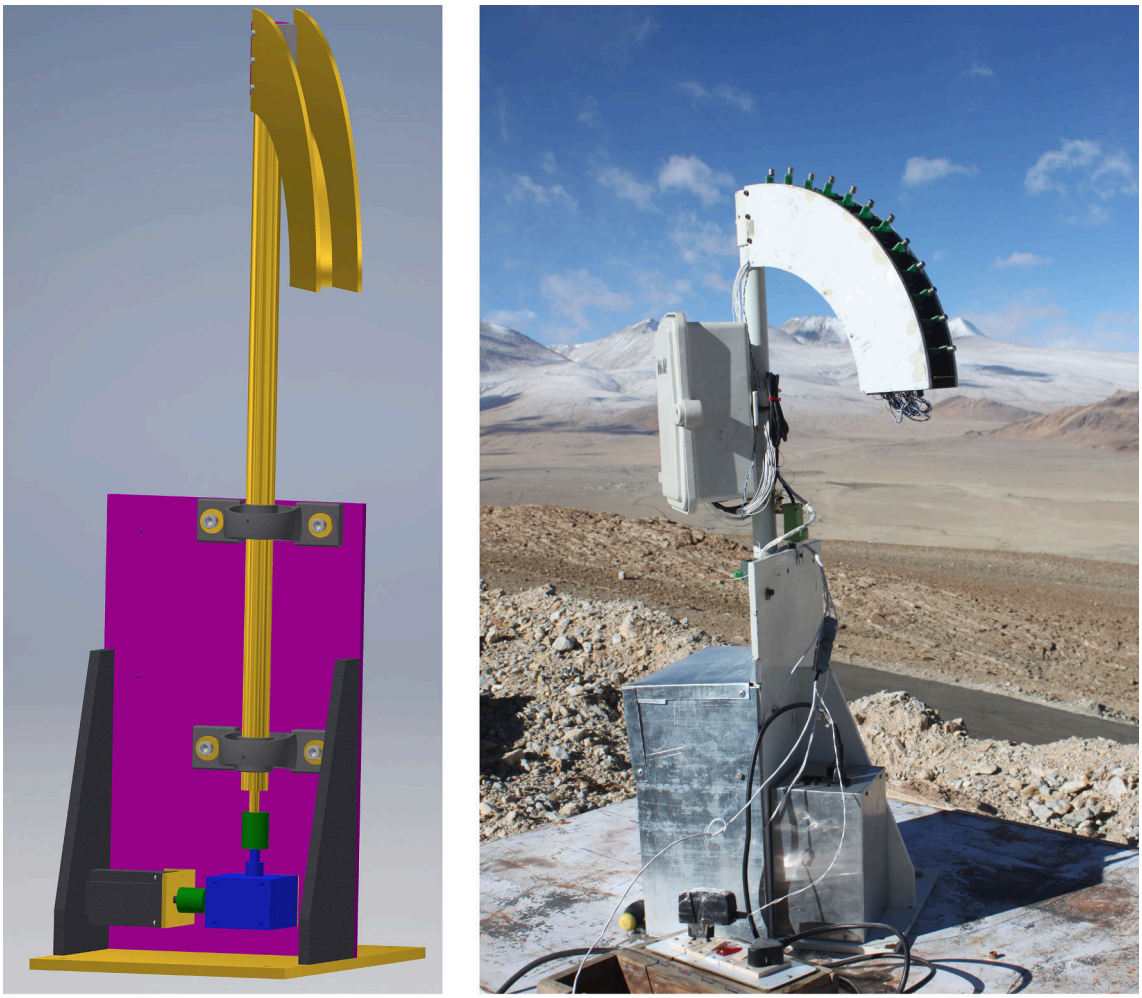

Fig. 4.6: (a) 3D model of the modified structure of the cloud monitor instrument, and (b) All sky scanning cloud monitor instrument installed at IAO Hanle.

A new mechanical structure was designed and fabricated locally at IIA Bangalore to overcome the shortcomings mentioned above of the first version of the instrument.

Figure 4.6(a) and Figure 4.6(b) shows the 3D model and the finished instrument respectively. Autodesk Inventor[2] was used as software design tool for designing the new structure. In the new version, only the sensor mounting unit was retained from the first version of the instrument. A worm gear based system was introduced to increase the drive stiffness. A small Autonics stepper motor A16K-M268 drives the worm gear which in turn rotates the scanning unit. The gear ratio of the worm gear is 15. All the electronics is mounted inside the waterproof outdoor box. The outdoor box itself is mounted on the main shaft of the instrument and rotates along with the scanning unit, thereby eliminating any relative motion between the electronic boards and the sensors. A Hall effect based limit switch is replaced with the industrial grade inductive limit switch, which acts as both the home and limit switch for the instrument.

4.8 Instrument electronics

Four electronic boards are developed for the cloud monitor instrument. These are Sensor Interface Board, Instrument Control and Data Acquisition Board, Stepper Motor Driver Board, and Optical Isolation Board. All these boards are described below:-

4.8.1 Sensor interface board

Thermopile sensor generates a voltage output which is proportional to the temperature difference between the two junctions of the sensor. Measurement junction senses the radiations coming from the sky, and the reference junction is exposed to ambient temperature. Reference junction temperature varies depending

[2] http://www.autodesk.in/products/inventor/overview

upon the ambient temperature. This means the output of the sensor will vary even if the radiations coming from the sky is constant since ambient temperature is varying. This makes it compulsory to either operate the sensor at a constant ambient temperature or to compensate the sensor output for changes in the ambient temperature. We have opted to correct the sensor output for changes in ambient temperature variations. A software based compensation scheme is developed, where the uncompensated sensor output and the ambient temperature is measured. The correction process takes place inside the computer while processing the data.

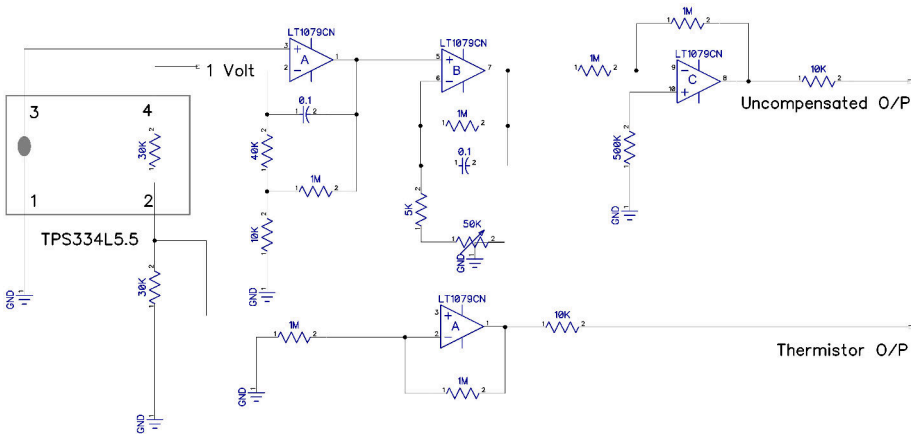

Fig. 4.7: Circuit schematic of the sensor interface board.

Figure 4.7 shows the circuit schematic of sensor interface board. We have modified the circuit used by Clay et.al. (1998) for their single channel cloud monitor (R. W. Clay et. al., 1998). Since the output voltage of thermopile is very small and is in microvolts range, two stage amplifier circuit consisting of precision amplifier LT1079[3] is used. The second stage also allows for changes in the gain of the circuit. The thermopile sensor is equipped with an inbuilt thermistor, which is used for the measurement of reference junction temperature. The thermistor is connected in series with another 30KΩ resistor. This series combination is biased with 1V, and the output voltage is measured at the 30KΩ resistor. The bias voltage is kept at only 1V to keep the

[3] http://www.linear.com/product/LT1079

thermistor self-heating effect at the minimum. The device generates two voltage outputs, one from the thermopile and other from the thermistor. Both of these outputs are used by the data analysis software to correct the thermopile output, and measure the sky temperature.

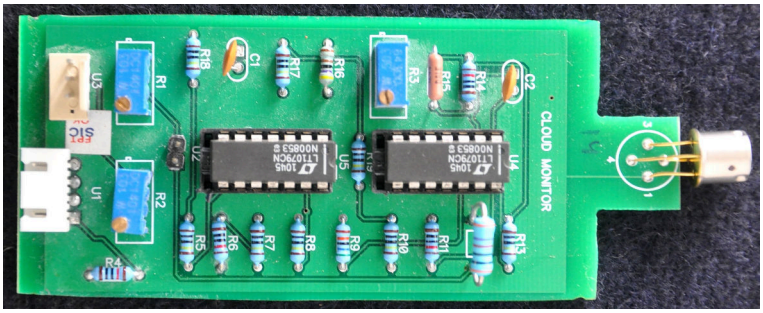

Fig. 4.8: Sensor interface PCB board.

PCB board for the circuit was designed using the free academic version of DipTrace software. The sensor is mounted on the PCB board itself to minimize noise as well as EMI. Figure 4.8 shows the finished PCB of the sensor interface board. 20 such board are made, 12 for the instrument and remaining as spares.

4.8.2 Instrument control and data acquisition board

The output of the thermopile sensor is analog, this needs to be converted to a digital value before any processing of data can take place. A customized network based data acquisition and logging board is developed for the instrument (T. K. Sharma and P. S. Parihar, 2014). Figure 4.9 shows the completed board with all the components mounted. The schematic and layout of the board were designed using the free academic version of PCB design software DipTrace. The board also control all the functionality of the instrument like initialization, homing, movement of the scanning unit, data acquisition, and logging. A high-end microcontroller PIC18F97J60 from Microchip is used as the main processor. An external ADC MAX1144 converts the analog output of the sensor to a digital value, and this data is stored on an SD card.

Onboard RTC (Real Time Clock) unit provides the time information which is required for time-stamping the data. Data can also be transmitted to the remote server using either serial or Ethernet connectivity. Important components of the board are described below:-

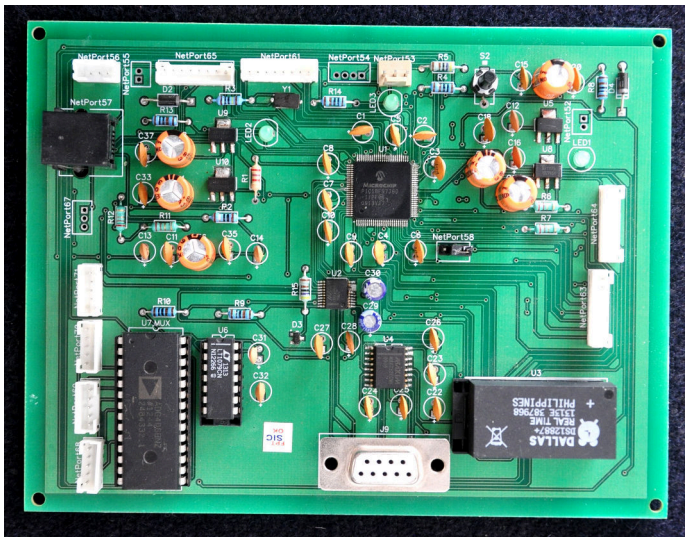

Fig. 4.9: Instrument control and Data acquisition PCB board.

4.8.2.1 PIC18F97J60 microcontroller

A PIC18F97J60 microcontroller from Microchip is used as the main processor of the board. This microcontroller is responsible for interfacing of ADC and analog multiplexer, interfacing of home and limit switch, generation of signals required for driving the stepper motor, interfacing of RTC chip, logging of data on the SD card, and the establishment of a communication link between the computer and instrument.

4.8.2.2 MAX1144 ADC

Although PIC18F97J60 microcontroller has an inbuilt ADC module, a separate ADC chip MAX1144[4] from Maxim Corporation is used for analog to digital conversion of the sensor output. There are two reasons for this choice. First reason is the resolution of the microcontroller ADC, which is only 10 bit. Another reason is the voltage range of the analog signal which can be interfaced to the microcontroller (it can accept analog signals up to 5V only). MAX1144 is a single channel 14-bit ADC, and it can accept bipolar analog signals up to ±6V. The communication protocol used is SPI. It has also got the internal calibration circuitry, which is used to correct for linearity and offset errors resulting from changes in operating temperature.

4.8.2.3 LM4040C20 voltage reference

The ADC MAX1144 requires a precision voltage reference for accurate conversion of the analog signal to equivalent digital value. Voltage level required for the reference is 2.048V. LM4040C20[5] voltage reference from Texas Instruments is used for generating this voltage. It is a precision voltage reference with very low noise of $35\mu\ V_{rms}$.

4.8.2.4 ADG406 analog multiplexer

The availability of only one analog channel on MAX1144 ADC led us to us an analog multiplexer. We have used ADG406[6] analog multiplexer from Analog Devices. It is a bipolar 16-channel analog multiplexer which can accept signals up to ±27V. Any one of the 16 analog inputs can be selected depending upon the logic present on the selection lines. This chip also has break-before-make switching action, which prevents

[4] https://www.maximintegrated.com/en/products/analog/data-converters/analog-to-digital-converters/MAX1144.html

[5] http://www.ti.com/product/LM4040C20

[6] http://www.analog.com/en/products/switches-multiplexers/analog-switches-multiplexers/adg406.html

momentary shorting of analog inputs while switching.

4.8.2.5 DS12887 RTC

A DS12887[7] RTC chip is used to provide time information, which is required for time-stamping of the data files which are stored in the SD card. The main reason for using DS12887 is the availability of all the supporting components like resistors, capacitors, crystal oscillator and the battery inside the single package. The chip only needs to be interfaced digitally with the microcontroller.

4.8.3 Stepper motor driver board

The cloud monitor instrument uses the same stepper motor driver board, which is developed for the AEM. Only one of the driver out of the three present on the board is used for driving the motor. Section 2.7.2 describes this board in detail.

4.8.4 Optical isolation board

A small stepper motor is used to drive the scanning unit of the instrument. In the initial stage of the instrument development, one dual 9V supply was used to power all the electronics like thermistor biasing, op-amps and the stepper motor driver board. This arrangement of power supply was introducing noise in the sensor output. The output of the thermopile sensor is very small and is sensitive to noise present in the power supply of the op-amps. OP-amps were picking up the small noise introduced by the motor driver and were adding it to the sensor output. To overcome the noise we have separated the power sources of the motor driver and the remaining sensing electronics. A small circuit consisting of Optocoupler(optical isolator)

[7] https://www.maximintegrated.com/en/datasheet/index.mvp/id/2680

MCT2E[8] was designed, and placed between the motor driver and the instrument control board. Optical isolation board accepts the inputs (microstep select lines, pulse, direction, enable and sleep signals required by drive) from the instrument control board. Two separate power supplies are used to power the motor driver and the rest of electronics.

4.9 Sensor calibration and ambient temperature compensation

There are 12 thermopile sensors used in scanning cloud monitor, and each sensor unit has got a separate electronic board. Although the electronic gain settings for all the boards are kept same, the output voltage range for different boards are different when they all are subjected to the same external excitation (IR radiation coming from some uniform source). The primary reason for this behavior is the offset voltages in the op-amps and the tolerances in the gain components like resistors and potentiometers. Also, the output voltage of all the thermopile sensors is not the same for same excitation. This makes it necessary to calibrate all the sensor boards.

The output voltage of the thermopile is a function of the object temperature and the ambient temperature(reference junction temperature). This relation can be expressed as

$$V = K.F(T_{obj}, T_{amb}) \tag{4.8}$$

Where V is output voltage of thermopile, K is a constant, T_{obj} and T_{amb} are object and ambient temperature respectively. It is not necessary to know the exact behavior of V for changes in both the T_{obj} and T_{amb}. We can expand the Equation 4.8 to include the

[8] http://www.ti.com/product/MCT2E

calibration temperature T_{ref}, which can be any arbitrary temperature at which sensors are calibrated. Expanded equation can be written as

$$V = K.F(T_{obj}, T_{ref}) - K.F(T_{amb}, T_{ref}) \tag{4.9}$$

The function $F(T_1, T_2)$ is obtained by observing the behavior of the thermopile output voltage at a constant ambient temperature when the thermopile sensor is exposed to an object whose temperature can be controlled. Equation 4.9 establishes the relationship between the output voltage of thermopile sensor (V), object temperature T_{obj}, the ambient temperature T_{amb}, and the reference temperature T_{ref} at which sensor is calibrated. For a constant ambient temperature, we can use an equation or a lookup table to determine the object temperature from the output voltage of thermopile sensor. But if the ambient temperature itself varies, the output voltage of the thermopile sensor will vary for the fixed object temperature. This implies we have to correct the output of the thermopile sensor for changes in the ambient temperature. We have developed and implemented a software-based or digital ambient temperature compensation scheme.

4.9.1 Thermistor calibration

All thermopile sensors are equipped with an inbuilt thermistor, which can be used for measurement of ambient temperature, and ambient temperature compensation. The thermistor is in contact with the reference junction internally and measures the temperature of the reference junction. Thermistors are characterized by two parameters, these are $\beta - value$ and the resistance R_0 of the thermistor at temperature T_0 (usually value of T_0 is specified at 25 °C) . Thermistor used in our sensor has a $\beta - value$ of 3964 and value of resistance at 25 °C is 30 KΩ. Resistance of the thermistor at any other temperature can be expressed as

$$R = R_0.e^{\beta(1/T - 1/T_0)} \tag{4.10}$$

Equation 4.10 can be used to calculate the resistance of thermistor at any given temperature, once $\beta - value$, R_0 and T_0 are known. The same equation can also be used to calculate the thermistor temperature, provided other constants are known. The thermistor is placed in series with another resistor of fixed value of 30 KΩ, and this combination is biased with a voltage of 1 V. This value of bias voltage is chosen to keep the thermistor self-heating effect at a minimum. The voltage output is taken at the other resistor and is fed to the op-amp with a gain of 2. This voltage output is read by the data acquisition board and saved in the data file for each scan. Data analysis software read these values and calculates the ambient temperature, which is required for further calculations.

4.9.2 Thermopile calibration

Thermopile calibration means knowing the sensor output when it is excited by a source having a known temperature. Two schemes are used to calibrate the sensor. In the first scheme called Two Point Calibration, the thermopile sensor is kept at a constant ambient temperature, and sensor output is recorded for an object at two different temperatures. The slope of the line connecting the two points gives the sensitivity of the sensor. This method of sensor calibration is not very accurate and results in an accuracy of the order of $\pm$1 or $\pm$2K, depending upon the object and ambient temperature range. Only over a very small range of object temperature, an accuracy of the order of $\pm$0.1K can be achieved (Schilz, 2011).

The other method of calibration involves recording the sensor output at variable object temperature. A linear fit to the plot between output voltage versus object temperature is the sensitivity. This method of sensor calibration is very accurate and

an accuracy of the order of $\pm$0.5K can be achieved even for the extended object and ambient temperature range. We have adopted the second method, and a special calibration set-up was designed and developed in the lab. Figure 4.10 shows the calibration set-up. A Peltier element (30mm$\times$30mm) was used as an object whose temperature can be varied in steps. Peltier element has two faces. When powered on, one of the faces becomes hot, and the other face becomes cold. This Peltier element was mounted on a heat sink to remove heat from the hot side. A small thermistor was attached on the front (cold) side of the Peltier element to measure its temperature. Heat sink compound was used to bond thermistor on Peltier screen. Heat sink compound provides better thermal coupling between the thermistor and the Peltier element, thereby allowing the thermistor to measure correct Peltier element temperature.

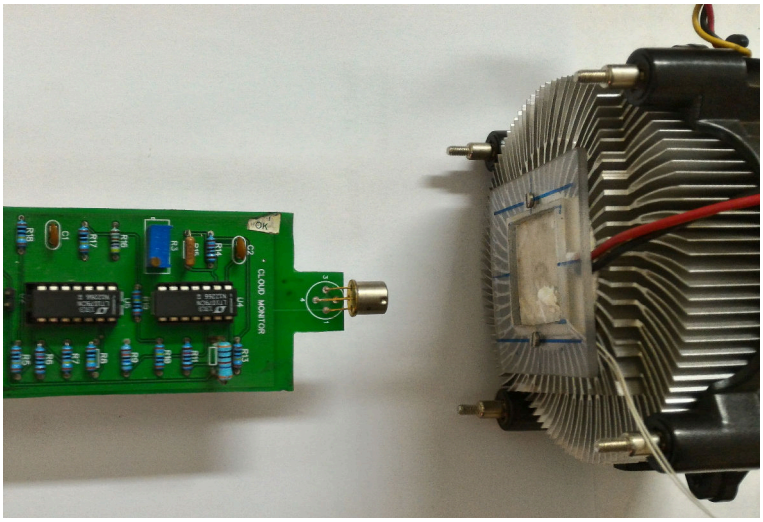

Fig. 4.10: Calibration setup consisting of sensor board, and Peltier element mounted on heat sink. A thermistor is attached to the front side of the Peltier element to measure its temperature.

The Sensor is placed near to the Peltier element in such a way that the sensor receives the radiation coming only from the Peltier element (sensor's 7° FoV was filled with Peltier element only). Then after the temperature of the Peltier element was varied in steps keeping the ambient temperature almost constant and the output of

the thermopile sensor was recorded. A data acquisition device NI-6008 from National Instruments was used for recording the data. Using this set-up, we have calibrated 20 sensor boards, 12 for the instrument and 8 spare boards. A LabVIEW[9] based software was developed for sensor calibration. The LabVIEW routine also plots and saves the data related to Peltier element temperature, ambient temperature(measured from the internal thermistor of the sensor) and the output of the sensor. Figure 4.11 shows the screen capture image of the software written for the calibration procedure.

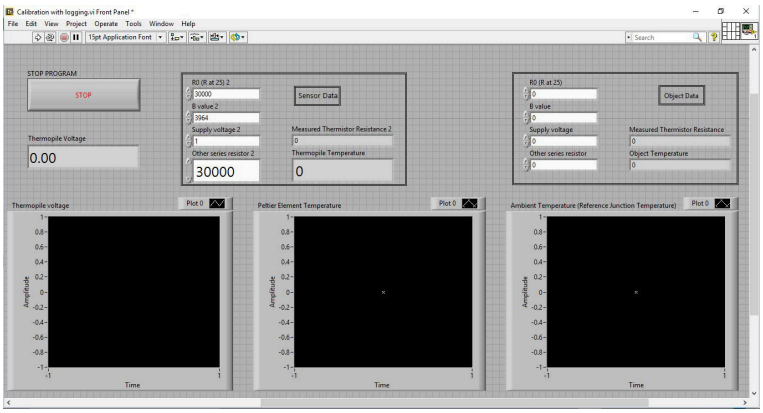

Fig. 4.11: Screen snap-shot of the sensor calibration GUI

[9] http://www.ni.com/labview/

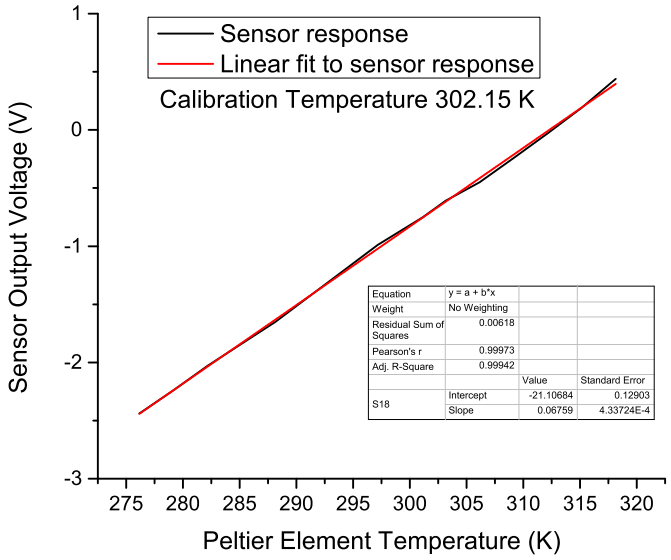

Fig. 4.12: Calibration curve and linear fit to the curve for one of the sensor board of the Cloud Monitor Instrument.

Using this setup, we have calibrated all the sensor boards from 0° to 50°C degree centigrade. The sensor response is found to be linear. Figure 4.12 shows the calibration curve and the linear fitted curve for one of the sensor. The relationship between the Peltier element temperature and the thermopile output voltage can be expressed as

$$V = I + B * T \tag{4.11}$$

where I and B are the fitting coefficients.

The calibration procedure gives separate values of I, B and sensor calibration temperature for each sensor. Table 4.1 lists the calibration coefficients for all the sensors

Table 4.1: Sensor calibration temperature and calibration coefficients for all sensor boards.

Sensor No	Calibration Temperature (K)	I	B
1	296.4	-26.18593	0.08294
2	301.4	-23.45028	0.07648
3	302.7	-24.78484	0.08141
4	301.2	-23.21909	0.07619
5	301.2	-23.77169	0.07616
6	301.5	-23.02530	0.07245
7	303.0	-23.29692	0.07517
8	300.8	-22.74316	0.07322
9	303.1	-22.10351	0.07069
10	303.1	-24.37116	0.07846
11	302.4	-21.81965	0.07109
12	303.2	-24.13787	0.07683
13	306.0	-25.10773	0.08036
14	301.1	-21.92556	0.07175
15	301.1	-24.65882	0.07973
16	301.1	-25.04442	0.08000
17	301.1	-23.37817	0.07805
18	302.1	-21.10684	0.06759
19	302.1	-23.05208	0.07532

All these values of the calibration constants are supplied to the data analysis software in a text file.

4.9.3 Ambient temperature compensation

As described earlier, the thermopile sensor generates a voltage output which is proportional to the temperature difference between the reference junction and the measurement junction. This means if the sensor is exposed to an object of constant temperature and the ambient temperature varies, the output of the sensor will also vary. There are two ways to correct for this effect. These are:-

1. The sensor unit can be kept in temperature controlled environment, where the temperature is constant(this constant temperature is equal to the calibration

temperature for the sensor). This will make the temperature of the reference junction constant.

2. The output of the sensor can be corrected for changes in the ambient temperature. A correction factor can be generated depending upon the difference between the calibration temperature and the ambient temperature. This correction factor is added to the thermopile output voltage, and the object temperature is calculated.

The first method of operating the sensor at constant ambient temperature is expensive, as it requires special temperature controlled enclosure with an IR transmitting window. This also makes the sensor unit bulky. This method is used primarily in the industry where the size of the instrument is not an issue. We have developed a software-based ambient temperature compensation scheme, in which all the calculations are performed inside the computer, and correction is applied to the sensor output. Following are the steps used in the scheme:-

1. The sensor is calibrated at fixed ambient temperature T_{ref} (calibration temperature).

2. The calibration procedure gives a relation between the output voltage of thermopile V_{meas} and the object temperature T_{obj} at a fixed ambient temperature T_{ref} similar to Equation 4.11.

3. Now the calibrated sensor is ready to measure the object temperature at any ambient temperature.

4. The sensor is exposed to the object, whose temperature is to be measured. The uncompensated thermopile output voltage V_{uncomp} is measured.

5. The thermistor output is measured and converted to the ambient temperature T_{amb}.

6. The calibration temperature T_{ref} is put in the relation obtained in step 2, and the voltage is calculated.

7. Present ambient temperature T_{amb} is put in the relation obtained in step 2, and the voltage is calculated.

8. A difference is taken of the voltages calculated in step 6 and 7, which is the correction factor.

9. The correction factor is added to the uncompensated thermopile output voltage V_{uncomp} to get the compensated output voltage V_{comp} .

10. This compensated thermopile voltage is put back in the equation obtained in step 2, and the present object temperature is calculated back.

Object temperature obtained in this way is independent of the variations in the ambient temperature. All these steps are followed by the data analysis software to measure the accurate sky temperature.

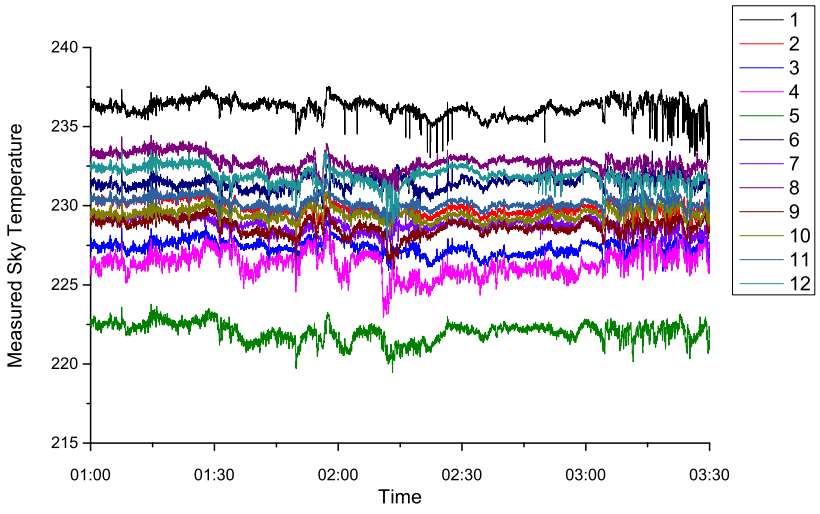

Fig. 4.13: Measured sky temperature from various sensors (all pointing towards zenith) before applying any correction.

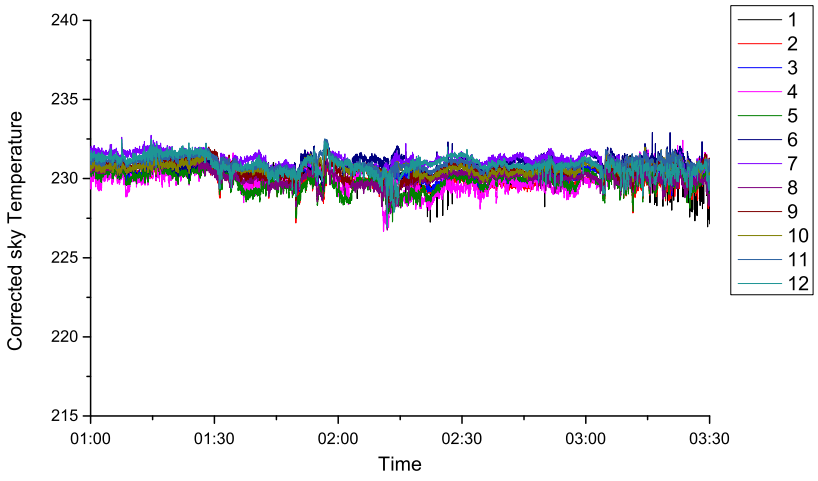

Fig. 4.14: Measured sky temperature from various sensors (all pointing towards zenith) after applying the correction.

4.9.4 On-site sky calibration of sensors

After lab calibration of the thermopile and thermistor, all sensors were checked for inter-sensor variations. For this experiment, a cloud free day was chosen, and all the sensors were pointed towards the same portion of the sky (near zenith), and sensor output were recorded. The voltage output of the sensors was converted to the temperature readings using the thermopile calibration coefficients and following the method described in the previous section. Since all the sensor are pointed to the same part of the sky, so they are exposed to same IR radiation coming from the sky and hence expected to give similar sky temperature. However, in practice, they gave slightly different sky temperatures. The primary reason for this offset is the temperature range (0 to 50 °C) used to calibrate the sensors. The sky temperature can be as low as -50 °C, whereas calibration has been done till 0 °. This made us to extrapolate Equation 4.11, which results in some offset. To correct for this effect, the temperature offsets was determined as described earlier and then intercept(I) term was adjusted and new I term with same slope (B) have been used to get the sky

temperature. Once I is revised then again all sensors were pointed toward zenith and sky temperature was measured. Figure 4.13 and Figure 4.14 shows the sky temperature before and after the correction respectively. The temperature scale is kept same in both the cases to better appreciate the correction.

4.10 Instrument software

Four different software are developed for fully automated operation of the instrument. These are- Embedded Software, Data Logging Software, Cloud Map Generation Software, and Data Analysis Software(percentage cloud cover). These software's are responsible for the operation of instrument, collection of data and generation of the results after processing the data respectively.

4.10.1 Embedded software

This is the lowest level of code, which resides and run inside the instrument control and data acquisition board. This part of the software is developed in MPLAB IDE programming environment from Microchip[10]. The programming language used is the embedded C. Free version of the C18 compiler is used to convert the C code to equivalent hex code, which was later uploaded to the instrument control and data acquisition board using ICD3[11] programmer from Microchip. These are the few tasks handled by the software:-

1. Generation of the control signal (analog multiplexer selection lines) to select any of the analog channel using analog multiplexer ADG406.

[10] http://www.microchip.com/

[11] http://www.microchip.com/Developmenttools/ProductDetails.aspx?PartNO=DV164035

2. Interfacing of analog to digital converter MAX1144 to the microcontroller. ADC converts the analog signal to the equivalent 14-bit digital value, which is transferred to the microcontroller using SPI communication protocol.

3. Providing serial and Ethernet connectivity to the instrument for transmitting the instrument data for the logging purpose.

4. Although data is transmitted to the computer using serial communication, it is stored locally on the SD card as well. Embedded software also handles the interfacing of the SD card to the microcontroller.

5. This software also interfaces an RTC chip (DS12887) to the board, which provides the time information.

6. Generation of control signals(micro-step select, pulse, direction, enable and sleep) for the motor driver to operate the scanning unit.

7. Interfacing the limit and home switch for the scanning unit of the instrument.

4.10.2 Data acquisition software

A Windows operating system based data acquisition software has been developed using QT[12] software development platform. The software logs the incoming data stream from the cloud monitor instrument. It saves the incoming data in text format, one file for each scan. The name of the file is a combination of the date and time of the observation (e.g. 01-01-2016_19-07-15.txt). The software GUI has two windows. The first window is the main window, which displays the incoming data from the instrument. Figure 4.15(a) shows the screen snapshot of the main window. The main window has 3 options. These are- Open port(open serial port, connect to the

[12] http://www.qt.io/

instrument and start data logging), Disconnect (stop data logging and close the serial port) and Tools menu.

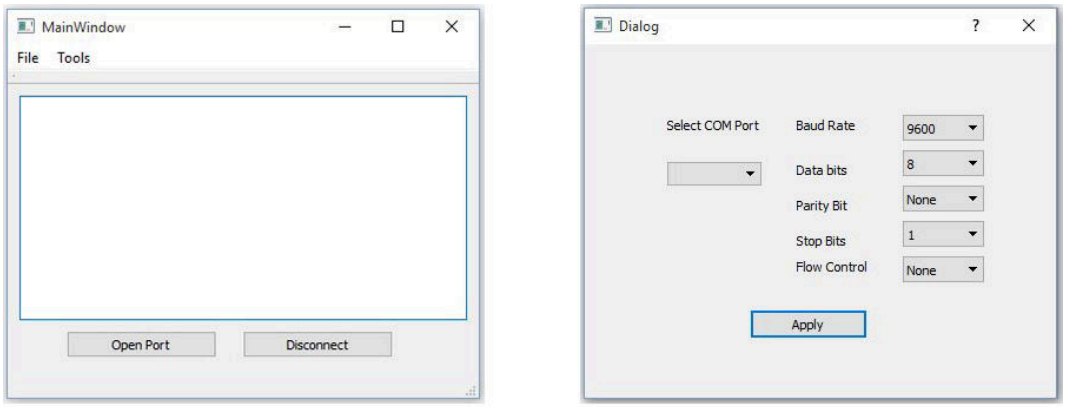

Fig. 4.15: Screen snapshot of the (a) Main window, and (b) Configuration window of the data logging software.

The other window is the Configuration window. Figure 4.15(b) shows a screen snapshot of the configuration window. This window is used for configuring the serial port. This window allows the user to set the serial port number, baud rate, parity and other parameters related to the serial communication. Default baud rate is 9600, which results in the lowest error at the crystal frequency of the microcontroller.

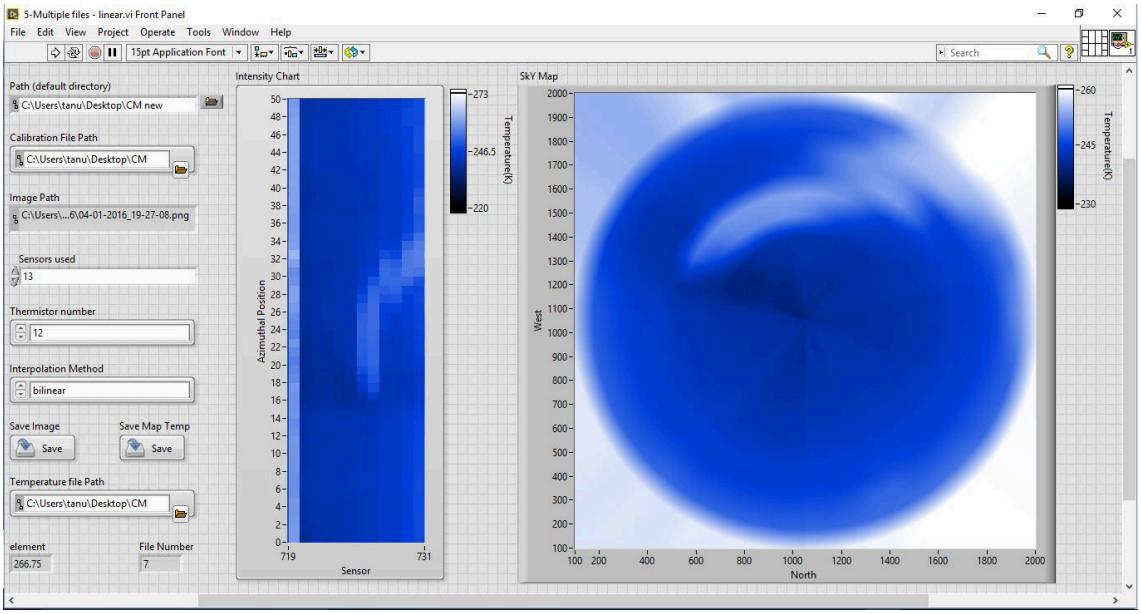

Fig. 4.16: Screen snapshot of Cloud Map Generation software.

4.10.3 Cloud map generation software

The raw data (ADC counts) generated by cloud monitor for each scan is saved into a text file. These raw data files need to be processed before the map of the sky is generated. We have developed a LabVIEW-based software for the instrument. A set of subroutines converts raw data into sky maps, which also includes different calibration steps describes in previous sections. The software developed by us is fully automated in the sense that once the user provides the path of the folder where raw data is stored, the path of calibration files and few other parameters, then the software processes all the data files present in that directory and generates the corresponding sky-maps. Software not only provides sky map in the form of images but also saves temperature data into text files. These files can be used later to get percentage cloud cover and related statistics. Figure 4.16 shows the screen capture image of the Cloud Map Generation software.

The steps followed by the software while processing the raw data files to generate

the cloud maps are given below:-

1. As an input software require the path of folders where raw data and calibration files are stored. The user can also select whether to save the sky maps, temperature files, etc. or not?

2. Out of four, the user can select one of the interpolation methods for map generation. The available interpolation methods are nearest, bilinear, bicubic and bicubic spline. These interpolation methods decide the way sky maps are generated. However, we found that the maps generated using the bilinear interpolation method best resembles the real sky condition.

3. Once the user provides all the inputs, the software starts executing the code. It reads all the data files one by one. It also reads the calibration file.

4. Since the data file contains the instrument data (12 Thermopile sensors and 3 thermistor outputs) in raw form or ADC numbers, software converts these numbers to the corresponding voltages.

5. The software extracts the ambient temperature information from the data file. This information is required for ambient temperature compensation. Although we get the ambient temperature information from the instrument itself, the software also has provision to read these values from the weather station data which is installed near to the instrument.

6. Sky temperature is calculated from the voltages after applying the correction factor for the ambient temperature compensation.

7. Cloud map is generated and displayed on the front panel of the software. Images are also saved depending upon the inputs provided by the user. Measured temperature data for each scan is also saved for each data file. The

analysis software utilizes this temperature data for automatic detection of clouds.

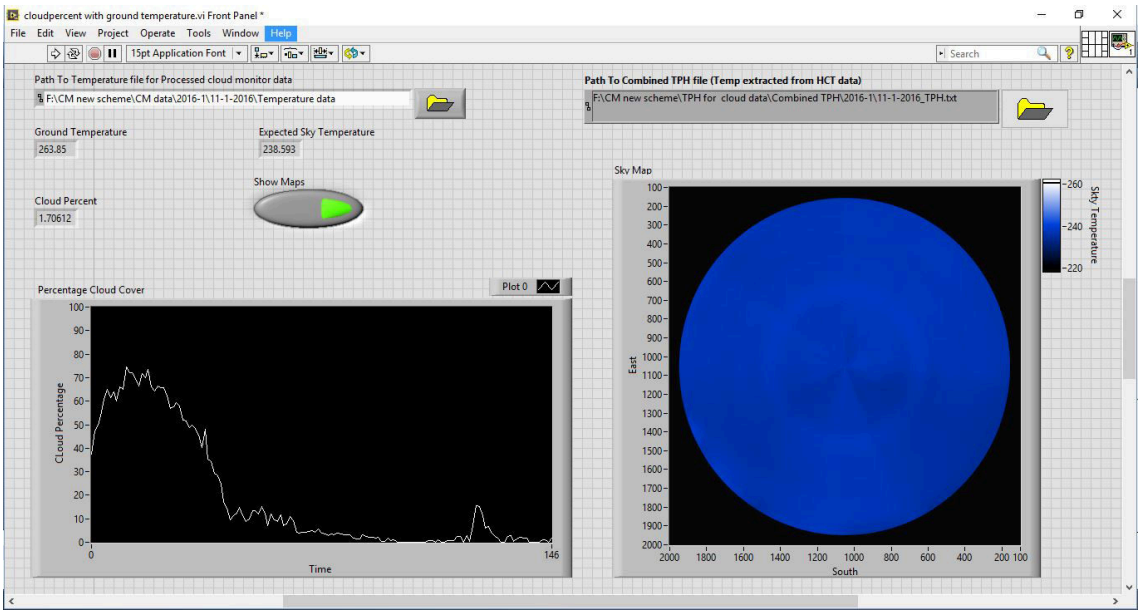

Fig. 4.17: Screen snapshot of percentage cloud cover calculation software.

4.10.4 Data analysis software (Percentage cloud cover calculation software)

This software is developed for automatic detection of clouds and calculating the percentage cloud cover. This piece of software uses the temperature file generated by the cloud map generation software, and the HCT met server file (TPH file) as an input. The software first discriminates clear and cloudy parts of the sky and calculates the percentage cloud cover for each of the scan and saves it in a text file along with time stamp. The local temperature, humidity, and pressure are extracted from the HCT met server file and also saved in the same file. Figure 4.17 shows the screen snapshot of the analysis software. Front GUI of the software shows the cloud map for each scan, ground temperature, expected sky temperature, cloud percentage in each scan and the plot of percentage cloud and time for the whole night.

4.11 Operation of instrument

The cloud monitor instrument is a fully automatic device. Once started, it does not require any assistance from the operator. Following are the steps, which the instrument follows while observation:-

1. On power up, the instrument control and data acquisition board initializes. Microcontroller initializes all other components like analog multiplexer, ADC, RTC, SD card and serial port.

2. Once initialization is complete, the scanning unit of the instrument starts rotating clockwise in search of home position (North direction).

3. After homing, the instrument starts the regular observation.

4. RTC time is read, and a file having time and date as the name is created on the SD card. Also, the start of scan identification signal is sent to the data logging computer.

5. The scanning unit of the instrument moves counter-clockwise direction in steps of 7°. At each position the scanning unit stops, output voltages from all the sensors are read multiple times and the mean value is computed. Then after sensor readings are transmitted to the computer via serial port, and also recorded on the SD card.

6. The scanning process continues till the entire 360° of the azimuth is scanned. This scanning process takes about 120 seconds to complete.

7. On completion of the scan, the file is saved and closed on the SD card. End of scan identification signal is also sent to the data logging computer to mark the completion of the scan.

8. Scanning unit is brought back to the home position by rotating in the clockwise direction, which takes about 80 seconds.

9. Steps 4 to 8 are repeated continuously as long as the observation is required. A new sky scan is generated every 200 seconds.

4.12 Results

The goal of the cloud monitor instrument is to generate a reliable temperature map of the whole sky which can be utilized to get information about cloud coverage. Even after going through very extensive laboratory and sky calibration procedures as described in previous sections, reliable sky maps can only be generated when we understand the effect of changing environment on the sky temperature measured by the instrument. Initial data collected over two months has been used to study the effect of ground temperature, humidity, pressure, etc. on the measured sky temperature. Furthermore, we explored the effect of airmass on measured sky temperature when the sensor is pointed at different zenith angle.

4.12.1 Effect of ground temperature and humidity on measured sky temperature

All the sensor are subjected to the variable environmental conditions. More importantly, ambient temperature and ground humidity goes through diurnal and seasonal changes. If the ambient temperature compensation is working properly and the sensor is not affected by RH, then we expect the measured sky temperature to be correct. To understand the effect of these two parameters on the sky temperature we extract the sky temperature of the sensor which is all the time pointed toward the zenith. Figure 4.18 shows the relation between the measured sky temperature (at

zenith) and the ground temperature for the first 50 nights. Initially, we plotted all the sky temperatures which include both clear and cloudy sky.

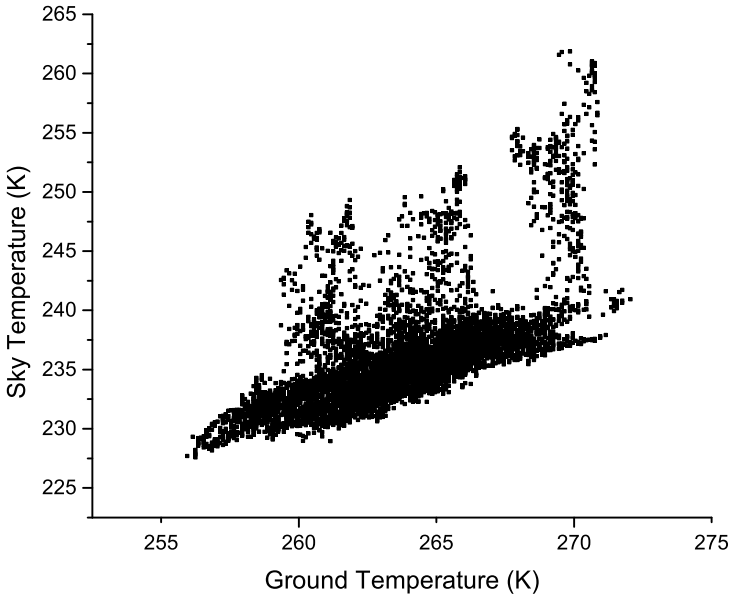

Fig. 4.18: Ground temperature Vs. sky temperature (at zenith) for 50 nights of observation(both clear and cloudy nights of January and February 2016).

Then after, to better understand the relation between the sky temperature and the ground temperature, we removed data from cloudy nights and plotted data for only clear nights. Information about clear and cloudy nights have been collected from both CONCAM and scanning cloud monitor. Resultant plot for clear nights is shown in Figure 4.19. Figure 4.19 also shows the linear fit (red line) to the curve. The linear relation between sky temperature(EST) and the ground temperature (GT) can be expressed as

$$\mathrm{EST} = 0.711 \times \mathrm{GT} + 46.98 \tag{4.12}$$

The reason for this linear relation seems to be not due to improper ambient

temperature compensation. Because at fixed clear sky temperature, but variable ambient temperature the sensor should give an inverse relation between ground and sky temperatures. Because an increase in ground temperature for a fixed sky temperature will increase the difference in junction temperature and hence should be reflected as lower sky temperature. The absolute measurement of the sky temperature has still some uncertainty(due to the sensor calibration temperature range), but we can use the relation in Equation 4.12 to determine the threshold sky temperature for any ambient temperature, and any temperature above this threshold can be assigned due to the presence of the cloud. Which in turn helps in automatic detection of the clouds by software.

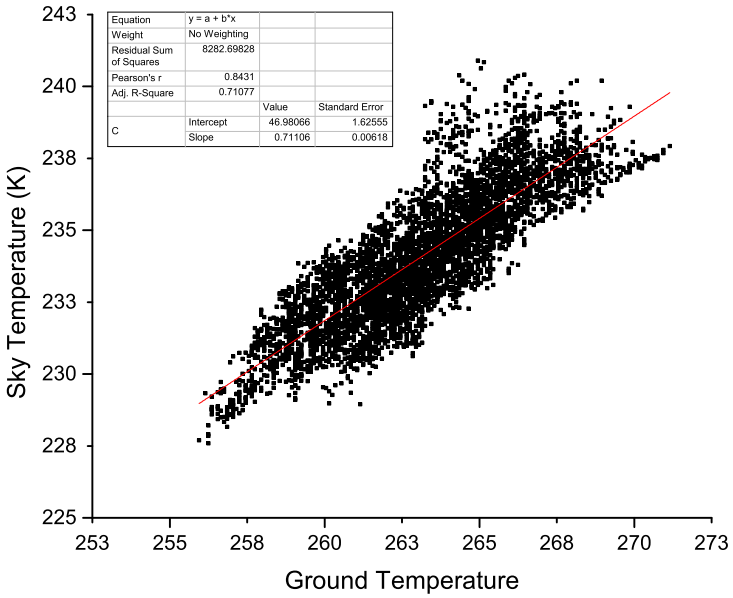

Fig. 4.19: Ground temperature Vs. sky temperature (at zenith) only for clear nights(January and February 2016).

With the expectation that humid local atmosphere will give excess IR emission due to the presence of a large number of OH molecules, we also attempted to search for any relation between the measured sky temperature and the humidity (RH). Figure 4.20

shows the plot between the sky temperature (at zenith) and the humidity and contrary to our expectation we do not find any tight relation between the sky temperature and the ground level humidity. From Figure 4.20 it is apparent that for most of the time humidity is below 30%, as a large number of points are concentrated in this region. There are very few data points above 30% and better relation may be established when we have better coverage in RH.

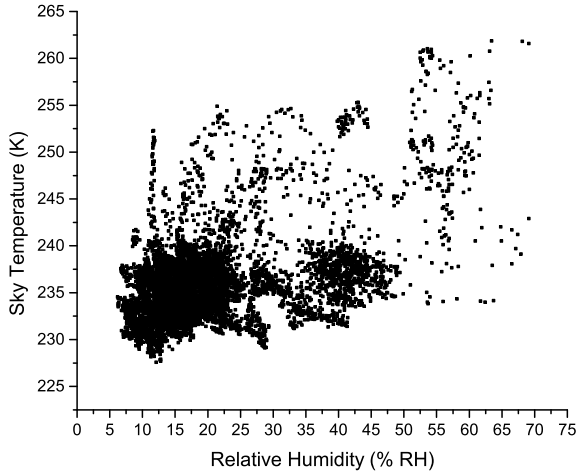

Fig. 4.20: Ground level humidity Vs. sky temperature (at zenith) for 50 nights of cloud monitor data.

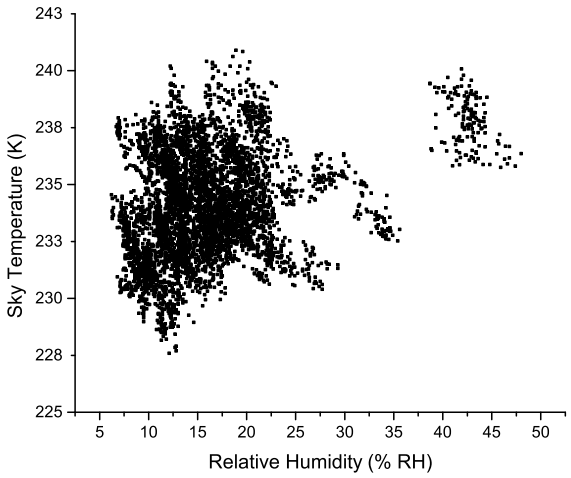

Fig. 4.21: Ground level humidity Vs. sky temperature (at zenith) only for clear nights out of 50 nights of cloud monitor data.

Figure 4.21 shows a plot between sky temperature (at zenith) and the humidity only for clear nights. Again we did not find a very clear relation between the sky temperature and the humidity. There is a possibility that RH may be linked with ground temperature in the sense higher RH can lead to increased ground temperature. Therefore, we need more data point to probe any relation between RH and the measured sky temperature.

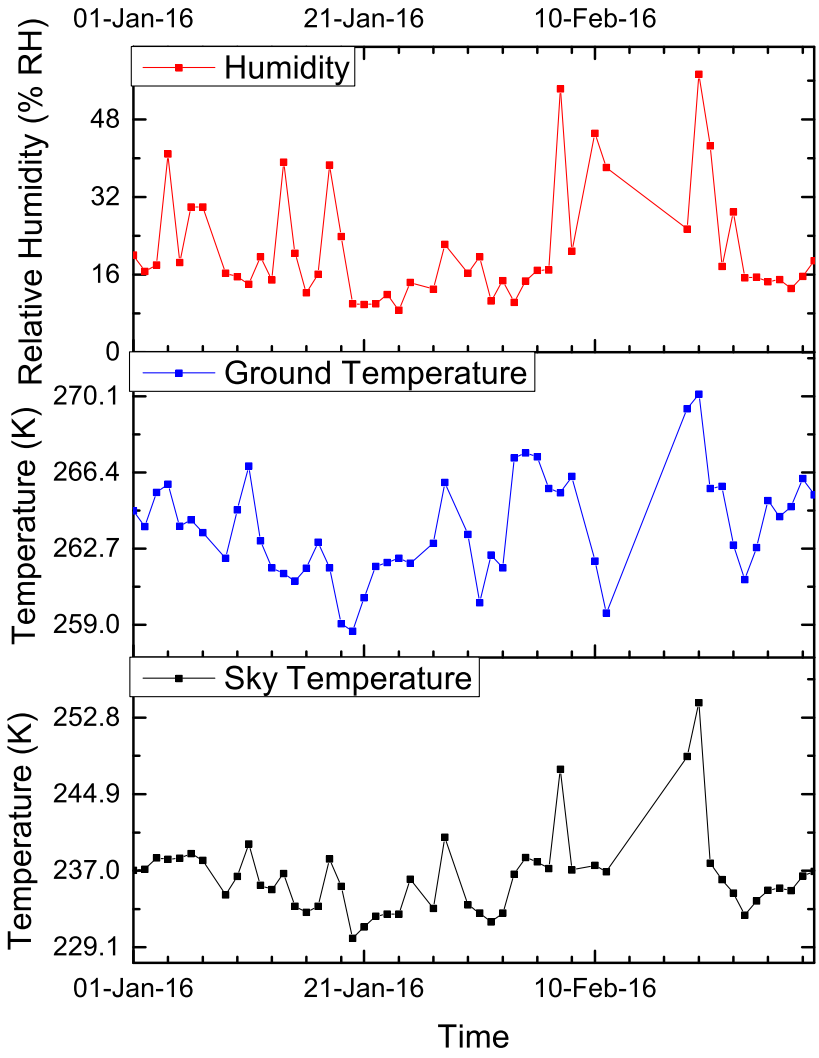

Fig. 4.22: Nightly averaged Ground level humidity, Ground temperature and Sky temperature plotted Vs. time for 50 nights of cloud monitor data. There is a gap from 12-17 February.

To extend the above study, we also plotted nightly average sky temperature against the average humidity and average ground temperature as shown in Figure 4.22 for initial 50 nights. There is an observation gap of 5 days between 12-17 February. Again, average sky temperature for night shows a strong correlation with the ground temperature. Whereas humidity shows a lesser effect on the sky temperature, there seems to be weak correlation above 30% RH.

4.12.2 Effect of airmass and its correction

The measured sky temperature depends on the zenith distance of the portion of the sky. The larger the zenith distance, the higher the measured sky temperature. At higher zenith distance, the sensor has to look through a larger column of air. A Larger column of air means that the sensor is looking at the sky through more water vapor and aerosol content. Measured sky temperature is lowest at zenith and comes close to the ground temperature near horizon. To generate all sky temperature map to detect clouds, one need to remove the effect of the airmass.

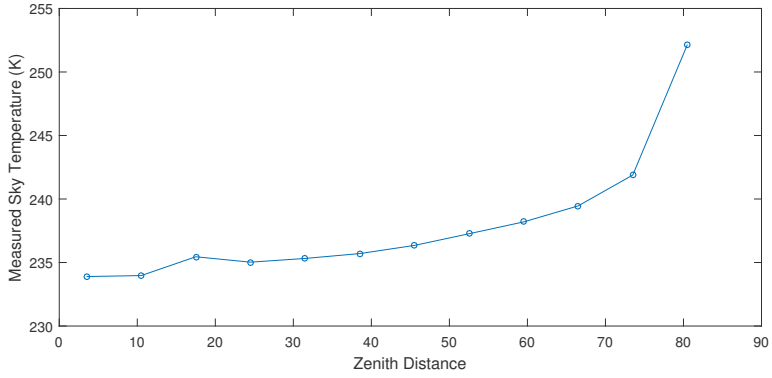

Fig. 4.23: Zenith angle Vs. Measured sky temperature for one of the scan on night (completely clear sky) of 24-02-2016.

Figure 4.23 shows a plot of Zenith distance Vs. Measured Sky Temperature for one of the scans on 24-02-2016(Completely clear sky).

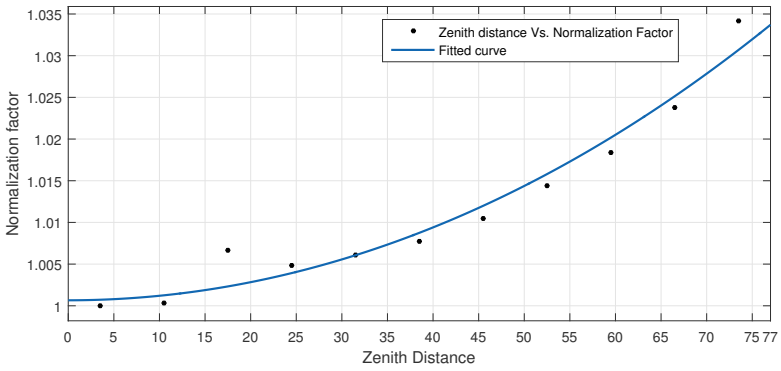

Fig. 4.24: Zenith angle Vs. Normalization factor for the sensor boards.

Figure 4.24 shows a plot between the normalization factor (Temperature at different zenith distance divided by the temperature measured by the sensor nearest to zenith), averaged over several clear nights for sensors pointing at different zenith angles. This effect is similar to the atmospheric extinction, except that we expect more IR radiations closer to the horizon. Figure 4.24 also shows the fit to the curve. For this fitting, the last sensor (pointing at 80.5° from zenith) is omitted. This last sensor (almost pointing to the horizon) is more affected by ground IR emission then radiation from the sky. The fitting equation can be expressed as

$$\text{ST} = \text{a*sec(b*ZD)} \tag{4.13}$$

Here ST is the sky temperature, and ZD is the zenith distance in degrees starting from 3.5°. Values of constants **a** and **b** are 1.001 and 0.1887 respectively.

The relation between the measured sky temperature and the zenith distance is used to calculate the normalization coefficients for sensors pointing in the different direction. Normalization process gives the sensor readings independent of the sensor direction. So far we have collected data for 65 nights, Figure 4.25 shows the time series plot of normalization coefficients obtained for clear nights (clear night means there is not even a single patch of cloud passes through the local sky). We do not find any noticeable changes in normalization factors over three months period. Then after these normalization coefficients are used to correct for airmass effect by following flat field procedure adopted in astronomy. Figure 4.26 and Figure 4.27 shows the cloud maps generated before and after applying zenith angle correction for a clear night (23-02-2016) and a cloudy night (04-02-2016) respectively.

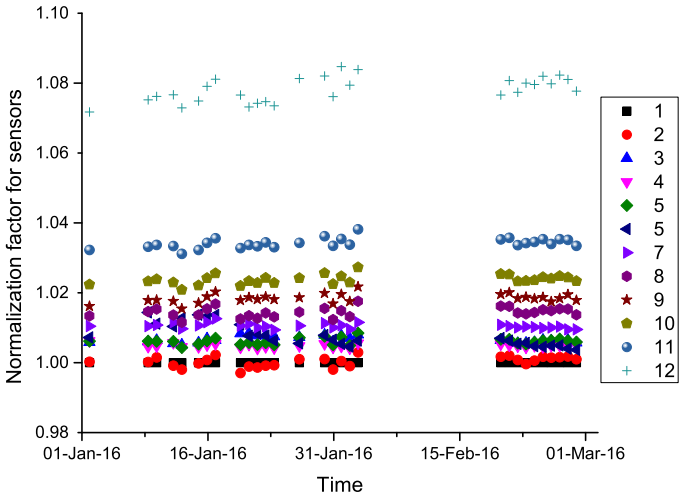

Fig. 4.25: Variations in the normalization factor for sensor boards only for clear nights (January to February 2016).

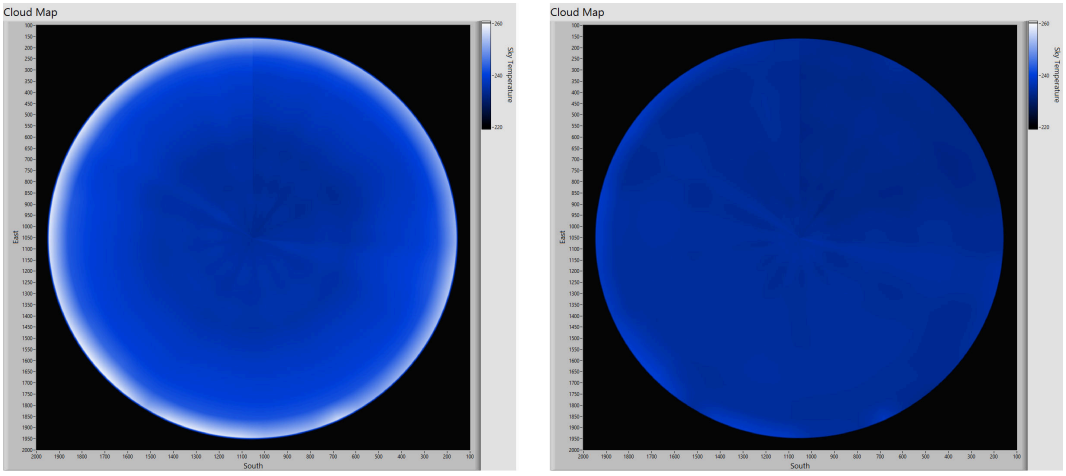

Fig. 4.26: Clear sky maps (a) Cloud map without correcting for airmass effect, and (b) Cloud map generated after applying the correction for airmass effect for the same night (23-02-2016, 19:12:41 PM).

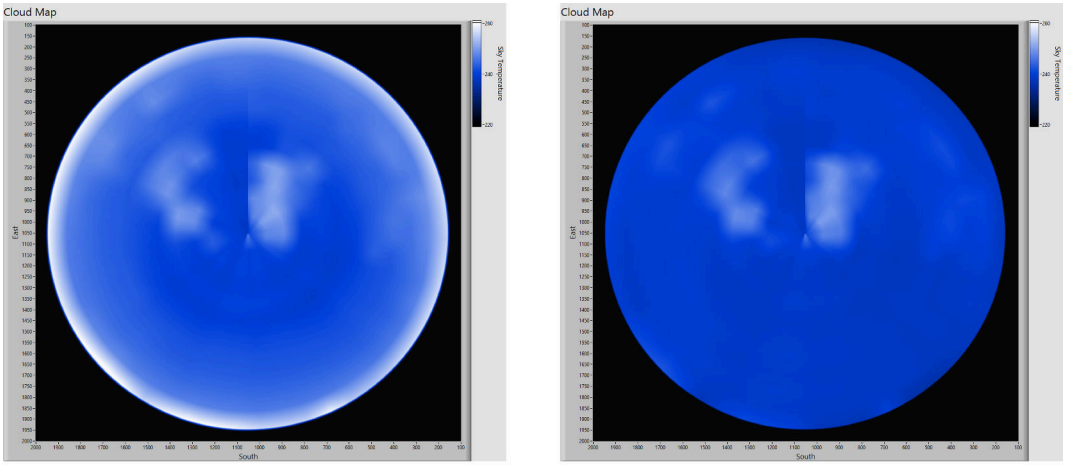

(a) (b)

Fig. 4.27: Cloudy sky maps (a) Cloud map without correcting for airmass effect, and (b) Cloud map generated after applying the correction for airmass effect for the same night (04-02-2016, 21:38:08 PM).

4.12.3 Comparison with CONCAM all-sky images

The All Sky Scanning Cloud Monitor instrument has been installed at IAO Hanle in December 2015. Then after the instrument is working continuously, whenever there are no rain or snowfall events. Observation could not be carried out on few nights due to unavailability of an operator who can start the instrument. We have reduced the cloud monitor data for a duration of 65 nights, although only first 50 nights were used to develop a relation between the ground and the sky temperature, and automatic detection of clouds. For the purpose of comparison and cross check, we collected CONCAM images simultaneously along with the cloud monitor data. We have compared the cloud maps generated by the scanning cloud monitor instrument with the images captured by the CONCAM camera. Figure 4.28 to Figure 4.33 shows the CONCAM images and the cloud map generated by cloud monitor at same time under below-mentioned sky conditions:-

1. Fully clear sky with Moon present in Figure 4.28.

2. Fully clear sky without Moon in Figure 4.29.

3. Fully cloudy sky with Moon present in Figure 4.30.

4. Fully cloudy sky without Moon in Figure 4.31.

5. Partly cloudy sky with Moon present in Figure 4.32.

6. Partly cloudy sky without Moon in Figure 4.33.

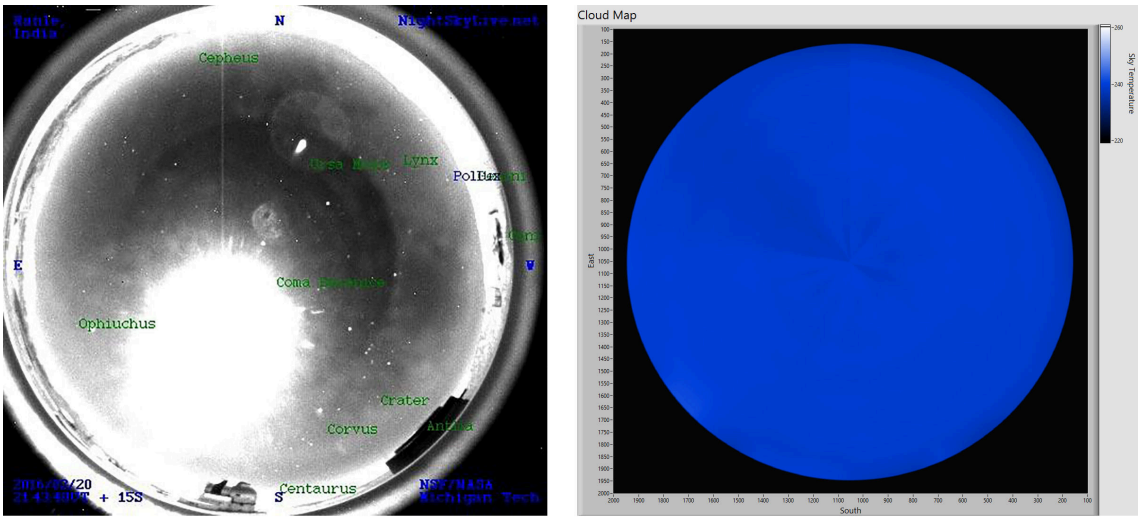

(a) (b)

Fig. 4.28: Image of the fully clear sky with moon as captured by (a) CONCAM all sky camera, and generated by (b) All sky scanning cloud monitor instrument (20-02-2016 20:43 PM).

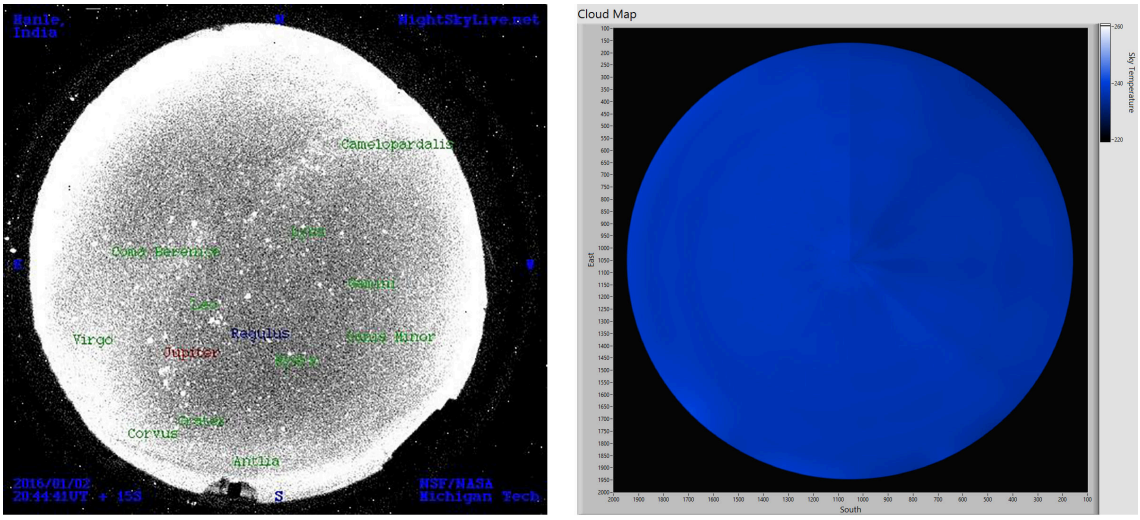

(a) (b)

Fig. 4.29: Image of the fully clear sky without moon as captured by (a) CONCAM all sky camera, and generated by (b) All sky scanning cloud monitor instrument (02-01-2016 20:44 PM).

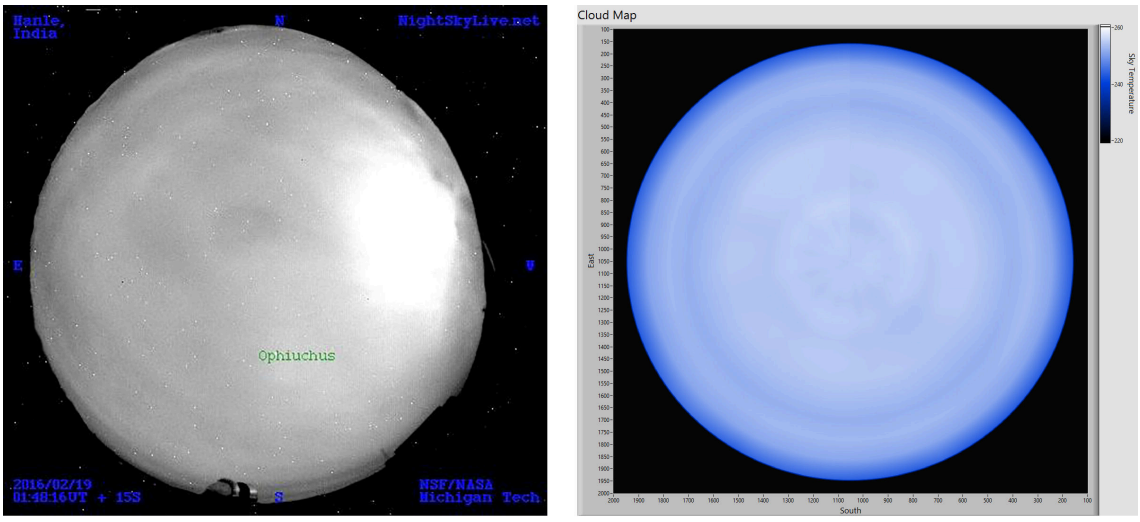

(a) (b)

Fig. 4.30: Image of the fully cloudy sky with moon as captured by (a) CONCAM all sky camera, and generated by (b) All sky scanning cloud monitor instrument (19-02-2016 01:48 AM).

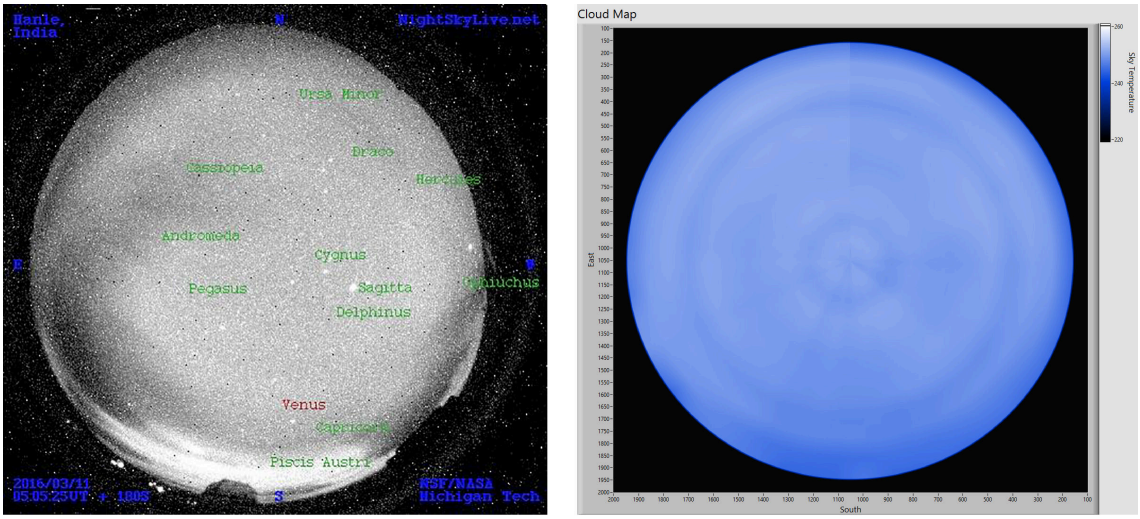

(a) (b)

Fig. 4.31: Image of the fully cloudy sky without moon as captured by (a) CONCAM all sky camera, and generated by (b) All sky scanning cloud monitor instrument (19-02-2016 01:48 AM).

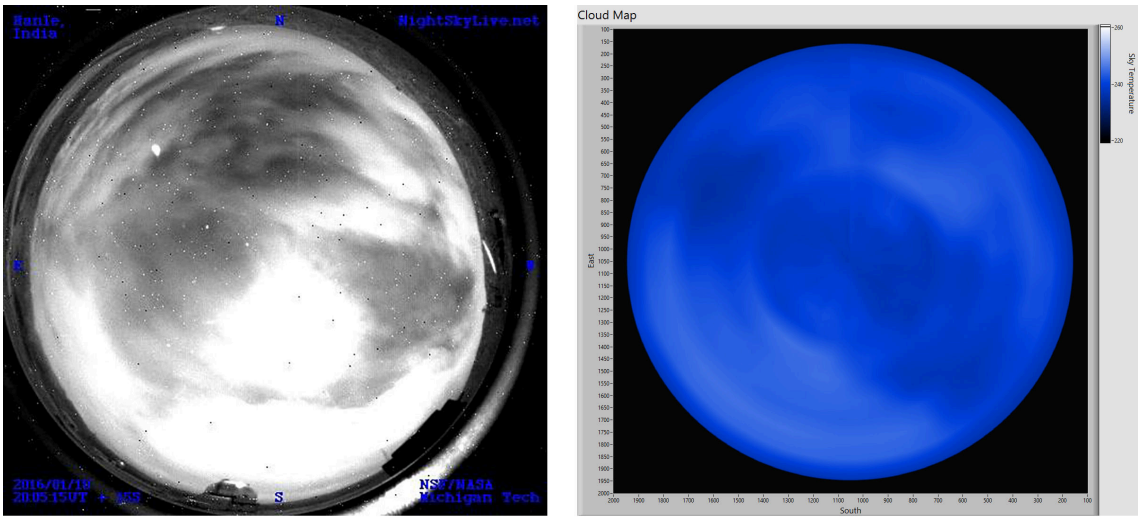

(a) (b)

Fig. 4.32: Image of the partly cloudy sky with moon as captured by (a) CONCAM all sky camera, and generated by (b) All sky scanning cloud monitor instrument (10-01-2016 08:05 PM).

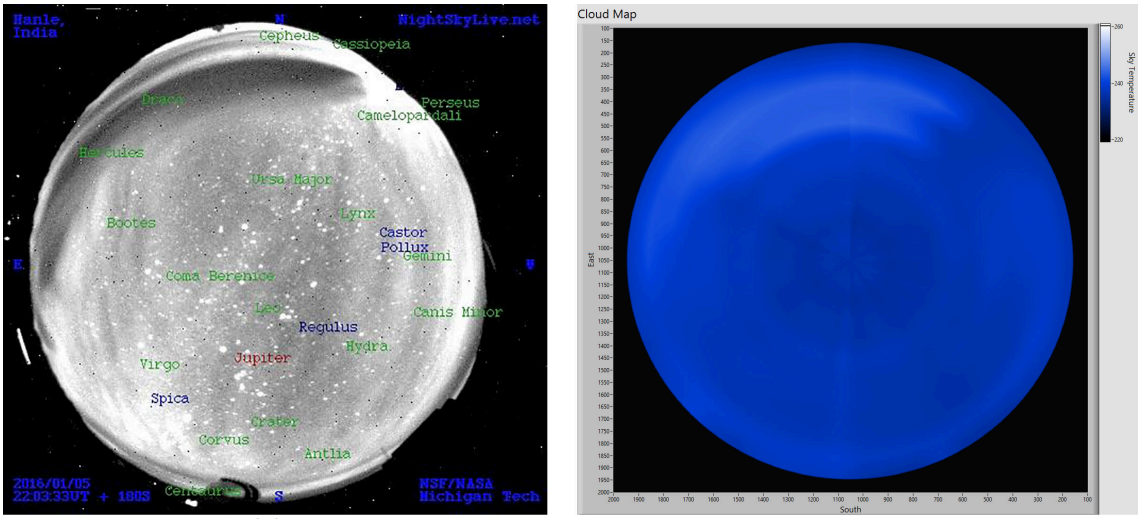

(a) (b)

Fig. 4.33: Image of the partly cloudy sky without moon as captured by (a) CONCAM all sky camera, and generated by (b) All sky scanning cloud monitor instrument (05-01-2016 22:03 PM).

Following conclusions can be drawn after comparing the images of 65 nights of both the instruments:-

1. The visual inspection of the CONCAM images and cloud maps generated by the cloud monitor instrument shows that they match very well, which proves that the sky map generated by scanning cloud monitor are reliable.

2. Cloud maps generated by the cloud monitor instrument are not affected at all by the presence of the moon in both the clear and the cloudy conditions (see the Figure 4.28 to Figure 4.33). Whereas, CONCAM (or any other visible all-sky camera) images are affected by the presence (and phase) of the moon. This way our device is performing better than CONCAM.

3. Cloud maps generated by the cloud monitor instrument and the percentage cloud cover calculation from it are not affected by the presence of the Milky Way.

4. Thin clouds remain almost undetectable using all-sky visible cameras unless

photometry and other techniques are used. Scanning type cloud monitor easily detects the presence of thin clouds.

5. The contrast between the clear and the cloudy sky is much better for the scanning cloud monitor than CONCAM, and hence it helps to determine the cloud cover reliably and automatically.

4.13 Automatic detection of clouds and percentage cloud cover calculation

With three months of cloud monitor instrument operation, we found a linear relationship between the local atmospheric temperature (or ground temperature) and the expected sky temperature. This linear relationship helps to predict the clear sky temperature on any night which has a certain ambient temperature. Once expected clear sky temperature is known, then, the threshold temperature above which sky can be considered cloudy can be decided. From Figure 4.19, the spread (σ) in the expected sky temperature for a given ground temperature is about $\pm 2^{\circ}$ from the mean value. Therefore, any temperature which is two σ above the expected sky temperature can be considered a cloud patch in the sky. Below are the steps followed by the software to calculate the percentage cloud cover of the sky:-

1. Software takes the temperature files folder and the Met server file (contains local atmospheric temperature, pressure, humidity, wind speed, etc.) as the input.

2. Temperature file is corrected for the zenith angle dependency (airmass correction) of the measured sky temperature.

3. Ground or atmospheric temperature is extracted from the Met server file for individual scans and expected sky temperature is computed by adding 4

degrees (2σ) to this, and this value is set as the threshold temperature above which cloudy sky can be distinguished from the clear sky.

4. Measured sky temperature for each sensor and every scan (basically 12×51 array) is compared with the expected sky temperature. This gives a binary array containing only 1's and 0's. Here 1 represents cloud and 0 represent the clear sky.

5. Sensors at different zenith angle samples the different areas of the sky, and there is overlapping in the scanned areas as we move from lowest sensor to the sensor near zenith. To overcome this, we have assigned different weighing constants to sensors at different zenith angles. Now the percentage cloud cover for each sensor is calculated.

6. Sum of the cloud cover of all the sensors give the cloud percentage percent.

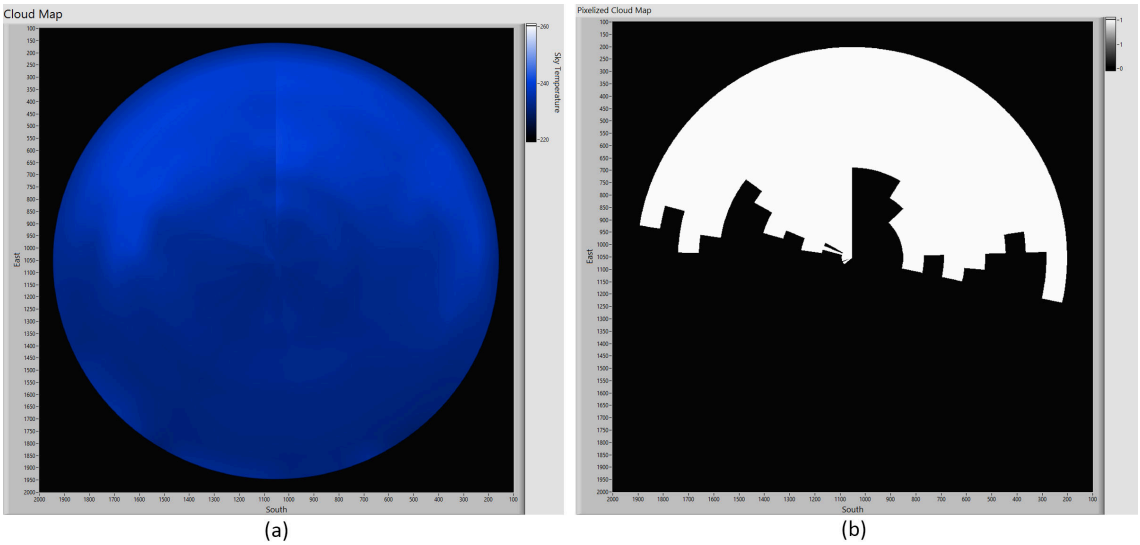

(a) (b)

Fig. 4.34: Image of the partly cloudy sky without the moon (a) Cloud map generated by scanning cloud monitor, and (b) Pixelized cloud map (12-02-2016 00:43 AM).

The GUI of the software as shown in Figure 4.17 shows the ground temperature, expected sky temperature, sky maps, and the plot for percent cloud cover for the whole

night of observation. It also generates a binary image (black for clear and white for cloudy part of the sky) along with the sky map for better comparison. One such image along with the associated cloud map is shown in Figure 4.34

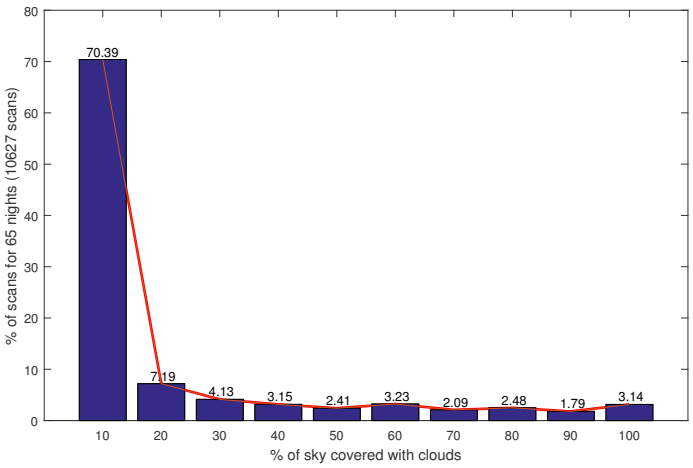

Fig. 4.35: Percentage cloud over Vs. percentage of total scans for 65 nights (10627 scans).

Altogether we have collected data for 65 nights in three months of instrument operation starting from December 2015. The data has been analyzed and also percentage cloud cover is computed. A histogram plot showing the distribution of clear and cloudy patches is given in the Figure 4.35. From this distribution, we get that nearly 70% of the time sky is completely clear (cloud cover less than 10%). Whereas, fully cloudy time is not more than 3%. Remaining time which is about 27% of total time is found to be partially clear. Once again to cross-check we have used the CONCAM data and confirmed that our scanning cloud monitor provides reliable results.

4.14 Discussion

The primary aim of this project was to develop a device which can provide a reliable measure of cloud coverage present in the local sky. One of the primary requirement

was that the device should not be affected by variable illumination of the Moon, environmental conditions and also facilitate automated detection of the cloud much more reliably than possible with a conventional CCD-based all-sky camera. After several years of effort and devising better laboratory and sky calibration techniques, finally, we could achieve this goal. Our scanning cloud monitor generates a reliable map of the sky with enhanced contrast between cloudy and clear sky, which helps to distinguish between clear and the cloudy part of the sky. The instrument generates a sky map, which is similar to the images captured by all-sky cameras working in visible or IR wavelengths. These images can be used to visualize the sky, and the temperature related data can be used to compute percentage cloud cover. The biggest advantage is that the changes in sky illumination by Moon has no effect on all-sky maps. Hence, irrespective of the presence and absence of Moon, we get similar sky map in which clouds are distinguished by looking at only the sky temperature. Similarly, the presence of a large number of stars distributed all over the sky and extended Milky-way, which indeed create problems to automated cloud detection technique for CCD based all-sky images has no effect. We also checked the stability of the device by operating it over more than three months and found that it indeed generated very consistent results. Our device is simple to develop and also less expensive and can be a very useful instrument to those existing observatories which can not afford to have very expensive IR imaging based all-sky camera. Undoubtedly our device is one of the very useful survey instrument and can play very important role to the groups exploring news site for future observatories.

CHAPTER 5

MASS-DIMM TELESCOPE

Light from the distant objects which is a plane wavefront gets distorted/corrugated while passing through the Earth's turbulent atmosphere. The image formed by such a distorted wavefront by a telescope is found to be blurred (due to distortion in the phase of the incoming wavefront) and also gives scintillation/twinkling effect. The MASS-DIMM (Multi Aperture Scintillation Sensor - Differential Image Motion Monitor) instrument uses these two observable effects of the turbulent atmosphere to understand the kinematic property of the atmosphere (Tokovinin and Kornilov, 2007). The MASS is a device which measures the Scintillation effect in stellar light and provides a vertical structure of atmospheric turbulence (Kornilov et al., 2007). Whereas, the DIMM uses the fluctuation in the phase of the incoming wavefront and provides the seeing (integrated effect of atmospheric turbulence). The knowledge of turbulence profile and its time variation is not only required while selecting a new site, but an effective implementation of Adoptive Optics to existing telescope also requires this information. For the purpose

of exploring the IAO Hanle site for the NLOT project, a MASS-DIMM device has been acquired from TMT Project USA. However, before it can be used, the device requires a lot of modifications to its software. Additionally to measure seeing and vertical turbulence profiles over a range of wind speeds it requires a very sturdy telescope. For the TMT project, a 14 inch customized telescope was purchased from a German telescope manufacturer Halfmann Teleskoptechnik. In the beginning, we planned to make use of commercially available Meade telescope, however, later we realized that Meade telescope is not the best choice for the MASS-DIMM instrument (explained in the subsequent section) and a new telescope needs to be designed and fabricated which can work in the windy environment.

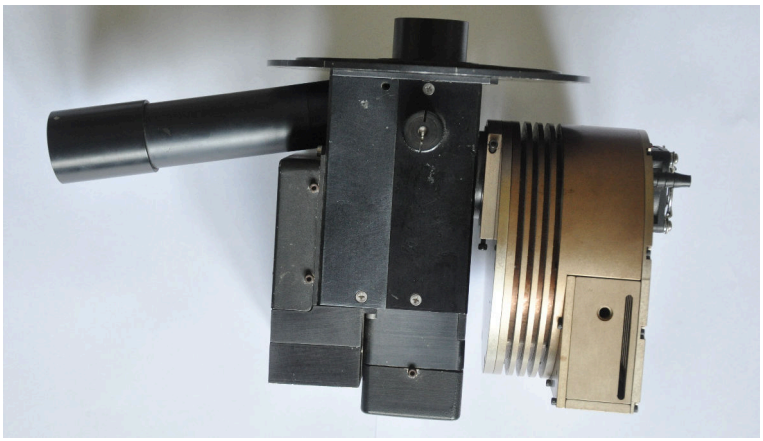

Fig. 5.1: Combined MASS-DIMM instrument acquired from TMT project USA.

5.1 MASS-DIMM Instrument

In the year 2001-2002, the MASS-DIMM instrument was designed and developed by a group working at Sternberg Institute (Moscow University) Moscow and Cerro-Tololo Inter-American Observatory. The MASS-DIMM is basically two different instruments embedded into the same body and fed by a single telescope. The MASS part of the instrument works on the principle of stellar scintillation and provides atmospheric

turbulence at 0.5, 1, 2, 4, 8, 16 Km above the ground and is insensitive to turbulence below the 500m altitude. The pupil segmenter splits telescope pupil into four concentric annular pupils. By making use of auxiliary optics, light from these pupils are focused onto PMTs (Photo Multiplier Tubes) which records intensity fluctuation in the form of scintillation indices. The Photon counts accumulated in 1 minute in the interval of 1 ms are converted to ten scintillation indices, four of which are normal (one per aperture) and six differential scintillation indices for each pair of apertures. These ten scintillation indices are fitted to a model of six turbulent layers at predefined altitudes.

The MASS-DIMM instrument is shown in Figure 5.1 and Figure 5.2 shows the typical output from it in the form or vertical turbulence profile. Whereas, the DIMM (Differential Image Motion Monitor) channel is a standard image motion based seeing measurement device being used around the world at many observatories (Sarazin and Roddier, 1990; Tokovinin, 2002). Combining MASS and DIMM in a single instrument has several distinct advantages. The first one being that it requires only one telescope for the pointing and tracking. Both instruments work on the same optical path, thus sample the same turbulent volume, so not subjected to any differential error. The working principle, optical design, instrument hardware and application of the instrument have been explained in many articles published by Victor Kornilov of SAI Moscow and Andre Tokovinin of CTIO (Kornilov et al., 2003, 2007; Tokovinin, 2007).

In modern observatories where Adaptive Optics (AO) and interferometry are used for studying the objects with extremely enhanced spatial resolution, knowing the seeing is not enough. Other atmospheric parameters like time constant and isoplanatic angle must also be known (Hardy, 1998). These parameters are also required for the performance evaluation of the AO systems. The results obtained from MASS and DIMM instrument on seeing are similar as long as the ground layer turbulence is not significant.

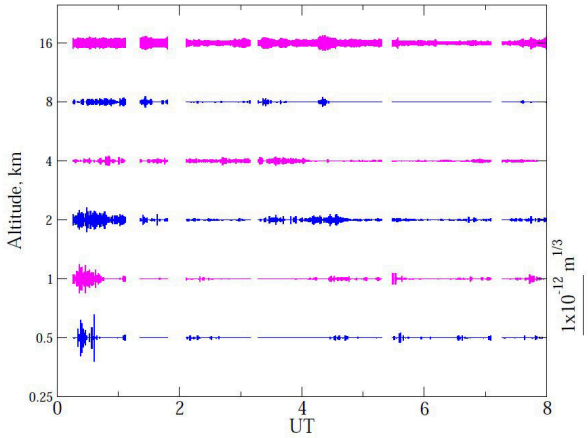

Fig. 5.2: A typical example of the vertical profile of atmospheric turbulence measured by MASS-DIMM instruments.

5.2 Telescope for MASS-DIMM Instrument

The MASS-DIMM instrument was originally designed to be operated with 254mm Meade telescope for CTIO program and 350mm Cassegrain telescope custom made by German company Halfmann for the TMT project. The instrument can also be used with other telescopes with suitable modifications. At present, a locally developed DIMM is being operated at IAO Hanle with a Meade telescope. Figure 5.3 shows the in-house developed DIMM instrument installed at IAO.

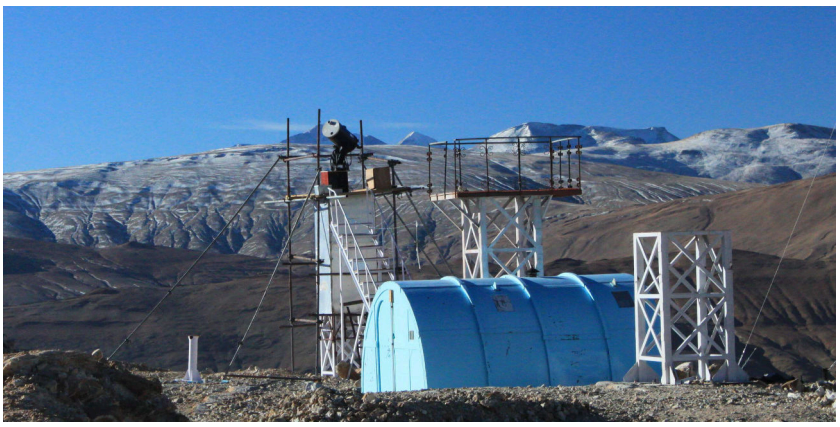

Fig. 5.3: In-house developed DIMM instrument installed at IAO Hanle.

IAO Hanle is subjected to very high wind speed, and with regular observation, we have found that the operation of the DIMM is affected by this high wind speed. The primary reason being the use of Meade telescope, which is mechanically not very stable. Both axes of the Meade telescope have got large worm wheel driven by a worm gear. The worm wheel unit is not anti-backlash type, and there is a small free movement in both the axes. Meade telescope also uses a tube instead of a truss. Hence, the wind loading is large. Both of these effects get combined and as a result, telescope starts shaking when wind speed is more than 5m/sec.

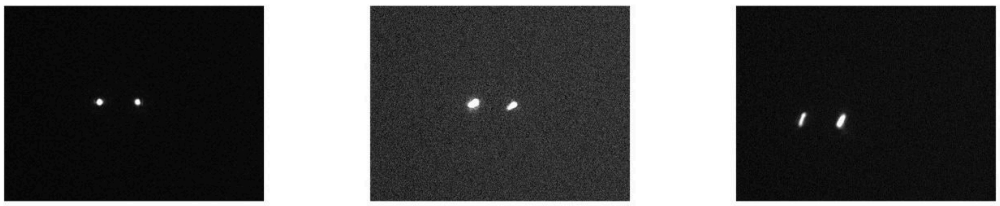

Fig. 5.4: Various images captured by DIMM instrument installed at IAO Hanle..

Figure 5.4 shows few images captured by the DIMM instrument, here the DIMM instruments integration time is 10 ms. In Figure 5.4(a), there is no effect of the wind induced vibration/shaking. The two images formed by the single star are nearly circular. Whereas, in Figure 5.4(b) and (c) the star spots have got affected by telescope shaking and no more circular. Such distorted images result in the unreliable seeing value, which depends on accurate measurement of the distance between center of two spots. Due to this problem, any seeing measurement obtained above 4-5 m/sec wind speed by the present DIMM system is not very reliable and mostly overestimated.

To overcome the above mentioned problems we decided to design and develop a customized telescope which can provide undistorted stellar images over a large range of wind speed. The proposed MASS-DIMM telescope is an Alt-Az (Altitude-Azimuth) mount telescope with provision for the equatorial mount as well. In order to reduce

wind induced shaking/disturbances, the cross section area of the telescope needs to be minimized. Additionally, light weight carbon fiber based truss is used to reduce the cross-section area and hence the wind effect. For the optimum performance over a range of wind speeds, the telescope structure needs to go through the process of modeling and analysis. The use of direct drive technology eliminates the backlash problem and provides an option to control telescope stiffness dynamically. However, direct drive technology requires the use of very high resolution on-axis encoder for the purpose of close loop control of position and speed.

5.3 Design requirements

Below we provide a few key requirements, which the proposed telescope is expected to fulfill:-

1. **Mount type:-** Alt-Az mount, with provision to be used in equatorial mode whenever required. A fork is proposed to hold the OTA.

2. **Wind loading:-** The main objective behind developing this telescope is that it should work in a windy environment. Wind effect on the telescope can be minimized by having optimum cross section area, high structural stiffness, light weight and use of direct drive motors which eliminates backlash problem.

3. **Weight and Moment of Inertia:-** Rotating parts of the telescope should be light weight. The design must also facilitate a requirement of the lower moment of inertia about azimuth and elevation axes.

4. **Motor and its housing:-** Two identical ETEL direct drive motors, TML0210-070-3TBS-SH2-NC will be used in azimuth and elevation axes. The motor is frameless and needs to be incorporated in the mount itself. Whenever required, both, stator as well as rotor should be easily removable.

5. **Cooling of motor:-** Motors will generate heat which needs to be dissipated through air convection. Motor housing design should allow natural/forced cooling.

6. **Encoder mount:-** Optical rotary encoder from Renishaw, which has got circular scale and reading head is planned to be used. The circular scale will be directly connected with the rotating shaft, whereas encoder head will be mounted on the stationary frame. There must be a provision to align the encoder, which requires the adjustment in tip/tilt and gap.

7. **Interface with OTA:-** A dove-tail type of interface is used between the telescope tube and the mount.

8. **Limit switch:-** Both azimuth and elevation axes require limit switches, to prevent telescope from overrun.

9. **Balancing Elevation Axis:-** There must be a provision to balance elevation axis. Dove-tail interface can handle this requirement up to some extent.

10. **Scalibility:-** In near future we plan to develop in-house, our mid-sized telescope, which can be used for a specific science project. The MASS-DIMM telescope should be designed in such way that it can be easily scaled-up to hold 1.0m size OTA.

11. **Reliability:-** The primary use of the telescope is regular monitoring. Therefore, it should be very reliable, and design should meet this requirement.

12. **Brake:-** Brake is required on both azimuth and elevation axis.

13. **Telescope pointing:-** To facilitate automation, all-sky telescope pointing should be better than ten arc-second.

14. **Telescope tracking:-** Open loop tracking performance better than 1 arc-second in 5 minutes.

15. **Wind Speed**

    (a) Operational wind speed :- 54 Km/h

    (b) Survival wind speed :- 150 Km/h

16. **Speed of Rotation**

    (a) Slewing speed

        i. Alt-Azimuth mount-Azimuth/Elevation axis :- 12 deg/sec

        ii. Equatorial mount - RA/Declination axis :- 5 deg/sec

    (b) Tracking Speed

        i. Polar axis (RA) :- $15''$/sec $\pm$ 0.5 sec/sec

    (c) Guiding Speed

        i. Vertical/RA/declination axis :- $10''$/sec

    (d) Fine guiding speed

        i. Vertical/RA/declination axis :- $1''$/sec

17. **Acceleration time**

    (a) Alt-Azimuth mount :- 2 sec

    (b) Equatorial mount :- 2 sec

5.4 The Telescope Mount

The MASS-DIMM telescope is designed primarily to be operated in Alt-Az Mode with provision to be used in Equatorial mode as well. Figure 5.5 and 5.6 shows the assembly

drawing of the telescope in Alt-Az and Equatorial mount schemes respectively. Both mounting schemes of the telescope are described below.

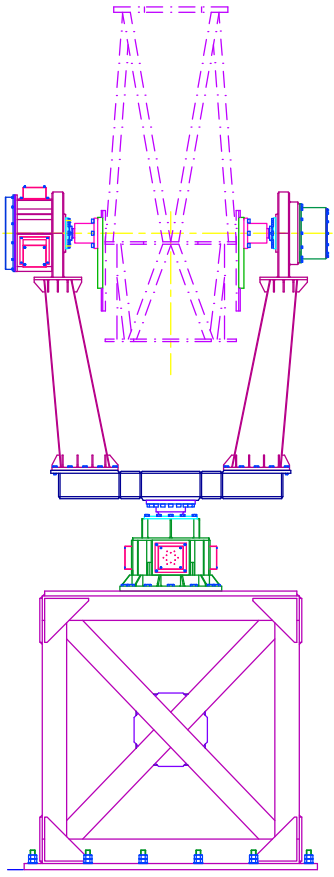

Fig. 5.5: Assembly drawing of the MASS-DIMM telescope in Alt/Az mount scheme. Left end of the Elevation axis is the drive end consisting of motor. Right end is the non-drive end, and consists of the encoder and brake.

Alt-Az scheme

The cross section area of the telescope is kept minimum to reduce the wind loading. Telescope mount assembly consists of the yoke base, onto which two arms of the fork are fixed. Direct drive motors are used on both of the axes. These motors are directly coupled with the telescope axes, which means no reduction mechanism is present. This

makes the Elevation and Azimuth drive assembly of the telescope compact and light weight. Cooling fans are provided in both of the drive assemblies for forced cooling of the motors. Azimuth (Equatorial) drive assembly consists of the motor, encoder, and a brake unit all mounted on the same shaft, which is interfaced with the yoke base. Elevation (Dec) axis has two ends. The left end of the axis is the drive end, which houses the motor and the cooling fan assembly. The right end of the axis is the non-drive end and consists of the encoder and brake units. Telescope truss is interfaced with the mount using dovetails. The telescope fork is designed to accommodate a tube or truss with maximum size of 20-inches. Azimuth drive assembly also acts as base of the telescope, and can be mounted on a metallic pier as shown in Figure 5.5 or a concrete pier.

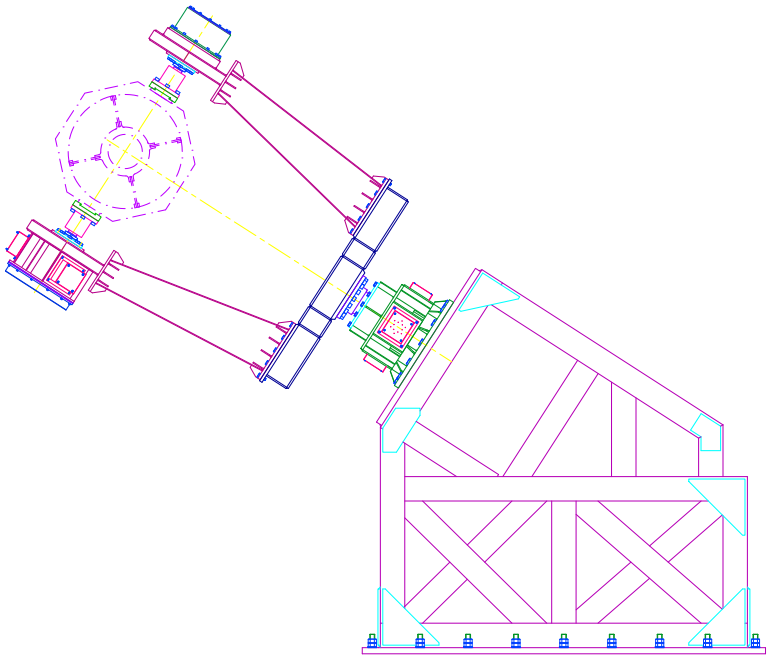

Fig. 5.6: Assembly drawing of the MASS-DIMM telescope in Equatorial mount scheme.

Equatorial Mount scheme

The immediate intended use of the telescope is to carry out seeing measurements using the MASS-DIMM instrument. The MASS-DIMM instrument uses on-axis star and hence no field derotator is required (when the telescope is working in Alt/Az mode). Whereas, there is a plan to use the mount designed for MASS-DIMM to hold the existing 20-inch OTA from Taurus optics and operate the telescope for few selected science applications which can be better done in equatorial mode. In Equatorial mount scheme the telescope configuration remains same as the Alt-Az mount scheme, the only difference is that the telescope is now aligned with the polar axis. The mount of the telescope is designed in such way that when it is used in equatorial mode then it should not introduce any flexure and also azimuth (RA) bearing should withstand against radial loads. In the equatorial mode, the RA axis is aligned to polar axis (Latitude of Hanle is 32°:46′:46″) with the help of an additional wedge.

5.5 Telescope hardware

The major components of the telescope hardware are briefly described in this section.

5.5.1 Telescope Optics

The TPO 16-inch F/8 Ritchey-Chretien truss OTA is used as the optics for the telescope. Primary reason for choosing the truss OTA over the tube OTA is the lower weight and the small cross section area. This truss is made of lightweight carbon fiber material. Carbon fiber has a very low thermal coefficient of expansion, hence, the shifts in the focus are minimized. The OTA has three cooling fans installed in the backside for forced cooling of the primary mirror to the ambient temperature, so the

effect of the telescope induced turbulence is minimized. The primary mirror of the OTA is fixed, hence, there is no image shift. The focusing is achieved by a Crayford-style focuser. This focuser has two knobs for coarse and micro focus adjustments. Truss can be interfaced with the telescope mount using the Losmandy Dovetails present on two sides of the OTA. Figure 5.7 shows the image of the OTA, and Table 5.1 lists some of the specifications of the OTA.

Table 5.1: Specifications of the TPO 16-inch F/8 Ritchey-Chretien truss OTA.

Parameter	Value
Optical design	Ritchey-Chretien
Telescope aperture	16 inch
Telescope focal length	3250 mm
Telescope focal ratio	f/8
Mirror Material	Low expansion Quartz
Optical coating	Dielectric
OTA mount type	Losmandy-Style Dovetail
Truss material	Carbon fiber
Focuser	3-inch dual speed linear bearing Crayford style focuser
Weight	42 Kg

Fig. 5.7: TPO 16-inch F/8 Ritchey-Chretien truss OTA.

A mechanical model and the drawings of the OTA was required for the purpose of designing the telescope mount and for carrying out wind loading related analysis. A mechanical model was also required for calculating the center of mass of the Truss and the torque required to rotate the telescope using direct drive motors. The manufacturer of the OTA did not agree to provide these drawings and other required information, so we decided to make a 3-D model of the OTA. For this, we took the precise measurement of the various parts of the truss while OTA was in assembled condition. Part drawings and 3D model for each part were generated in Autodesk Inventor, and materials were assigned correctly. All these parts were assembled in assembly environment of the Inventor, and the center of mass of the truss was determined. Figure 5.8 shows the 3D model of the truss, the center of mass is also visible in the same figure. Total weight of the designed truss model came out to be 41.4 Kg, which is quite close to the actual weight 42 Kg. Same 3D model of the truss was also used for wind load analysis of the truss.

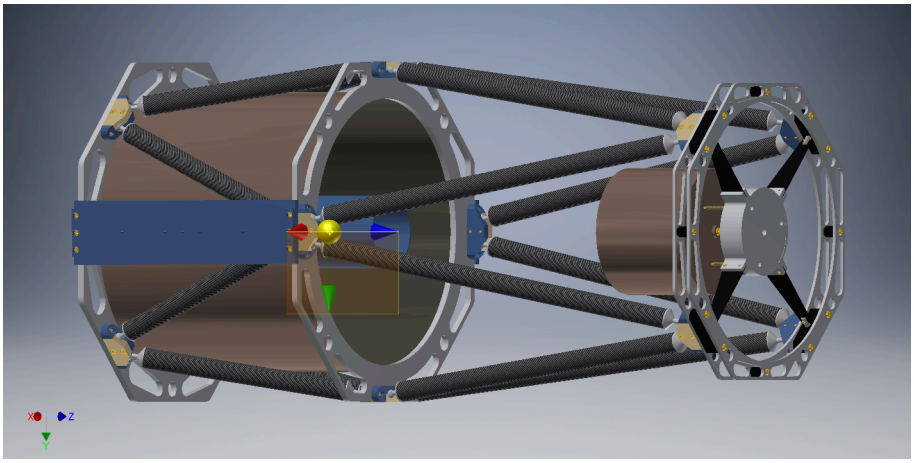

Fig. 5.8: 3D model of the TPO truss designed using Autodek Inventor.

5.5.2 ETEL direct drive motor

A direct drive motor TMLO210-070-3TBS-SH2-NC from ETEL is used for driving the RA and DEC axis of the telescope. These are high torque motor with a large number

of poles, which allows the motor to move at a very slow speed required for telescope operation. Specifications of the motor are listed in Table 5.2. These are frameless motors, where rotor and stator are supplied as separate units. These motors consume a large amount of current to produce high torque, hence forced cooling is required to keep the motor temperature below 130 °C. If operated above 130 °C, the magnets on the rotor may get demagnetized. The azimuth and the elevation drive assembly of the telescope are designed with exhaust fans for forced cooling of the motor.

Table 5.2: ETEL Motor Specifications.

Parameter	Value
Nominal input voltage	600 V
Number of poles	44
Rotor mass	3.48 Kg
Stator mass	7.41 Kg
Peak torque	309 Nm
Continuous torque	52.1 Nm
Torque constant	7.78 Nm/A
Motor constant	4.44 Nm/$\sqrt{W}$
Peak current	56.2 A
Continuous current	6.78 A
Maximum Continuous power dissipation	194 W

Fig. 5.9: ETEL motor thermal protection unit.

5.5.3 Thermal protection unit(IMTHP)

High magnetic strength Neodymium magnets are used in the direct drive motors. These magnets may get irreversibly demagnetized if the temperature exceeds 130 °C. This calls for keeping the motor temperature below 130 °C, while in operation. ETEL supplies the IMTHP unit (Thermal Protection Unit), which allows monitoring the internal temperature of the motor. Three phases of the motor winding are in contact with the KTY series temperature sensor. The output of these sensors can be connected to the IMTHP unit which is shown in Figure 5.9. The temperature sensor provides three outputs, and these are: - analog sensor output proportional to the temperature, one digital warning signal, and one digital error signal. These signals can be supplied to the motion controller operating the motor. Motion controller can decide to operate the motor or not, depending upon the alarm and error signals.

Fig. 5.10: Renishaw ring type encoder and the Tonic series readhead. Index mark (a vertical line on encoder ring) can also be seen.

5.5.4 Renishaw Encoder

Since the direct drive motors are directly coupled to the telescope Azimuth and Elevation axes without any gear system, it requires a very precise high-resolution encoder to be mounted directly on the telescope axes. A ring type encoder from Renishaw has been selected for the purpose. This encoder has a separate ring

(RESM-20u-S-S-150), a read-head (T2001-50A), and an interface (TI20KDA20A). The diameter of the ring is 150 mm, and the number of lines are 23600 with one index mark. The read-head interpolates these lines by a factor of 20000 and provides a linear resolution of 1 nm. In terms of the angular resolution it corresponds to 0.0027″. The output end of the encoder is a 15 pin DB-15 connector. Various outputs are A, B, Z, $\overline{A}$,$\overline{B}$, $\overline{Z}$, Alarm and Limits. Figure 5.10 shows the encoder ring and the read-head.

5.5.5 Brake

The use of direct drive motors to drive both the telescope axes makes it necessary to have a break on both the axis since there is nothing to restrict the telescope movement once the motors are powered off. A VAR02 series brake from Warner Electric[1] is used on both axes. This unit operates at a voltage of 24V and provides a braking torque of 35 Nm, which is enough to hold the telescope in its position. Figure 5.11 shows the brake unit.

Fig. 5.11: VAR02 series brake from Warner Electric.

The brake unit also comes with manual hand release (not shown in the figure), which is very useful in case of a power failure. The brakes automatically returns to the neutral position, once the hand release is released.

[1] http://www.warnerelectric.com/

5.6 Mechanical Analysis of telescope

The design process of any system involves the creation of a mathematical model of the physical aspects and characteristics of the system. A similar process applies in the case of telescopes as well. However, for a telescope the tolerances are very demanding. Deformation of the optical elements should not be greater than of the order of $\lambda/20$. Alignment tolerances are of the order of λ (Bely, 2003). The designed telescope must satisfy these deformation and alignment tolerances, when subjected to the following:-

1. **Static Loads:-** Loads due to gravity, static forces due to the wind, etc.
2. **Dynamic loads:-** Loads due to the wind gust, changing loads with changing telescope orientation, etc.
3. **Thermal Changes:-** Day to day and seasonal changes in the temperature can result in alignment and deformation errors if the materials are not chosen carefully. In bigger telescopes, optical elements are usually made of low expansion (ULE or Zerodur) glass, while critical mechanical assemblies are made of invar or low expansion ceramics. However, such expensive material may not be affordable while making a small telescope like ours.

To understand the effect of various disturbances in large telescopes, it is necessary to model both the mechanical structure and the optics of the system. While designing a large telescope, one need to carry out much more complex and integrated modeling work. Whereas, smaller telescope hardly goes through the process of modeling and analysis. Since the primary goal of having a customized MASS-DIMM telescope is to have a very sturdy telescope which will provide a decent image quality at high wind speed (up to 15m/sec), therefore, extreme care was required, and we decided to go through detailed modeling and optimization process. There are two primary requirements which any telescope is supposed to fulfill, these are:-

1. **Operational:-** These are the requirements which the telescope must fulfill on day to day basis during observation. Some of these requirements can be the maximum permissible strain in different parts of telescope under various load conditions, changes in focus due to changes in temperature, alignment tolerances, etc.

2. **Survival:-** These requirements are related to the extreme conditions, or to the survival of the facility. Some of these requirements are the survival wind speed, survival earthquake magnitude, etc.

The above mentioned requirements can be met, if the designed structure is analyzed for both conditions. The telescope structure is best analyzed with a finite element model (FEM) method.

FEM Model of telescope

We have analyzed the designed telescope structure using FEM method. The telescope is analyzed for static payload and wind loads (maximum operational wind speed 54 Km/h of and maximum survival wind speed of 150 Km/h). Figure 5.12 shows the FEM model of the telescope in Equatorial mount scheme. A finite element model of the mount is made using plate elements. Beam elements are used for interfacing the shaft to the sleeves. Bolted joints between the plates are represented by merging the nodes on the two surfaces. The origin of the model is at the intersection of the OTA and the declination axis (shown as a small black dot in Figure 5.12). X axis is along the declination axis and positive towards the non-drive end, and the Y axis is positive upwards. Constraints are kept at azimuth drive housing bolt locations. Load due to wind acting on the tube (X negative) is applied as the nodal load on the dovetail. The differential moment due to wind acting on the tube (torque about declination axis) is applied as couple force on the nodes of the dovetail. The pressure load is applied as the elemental load on the elements (in the mount) which are exposed to the wind blowing

west. In the present configuration a 16-inch OTA is used, a 20-inch OTA can also be used on the same mount. Therefore, analysis is carried out for the 20-inch OTA to get the maximum safety factor.

Below are the goals of the FEM analysis of the telescope:-

1. To check the stress in critical parts of the telescope in both operational and survival conditions.

2. To calculate the natural frequency, and torsional frequency of the Azimuth shaft of the telescope.

3. To calculate the maximum torque required by the motor to be generated in various load conditions in both the Alt/Az and Equatorial mount scheme.

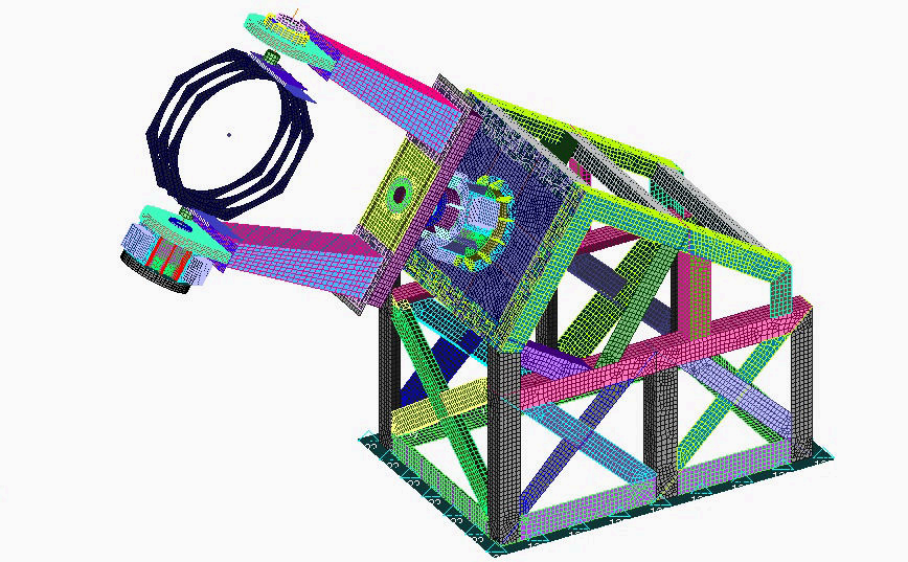

Fig. 5.12: FEM model of the telescope in Equatorial mount scheme.

The different elements forming the structure are made of Mild Steel. The material properties of the mild steel used for the FEM analysis are listed in Table 5.3.

Table 5.3: Properties of Mild steel

Parameter	Value
Density	$7.85E^{-9}$ N/mm^3
UTS	420 MPa
Yield Strength	210 MPa

The telescope mount is analyzed for the below mentioned static load cases:-

1. Alt-Azimuth Mount (Tube Pointing 30° off North) Wind at 54 Km/h blowing west:- 20AZM30NWX54S
2. Alt-Azimuth Mount (Tube pointing Zenith)Wind at 150 km/h in a direction normal to declination axis:- 20AZMZENW150S
3. Equatorial Mount 12 'O' Clock Position (Tube pointing Zenith)Wind at 54 km/h blowing north:- 20EQM12ZENWZ54S
4. Equatorial Mount 12 'O' Clock Position (Tube pointing Zenith)Wind at 150 Km/h blowing north:- 20EQM12ZENWZ150S
5. Equatorial Mount 6 'O' Clock Position (Tube pointing East)Wind at 150 Km/h blowing north:- 20EQM6EWX150S
6. Equatorial Mount 6 'O' Clock Position (Tube pointing North)Wind 150 km/h blowing east:- 20EQM6NWZ150S

Table 5.4 lists wind load and pressure acting on telescope under various load conditions in both the Alt/Az and Equatorial mount schemes.

Table 5.4: Wind load and pressure on telescope under various load conditions.

Load condition	Weight of Tube (20 inch)(Kg)	Torque about Dec axis (Nmm)	Wind load (N)	Pressure due to wind (MPa)
20AZM30NWX54S	60	1407	65.1	1.4E-4
20AZMZENW150S	60	175905	502	1.1E-3
20EQM12ZENWZ54S	60	1407	65.1	1.4E-4
20EQM12ZENWZ150S	60	175905	502	1.1E-3
20EQM6EWX150S	60	175905	502	1.1E-3
20EQM6NWZ150S	60	175905	502	1.1E-3

Figure 5.14 shows the stress at the yoke base in one of the load condition(Alt-Azimuth Mount (Tube Pointing 30° off North) Wind at 54 Km/h blowing west:- 20AZM30NWX54S). The telescope orientation in this load condition is shown in Figure 5.13.

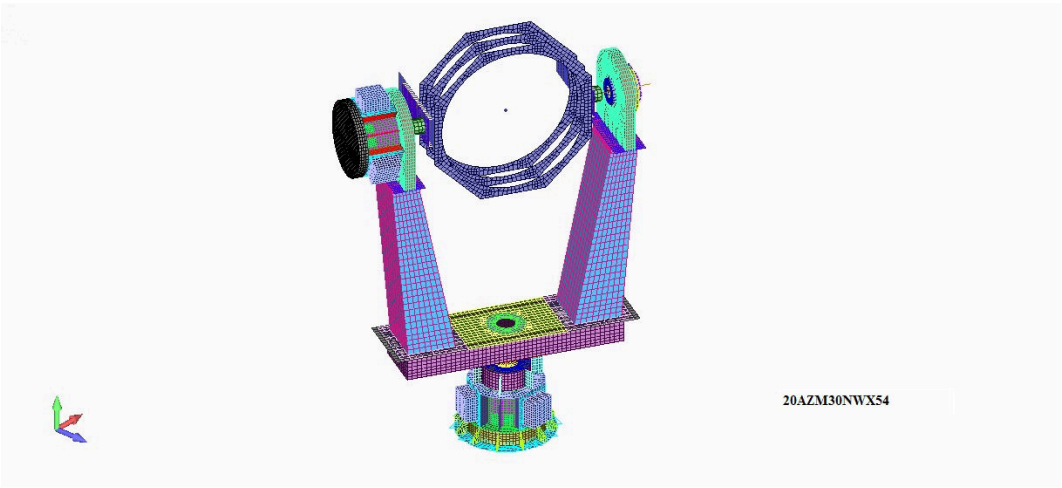

Fig. 5.13: Alt-Az mount scheme, tube pointing towards horizon(30° off North), and Wind at 54 Km/h blowing towards west.

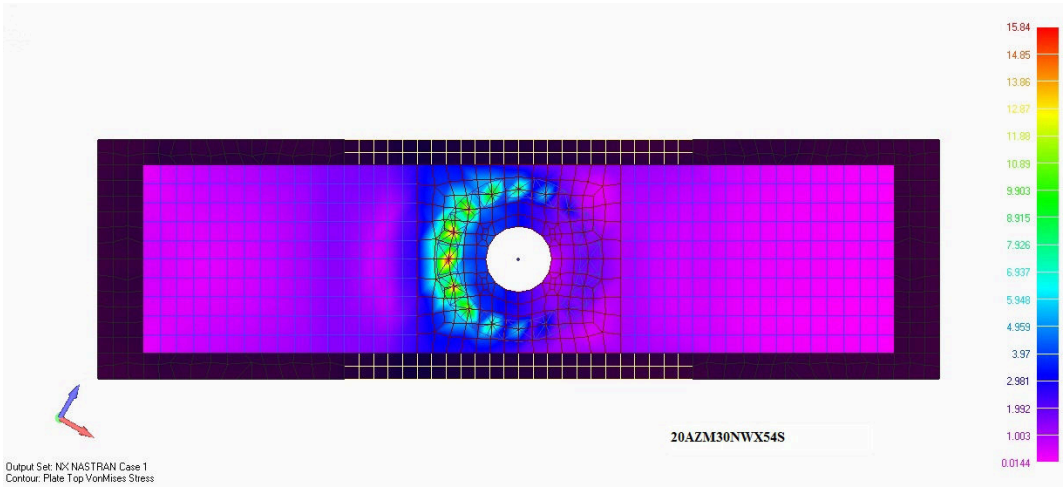

Fig. 5.14: Stress at the Yoke base in load conditions shown in Figure 5.13, (tube pointing towards horizon(30° off North), and Wind at 54 Km/h blowing towards west).

Stresses in telescope parts

We found that the stresses in most parts of the telescope are much lower compared to the yoke base. Table 5.5 shows the stresses computed at yoke base in different load conditions. Also, the stresses due to the wind are much lower.

Table 5.5: Maximum stress and safety factor at yoke base of telescope in different load conditions.

S. No.	Location	Load condition	Stress (MPa)	Factor of safety
1	Yoke base	20AZM30NWX54S	15.8	26.5
2	Yoke base	20AZMZENW150S	37.7	10.8
3	Yoke base	20EQM12ZENWZ54S	57.9	7.2
4	Yoke base	20EQM12ZENWZ150S	76.8	5.4
5	Yoke base	20EQM6EWX150S	82.1	5.1
6	Yoke base	20EQM6NWZ150S	64.6	6.5

Frequency Analysis of the Azimuth shaft

It is important to know the modal frequencies of a structure, as it enables to ensure that the frequency of any applied force does not coincide with the natural frequency of the system. The coinciding frequencies can lead to the resonance and large oscillations. The natural frequency of a system can be defined as a frequency at which the system tends to oscillate in the absence of any driving or damping force. It depends on the

structural stiffness and the mass of the system. Stresses in most parts of the telescope are very low when compared to the stress in the yoke base and the Azimuth shaft. We have also conducted the frequency analysis of the Azimuth shaft. Below are the frequencies computed from the analysis:-

1. Natural frequency
   (a) Bending of azimuth shaft (in Dec. plane) :- **13.4 Hz**
   (b) Bending of azimuth shaft (in plane perpendicular to Dec. axis) :- **16.1 Hz**
2. Torsional frequency
   (a) Stiffness of shaft:- 3 E+8 Nmm/rad
   (b) Mass moment of inertia of telescope about Az. axis:- 61083 Nmm sec^2
   (c) Torsional (lock rotor) frequency:- **12.8 Hz**

Azimuth Drive Torque

Various loads acting on the telescope such as wind load, friction in bearings, the inertia of the telescope, etc. manifest themselves in the form of a torque required either to move or to keep the telescope in its position. It is assumed that the telescope is perfectly balanced in both axis. Value of various torques calculated in Alt/Az and Equatorial mount scheme are listed below:-

1. Maximum torque due to the wind:- 3.8 Nm
2. Maximum bearing friction torque for Alt-Az mount:- 0.38 Nm
3. Maximum bearing friction torque for Equatorial mount:- 11 Nm
4. Inertia torque for Alt-Az:- 6.4 Nm
5. Inertia torque for Equatorial mount:- 2.7 Nm

6. Maximum starting drive torque for Alt-Az mount:- 10.6 Nm
7. Maximum running torque for Alt-Az mount:- 4.2 Nm
8. Maximum starting drive torque for Equatorial mount:- 17.5 Nm
9. Maximum running torque for Equatorial mount:- 14.8 Nm

Only torques in the Azimuth(Equatorial) drive are calculated, as this drive unit experience the load of the full telescope (including fork, truss and elevation drive). Torque values for the Elevation (Declination) drive will be much lower as the only load in this axis is the telescope truss. Although Friction torques will be the same.

Motor torques

Various motor torques (for ETEL motor) are listed below:-

1. Peak torque: - Maximum torque motor can generate. The value of this torque is 309 Nm. This torque is generated at maximum current of 56.2 A. This current can not flow through the motor continuously, as it can result in damage (demagnetization of magnets due to rise in temperature).
2. Continuous torque: - It is a maximum torque, which the motor can produce continuously without any damage to the motor. The value of this torque is 52.1 Nm, and it is generated at 6.78 A current.
3. Stall torque: - This value corresponds to the torque which motor produces in the stall condition. Its value is 39.3 Nm.

Conclusion

The following conclusions can be drawn from the FEM analysis of the telescope:-

1. The stresses induced in the components are mainly due to the weight of the mount and the effect of wind on stress is marginal.

2. The displacements due to change of wind load are not significant.

3. The stress values in the plates of the mount are small. To maintain the stiffness of the mount necessary for smooth rotation, the weights of various parts cannot be reduced further.

4. The natural frequencies in bending for Azimuth shaft in two planes are 13.4 Hz and 16.1 Hz. The torsional frequency of the Azimuth shaft is 12.8 Hz, which provides the required stiffness.

5. The torque requirement of the telescope after taking care of wind load, friction in bearings, etc. are well within the continuous torque capacity of the motor.

5.7 Wind analysis of the Telescope OTA

3D model of the telescope OTA was prepared using the Autodesk Inventor. We have also studied the effect of the wind on the telescope truss when the truss is pointing in the different direction from zenith. Autodesk Flow Design software was used for conducting this study. Wind tunnel dimensions were decided according to the rules provided in software documentation. This study was conducted at a constant wind speed of 10 m/s. Truss was oriented at different zenith angles and wind loads were determined. Figure 5.15 shows the screen capture image of the simulation window when the truss is pointing towards the zenith.

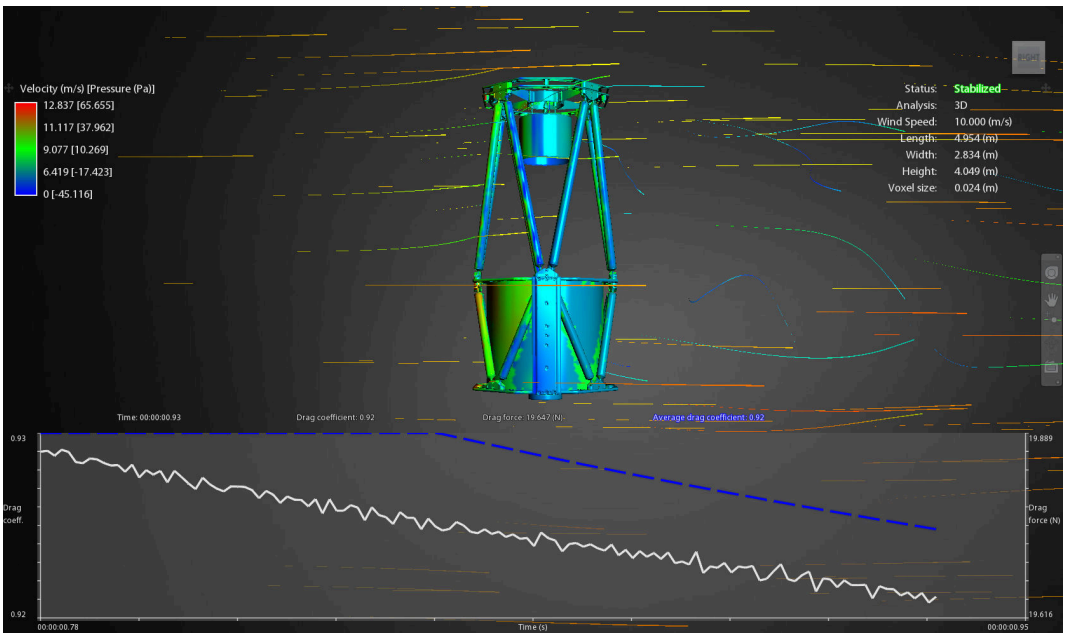

Fig. 5.15: Drag force on TPO truss in 0° orientation from zenith and at 10 m/s wind speed.

We have also conducted a comparative study of wind load on the TPO truss OTA and a telescope tube OTA of similar size when the truss is replaced with the full tube (keeping the same wind speed and the wind tunnel dimensions). Figure 5.16 shows the screen capture image of the simulation window when the tube is pointing towards the zenith.

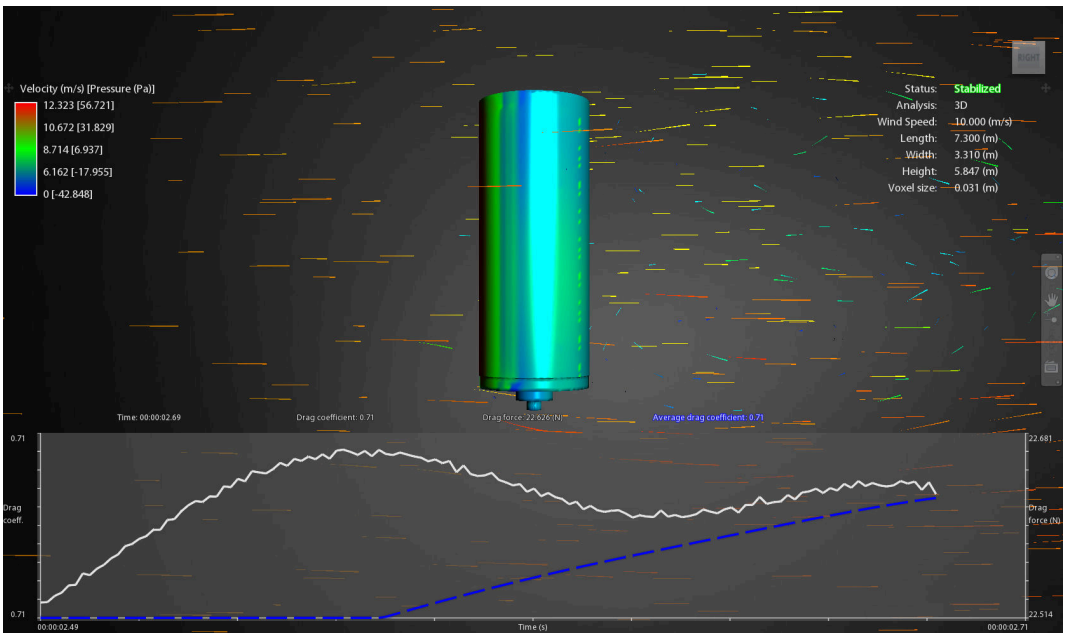

Fig. 5.16: Drag force on telescope tube in 0° orientation from zenith and at 10 m/s wind speed (wind direction left to right).

Table 5.6: Comparison between Drag force and Drag coefficient C_D for telescope tube and TPO truss for different orientation at wind speed of 10 m/s (wind direction left to right).

Orientation	Drag Force Tube(N)	Drag Force TPO(N)	C_D(Tube)	C_D(TPO)
300°	20.08	18.14	0.61	0.74
320°	22.68	19.70	0.53	0.68
340°	18.82	19.26	0.48	0.66
0°	27.86	19.64	0.71	0.92
20°	17.14	18.48	0.49	0.65
40°	16.80	19.20	0.48	0.66
60°	15.60	17.32	0.54	0.70

Table 5.6 lists the drag force and the drag coefficients for the TPO truss and the telescope tube of similar size for different zenith angles. These are the important conclusions which can be drawn from the table:-

1. The drag force acting on the TPO truss is almost independent of the zenith angle as it's value is almost same in all of the cases. Also, the difference between the minimum and maximum drag force is just 2.32 N.

2. The drag force for the telescope tube is highly dependent upon its orientation and varies a lot from 15.6 to 27.86 N. Also the maximum drag force is much higher when compared to the TPO truss.

3. The drag force acting on any object depends not only on the cross section area but also on the geometry of the object.

5.8 Laboratory test of the telescope control

Direct drive technology is being for the first time implemented by us in India and design and manufacturing of the telescope mount were expected to take at least a year time. Therefore, before the telescope mount was ready, we initiated a laboratory experiment to develop and test the single axis control of the telescope. For this purpose, a test bed was created which includes motor, encoder, and customized controller. In this section, we describe the test bed, and the experiment carried out with it. The telescope performance has been tested for tracking in Equatorial mode, i.e. when the motor is moving at a constant speed of 15″/s. This experiment is conducted using the in-house developed drive and controller (Explained in detail in Section 6.2 of Chapter 6) for testing the motor. A test set-up was designed and fabricated locally for this experiment. The primary goal of this experiment was to ensure that the motor can move with the slowest speed required for the telescope operation.

Test Set-up

Figure 5.17 shows the set-up for testing the performance of the ETEL direct drive motor. The set-up consists of a base plate, over which two brackets are mounted using screws. The bearing blocks are mounted on the two brackets for the motor shaft. There is one large bracket between the two small brackets for mounting the stator of

the motor. The larger bracket has an opening in it, where the stator is mounted using screws. The rotor is placed concentrically inside the stator over the shaft. This set-up also consists of a very high-resolution optical encoder, Mercury 5000 series from MicroE Systems[2]. Mercury encoders are similar to the Renishaw encoder, planned to be used in the actual telescope (during this experiment Renishaw encoder was not available). This encoder consists of separate encoder disk and a read-head. The encoder disk is made of glass with lines on it, and a read-head is placed parallel to the disk at some distance. There are 8192 lines on the encoder disk, and the read-head interpolates these lines by a factor of 16384. The quadrature output of the encoder is further interpolated by four times by the encoder interface IC HCTL2022[3]. This gives the resolution of 0.00241″/count.The encoder disk is mounted on the motor shaft concentrically, and the readhead is mounted on a bracket. The distance and the angle between the encoder disk and the read-head can be changed to get the optimum encoder signal, while observing the encoder signal strength using the encoder alignment tool (SmartPrecision Alignment Tool) and the alignment software (SmartPrecision Software).

[2] http://www.microesystems.com/products-services/linear-encoders-compact/mii5000

[3] http://www.avagotech.com/products/motion-control-encoders/integrated-circuits/decoder-ic/hctl-2022

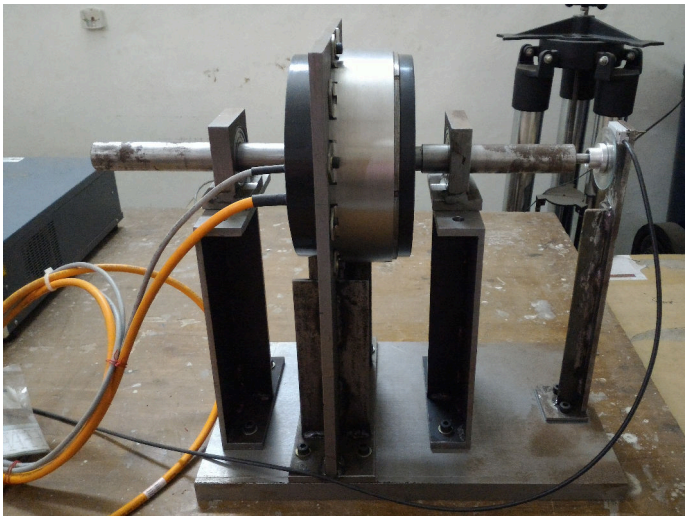

Fig. 5.17: Test set-up consisting of ETEL motor and Mercury 5000 series encoder (extreme right).

Closed loop operation of motor

We have operated the motor in closed loop condition using proportional and integral control. Since the encoder gives a large number of pulses (6213.8 pulses per second) for equatorial track rate of 15″/s, we were able to close the control loop (speed loop) at a high rate of 100 Hz. This means in every iteration of control loop 62.13 encoder counts are expected. Motor tracking performance was tested for short duration tracking (3 minutes) and long duration tracking (15 minutes). Both of these experiments were conducted in no load condition.

1. **Short duration tracking (3 Minutes)**

   Figure 5.18 shows the track (black line) curve for the ETEL motor for a 3 minutes duration. Linear fit (red line) and the statistics related to the fitting are also shown in the same figure. The mean encoder count for each iteration obtained from the linear fit is 62.16, which is quite close to the desired encoder count of 62.13.

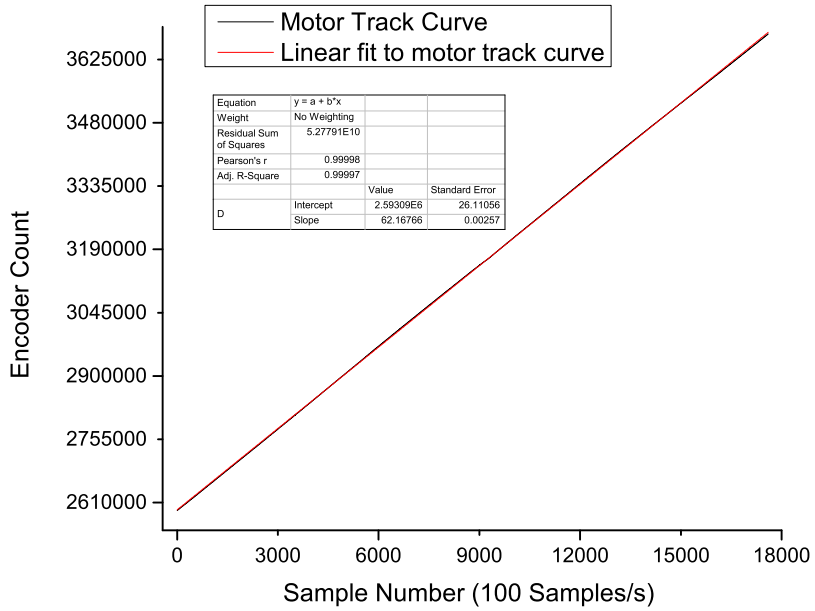

Fig. 5.18: Encoder count Vs time for 3 minutes of tracking.

Figure 5.19 shows the curve for mean arcseconds moved by the motor for each iteration of the control loop. The value is 0.149", which is very near to the desired value of 0.150. Also, the system just lags by 4.07" after the tracking of 3 minutes. These results were obtained by optimizing the values of gains for the proportional and integral part of the control algorithm. Although we expect to improve further upon these gain settings to achieve a much-improved tracking performance.

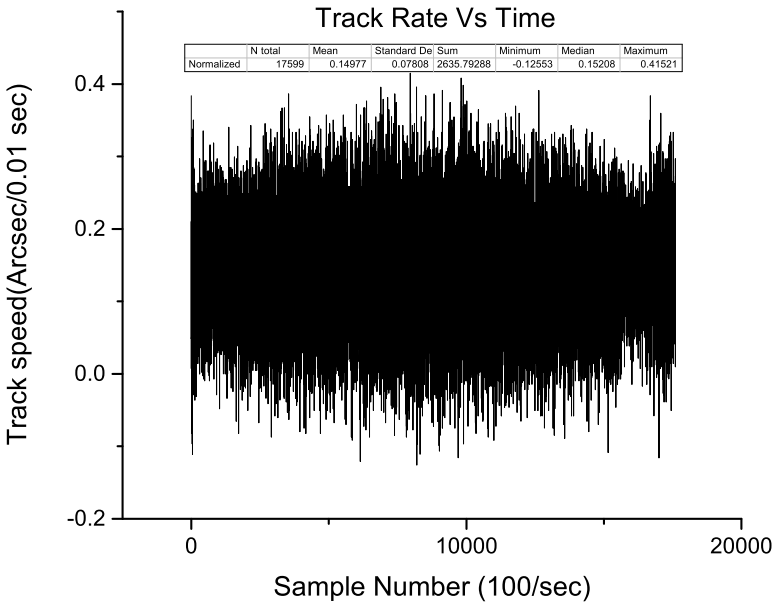

Fig. 5.19: Track rate Vs time for 3 minutes of tracking.

2. **Long duration tracking (15 Minutes)**

   Figure 5.20 shows the motor track curve for the 15-minute duration of tracking. The curve is linear as expected, and there is no large amplitude departure. After 15 minutes of tracking at the equatorial rate, motor lags about 32.4″. The mean track rate is 14.964″/s as opposed to 15″/s. Figure 5.21 shows the curve for Track rate Vs Time. From this plot, we can see sudden sharp changes in the track rate. The amplitude of these pulses is about 2″, and the period is about 150-190 sec. After conducting various experiments, it appears that the origin for these sharp and periodic changes in the track rate is electronic in origin. Initially, the amplitude of these pulses was quite large, and with the addition of capacitor based filters on the motor end, we were able to limit it to 2″.

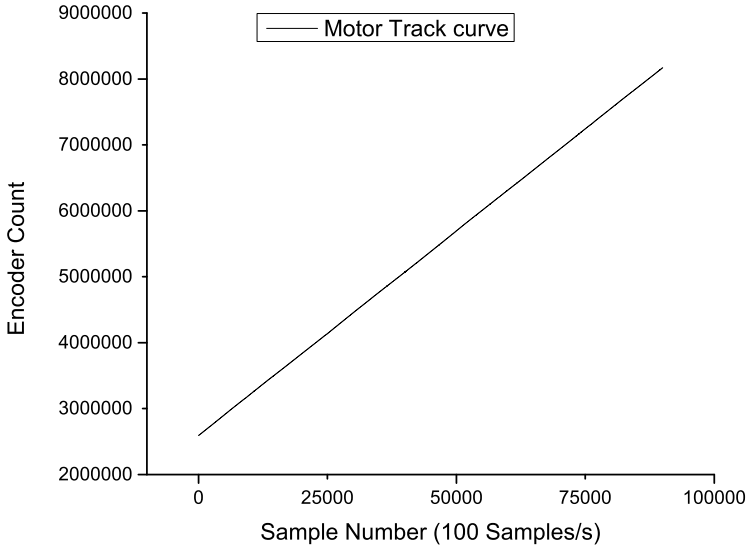

Fig. 5.20: Encoder count Vs time for 15 minutes of tracking.

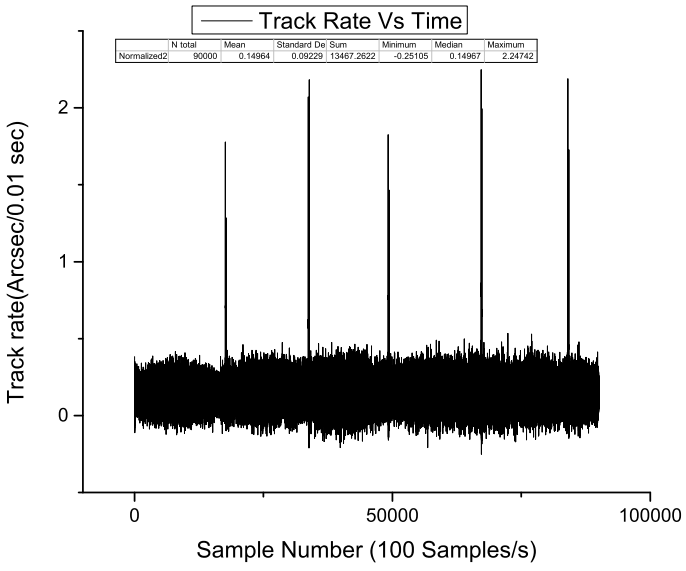

Fig. 5.21: Track rate count Vs time for 15 minutes of tracking.

The operation of ETEL motor with such a simple custom made drive (using only sinusoidal PWM technique to control the motor) confirmed that the motor will be able to move the telescope at desired speed in both the axes. A Delta-Tau PMAC controller

and PWM based drive will be used for the operation of the completed telescope. We expect to achieve much-improved motor performance using Delta-Tau controllers (using vector control technique), as these are very advanced dedicated motor controllers.

5.9 Manufacturing, assembly and initial testing of telescope

A contract was awarded to a Bangalore-based company to manufacture and assemble the telescope as per drawing. The manufacturing activities started in February 2016 and at present most of the telescope components are ready. Figure 5.22 shows the image of the assembled MASS-DIMM telescope at the manufacturing facility. At the time of writing this thesis, few parts of the Azimuth drive unit are still under fabrication and hence the Azimuth drive unit is not shown in the image. We have completed the preliminary factory inspection of the various parts of the telescope. We have also checked the compatibility of various bought out items like motor, encoder, brake, and telescope tube. All the bought out items are found to be matching with the fabricated components. The telescope tube is also tested for the smooth movement in Elevation axis and found to be rotating without any obstruction during visual inspection. We expect that manufacturing of few remaining parts will be completed shortly, and then full telescope will be assembled. After that telescope will be ready for factory testing where we will mainly check the functionality and then go for full sky pointing and tracking test at CREST (Hosakote) campus of IIA, Bangalore. The completed telescope is expected to start regular seeing observation by the end of the year 2016 at IAO Hanle.

Fig. 5.22: Assembled MASS-DIMM telescope at the manufacturing facility. The azimuth drive unit is not yet completed, hence, not shown in the image.

CHAPTER 6

AXIAL FLUX MOTOR AND MOTOR DRIVE

Motors are the main driving component for the telescopes. In the past, various kind of motors like Stepper motors, DC motors, Induction motors, etc. have been used along with the suitable gear system to drive the telescope. But in the recent years, the trend is to use the direct drive motors without any intermediate gear systems. Commercial direct drive motors can be used for smaller telescopes. However, large telescopes (such as NLOT) require a very customized motors. There are two primary motivations to carry out this project. The first one is to start some research and development activity on making customized motor required for any large telescope such as NLOT. Whereas the second one is to explore the possibility of developing an inexpensive motor controller and drive system which can be adopted by armature astronomers to built their small telescopes driven by custom made direct drive system. In this chapter, we describe our efforts to develop a direct drive motor

and related control and driving electronics.

6.1 Axial Flux Motor-Design and simulation

There are different configuration/topology to choose from for the stator-rotor arrangement of a motor. The topology we have selected for the prototype motor is single-sided, single-stage Axial flux motor. This topology was selected because it provides high torque, and is easy to design and construct. Additionally, the chosen configuration also provides high efficiency, power and torque density (Gieras et al., 2004). It also allows accommodating a large number of poles. Hence, these machines are ideal for low-speed applications. In conventional motors (radial flux motors) stator and rotor are cylindrical in shape, and usually, the rotor is placed concentrically inside the stator. On the other hand, in Axial Flux motors the rotor and stator are disk-shaped and placed parallel to each other separated by a small airgap.

Motor Construction

The axial flux motor is designed using basic analytical formulas, which relates the number of poles (coils), air-gap, current, magnetic flux in the gap, motor geometry, etc. with the torque. Table 6.1 and Table 6.2 lists the important parameters of the rotor and stator of the designed motor. Figure 6.1 (a) and Figure 6.1 (b) shows the completed rotor and stator respectively. The rotor consists of 16 High strength N35 NdFeB bar magnets separated by 22.5° and installed on a mild steel disk. The mild steel disk completes the magnetic loop and hence provide very high flux density. Magnets are fixed to the steel disk using high strength epoxy resin so that configuration of the magnetic poles are undisturbed during assembly and operation. Since magnets are of very high strength, it was difficult to arrange them on steel disk and therefore a customized fixture was designed. The fixture is made of plywood, consisting of the slots (dimensions equal to the magnet) and fixed to the mild steel

disk with screws as shown in Figure 6.2(a). After that, the magnets were fixed to the disk using epoxy resin. The magnets are arranged in such a way that the alternate magnet's North and South poles are in the same direction. The disk consisting of magnets, mounted on the circular plywood makes the rotor of the motor. Plywood was chosen for motor construction as opposed to the aluminum to reduce the prototyping time, as significantly large duration of time was required to procure and machine the aluminum block to suit the motor.

Table 6.1: Specifications of the Axial Flux Motor rotor.

Parameter	Value
Number of magnets	16
Magnet Material	NdFeB
Magnet grade	N35
Magnet Dimensions	50×25×12.5mm
Pole pitch	22.5°
Inner diameter	175mm
Outer diameter	280mm

Table 6.2: Specifications of the Axial Flux Motor stator.

Parameter	Value
Number of coils	12
Coil dimensions	70×45×10mm
Coil turns	105
Coil wire gauge	20 (0.914mm)
Slot pitch	30°
Phase resistance	2.2 Ω

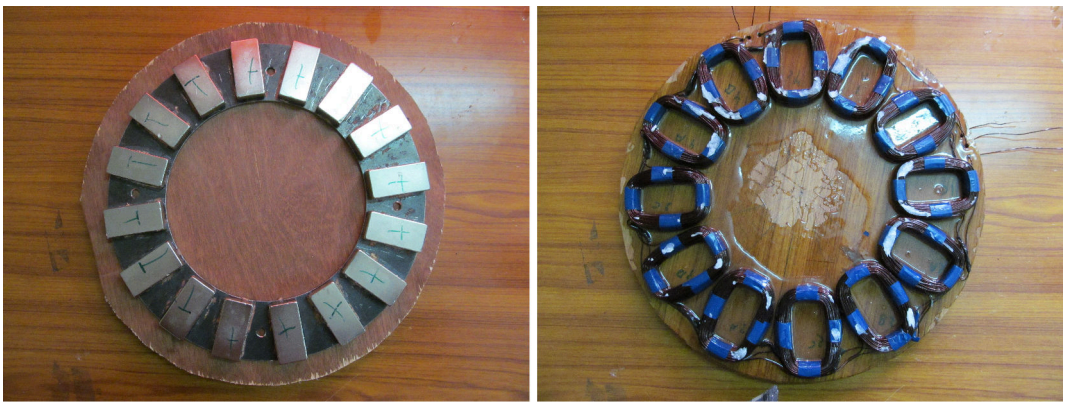

(a) (b)

Fig. 6.1: (a) Rotor and (b) Stator unit of the Axial Flux Direct Drive motor.

The stator of the motor consists of 12 coils. These coils are made from 20 Gauge (0.914mm diameter) laminated copper wire. A rectangular bobbin made of plywood was used for winding the coils on a coil winding machine displaying the number of turns wounded. Figure 6.2(b) shows the set-up for winding coils. Finished coils are fixed on the circular plywood using epoxy resin. The coils of the stator are connected in such way that it forms a 3-phases motor (star connection). The coils mounted on the disk act like a stator of the motor. A hole was drilled in the center of the stator, and a bearing was placed.

(a) (b)

Fig. 6.2: (a) Plywood section attached to mild steel disk for fixing magnets, and (b) Rectangular bobbin made of plywood mounted on the coil winding machine.

A simple laboratory test setup to evaluate the performance of the motor has been

designed and built. Figure 6.8 shows the set-up along with power supply and drive electronics. The test set-up consists of a wooden base and two vertical supports onto which two bearing blocks are mounted on the same height. The stator is fixed to one of the vertical blocks, and an aluminum shaft runs through the center of the stator. Rotor is fixed to the shaft, and placed parallel to the stator. The gap between the rotor and stator is kept about 2mm. With the help of an additional bracket, an incremental encoder CP850 from Computer Optics is mounted on the shaft projected beyond the bearing block at one of the ends. This encoder provides 1.25 Million counts per revolution, which is equivalent to nearly 1″/count. That means when the motor is moving at the equatorial track speed then encoder provides about 15 counts/second, which is barely enough to test the motor for its tracking performance.

Analysis of Axial Flux Motor using COMSOL Multiphysics

The prototype motor described earlier is built primarily to check the concept rather than intend to be used in a real telescope. Therefore, it has not gone through the standard procedure of first design and analysis then the fabrication. To check how well the custom made motor meets expected performance a static modeling/analysis of the motor using COMSOL Multiphysics software has been also carried out. The model allows the user to set different parameters like operating voltage, magnetic field strength of the rotor magnets and motor material. The model provides the information like static torque generated by the motor, magnetic flux density in different parts of the motor, and the current flowing through the different coils of the motor. Below are the steps followed while simulating motor using the COMSOL software:-

1. **Geometry:-** Coils, magnets, the magnet mounting steel disk, etc. are designed separately in COMSOL, and their geometries are saved. These geometries are imported in the final model and assembled according to the motor construction. A volume filled with air is also designed around the motor assembly. Figure 6.3

shows the rotor and stator geometry created in COMSOL.

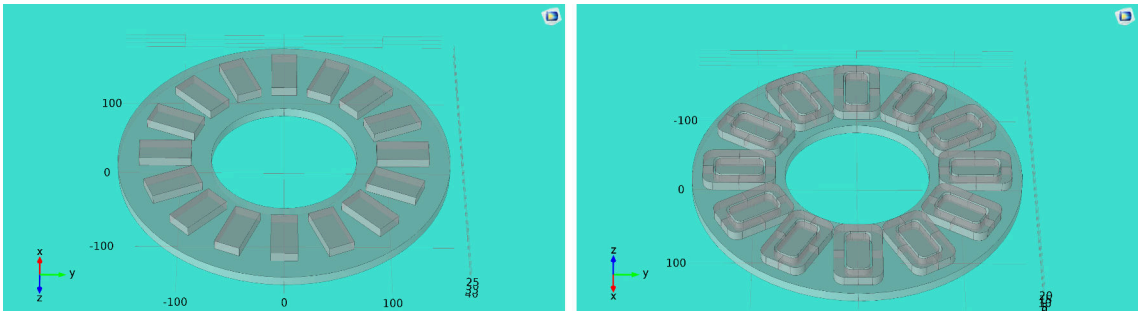

Fig. 6.3: Rotor geometry (Left) and the Stator geometry (Right) of the Axial Flux motor designed in COMSOL Multiphysics software.

2. **Parameters:-** Various parameters are supplied to the COMSOL software like the number of coil turns, coil conductivity, coil wire area, supply voltage, supply frequency, the phase difference between 3 phases of the motor and the magnetic flux density of the rotor magnets.

3. **Material:-** Material for different parts like magnets, magnet mounting disk are assigned correctly. Magnet material is assigned as air since NdFeB and air have almost similar relative permeability. Volume surrounding the motor assembly is also defined as air.

4. **Physics:-** Magnetic field physics is used to simulate the effect of magnets and coils. The multi-turn coil is used to define the stator coils and Ampere's Law for defining the magnets.

5. **Mesh:-** FEM analysis requires the meshing of the object geometry. A physics controlled mesh of the whole geometry is created for the analysis.

6. **Stationary solver:-** We have used stationary solver to compute the various parameters like the current through the different coils, torque produced by the motor and the magnetic flux density in various parts of the motor.

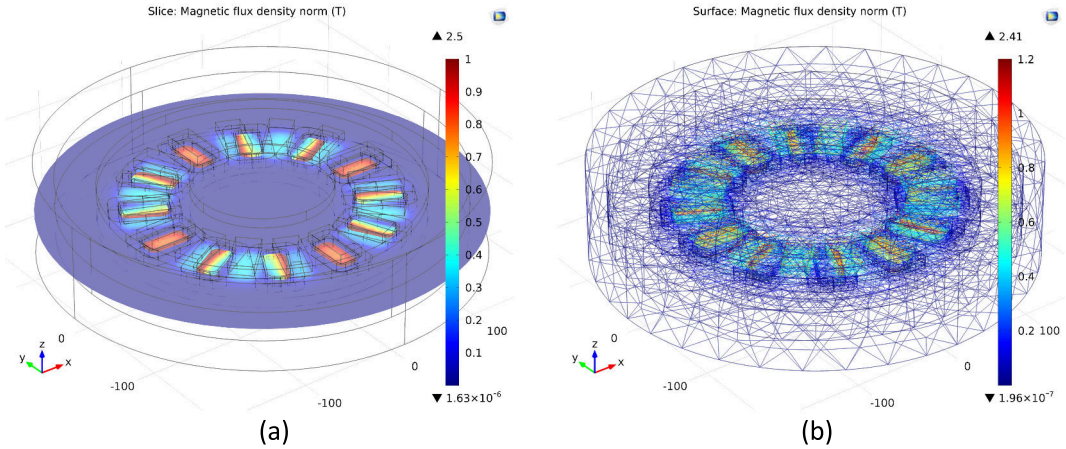

Fig. 6.4: (a) Magnetic flux density in a plane of the motor, and (b) Magnetic field lines and surface magnetic flux density in different parts of the motor.

7. **Results:-** We have calculated the torque produced by the motor in the stationary condition. The calculated torque comes out to be 28.5 Nm at 5 A current and 2mm airgap between the rotor and stator. Due to the absence of right kind of testing setup, the motor torque determined by COMSOL analysis could not be verified experimentally. Figure 6.4 (a) and 6.4 (b) shows the magnetic flux density in plane of the motor and Surface magnetic flux density in different parts of the motor respectively.

6.2 Microcontroller based controller and drive

A Turbo PMAC and Direct PWM drive from Delta-Tau will be used for driving the MASS-DIMM telescope. However, a simple microcontroller based controller and Mosfet based driver have been developed for testing the axial flux motor and the ETEL motor. Figure 6.5 shows the block diagram of the motor controller and drive. Only the microcontroller board is made of commercial grade PCB. Whereas, other boards are made of discrete components mounted on the general purpose PCB boards and hence, easily re-configurable. The basic functionality of the controller-driver unit

is to generate the three phase variable frequency output with desired voltage (current) so that motor can be rotated. The motor speed can be controlled by changing the frequency of the three-phase signal. Whereas, torque can be controlled by varying voltage/current flowing in the coils.

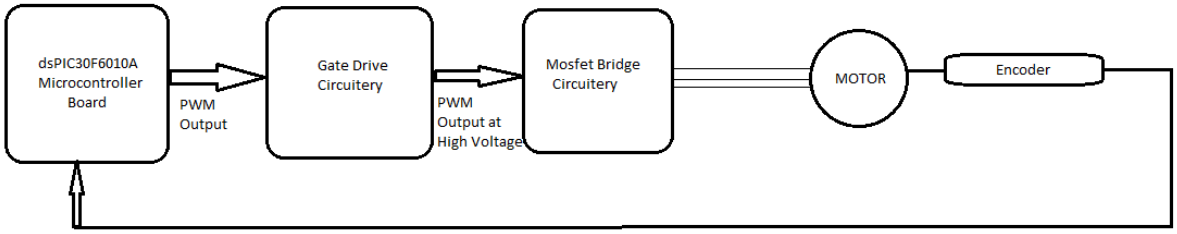

Fig. 6.5: Block diagram of the dsPIC30F6010A microcontroller based motor drive.

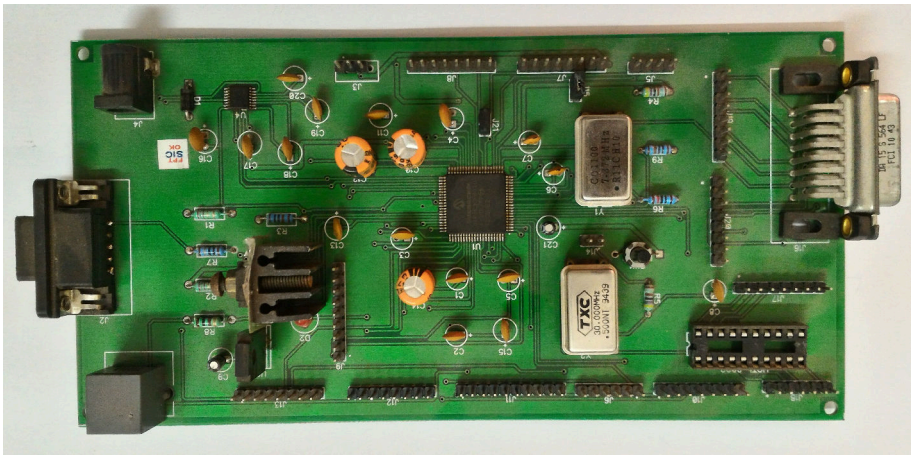

Fig. 6.6: dsPIC30F6010A Microcontroller based controller board developed for testing Axial Flux motor and ETEL motor.

Microcontroller Board

Figure 6.6 shows the microcontroller board designed in-house for the motor drive. It generates the required signals for motor operation as well as reads output of the encoder. The microcontroller used in the drive is dsPIC30F6010A from Microchip. This microcontroller comes with an inbuilt Motor Control Module and provides up to eight 16-bit PWM output channels. A 7.372 MHz crystal is used on the board. Microcontroller accepts this clock and multiplies it by 16 times to 117.952 MHz using

internal PLL block. A quadrature encoder interface IC HCTL2022 from Digilent is also provided on the board. A 30 MHz crystal provides the clock for the operation of this IC. This IC accepts the A, B and I pulses coming from the encoder and provides absolute position information. Data can be read in four separate bytes. All the I/O pins of the microcontroller are provided as ports for interfacing the HCTL2022 and other drive electronics to the board. A serial port is also provided on the board to communicate with the PC.

Drive operation

Figure 6.7 shows the PCB implementation of the motor drive as depicted in the block diagram shown in the Figure 6.5. Various boards present in the drive are Differential line receiver for the encoder, Microcontroller board, Level shifting board, Optical isolation and gate drive board, and the Mosfet bridge board respectively (left to right).

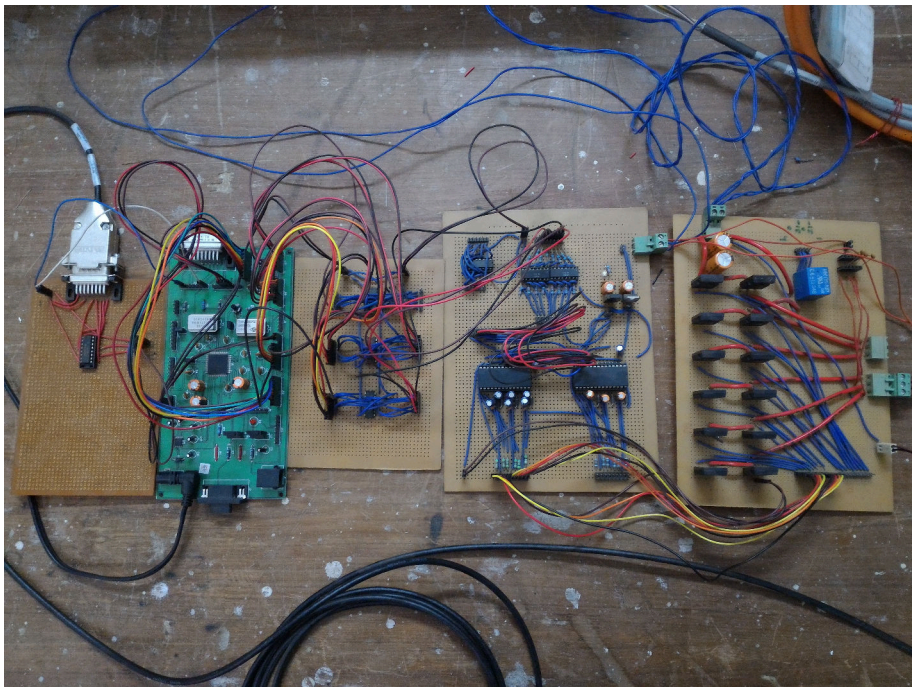

Fig. 6.7: dsPIC30F6010A Microcontroller based drive for testing Axial Flux motor and ETEL motor. Various blocks of the drive from left to right are Differential line receiver for encoder, Microcontroller board, Level shifting board, Optical isolation and gate drive board, and the Mosfte bridge board respectively.

The drive works on the principle of sinusoidal PWM modulation. Since the motor has 3-phases, a 3-phase control signal is required to operate it. The microcontroller board has 8 PWM modules, out of which six are used to generate the control signal. Three signals are normal, and the remaining 3 are complementary to first three signals. These PWM modules generate three separate constant frequency sinusoidal wave, which are 120° phase apart. These low-frequency sinusoidal waves are generated by the microcontroller using PWM technique by varying the duty cycle of the square wave. The control signal can not be used directly to drive the motor, as it does not have the required power. This microcontroller output at 3.3V is fed to a level shifter board, which converts it to 5V level. This signal at 5V goes to an optical isolation network made of A844 optocoupler IC that separates the low power microcontroller board from high power motor side. The output of the optical isolation network at 5V is supplied to a gate drive circuitry made of IR2136 gate drive IC. This IC accepts the control signal at 5V and converts it to a voltage level (15V) required to drive the MOSFET bridge made of six IRFP4227 MOSFETs. Three output sections of the IR2136 drives the three high and low side of the MOSFET bridge respectively, one high and one low side for each phase.

HCTL2022 accepts the incremental quadrature signal from the encoder, and converts it to the absolute position information provided encoder passes through the index pulse (or home position) before starting counting. Microcontroller board accepts the encoder output coming from HCTL2022 ic (encoder interface). This way the encoder output can be used to operate the motor in closed loop condition using PID control technique. The speed of the motor is changed by changing the frequency of the 3-phase sinusoidal signal generated by the microcontroller, and the torque produced by motor can be changed by changing the current flowing through the motor coils.

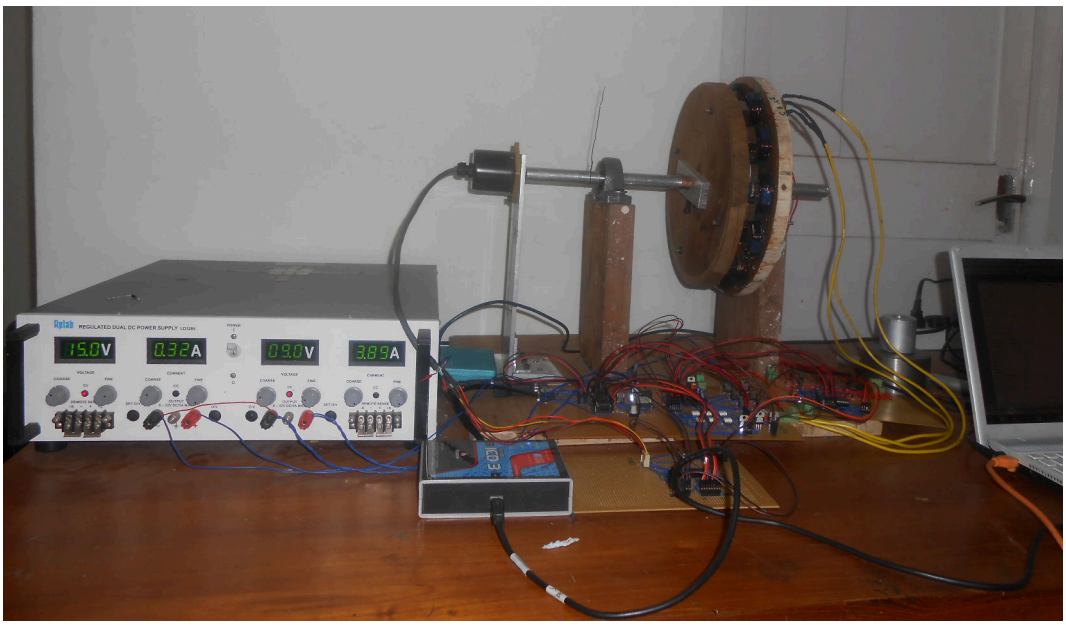

Fig. 6.8: Test set-up for axial flux motor consisting of motor, power supply, drive electronics, Microchip ICD3 programmer and encoder mounted on shaft.

6.3 Axial flux motor tests

Figure 6.8 shows the set-up for testing the axial flux motor. Equatorial telescopes require tracking in only one axis, i.e. RA axis. Perfect tracking of the stellar objects requires the RA axis of the telescope to be moved at a constant rate of 15″/sec. We have tested the axial flux motor performance in two operating conditions. These are open loop and closed loop(only proportional control) operation. The encoder used in the test is CP850 from Computer Optical Products. This encoder generates 1.25 million counts per revolution, which increases to 5 million counts per revolution after an interpolation of 4 provided by the encoder interface IC HCTL2022. In terms of angular resolution, it is 0.2596″, and we expect 57.87 counts/s when the motor moves at equatorial track rate. Due to this low count rate we were not able to close the control loop at a high rate, and only 4 Hz correction rate have been used, which is indeed very slow.

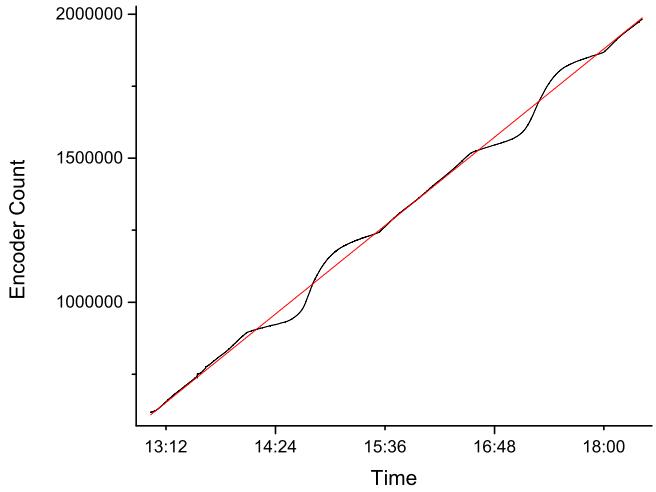

Fig. 6.9: Encoder value Vs. Time plot for axial flux motor for about 6 hours of operation, when motor is moving at equatorial track rate. Black curve shows the actual motor response, and red curve is the linear fit to the motor response.

6.3.1 Open Loop Operation

In open loop mode of operation, the motor is fed with 3-phase constant frequency sinusoidal voltage generated by the controller board and drive. No real time corrections were applied. Figure 6.9 shows the plot for Time Vs. Encoder count(black curve), when the motor moves at the equatorial rate. Linear fir (red curve) to the encoder count is also shown in the same figure. Duration of this experiment is 5 hours and 25 minutes.

From Figure 6.9, it is clear that on average the motor is able to move at the required track rate. However, there were oscillations in the motor response. Sometimes motor slows down and sometimes it speeds up. To investigate the reason behind these oscillations, we decided to move the motor by one full revolution. To keep the test time smaller, we decided to move the motor at a rate higher than the track rate. The time required by the motor to complete one rotation at this speed is 9

hours and 45 minutes. Figure 6.10 shows the plot (black curve) for Time Vs. Encoder counts for one full revolution of the motor. Linear fit (red curve) to the encoder count is also shown in the same figure.

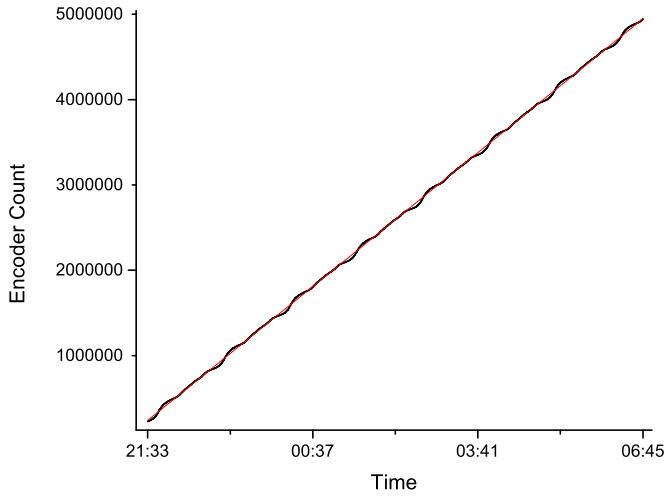

Fig. 6.10: Encoder value Vs. Time plot for axial flux motor for one full revolution.

Full rotation of the motor shows large amplitude oscillations in the motor's open loop response. The nature of these oscillations is strictly periodic. There are low amplitude oscillations present as well. The number of oscillations is 8, which is equal to the number of rotor pole pairs in the motor. This behavior resembles the stepper motor response operating in open loop condition in the microstepping mode. Friction (static and dynamic), detent effect and quantization (due to the drive and controller) are the factors which contribute to this type of response [1]. Figure 6.11 shows how the track (in terms of encoder count) error changes with time. The maximum position error of the motor shaft is as large as 50000 encoder counts (3.6 °).

[1] http://homepage.cs.uiowa.edu/~jones/step/micro.html

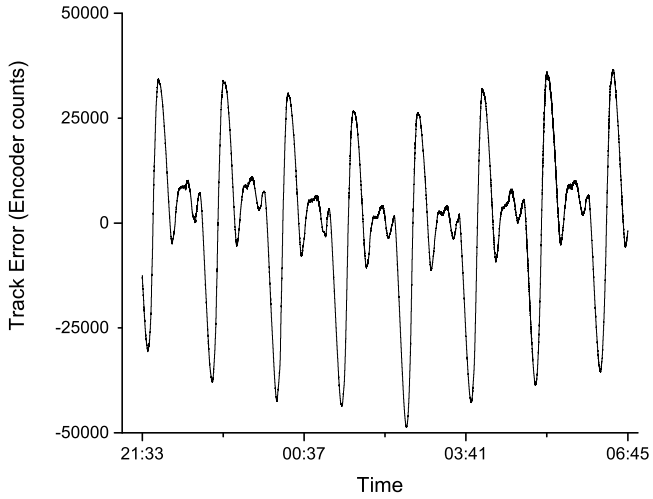

Fig. 6.11: Track error Vs. Time plot for axial flux motor for one full revolution.

6.3.2 Closed Loop Operation

To overcome the shortcomings of operating the motor in open loop mode and to get better tracking performance, we have implemented the closed loop in the drive and controller. Due to the limited encoder resolution (57.87 counts/s), we were unable to run the control loop better than 4 Hz. Also, we have used only the proportion control. Figure 6.12 shows the Encoder Count Vs. Time for the motor operation in closed loop condition for about 7 hours and 30 minutes of operation. Linear fit to the curve (red line) is also shown in the same figure. Operating the motor in closed loop removes the large amplitude oscillations from the motor as observed in open loop operation. Zoomed portion of the curve in Figure 6.12 is shown in Figure 6.13 for one minute of tracking.

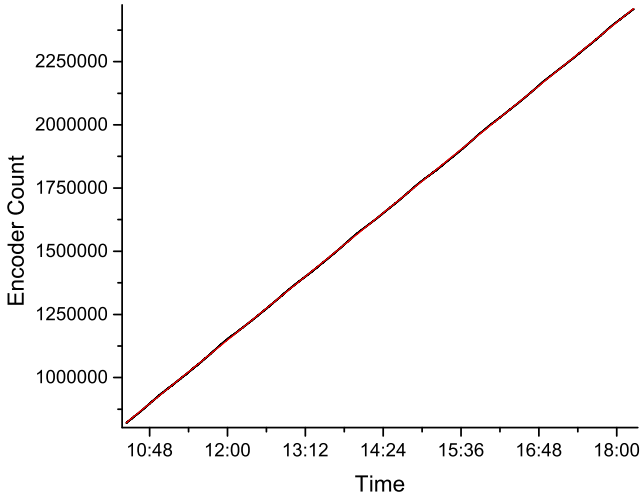

Fig. 6.12: Encoder count Vs. time (Black line) for the axial flux motor operation in closed loop condition, only proportional control is used. Linear fit to the curve is shown in red line.

Figure 6.14 shows the plot of Track Error Vs. Time for the similar duration of the motor operation. Use of proportional control removes the large amplitude oscillations. Now the maximum amplitude of oscillations is about 4000 counts (17.28′) as opposed to the 50000 counts (3.6°) of the open loop operation. Though it is a substantial improvement over the open loop performance, however, far from needed requirement for a telescope drive where it requires sub-arc second following error.

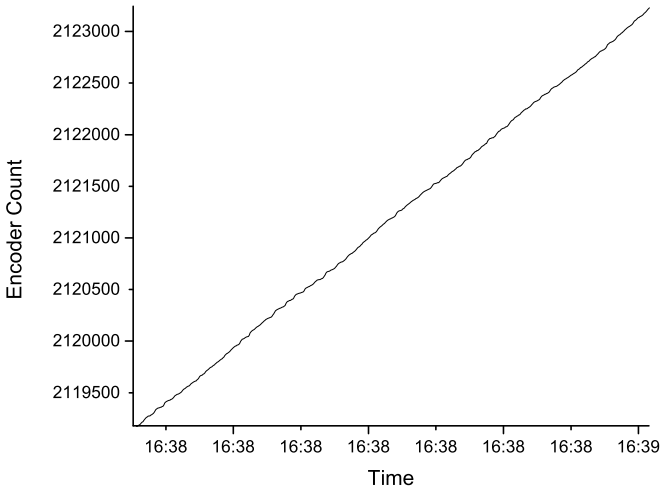

Fig. 6.13: Encoder count Vs. time for the axial flux motor operation in closed loop condition for one minute duration, only proportional control is used.

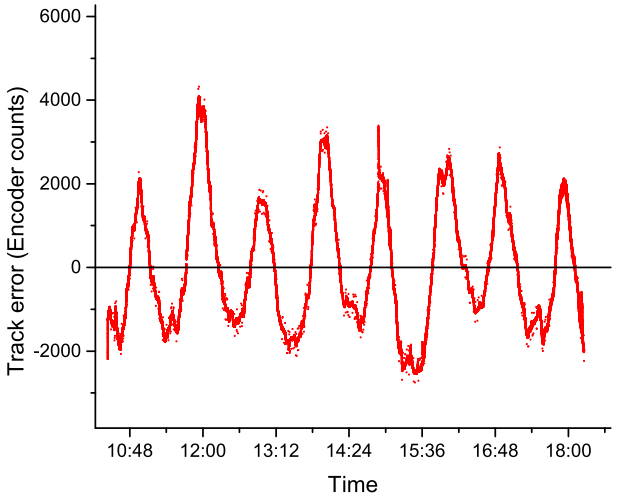

Fig. 6.14: Track error Vs. Time plot for axial flux motor for 7 Hour 30 minutes of motor operation.

One of the reasons for this large following error seems to be the implementation of velocity loop with only proportional control, that too at a slow correction rate of only 4Hz. If we close the loop for the position and torque (current) then we expect much

better performance. Other reasons may be limited encoder resolution, differences in the coils, magnets, and their geometries. Additionally, the structure of the stator and rotor is made of wood which is not mechanically very rigid and hence can introduce errors.

6.4 GPS

All telescopes need accurate time and location information for precise pointing and tracking of the stellar object. In case of Alt/Az Telescopes this information is very critical. Usually, time information is obtained from computers synchronized with time servers. But this system can introduce serious errors in case of network shutdown for a telescope located in a remote location like Hanle. Thus, we decided to use a GPS for obtaining both the time and location information. The GPS used is PMOD MT3329 from Digilent. Table 6.3 lists some of the specification of the GPS unit.

Table 6.3: Specifications of the PMOD MT3329 GPS.

Parameter	Value
Interface	UART
Default data Baud rate	9600 bps
Data protocol	NMEA
Antenna type	Inbuilt ceramic antenna with connector for external antenna
Operating voltage	3-3.6V
Update rate	1 Hz default (10 Hz maximum)
No. of channels	66
Positional accuracy	3m
Maximum Altitude	18000m
Maximum speed	515 m/s

GPS provides data through the serial portand also generates a 1 Hz output pulse, this can be used to synchronize other electronic circuitry and local clocks. The output data of the GPS follows the NMEA (National Marine Electronics Association) protocol. Output data contains many lines of strings, each line of string start with an

identifier (GPGGA, GPGSA, GPRMC, GPGSV, GPVTG). Time information is output by GPS in UT (Universal Time) format, and location is provided in latitude, longitude, and altitude format. Figure 6.15 shows the screen capture image of the LabVIEW-based software developed to extract the desired information from the GPS output strings. Figure 6.16 shows the path of the GPS device created by opening the logged data file in Google Earth.

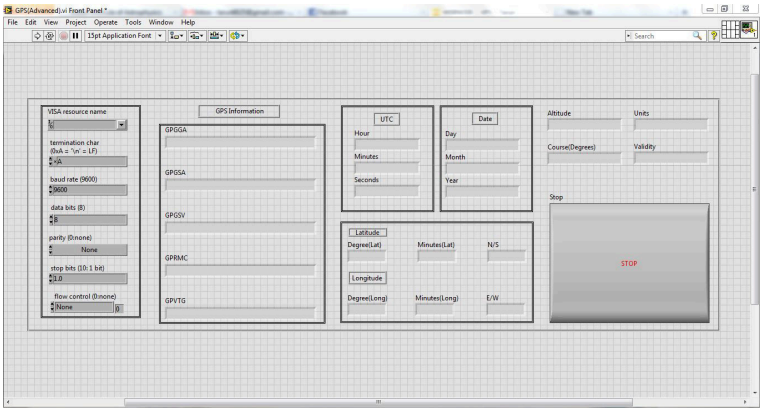

Fig. 6.15: Screen snapshot of LabVIEW base software developed for GPS information display.

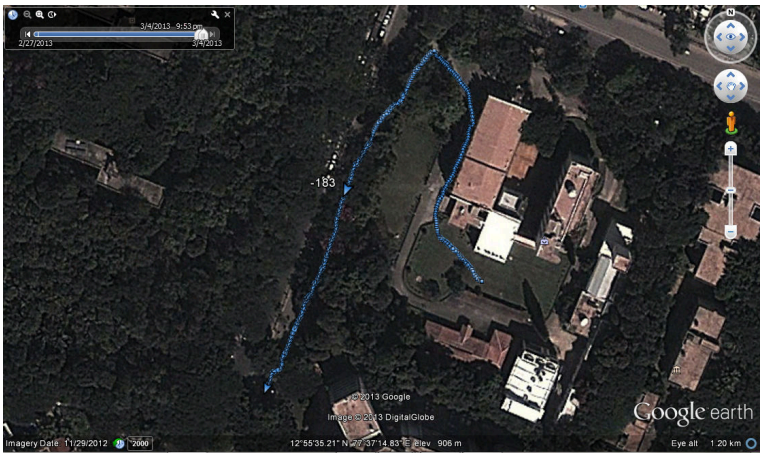

Fig. 6.16: Track of the GPS device created by opening the logged data file in Google Earth.

CHAPTER 7

CONCLUSION

The primary aim of this thesis was to develop new instruments for Astronomical site characterization, not just the replication of existing instruments. In this process, we have developed two very Innovative instruments. These are the Automated Extinction Monitor and the Scanning Cloud Monitor. Both of these instruments overcome the shortcomings associated with the use of existing instruments. We have also attempted to design and develop a direct drive based telescope for the MASS-DIMM instrument, which has been acquired from the TMT Project, USA.

7.1 AEM

Automated Extinction Monitor is a very innovative instrument in a sense that it takes off the burden from the larger telescope for measurement of extinction and sky-brightness. The same instrument is also used for variability studies, as the time

required for extinction measurement is just a part of the whole night. We have developed a fully automatic network-based instrument, which can be operated remotely. A commercially available telephoto lens attached with a CCD camera is mounted on customized equatorial telescope mount. Each telescope axes consist of a stepper motor, directly coupled high resolution encoder and a reduction gear ensure accurate pointing and open loop tracking performance. The robust telescope control system has been developed for the instrument. Intelligent software developed for the instrument facilitates the automatic operation. The whole devices is kept inside a sliding roof enclosure. The instrument has been installed at IAO Hanle and is in continuous use.

Table 7.1: Sky-brightness and atmospheric extinction as measured from HCT and AEM at IAO, Hanle.

Parameter	RMS	Corr. Coefficients
V-Bnad Sky Brightness(average)	21.54±0.37	21.57±0.14
V-Band Atmospheric Extinction(average)	0.120±0.04	0.111±0.043

With the data collected over 150 nights, we were able to generate interesting results for extinction, sky brightness and variability study. The results generated by AEM matches with the results obtained from the previous studies conducted using HCT telescope data. The average extinction in V-band at IAO Hanle is found to be 0.111±0.043, which is very close to the extinction determined by the HCT telescope. An effort has also been made to correlate extinction with weather parameters and search for the cause of variability. Table 4 lists the average V-Band sky brightness and atmospheric extinction measured using HCT telescope and AEM at IAO, Hanle. The automated extinction monitor is found to be very suitable for getting the reliable measurement of sky brightness. The average V-band sky brightness is found to be 21.57±0.14, which again very well matches with sky brightness measured using 2m HCT telescope. AEM can also detect the presence of thin clouds passing through the

local atmosphere, which otherwise remains unnoticed by other means of cloud monitoring. As expected AEM can also be very effectively used to discover/follow up a large number of bright variables.

In brief, AEM is indeed proven to be a very useful supporting instrument for any observatory. AEM can regularly monitor extinction and sky-brightness, and can generate a very accurate statistics which is otherwise not possible with larger telescopes. We hope to collect such useful data for many years to come and thoroughly characterize the Hanle, and other nearby sites.

7.2 All Sky Scanning Cloud Monitor

All Sky Scanning Cloud Monitor has been primarily developed to overcome the difficulties associated with the automatic data reduction of all-sky cameras working in visible wavelengths. This instrument relies on the measurement of sky temperature using thermopile sensors to distinguish between the clear and cloudy sky, and it consists of multiple IR sensors and scans the sky periodically. All the electronic boards like sensor interface board, data acquisition board, and stepper motor driver board are designed and developed in-house. LabVIEW based software analyzes the instrument data and generates various type of results like sky maps, percentage cloud cover, and relation with weather parameters. Sky maps generated by the instrument looks similar to the all-sky images, but not affected by the presence of the moon, milky way and stars.

A detailed laboratory and on-sky calibration schemes have been developed to calibrate the sensors so that very reliable estimate of sky temperature can be obtained. The instrument has gone through laboratory testing as well as field testing. From these tests, we found that indeed our scanning cloud monitor is a reliable and unique

instrument, free from shortcomings faced by other cloud monitoring devices. The instrument is installed at IAO Hanle and is in continuous operation.

Data collected over 65 nights has been analyzed, which clearly shows the dependency of sky temperature on the ground temperature and the ground level humidity. Measured sky temperature is also found to be dependent on the airmass, and the analysis software corrects for this effect. By making use of proper thresholding scheme, we could easily and reliably generate percentage cloud cover information from the collected data. We hope to produce an accurate statistics of cloud cover over Hanle with regular observation using the scanning cloud monitor.

7.3 Direct Drive Telescope for MASS-DIMM Instrument

The operation of the DIMM instrument installed on Meade telescope at IAO Hanle is found to be getting affected by the wind. Solution to above the problem is to develop a new Alt-Az mount telescope for the MASS-DIMM instrument. Direct drive technology has been selected for driving the telescope axes, which provides stiffness and the fast dynamic response. The telescope cross section area is minimized by using a truss OTA in place of the tube OTA. The designed telescope is also analyzed for various loading conditions using FEM method. We have also studied the effect of wind on the truss OTA. A commercial controller and drive will be used for driving the telescope. At present, the telescope is in the final stage of fabrication and will be ready by the end of July 2016. Complete telescope along with MASS-DIMM instrument is expected to start regular observation by end of year 2016.

Efforts was also made to design and build an axial flux direct drive motor, which can be used to drive a medium size telescope. A COMSOL Multiphysics model of the motor was developed, and various motor parameters are calculated. We have also

developed a Sinusoidal PWM based drive and controller, which can drive the motor at a slow speed required for the telescope operation. Same drive and controller has been used to test the commercial motor used in the telescope and the axial flux motor. Drive performance was found to be satisfactory. In future, we hope to achieve much-improved drive and motor performance by making use of vector control in place of Sinusoidal PWM control scheme.

REFERENCES

Akerlof, C. Rapid Optical Follow-up Observations of SGR Events with ROTSE-I. *ApJ*, 542:251–256, 2000. doi: 10.1086/309535.

Ananthasubramanian, P. G., Yamamoto, S., Prabhu, T. P., and Angchuk, D. Measurements of 220 GHz atmospheric transparency at IAO, Hanle, during 2000-2003. *BASI*, 32:99, 2004.

Angione, R. J. and de Vaucouleurs, G. Twenty years of atmospheric extinction at McDonald Observatory. *PASP*, 98:1201–1207, 1986. doi: 10.1086/131922.

Arne, A. H. and Ronald, H. K. *Astronomical Photometry, Text and Handbook for the Advanced Amateur and Professional Astronomer*. Willmann-Bell, Virginia 23235 USA, 1990.

B. Kumar et. al. Sky Transparency over Naini Tal : A perspective study. In *BASI*, volume 28, pages 675–686, 2000.

Bakos, G. Wide-Field Millimagnitude Photometry with the HAT: A Tool for Extrasolar Planet Detection. *PASP*, 116:266–277, 2004. doi: 10.1086/382735.

Bely, P. Y. *The Design and Construction of Large Telescopes*. Springer, 2003.

Bessell, M. S. UBVRI passbands. PASP, 102:1181–1199, 1990.

Bhatt, B. C., Prabhu, T. P., and Anupama, G. C. Site characteristics of The Indian Astronomical Observatory, Hanle. *BASI*, 28:441–443, 2000.

B.Howell, S. Two-dimensional aperture photometry - Signal-to-noise ratio of point-source observations and optimal data-extraction techniques. PASP, 101:616–622, 1989.

Burki, G. The atmospheric extinction at the E.S.O. La Silla observatory. *A&AS*, 112:383, 1995.

Buton, C. Atmospheric extinction properties above Mauna Kea from the Nearby SuperNova Factory spectro-photometric data set. *A&A*, 549:A8, 2013. doi: 10.1051/0004-6361/201219834.

C. S. Stalin et. al. Night sky at the Indian Astronomical Observatory during 2000–2008. In *BASI*, volume 36, pages 111–127, 2008.

Cowsik, R., Srinivasan, R., and Prabhu, T. Indian Astronomical Observatory, Hanle. In *Astronomical Site Evaluation in the Visible and Radio Range*, volume 266, page 424, 2002a.

Cowsik, R., Srinivasan, R., and Prabhu, T. P. An introduction to the Indian Astronomical Observatory, Hanle. *Bulletin of the Astronomical Society of India*, 30:105–114, 2002b.

D. L. Pollacco et. al. The WASP Project and the SuperWASP Cameras. *PASP*, 118:1407–1418, 2006. doi: 10.1086/508556.

Everett, M. E. and Howell, S. B. A Technique for Ultrahigh-Precision CCD Photometry. PASP, 113: 1428–1435, 2001.

Garcia-Gil, A., Munoz-Tunon, C., and Varela, A. M. Atmosphere Extinction at the ORM on La Palma: A 20 yr Statistical Database Gathered at the Carlsberg Meridian Telescope. *PASP*, 122:1109–1121, 2010. doi: 10.1086/656329.

Gieras, J. F., Wang, R.-J., and Kempar, M. J. *Axial Flux Permanent Magnet Brushless Machines*. Springer, 2004.

Gilliland, R. L. and Brown, T. M. Time-resolved CCD photometry of an ensemble of stars. PASP, 100: 754–765, 1988.

Hardy, J. W. *Adaptive Optics for Astronomical Telescopes*. Oxford, 1998.

Hayes, D. S. and Latham, D. W. A rediscussion of the atmospheric extinction and the absolute spectral-energy distribution of VEGA. *ApJ*, 197:593–601, 1975.

Il'Yasov, S. P., Baizhumanov, A. K., Sarazin, M., Sultanov, K. B., and Egamberdiev, S. A. Measurement of night seeing at Mount Maidanak with the ESO differential image motion monitor. *Astronomy Letters*, 25:122–125, 1999.

J. Sebag et. al. LSST all-sky IR camera cloud monitoring test results. In *Society of Photo-Optical Instrumentation Engineers (SPIE) Conference Series*, volume 7733, page 48, 2010. doi: 10.1117/12.856337.

Kornilov, V., Tokovinin, A. A., Vozyakova, O., et al. MASS: a monitor of the vertical turbulence distribution. In *Adaptive Optical System Technologies II*, volume 4839 of Proc. SPIE, pages 837–845, 2003.

Kornilov, V., Tokovinin, A., Shatsky, N., et al. Combined MASS-DIMM instruments for atmospheric turbulence studies. *MNRAS*, 382:1268–1278, 2007. doi: 10.1111/j.1365-2966.2007.12467.x.

Kornilov, V., Ilyasov, S., Vozyakova, O., et al. Measurements of optical turbulence in the free atmosphere above Mount Maidanak in 2005-2007. *Astronomy Letters*, 35:547–554, 2009.

L. Shamir and R. J. Nemiroff. All-Sky Relative Opacity Mapping Using Nighttime Panoramic Images. *PASP*, 117:972–977, 2005. doi: 10.1086/432689.

Lockwood, G. W. and Thompson, D. T. Atmospheric extinction - The ordinary and volcanically induced variations, 1972-1985. *AJ*, 92:976–985, 1986.

M. C. B. Ashley and J. S. Jurcevic. A cloud detector for automated telescopes. *Proceedings of the Astronomical Society of Australia*, 9:334, 1991.

M. Suganuma et. al. The Infrared Cloud Monitor for the MAGNUM Robotic Telescope at Haleakala. *PASP*, 119:567–582, 2007. doi: 10.1086/518697.

McCormick, M. P. and Veiga, R. E. SAGE II measurements of early Pinatubo aerosols. Geophys. Res. Lett., 19:155–158, 1992.

Metlov, V. G. Seasonal and long-term variations in the atmospheric extinction in Crimea on the basis of the 1979-2002 observations. *Astronomical and Astrophysical Transactions*, 23:197–207, 2004. doi: 10.1080/1055679031000153879.

Mohan, V., Uddin, W., Sagar, R., and Gupta, S. K. Atmospheric extinction at Devasthal, Naini Tal. *Bulletin of the Astronomical Society of India*, 27:601, 1999.

Parihar, P., Messina, S., Distefano, E., Shantikumar, N. S., and Medhi, B. J. Exploring pre-main-sequence variables of the ONC: the new variables. MNRAS, 400:603–621, 2009.

Patat, F. A robust algorithm for sky background computation in CCD images. *A&A*, 401:797–807, 2003. doi: 10.1051/0004-6361:20030137.

Pojmanski, G. The All Sky Automated Survey. *Acta Astronomica*, 47:467–481, 1997.

Poretti, E. and Zerbi, F. Spurious effects in presence of a variable extinction coefficient in photoelectric photometry. *A&A*, 268:369–373, 1993a.

Poretti, E. and Zerbi, F. Spurious effects in presence of a variable extinction coefficient in photoelectric photometry. A&A, 268:369–373, 1993b.

Prabhu, T. P. Indian Astronomical Observatory, Leh-Hanle. *Proceedings of the Indian National Science Academy Part A*, 80:887–912, 2014.

R. Sloan and J. H. Shaw and D. Williams. Infrared Emission Spectrum of the Atmosphere. *Optical society of America*, 45:455, 1955.

R. W. Clay et. al. A Cloud Monitoring System for Remote Sites. *Proceedings of the Astronomical Society of Australia*, 15:332–335, 1998. doi: 10.1071/AS98332.

Reimann, H. G., Ossenkopf, V., and Beyersdorfer, S. Atmospheric extinction and meteorological conditions - A long time photometric study. *A&A*, 265:360–369, 1992.

Rufener, F. The evolution of atmospheric extinction at La Silla. A&A, 165:275–286, 1986.

S. Stefan, et. al. VLT ASTRONOMICAL SITE MONITOR: CONTROL, AUTOMATION, AND DATA FLOW. *SPIE Proceedding Advanced Telescope and Instrumentation Control Software, Ed. Hilton Lewis Munich, Germany, 2000*, 4009:338, 2000. doi: 10.1117/12.388404.

Sarazin, M. and Roddier, F. The ESO differential image motion monitor. *A&A*, 227:294–300, 1990.

Schilz, J. Remote Temperature Measurement with Perkin Elmer Thermopile Sensors (Pyrometry): A Practical Guide to Quantative Results. Technical report, PerkinElmer, 2001. URL `http://www.mantech.co.za/Technical/Attachments/TEMP_MEASUREMENT.PDF`.

Schilz, J. Thermoelectric Infrared Sensors (Thermopile) for Remote Temperature measurement; Pyromerty. Technical report, PerkinElmer, 2011. URL `https://www.tuhh.de/mt/ftir/lib/RemoteTemperature/pyrometry.pdf`.

Smith, W. J. *Modern Optical Engineering, The design of Optical Systems, Optical and Electro-Optical Engineering Series*. McGraw Hill, 1990.

Steinbring, E., Cuillandre, J. C., and Magnier, E. Mauna Kea Sky Transparency from CFHT SkyProbe Data. *PASP*, 121:295–302, 2009. doi: 10.1086/597766.

Sterken, C. and Jerzykiewicz, M. Atmospheric extinction coefficients in the UVBY system for La Silla. A&AS, 29:319, 1977.

Sterken, C. and Manfroid, J. The evolution of atmospheric extinction at La Silla derived from measurements in the Stromgren photometric system. *A&A*, 266:619–627, 1992.

T. E.Pickering. The MMT all-sky camera. In *Society of Photo-Optical Instrumentation Engineers (SPIE) Conference Series*, volume 6267, page 1, 2006. doi: 10.1117/12.672508.

T. K. Sharma and P. S. Parihar. Network Based Data Acquisition and Logging System using PIC Microcontroller. *International Journal of Engineering (IJE)*, 8:22–29, 2014.

Tokovinin, A. From Differential Image Motion to Seeing. *PASP*, 114:1156–1166, 2002.

Tokovinin, A. Turbulence profiles from the scintillation of Stars, Planets, and Moon. In *Revista Mexicana de Astronomia y Astrofisica Conference Series*, volume 31 of *Revista Mexicana de Astronomia y Astrofisica Conference Series*, pages 61–70, 2007.

Tokovinin, A. and Kornilov, V. Accurate seeing measurements with MASS and DIMM. *MNRAS*, 381: 1179–1189, 2007. doi: 10.1111/j.1365-2966.2007.12307.x.

Tug, H. Vertical Extinction on La Silla. *The Messenger*, 11:7–8, 1977.

W. Skidmore et. al. All Sky Camera Observations of Cloud and Light Pollution at Thirty Meter Telescope Candidate Sites. In *Revista Mexicana de Astronomia y Astrofisica Conference Series*, volume 41, pages 70–73, 2011.

Weber, R. J. and McMurry, P. H. Fine particle size distribution at Mouna Lua Observatory, Hawaii. *Journal of Geophysical Research*, 101:14767–14775, 1996.

Yao, Y., Wang, H., Liu, L., et al. Site characterization studies in high plateau of Tibet. In *Ground-based and Airborne Telescopes IV*, volume 8444 of Proc. SPIE, page 84441K, 2012.

Ye, Q. Z., Su, M., Li, H., and Zhang, X. Tibet's Ali: Asia's Atacama? MNRAS, 457:L1–L4, 2016.

Appendix

APPENDIX A

CONTROLLER BOARD SCHEMATIC

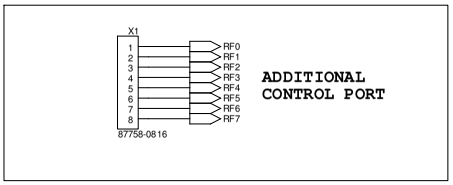

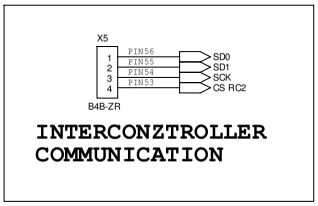

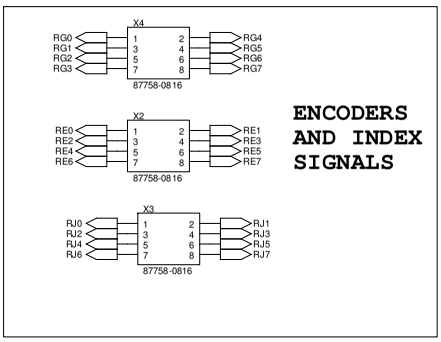

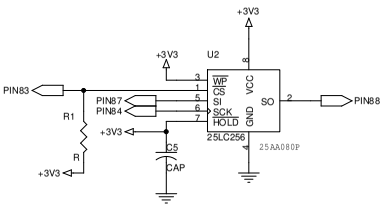

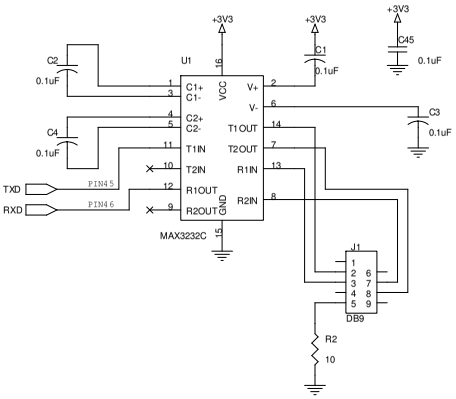

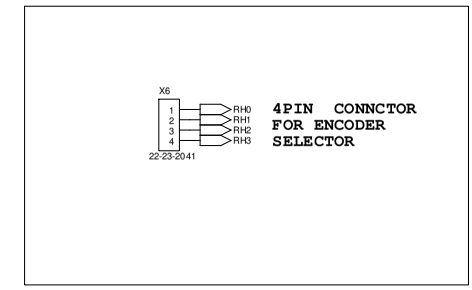

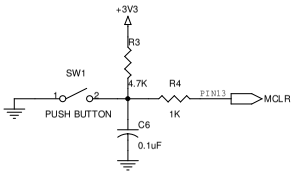

Title	<Title>	
Size B	Document Number <Doc>	Rev <RevCode>
Date: Thursday, June 30, 2011	Sheet 1 of 6	

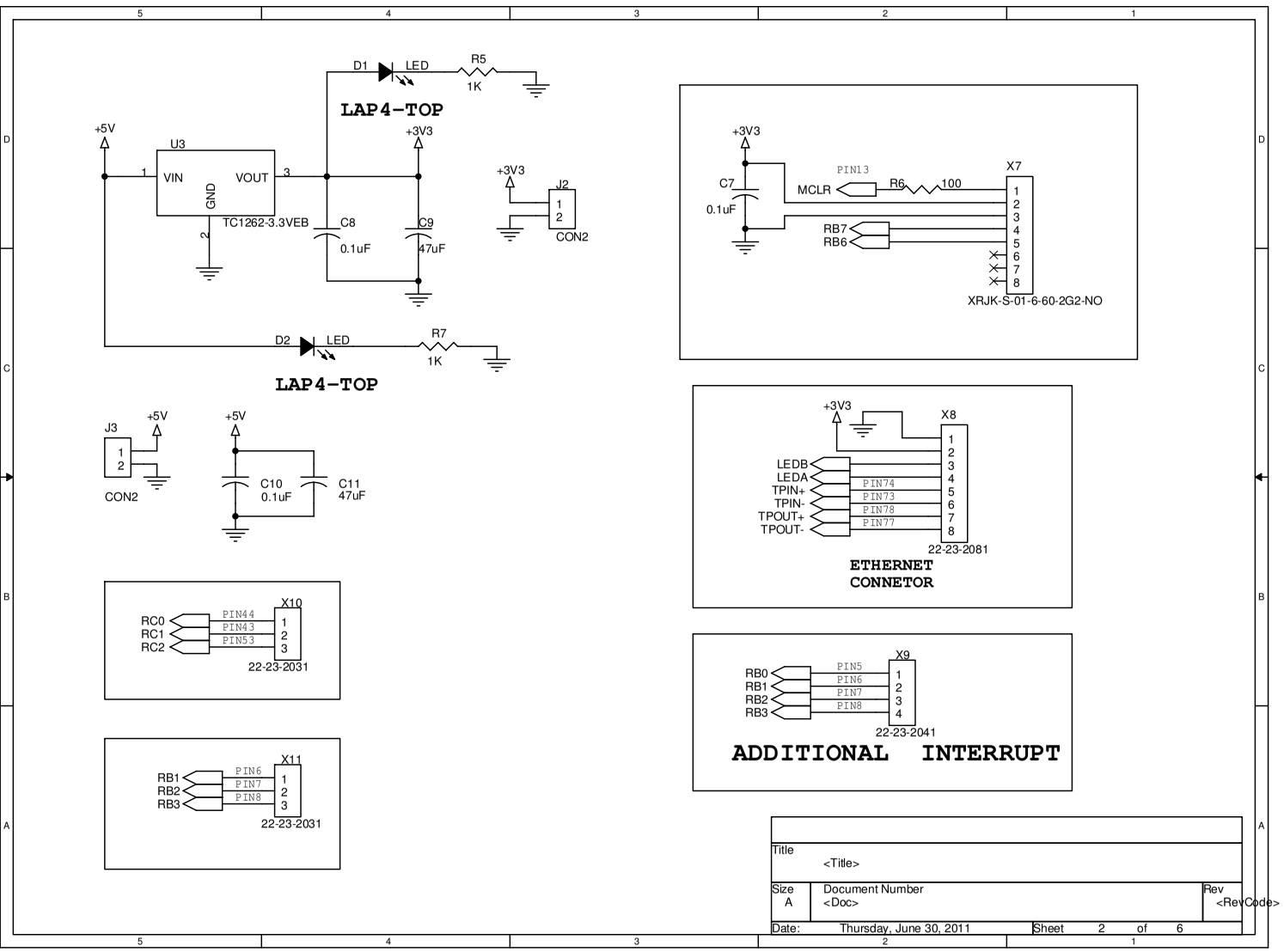

Title <Title>		
Size A	Document Number <Doc>	Rev <RevCode>
Date: Thursday, June 30, 2011	Sheet 2 of 6	

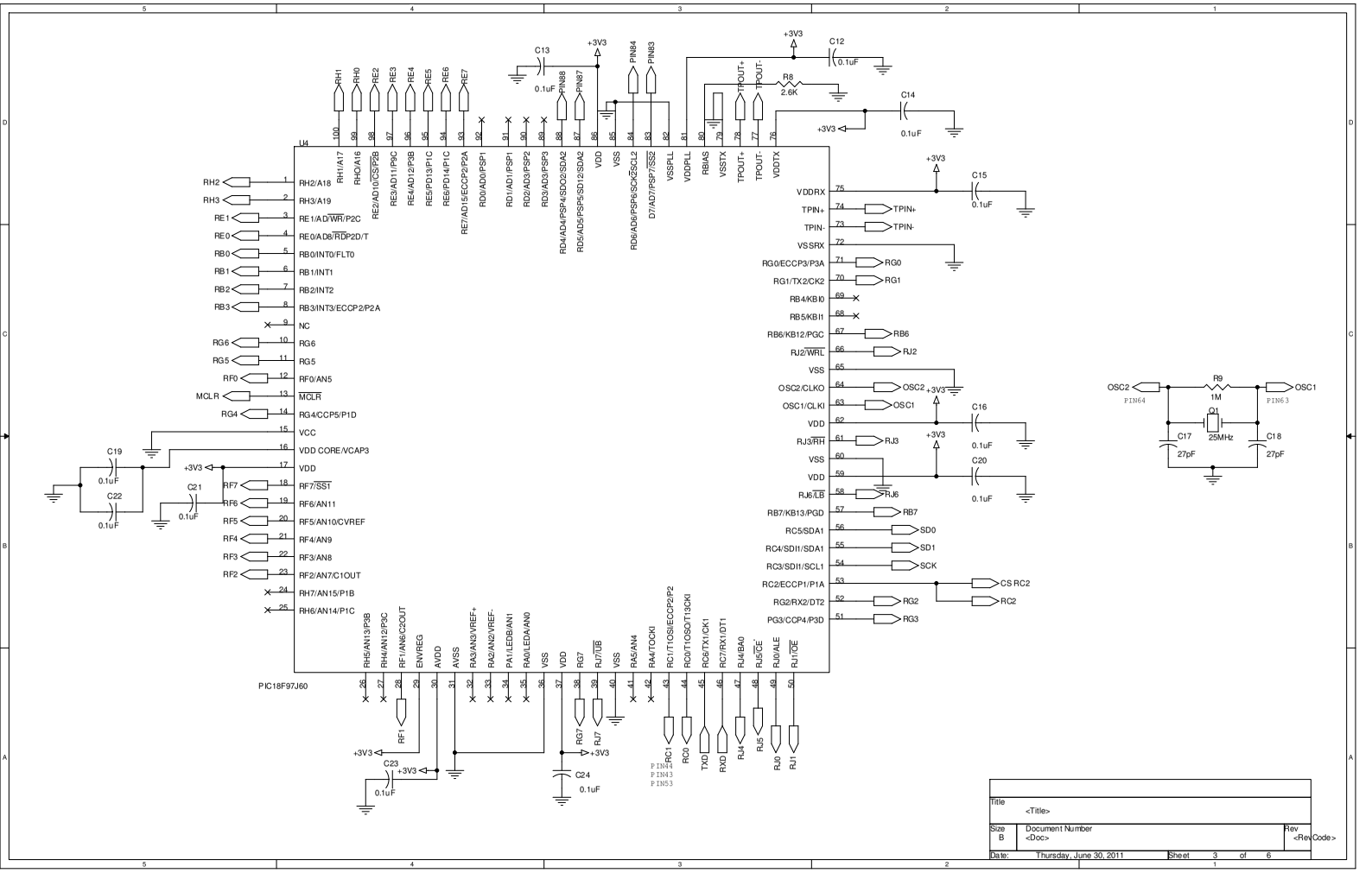

Title	<Title>	
Size B	Document Number <Doc>	Rev <RevCode>
Date: Thursday, June 30, 2011	Sheet 3 of 6	

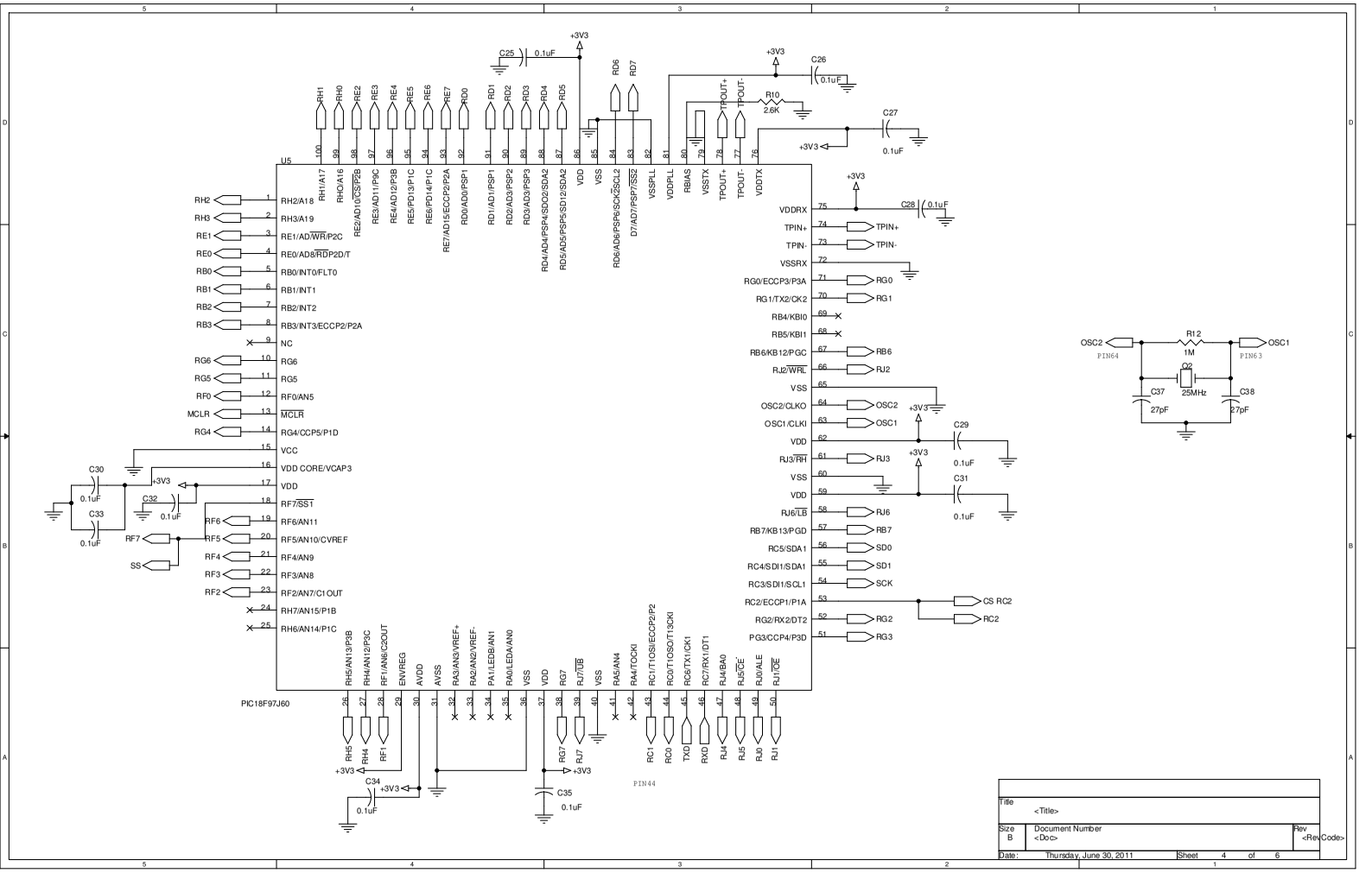

Title	<Title>	
Size B	Document Number <Doc>	Rev <RevCode>
Date: Thursday, June 30, 2011	Sheet 4 of 6	

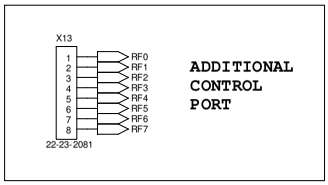

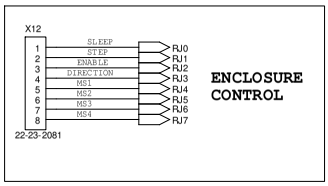

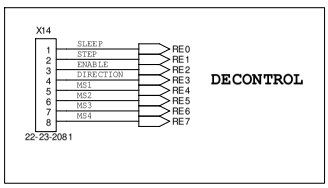

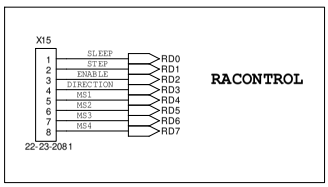

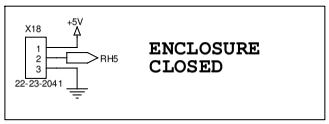

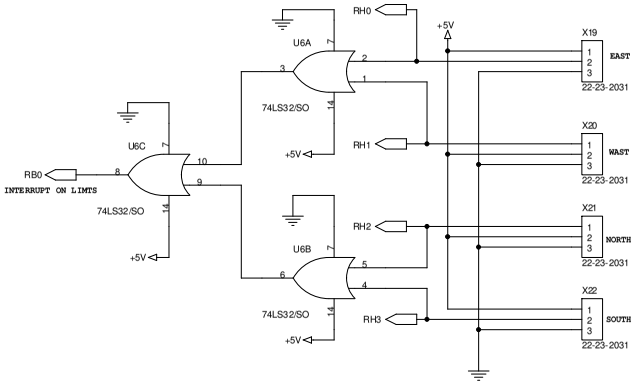

Title	<Title>	
Size B	Document Number <Doc>	Rev <RevCode>
Date: Thursday, June 30, 2011	Sheet 5 of 6	

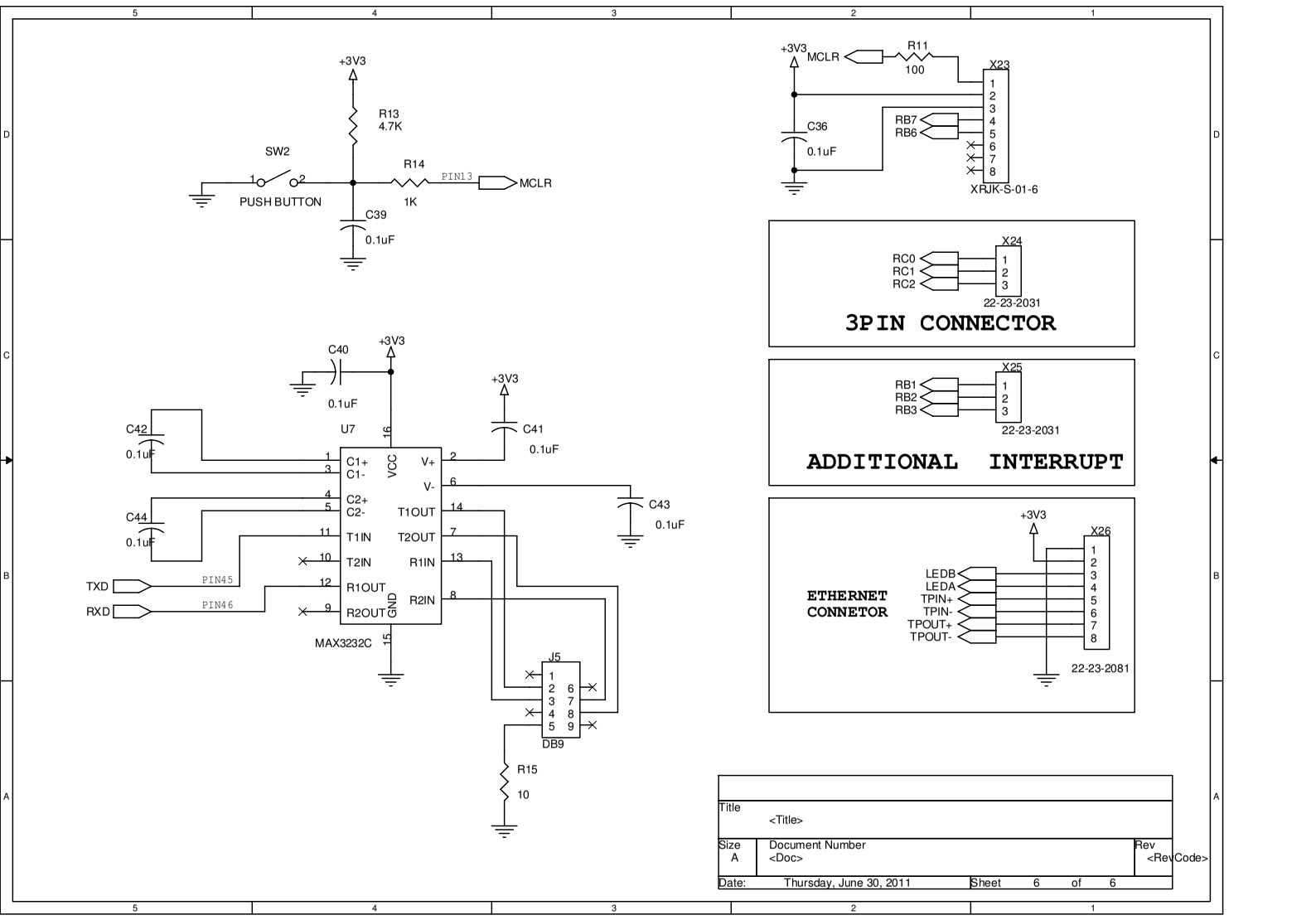

Title	<Title>	
Size A	Document Number <Doc>	Rev <RevCode>
Date: Thursday, June 30, 2011	Sheet 6 of 6	

APPENDIX B

STEPPER MOTOR DRIVER BOARD SCHEMATIC

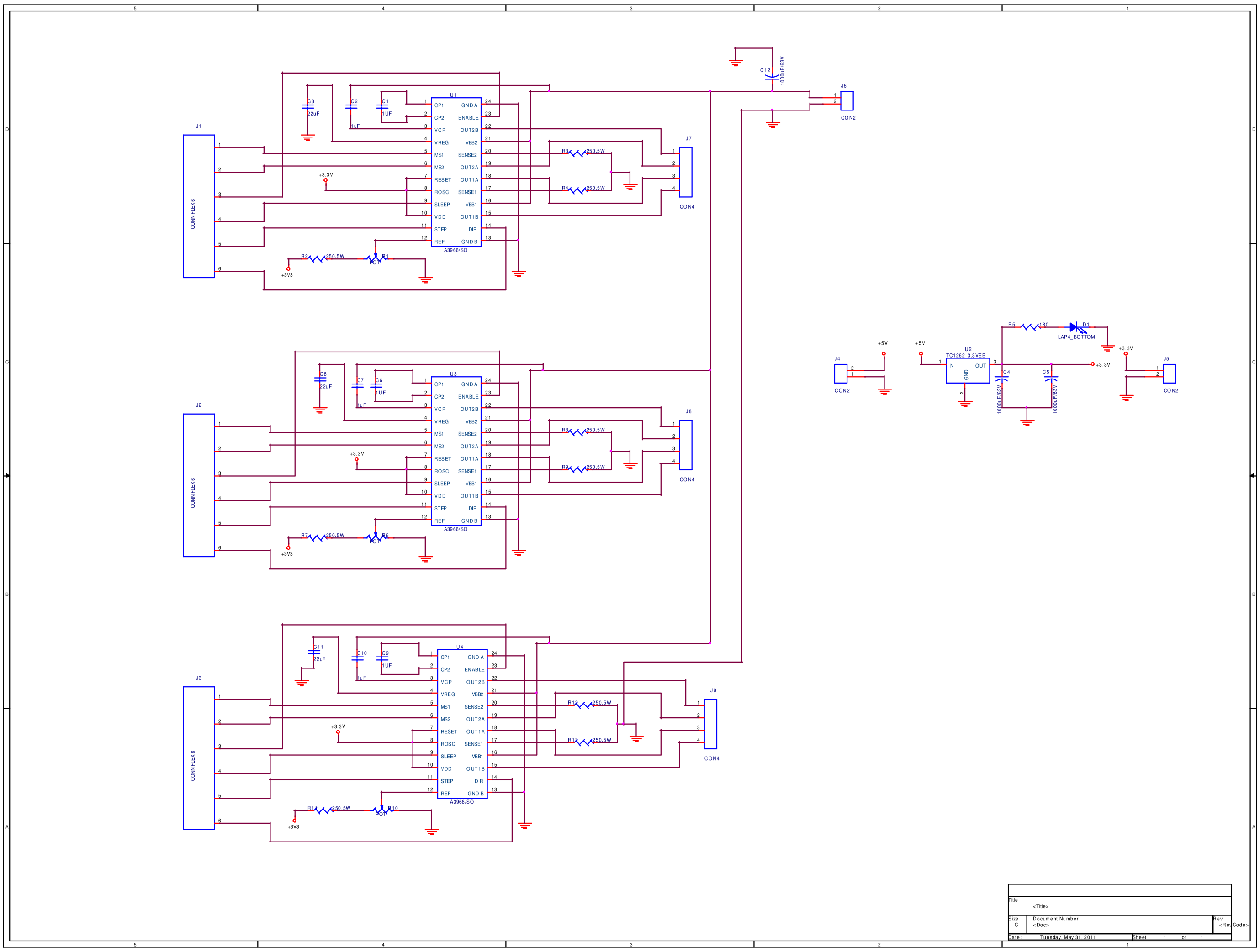

J1
CONN FLEX 6
U1
A3966/SO
J2
U3
J3
U4
J7
J8
J9
CON4
J6
CON2
C12
1000uF/63V
J4
J5
U2
TC1262_3.3VEB
+5V
+3.3V
+3V3
LAP4_BOTTOM
Title
<Title>
Size
C
Document Number
<Doc>
Rev
<RevCode>
Date:
Tuesday, May 31, 2011
Sheet
1
of
1

APPENDIX C

ENCODER PROCESSOR AND MULTIPLEXER BOARD SCHEMATIC

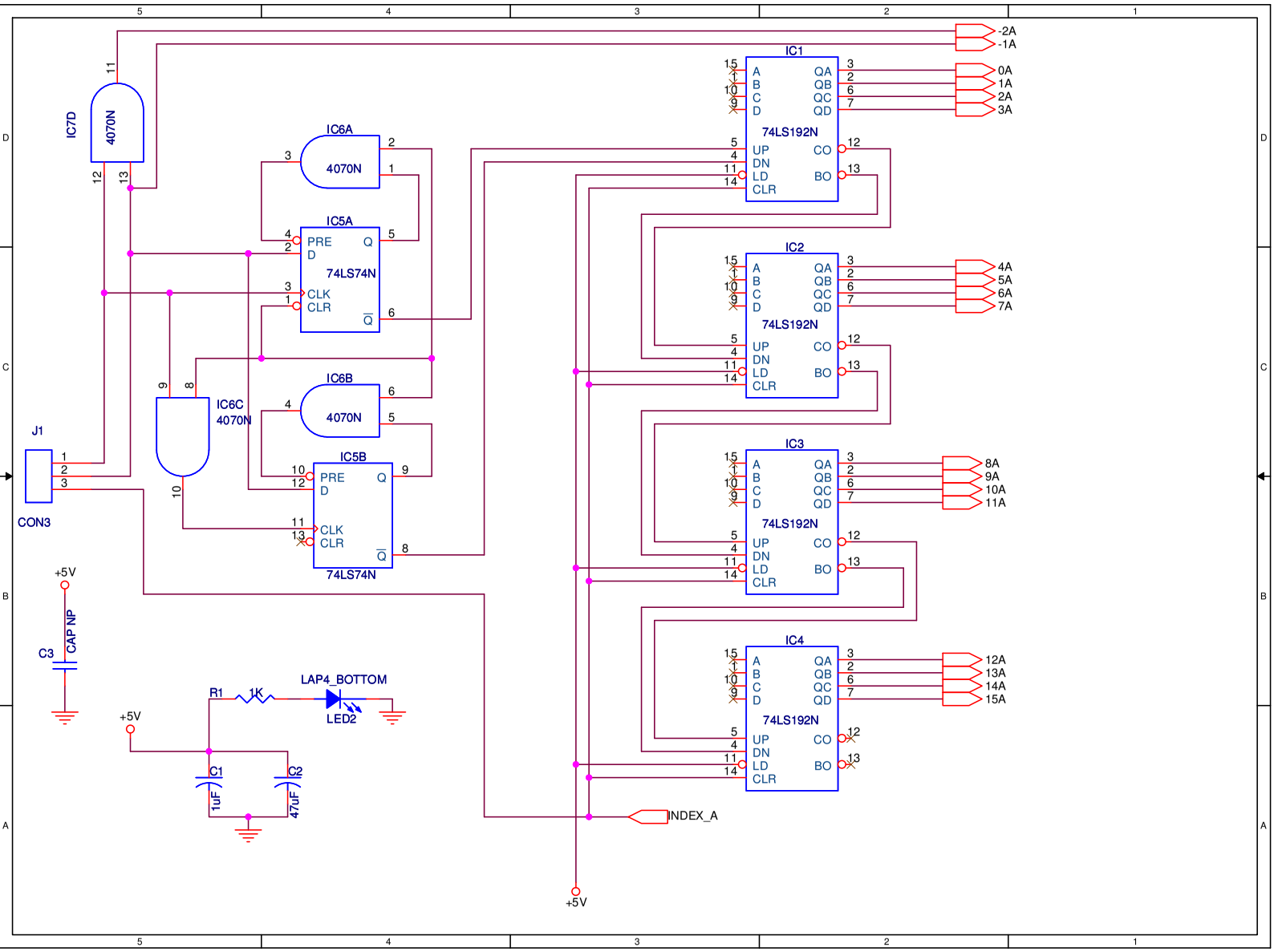
IC7D
4070N
IC6A
4070N
IC5A
PRE
D
74LS74N
CLK
CLR
Q
IC6B
4070N
IC6C
4070N
IC5B
PRE
D
74LS74N
CLK
CLR
Q
J1
CON3
+5V
C3
CAP NP
R1
1K
LAP4_BOTTOM
LED2
C1
1uF
C2
47uF
IC1
74LS192N
A
B
C
D
QA
QB
QC
QD
UP
DN
LD
CLR
CO
BO
IC2
74LS192N
IC3
74LS192N
IC4
74LS192N
-2A
-1A
0A
1A
2A
3A
4A
5A
6A
7A
8A
9A
10A
11A
12A
13A
14A
15A
INDEX_A
+5V

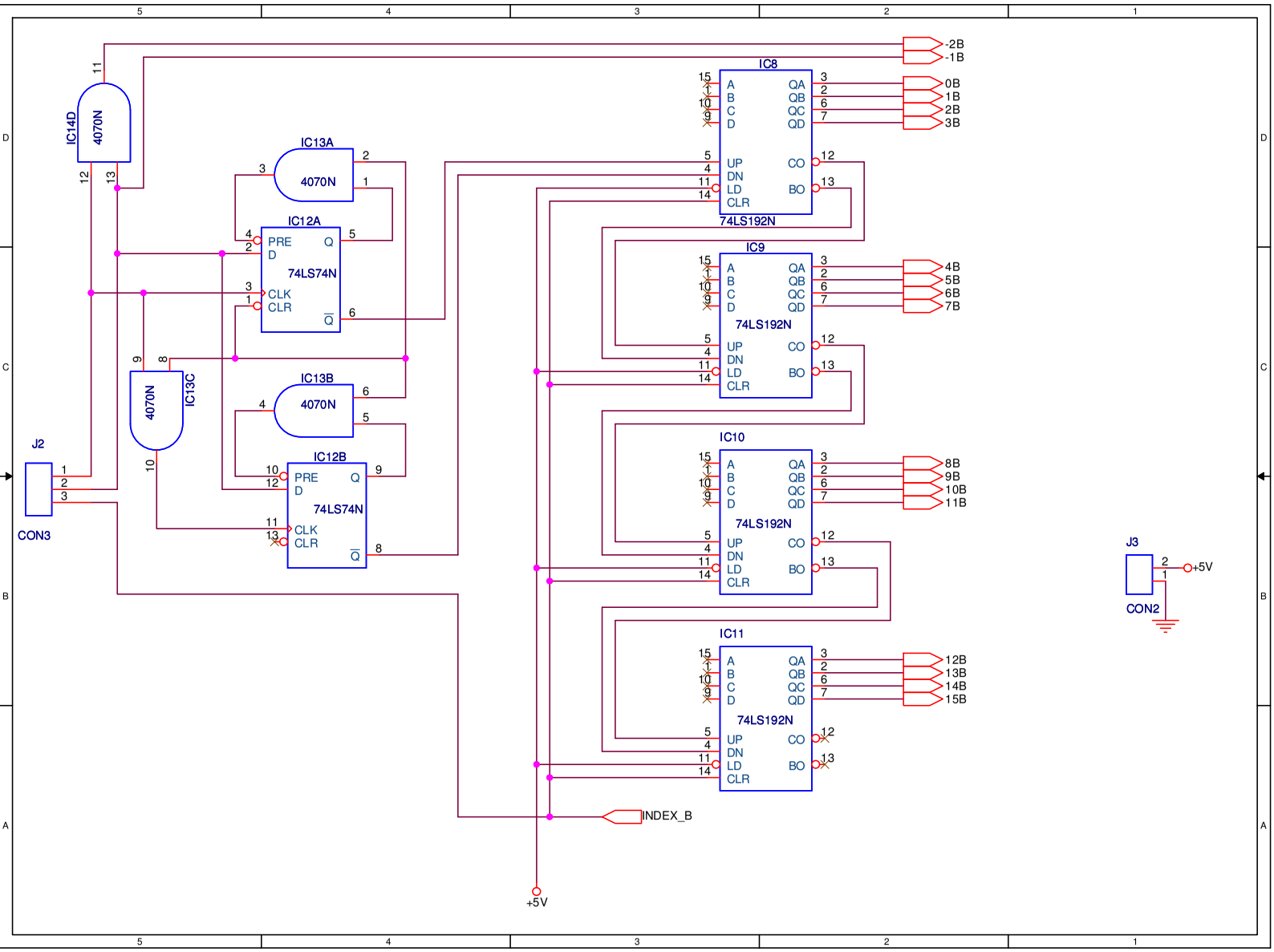
IC14D
4070N
IC13A
4070N
IC12A
PRE
D
74LS74N
CLK
CLR
Q
IC13B
4070N
IC12B
PRE
D
74LS74N
CLK
CLR
Q
IC13C
4070N
J2
CON3
IC8
A
B
C
D
QA
QB
QC
QD
UP
DN
LD
CLR
CO
BO
74LS192N
IC9
74LS192N
IC10
74LS192N
IC11
74LS192N
-2B
-1B
0B
1B
2B
3B
4B
5B
6B
7B
8B
9B
10B
11B
12B
13B
14B
15B
INDEX_B
+5V
J3
CON2
+5V

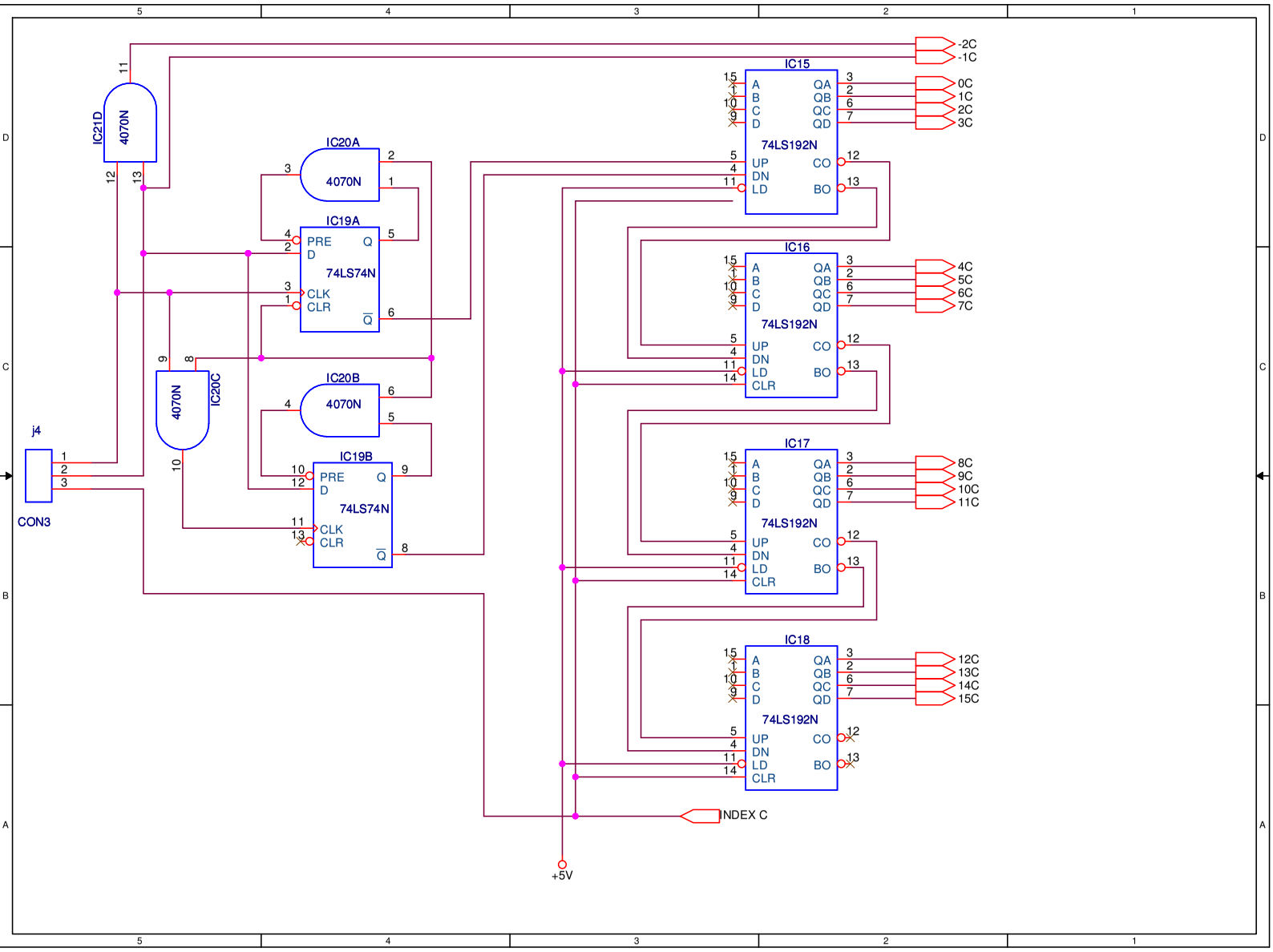
IC21D
4070N
IC20A
4070N
IC19A
PRE
D
74LS74N
CLK
CLR
Q
IC20B
4070N
IC19B
PRE
D
74LS74N
CLK
CLR
Q
IC20C
4070N
j4
CON3
IC15
IC16
IC17
IC18
A
B
C
D
QA
QB
QC
QD
74LS192N
UP
DN
LD
CLR
CO
BO
-2C
-1C
0C
1C
2C
3C
4C
5C
6C
7C
8C
9C
10C
11C
12C
13C
14C
15C
INDEX C
+5V

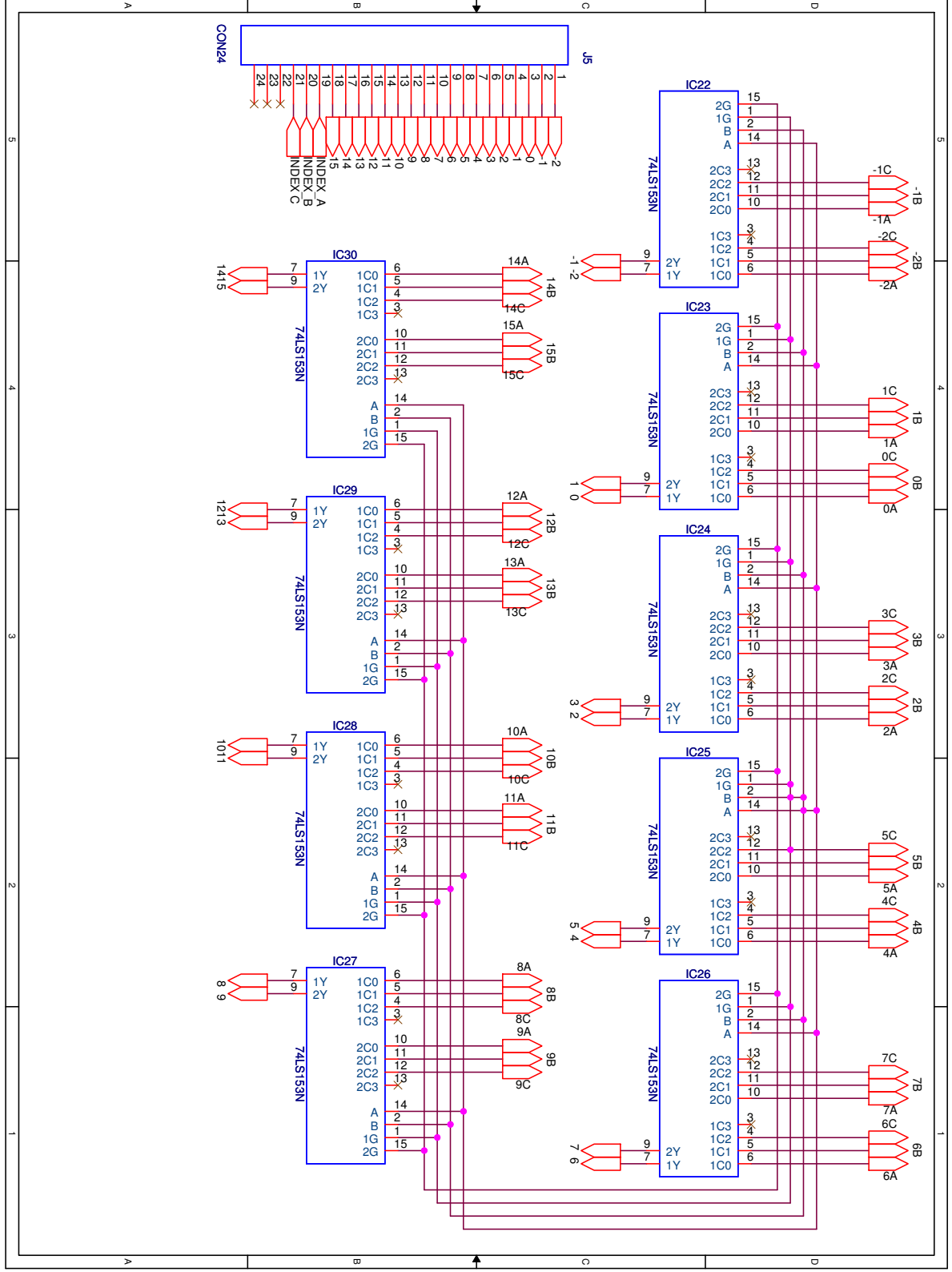
CON24
J5
INDEX_A
INDEX_B
INDEX_C
IC22
IC23
IC24
IC25
IC26
IC27
IC28
IC29
IC30
74LS153N
-1C
-1B
-1A
-2C
-2B
-2A
1C
1B
1A
0C
0B
0A
3C
3B
3A
2C
2B
2A
5C
5B
5A
4C
4B
4A
7C
7B
7A
6C
6B
6A
8A
8B
8C
9A
9B
9C
10A
10B
10C
11A
11B
11C
12A
12B
12C
13A
13B
13C
14A
14B
14C
15A
15B
15C

APPENDIX D

CONTROL SIGNALS FOR STEPPER MOTOR DRIVER

Following are the control signals which are generated by the Stepper Motor Driver Controller to operate the driver board:-

RESET Input (RESET):-

The RESET input is used for resetting the driver operation. A low signal on this input pin sets the driver translator to the initial state. This also disables the internal MOSFET outputs, and drive ignores all other inputs as long as this pin is brought back to high level.

Step Input (STEP):-

STEP input causes the driver translator to increase or decrease by one count, depending upon the logic present at the DIRECTION input. Internally the driver changes the phase currents of the motor and causes it to move by a step.

Microstep Select (MS1 and MS2):-

These two lines are used to set the microstepping mode of the driver. Depending upon the logic, the motor can move full, half, quarter or 1/16 step. Table D.1 shows the MS1 and MS2 logic, and the corresponding micro-stepping mode.

Table D.1: Microstep resolution selection table for stepper motor driver.

MS1	MS2	Microstep	Excitation Mode
L	L	Full step	2 Phase
H	L	Half step	1-2 Phase
L	H	Quarter step	W1-2 Phase
H	H	Sixteenth step	4W1-2 Phase

Direction Input (DIR):-

The DIR input determines the motor rotation direction. A low on this input causes the motor to rotate clockwise, and High causes anti-clockwise rotation.

Enable Input (ENABLE):-

A High logic on this input pin disables the driver operation. The driver does not respond to other input signals as long as this pin remains at High level.

Sleep Mode (SLEEP):-

A Low logic on this pin causes the driver to enter SLEEP mode. In sleep mode, most of the internal circuitry of the driver is disabled to reduce the power consumption.

Internal PWM Current Control:-

Apart from the digital inputs described above, the driver board also accepts an analog input V_{ref}. This input is used to set the maximum current limit for the motor operation. Expression for the maximum current limit $I_{TripMax}$ in Amps is given as

$$I_{TripMax} = \frac{V_{ref}}{(8 \times R_s)} \tag{D.1}$$

Where R_s is the resistance of the sense resistor (Ω) and V_{ref} is the input voltage on the REF pin (V).

APPENDIX E

EXTINCTION PLOTS AND TABLES

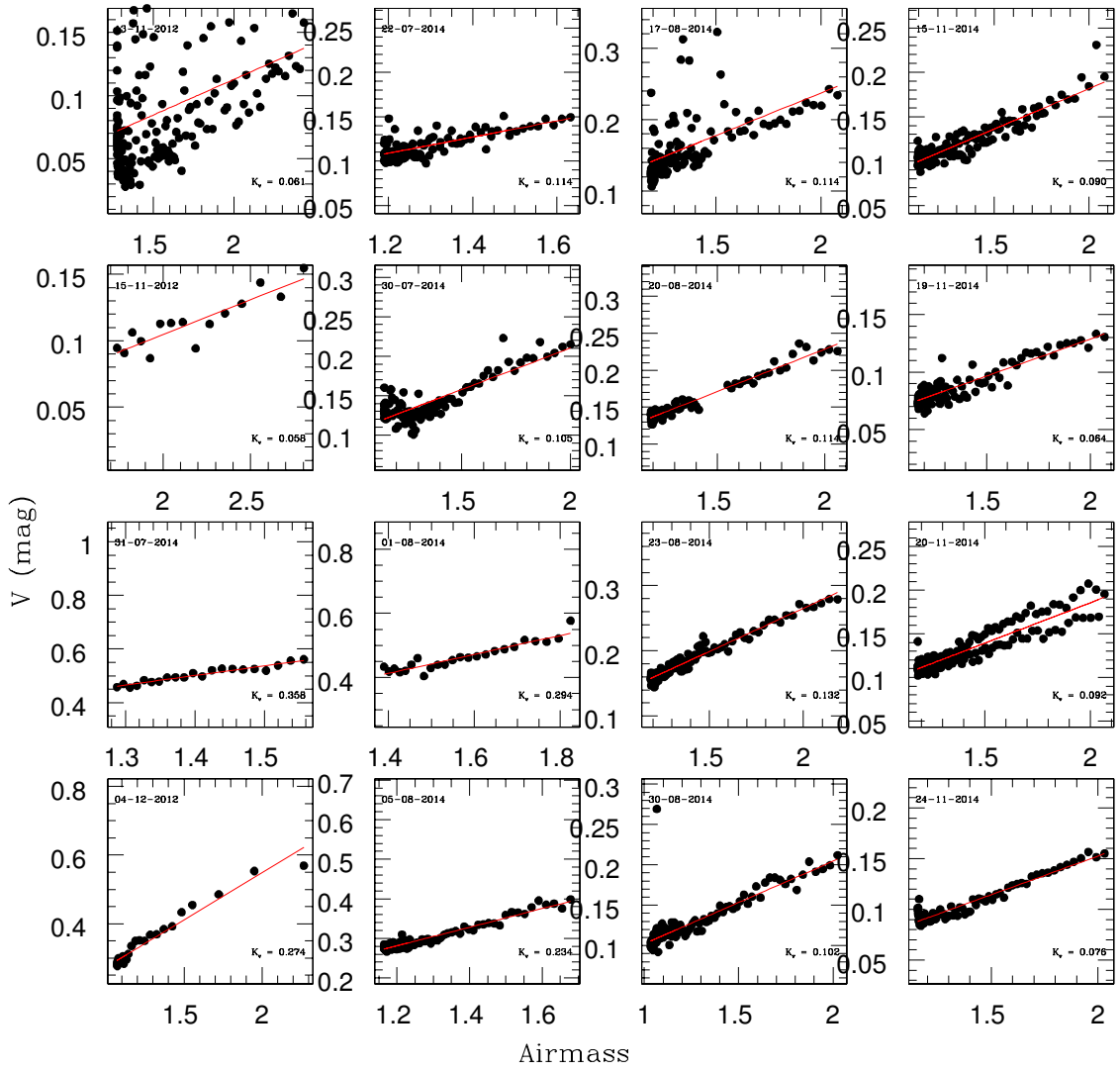

Fig. E.1: Extinction plots generated using AEM data.

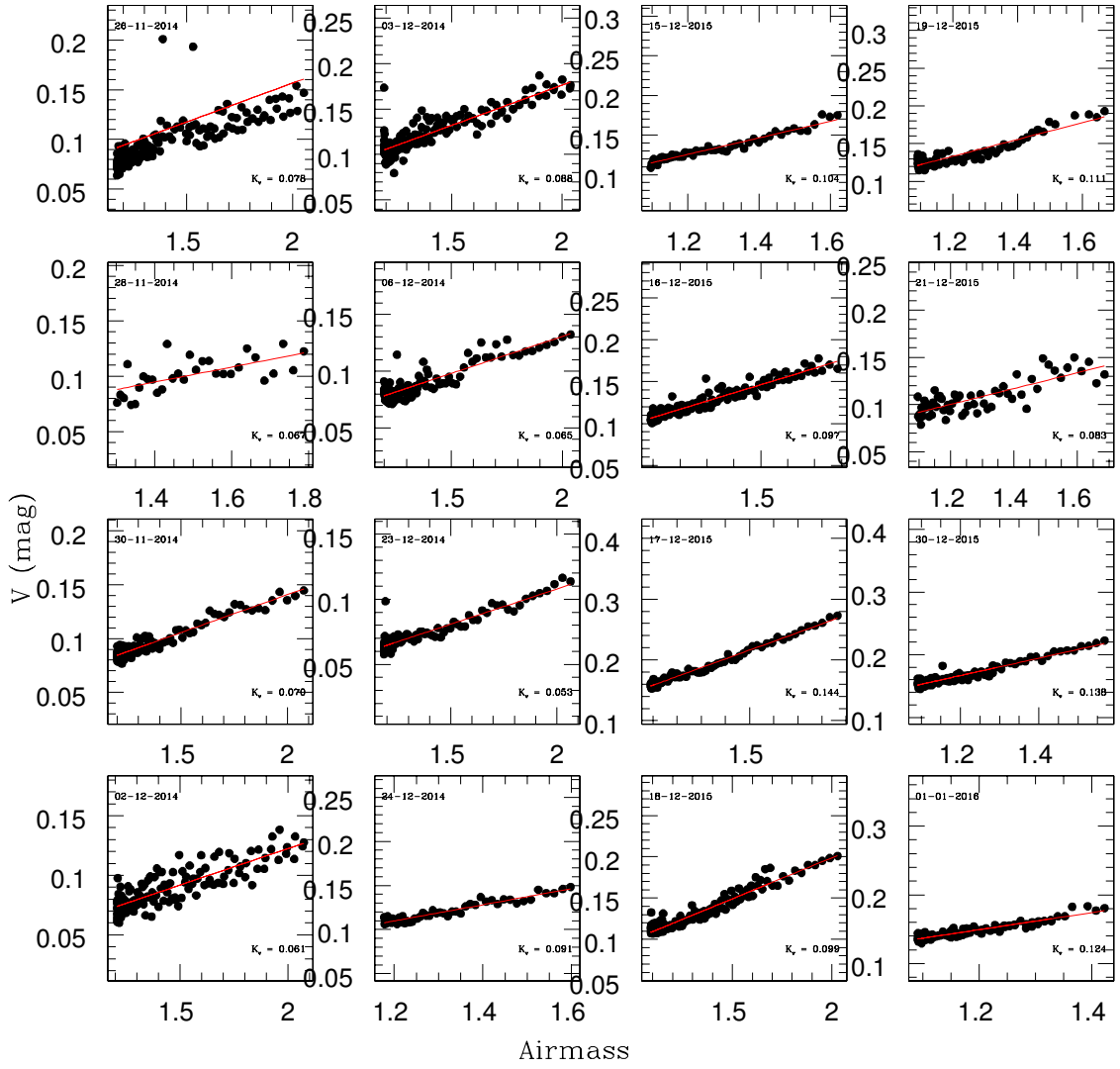

Fig. E.2: Extinction plots generated using AEM data.

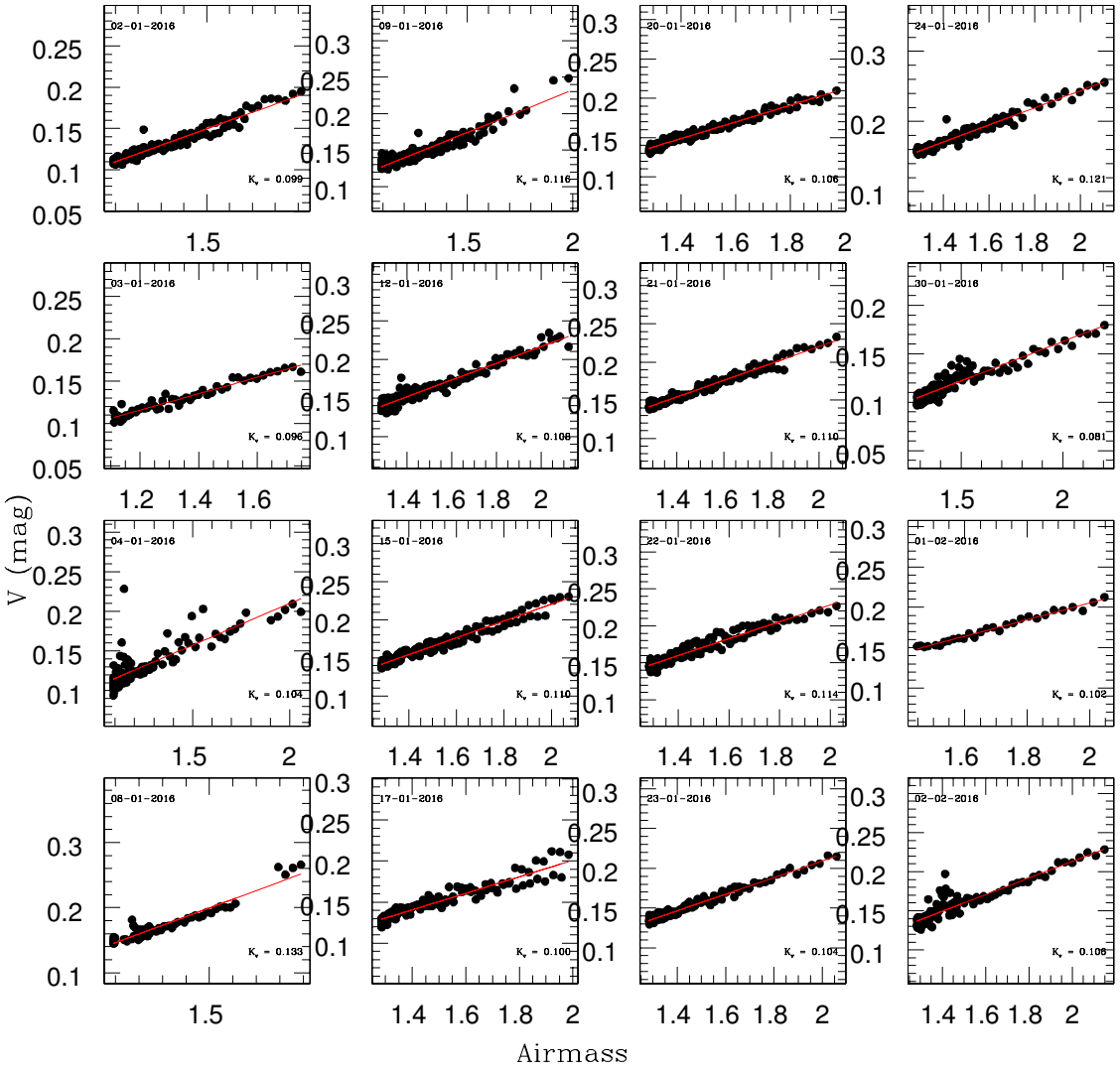

Fig. E.3: Extinction plots generated using AEM data.

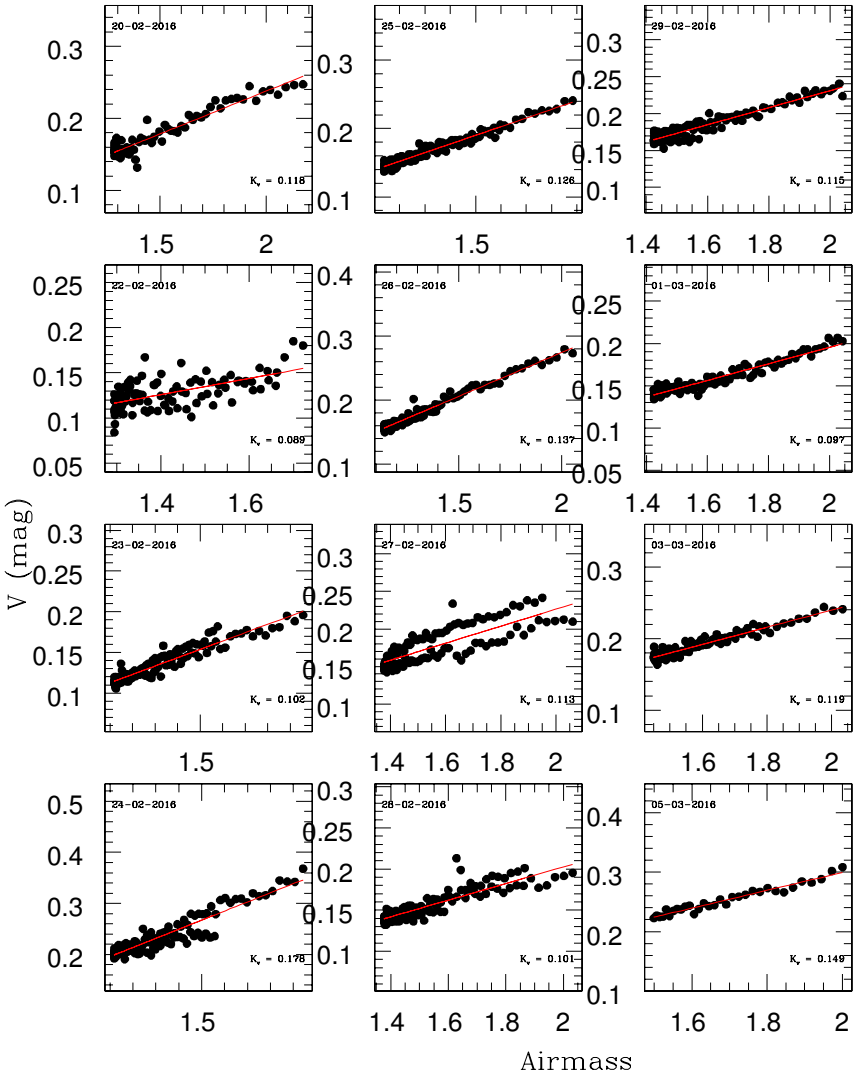

Fig. E.4: Extinction plots generated using AEM data.

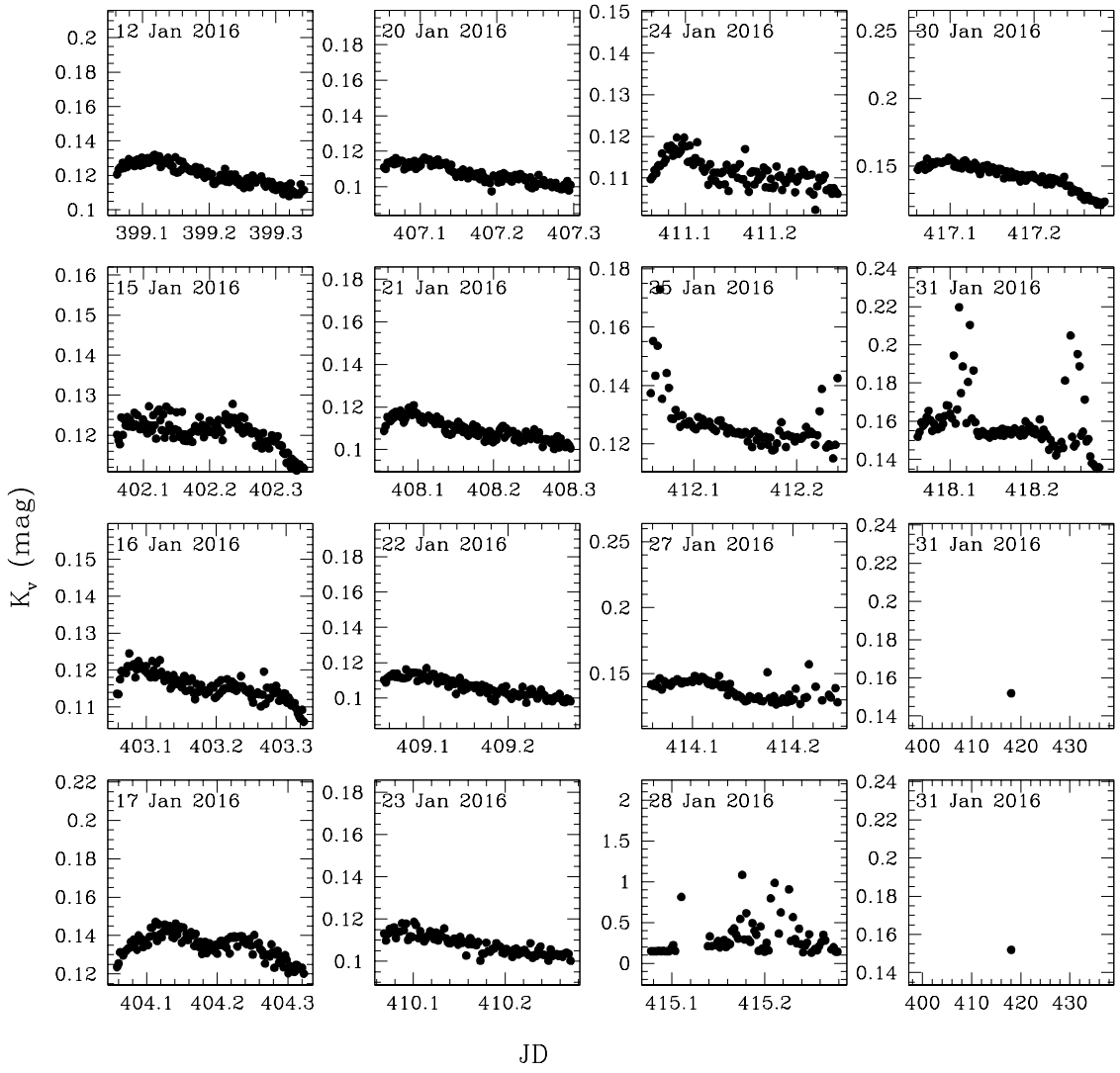

Fig. E.5: Nights showing variable extinction.

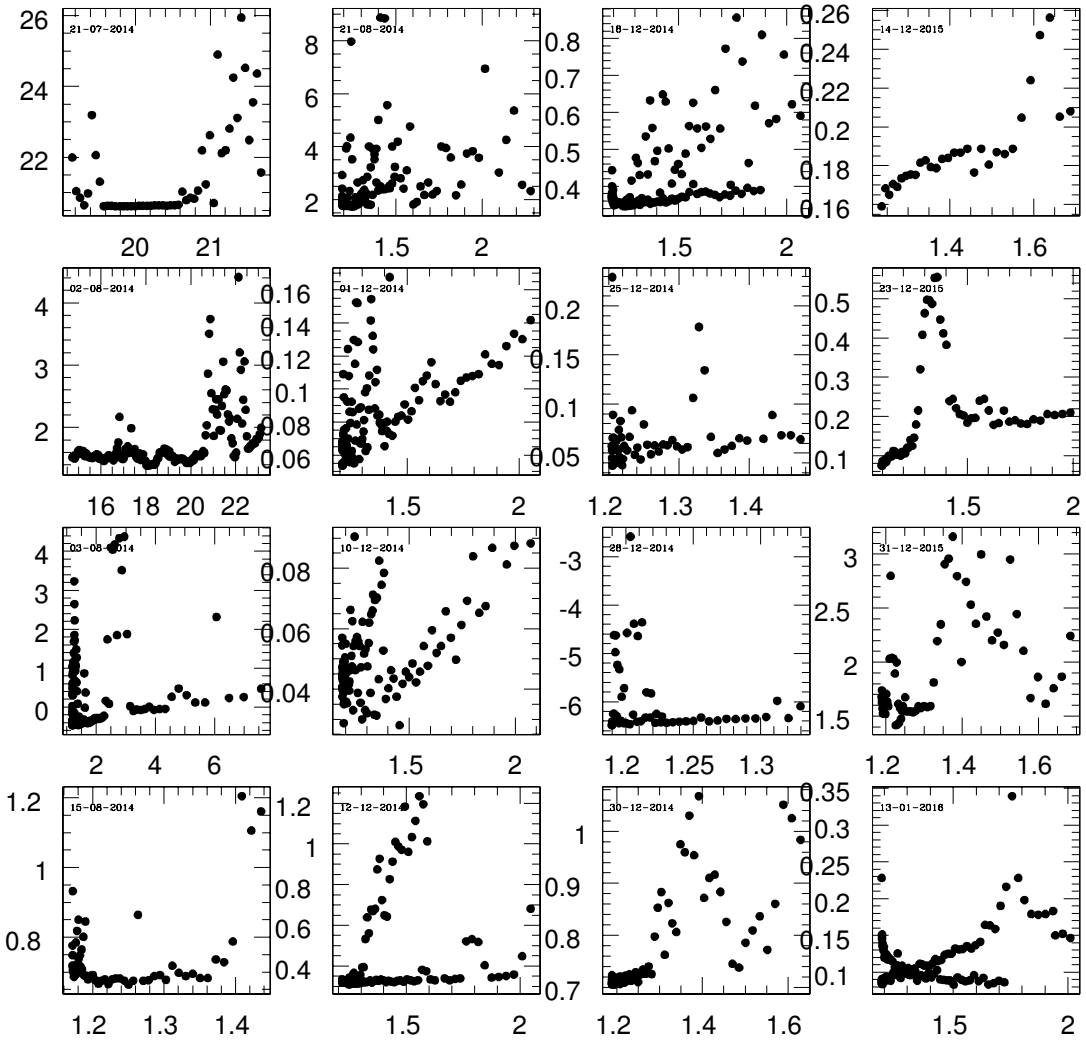

Fig. E.6: Plots for which extinction could not be determined.

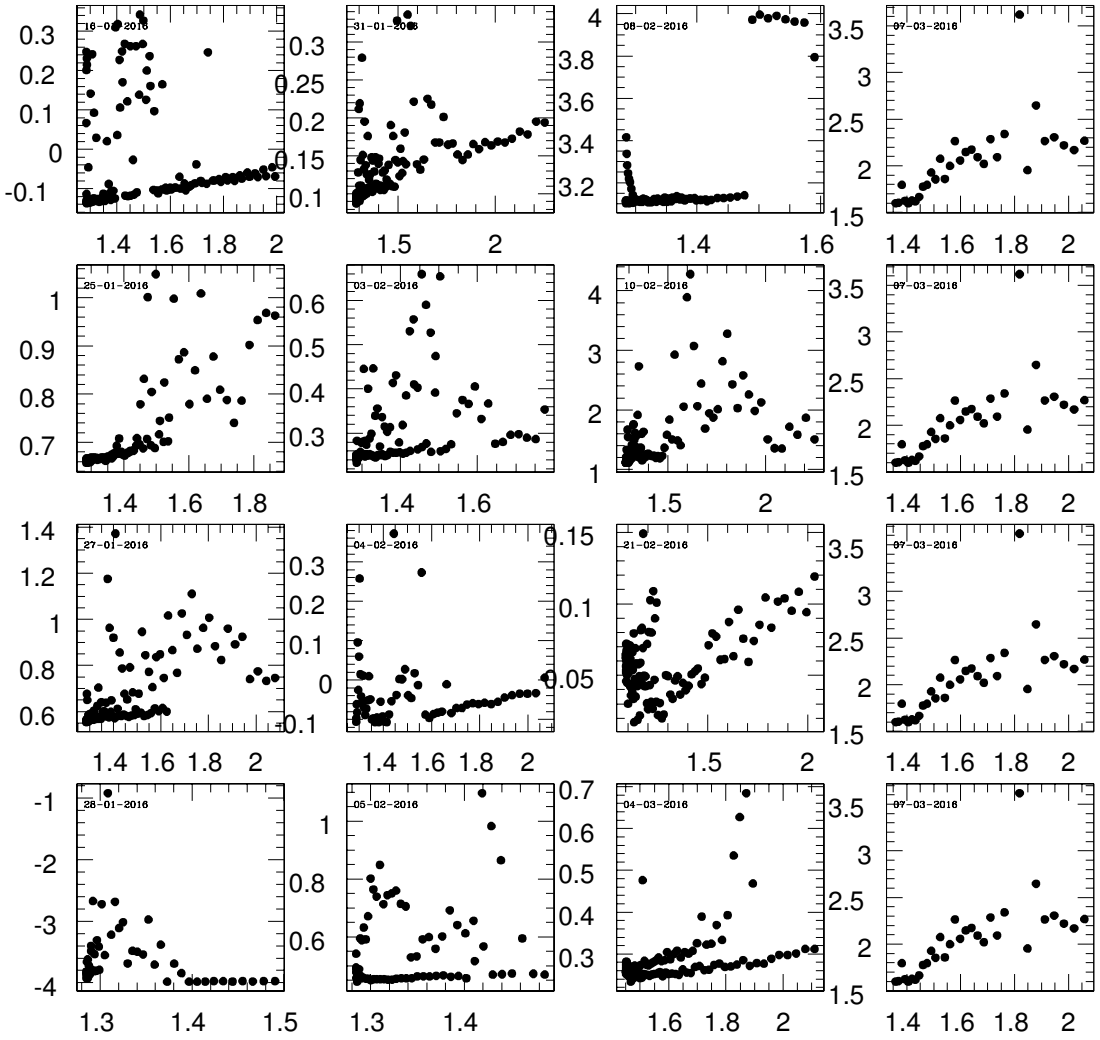

Fig. E.7: Plots for which extinction could not be determined.

Table E.1: Extinction coefficients and weather parameter for AEM observation.

Date	K_v	EK_v	Temperature	RH	Wind Speed	Pressure
13-11-2012	0.061	0.046	-7.02	16.54	2.16	587.92
04-12-2012	0.274	0.016	-7.98	14.63	1.04	592.05
22-07-2014	0.114	0.023	13.56	40.90	4.23	591.00
30-07-2014	0.105	0.014	11.59	48.06	2.26	591.42
01-08-2014	0.294	0.014	11.97	44.80	3.93	589.55
05-08-2014	0.234	0.007	11.95	47.27	8.68	590.95
20-08-2014	0.114	0.005	7.87	27.21	2.77	591.29
30-08-2014	0.102	0.015	7.37	38.31	1.99	592.20
15-11-2014	0.090	0.008	-5.38	11.12	2.29	590.01
19-11-2014	0.064	0.006	-5.65	16.98	1.16	591.09
20-11-2014	0.092	0.009	-5.76	16.88	4.50	588.50
24-11-2014	0.076	0.005	-4.54	11.95	1.58	590.12
26-11-2014	0.078	0.063	-5.88	16.84	1.10	587.08
28-11-2014	0.067	0.011	-8.42	19.84	2.39	577.81
30-11-2014	0.070	0.004	-7.29	14.03	2.53	589.32
02-12-2014	0.061	0.009	-3.91	10.16	5.75	590.65
03-12-2014	0.088	0.010	-5.91	11.22	2.62	590.21
06-12-2014	0.065	0.006	-6.61	9.67	4.63	589.46
23-12-2014	0.053	0.004	-13.10	37.08	2.26	586.27
24-12-2014	0.091	0.003	-5.79	13.08	7.11	586.59
15-12-2015	0.104	0.003	-10.62	10.65	1.08	585.99
16-12-2015	0.097	0.005	-10.38	19.86	8.00	581.91
17-12-2015	0.144	0.003	-15.26	45.75	1.77	583.04
18-12-2015	0.099	0.005	-12.56	20.91	1.46	585.83
19-12-2015	0.111	0.006	-12.48	21.31	4.14	582.93
21-12-2015	0.083	0.010	-12.95	18.46	4.33	583.11
01-01-2016	0.124	0.003	-8.87	20.79	1.63	590.21
02-01-2016	0.099	0.004	-9.85	17.40	1.22	590.57
03-01-2016	0.096	0.004	-8.02	18.66	1.14	591.08
04-01-2016	0.104	0.016	-7.49	41.23	7.59	587.84
09-01-2016	0.116	0.007	-11.84	17.89	0.60	588.44
12-01-2016	0.108	0.006	-10.92	20.86	2.29	584.89
15-01-2016	0.110	0.005	-12.50	21.42	1.47	586.10
17-01-2016	0.100	0.006	-10.48	16.37	3.95	583.41
20-01-2016	0.106	0.003	-15.24	10.83	0.66	586.04
21-01-2016	0.110	0.003	-13.78	10.54	1.17	587.32
22-01-2016	0.114	0.005	-12.51	11.16	0.87	587.17
23-01-2016	0.104	0.003	-11.85	12.63	0.86	586.65
24-01-2016	0.121	0.005	-11.80	9.47	1.31	585.69
30-01-2016	0.081	0.006	-10.24	16.21	2.46	583.11
01-02-2016	0.102	0.002	-11.33	10.15	4.53	585.09
02-02-2016	0.106	0.008	-11.71	14.99	1.70	585.02
20-02-2016	0.118	0.008	-8.49	44.36	1.19	588.40
22-02-2016	0.089	0.013	-10.98	30.36	2.73	589.47
23-02-2016	0.102	0.006	-12.64	16.34	2.22	590.38
24-02-2016	0.178	0.012	-11.02	16.35	1.82	590.92
25-02-2016	0.126	0.004	-8.97	16.22	1.49	591.39
26-02-2016	0.137	0.004	-9.43	15.67	2.46	592.82
27-02-2016	0.113	0.014	-8.93	13.61	1.68	592.05
28-02-2016	0.101	0.008	-7.75	16.82	0.97	592.49
29-02-2016	0.115	0.006	-8.91	20.69	2.24	591.31
01-03-2016	0.097	0.004	-7.55	16.04	2.19	591.57
03-03-2016	0.119	0.005	-5.90	31.50	1.96	591.64

Table E.2: Extinction coefficients and weather parameter for HCT observation.

Date	K_v	EK_v	Temperature	RH	Wind Speed	Pressure
19-09-2003	0.115	0.009	8.56	18.98	1.35	593.94
30-09-2003	0.316	0.033	-1.78	10.21	2.27	574.28
05-02-2004	0.095	0.006	-14.05	12.39	2.44	581.13
24-02-2004	0.147	0.002	-5.29	12.51	0.95	593.10
01-03-2004	0.130	0.006	-8.66	15.14	1.37	587.74
10-03-2004	0.137	0.009	-4.20	32.36	2.38	588.52
11-05-2004	0.110	0.010	2.63	27.71	2.68	589.44
13-05-2004	0.127	0.005	4.05	14.39	2.55	589.42
11-08-2004	0.242	0.009	9.82	40.20	6.85	589.73
06-10-2004	0.102	0.012	2.95	12.94	1.88	591.49
07-10-2004	0.102	0.004	0.47	21.74	2.86	589.87
03-11-2004	0.135	0.006	-7.24	11.35	1.17	591.99
08-11-2004	0.079	0.011	-5.96	12.17	1.47	589.47
02-12-2004	0.061	0.005	-8.63	13.97	1.34	592.44
04-12-2004	0.083	0.007	-5.76	10.10	3.01	589.00
26-01-2005	0.111	0.070	-13.30	21.62	1.97	588.50
21-02-2005	0.111	0.003	-11.71	38.19	2.28	586.07
22-02-2005	0.163	0.019	-2.63	38.19	3.80	586.07
25-02-2005	0.240	0.010	-1.12	28.25	2.22	592.18
27-05-2005	0.143	0.004	-1.12	28.25	2.22	592.18
20-06-2005	0.152	0.006	9.16	15.96	8.51	593.63
16-11-2005	0.012	0.011	-4.13	10.60	3.71	590.57
07-09-2005	0.152	0.006	9.06	15.39	3.08	594.79
26-10-2005	0.110	0.004	-4.13	10.60	3.71	590.57
16-11-2005	0.120	0.011	-6.88	6.36	2.98	586.10
28-12-2005	0.101	0.007	-6.88	6.36	2.98	586.10
23-01-2006	0.125	0.004	-11.00	21.72	1.22	586.61
17-03-2006	0.129	0.008	-16.57	43.01	2.15	581.40
24-09-2006	0.126	0.005	2.68	24.68	3.43	591.14
27-12-2006	0.102	0.006	-12.88	19.45	0.91	587.73

Corrections

RECOMMENDED CHANGES

Below is a list of changes recommended by the examiner. As recommended by the examiner, we have added text in the thesis at appropriate places. This has changed the page number for the recommended changes in the corrected copy of the thesis, new page numbers are mentioned in the response. Itemwise response to the each comment is presented.

1. In the introduction, a few paragraphs should be added to summarize the state of knowledge of the science. In this case that means showing what sites conditions are at the most common observatories around the world.

   Response:- Page 4, As suggested by the examiner we have added a section titled "Best astronomical sites in the world" in the Introduction chapter. The contents of this section are as follows:-

   Astronomical observatories are usually located at high altitude and far from the urban population. One of the prerequisites for any good site is that it should have a large number of clear nights, preferably distributed to all through the year. The impact of cloud cover on the science capability of the facility is quite clear. Sites with a low fraction of clear nights are less productive than sites with the high

fraction of photometric and usable nights. Observatory should be also located at the place which is free from significant light pollution at the time of construction. Additionally, it should have less prospects for habitation, which ultimately lead to the light pollution.

Another parameter which plays a very important role in deciding whether the site is suitable to host a big observatory or not is the atmospheric seeing. The impact of good natural seeing on the scientific productivity of any observatory cannot be overstated. Resolution-critical problems, such as strong-lensing, crowded field photometry, and velocity dispersion in the galactic nucleus are strongly seeing dependent, and the depth of all sky-limited observations depend on seeing to somewhere between the first and second power. There are host of new exciting science cases getting benefited with the Adaptive Optics system, which boost the spatial resolution of the telescope to the extent of diffraction limit. The effective AO corrections are highly sensitive to the native seeing through the size of the isoplanatic angle and length of the coherence time.

The ground-based infrared observations till mid-IR is slowly becoming more effective technique to probe a large number of science problems. The near and mid-IR atmospheric windows are set by the absorption spectrum of water and CO2. Sites with high precipitable water vapor are found to have narrower and less stable observing windows, as well as high thermal-IR background. Therefore, the best sites, where both optical and IR observation can be effectively carried out should be a cold site having extremely low precipitable water vapor, preferably less than 2 mm.

Other parameters which also contribute in making any site suitable for astronomical observatory are minimal change in diurnal and seasonal temperatures, low wind speed and gust, easy approachability, the high mechanical integrity of soil and low seismicity. Since big observatories are

expected to host a number of large telescopes, which requires huge investment, therefore, it is expected that the chosen site should have stable weather patterns over extended period say years or even decades.

Most world-class astronomical observatories are located close to coastal mountain ranges and islands. Chile is one of the few places on Earth with mountains that meet the stringent requirements of astronomical observatories. There are a number sites in Chile, which either already host an observatory or proposed for futures large telescopes such as E-ELT, GMT etc. These sites may be divided into two classes: moderate elevation, primarily coastal sites, and high elevation inland sites. Las Campanas, La Silla, Cerro Tololo and Paranal are all examples of moderate elevation sites in coastal ranges. Whereas, the ALMA site Chajnantor in the middle of the Atacama desert is the best example of the high altitude sites in the Chile.

On the Island of Hawaii, Mauna Kea is considered the highest (4200m from sea level) island mountain in the world. The place was first identified by Gerard Kuiper to be used for ground-based infrared astronomical observation. However, it was John Jefferies, a professor at university of Hawaii, who succeeded in getting NASA grant to install a relatively large size (2.2m) telescope, which saw the first light in 1970. After recognizing the importance of the Mauna Kea site for both optical and NIR observations, a number of other observing facilities such as CFHT, UKIRT, SUBARU and the Keck telescopes have been installed by different astronomical groups. Mauna Kea is also considered to be one of the preferred site for forthcoming TMT project.

Roque de Los Muchachos Observatory (ORM), in La Palma, Canary Islands, Spain, is another place which hosts a large number of telescopes ranging from few tens of inches to 10m size, mostly from Europe. The site infrastructure is managed by the Instituto de Astrofisica de Canarias, which includes providing

the access road, utilities, high-speed data links and the mountain-top residential facilities for observers. Altitude of ORM is moderate (2300m), however, parameters which characterizes any site such as seeing, sky brightness, number of clears nights are as good as other best sites in the world.

In addition to coastal and sites in Islands, continental places such as Maidanak in Uzbekistan, Hanle in India and Ali in China, can be considered equally good sites in Asia. These are very high altitude, thinly populated, extremely cold and dry desert sites, best suited for Optical, IR and Submillimeter astronomy. Some activities are already undertaken to characterize these sites for creating future large observing infrastructure, however, more efforts are needed to draw any conclusion.

Table 3 provide all relevant parameters, which can be used to judge the relative observing quality of the worlds few best sites.

Table 3: Site parameters for few best observatories around the world.

Parameter	IAO	Mauna Kea	La Silla	La Palma (ORM)	Aromazones (E-ELT)
Altitude(m)	4467	4200	2400	2250	3064
Median Seeing(arc-sec)	1.2	0.5	0.76	0.55	0.41
Extinction in V Band (mag)	0.120	0.119	0.164	0.137	0.162
Sky Brightness in V Band (mag)	21.28	21.5	21.7	21.9	21.9
Usable Nights(%)	81	72	-	72	89
PWV (mm)	1.5	1.9	4.0	4.14	-
Isoplanatic Angle(arc-sec)	-	2.69	1.26	2.33	2.04
Coherence Time(ms)	-	5.1	-	6.0	4.6
Average Night Temperature(C)	-1.0	2.3	-	7.3	7.5
Median Night wind speed(m/s)	4.0	5.7	-	8.2	7.2

2. Page 42, Manually controlled or linked to a rain gauge? Please explain how your instrument handles weather.

   Response:- Page 45, As suggested by the examiner we have corrected the contents of this section. Text " At present, the enclosure operation is manual and not linked to weather station. Which means, operator is required to manually start the instrument. From this point onwards, the instrument operates on its own." is added in this section for explaining how the instrument handles

weather.

3. Put page 49 and half of 50 in an Appendix.

   Response:- As suggested by the examiner the contents of page 49 and 50 are put into the Appendix D.

4. Page 61, regarding the 2.1 to 2.7. Diffraction limit and seeing dont add up (not even in quadrature).

   Response:- Page 64, Text "The diffraction limited image for the 75mm aperture telephoto lens is 1.84″, and the seeing at the site varies from 1-2 arc-second. Therefore, FWHM of the star in our field is expected to be about 2.1-2.7 arc-second and at the best focus, the whole starlight will get confined to within one pixel." is replaced with "The diffraction limited image for the 75mm aperture telephoto lens is 1.84", and the seeing at the site varies from 1-2 arc-second. Therefore, at the best focus, the whole starlight will get confined within one pixel."

5. Page 72, no comparison of the two techniques is shown and it would be valuable to see how well they correlate and why they differ.

   Response:- Page 74, Text "Till 2.5 air-mass, we do not find much difference between the extinction values derived using above two techniques. Therefore, extinction values for all the observed nights were obtained using the first techniques only. " is added in the paragraph to show that we have used only one technique, and comparison is not possible.

6. Page 119, How long is a full scan?

   Response:- Page 124, One full scan of the sky takes 200 seconds. This time include the time required to scan the sky (120 seconds) and the time required for bringing back the scanning unit to the home position. Enumeration 6, 8 and 9 are added to explain these facts.

7. Page 132, give a comparison of the cloud cover statistics between the 2 instruments.

   Response:-Page 138, At present, we have not determined the cloud cover statistics using the CONCAM visible all sky camera at IAO, Hanle.

8. Page 141, what is the DIMM integration time in Figure 5.4?

   Response:-Page 147, DIMM integration time is 10 milli-seconds. Text "here the DIMM instruments integration time is 10 ms." is added to in the paragraph.

9. Page 171, why using plywood for the motor construction as opposed to aluminum?

   Response:- Page 179, The reason for using plywood as opposed to amuminum is explained. Text "Plywood was chosen for motor construction as opposed to the aluminum to reduce the prototyping time, as significantly large duration of time was required to procure and machine the aluminum block to suit the motor." is added in this section.

10. Page 188, a comparison with the HCT, possibly in form of a table would be valuable.

    Response:- Page 197, As suggested by the examiner table and text "Table 4 lists the average V-Band sky brightness and atmospheric extinction measured using HCT telescope and AEM at IAO, Hanle." is added in the thesis at the relevant place.

Table 4: Sky-brightness and atmospheric extinction as measured from HCT and AEM at IAO, Hanle.

Parameter	RMS	Corr. Coefficients
V-Bnad Sky Brightness(average)	21.54±0.37	21.57±0.14
V-Band Atmospheric Extinction(average)	0.120±0.04	0.111±0.043

TYPOGRAPHICAL ERRORS

Below is a list of typographical errors pointed out by the examiner. As recommended by the examiner, we have added text in the thesis at appropriate places. This has changed the page number for the typographical errors in the corrected copy of the thesis, new page numbers are mentioned in the response. Itemwise response to the each comment is presented.

- Page 3, Line 2, remove “very”

  Response:-Page 3, Line 2, removed “very”

- Page 3, Line 6, “The mount”-> “Mount”

  Response:-Page 3, Line 6, “The mount”changed to “Mount”

- Page 3, Line 12, “would like to develop”

  Response:-Page 3, Line 12, “would”added before “like to develop”

- Page 3, Line 13, “Like Chile, these two sites may be populated with...”

  Response:-Page 3, Line 13, “Likewise Chilean sites, no wonder if in near future these two sites may be populated with...”changed to“Like Chile, these two sites may be populated with...”

- Page 3, Line 25, “little affected by monsoon”

  Response:- Page 3, Line 25, “not much affected by monsoon”changed to “little affected by monsoon”

- Page 3, Line 26, “This place”-> “It”

  Response:-Page 3, Line 26, “This place”changed to “It”

- Page 4, Line 3, “all the required”

  Response:-Page 4, Line 3, “all required”changed to“all the required”

- Page 4, Line 2 from the end, “station”-> “stations”

  Response:-Page 7, Line 5 from the end, “station”changed to “stations”

- Page 6, Line 1, “Seasonal”-> “seasonal”

  Response:-Page 8, Line 13 from bottom, “Seasonal”changed to “seasonal”

- Page 6, Line 3 from the end, “During the last two decades”

  Response:-Page 9, Line 6 from the end, “During last two decades”replaced with“During the last two decades”

- Page 9, Line 14, “all through year”-> “throughout the year”

  Response:- Page 12, Line 11, “all through year”changed to “throughout the year”

- Page 13, Line 2, “from”-> “by”

  Response:-Page 15, Line 5 from end, “from”changed to “by”

- Page 28, Section 2.5.1, Line 4, “gives the extinction”

  Response:-Page 31, Section 2.5.1, Line 4, “gives extinction”changed to “gives the extinction”

- Page 29, Line 2, “match”

  Response:-Page 32, Line 2, “matches”changed to “match”

- Page 31, Line 1, “ourselves”

  Response:- Page 34, Line 1, “our-self”changed to“ourselves”

- Page 31, Line 4, “is the main optics”

  Response:- Page 34, Line 4, “is main optics”changed to “is the main optics”

- Page 37, Line 2, “ourselves”, “by an external”

  Response:-Page 40, Line 2, “our-self”and “by external”changed to “ourselves”and “by an external”respectively

- Page 37, Section 2.6.3.1, Line 1, “The Equatorial telescope requires its”

  Response:-Page 40, Section 2.6.3.1, Line 1, “Equatorial telescope requires its”changed to “The Equatorial telescope requires its”

- Page 37, Section 2.6.3.1, Line 2, “this is a one time”

  Response:-Page 40, Section 2.6.3.1, Line 2, “this is one time”changed to “this is a one time”

- Page 37, Section 2.6.3.1, Line 3, remove “usually”and add “also”on the last line in “may also have to be installed”

  Response:-Page 37, Section 2.6.3.1, Line 3, “usually”removed and “also”added on the last line in “may also have to be installed”

- Page 38, 2 lines before Equation 2.18, “Hence, the total”

  Response:-Page 41, 2 lines before Equation 2.18, “Hence, total”changed to “Hence, the total”

- Page 39, Line1, “This means the RA axis can move as little as 0.405″, The equatorial...”

  Response:- Page 42, Line1, “This means the RA axis can move as little as 0.405″. Equatorial...”changed to “This means the RA axis can move as little as 0.405″. The equatorial...”

- Page 39, Section 2.6.3.3, Line 3, “However, it was soon realized”

  Response:-Page 42, Section 2.6.3.3, Line 3, “However, soon we realized”changed to “However, it was soon realized”

- Page 39, Section 2.6.3.3, Line 4, “the Dec axis”

  Response:-Page 42, Section 2.6.3.3, Line 4, “Dec axis”changed to“the Dec axis”

- Page 39, Section 2.6.3.3, Line 5, “we modified the DEC drive to use a small...”

  Response:-Page 42, Section 2.6.3.3, Line 5, “we have modified the DEC drive, and now it uses a...”changed to “we modified the DEC drive to use a small...”

- Page 39, Section 2.6.3.3, Line 7, “with a timing belt....The motor”

  Response:-Page 42, Section 2.6.3.3, Line 7, “with a timing belt....Motor”changed to “with a timing belt....The motor”

- Page 39, Section 2.6.3.3, Line 8, “The total”

  Response:-Page 42, Section 2.6.3.3, Line 8, “Total”changed to“The total”

- Page 40, Line 2, “The use of Large”

  Response:-Page 43, Line 2, “Use of Large”changed to “The use of Large”

- Page 40, Line 4, “observations....measurements”

  Response:-Page 43, Line 4, “observation....measurement”changed to “observations....measurements”

- Page 40, Section 2.6.3.4, Line 1, “axis”-> “axes”

  Response:-Page 43, Section 2.6.3.4, Line 1, “axis”changed to “axes”

- Page 40, Section 2.6.3.4, “driven”-> “driving”

  Response:-Page 43, Section 2.6.3.4, “driven”changed to “driving”

- Page 40, second to last line, “number by 4 bringing the number of pulses to”

  Response:-Page 43, second to last line, “number by 4. Now the number of pulses

is”changed to “number by 4 bringing the number of pulses to”

- Page 40, last line, “pulse now”

  Response:-Page 43, last line, “pulse”changed to“pulse now”

- Page 41, Line 3, “The CCD”

  Response:-Page 44, Line 3, “CCD”changed to “The CCD”

- Page 41, Line 5, “the CCD but it can also”

  Response:-Page 44, Line 5, “CCD. CCD can also be”changed to “the CCD but it can also be”

- Page 41, Line 10, “Once the correct focus is achieved, a threaded locking ring is”

  Response:-Page 44, Line 10, “Once correct focus is achieved then a threaded locking ring is”changed to“Once the correct focus is achieved, a threaded locking ring is”

- Page 42, Section 2.6.4, Line 1, “has been”-> “was”

  Response:-Page 44, Section 2.6.4, Line 1, “has been”changed to “was”

- Page 43, Line 1, “The mechanical”

  Response:-Page 46, Line 4, “The mechanical”changed to “Mechanical”

- Page 43, Line 3, “opened or closed and, this way, prevent”

  Response:-Page 436, Line 6, “opened or closed. And this way”changed to “opened or closed and, this way, prevent”

- Page 43, Section 2.7, Line 1, “although the AEM”

  Response:-Page 46, Section 2.7, Line 1, “although AEM”changed to “although the AEM”

- Page 43, Section 2.7, Line 5, “The telescope”

  Response:-Page 46, Section 2.7, Line 5, “Telescope”changed to “The telescope”

- Page 44, Line 1, “data are sent”

  Response:-Page 47, Line 4, “data is sent”changed to “data are sent”

- Page 44, Section 2.7.1, Line 2, “These are important”

  Response:-Page 47, Section 2.7.1, Line 2, “These are few important”changed to “These are important”

- Page 45, Line 6, “An internal RAM”

  Response:-Page 48, Line 9, “An internal ram”changed to “An internal RAM”

- Page 45, Line 7, “Five external interrupts, some of which”

  Response:-Page 48, Line 10, “five external interrupts, few of them”changed to “five external interrupts, some of which”

- Page 46, Section 2.7.1.1, Line 1, “The encoder”

  Response:-Page 49, Section 2.7.1.1, Line 1, “Encoder”changed to “The encoder”

- Page 47, Line 1, “The controller”

  Response:-Page 50, Line 12, “Controller”“The controller”

- Page 47, Section 2.7.1.2, Line 1, “by the stepper”

  Response:-Page 50, Section 2.7.1.2, Line 1, “by stepper”changed to “by the stepper”

- Page 47, Section 2.7.2, Line 1, “The stepper”

  Response:-Page 51, Section 2.7.2, Line 1, “Stepper”changed to“The stepper”

- Page 47, Section 2.7.2, Line 2, “on its own”

  Response:- Page 51, Section 2.7.2, Line 2, “by its own”changed to“on its own”

- Page 50, Section 2.7.3, Line 1, “An incremental encoder”

  Response:-Page 52, Section 2.7.3, Line 1, “Incremental encoder”changed to “An incremental encoder”

- Page 50, Section 2.7.3, Line 3, “Another output”

  Response:-Page 53, Section 2.7.3, Line 3, “Other output”changed to “Another output”

- Page 52, Line 4, “The absolute position”

  Response:-Page 54, Line 10, “Absolute position”changed to“The absolute position”

- Page 52, Section 2.8, Line 1, “fully-automatic”

  Response:-Page 54, Section 2.8, Line 1, “fully automatic”changed to“fully-automatic”

- Page 52, Section 2.8.1 title, “Embedded software”

  Response:-Page 55, Section 2.8.1 title, “Ebmedded software”changed to “Embedded software”

- Page 52, Section 2.8.1, Line 3, “The first code is for the stepper motor”

  Response:-Page 55, Section 2.8.1, Line 3, “First code is for the stepper motor”changed to “The first code is for the stepper motor”

- Page 53, Line 5, “This code receives”

  Response:-Page 55, Line 11, “This code receive”changed to “This code receives”

- Page 53, Line 10, “Depending on the needed”

  Response:-Page 55, Line 16, “Depending on needed”changed to “Depending on the needed”

- Page 54, Line 1, “Since microcontrollers have limited memory”

  Response:-Page 56, Line 1, “Since microcontrollers have got limited memory”changed to “Since microcontrollers have limited memory”

- Page 54, Section 2.8.2, Line 4, “the CCD, telescope controller and instrument enclosure”

Response:-Page 57, Section 2.8.2, Line 2, “CCD, telescope controller and the instrument enclosure”changed to “the CCD, telescope controller and instrument enclosure”

- Page 54, Section 2.8.2, Line 10, “All the required”

  Response:-Page 57, Section 2.8.2, Line 9, “All required”changed to “All the required”

- Page 55, in section configuration file, replace all instances of “place”with “site”and “weather”with “whether”

  Response:-Page 58, in section configuration file, all instances of “place”and “weather”are replaced with “site”and “whether”respectively

- Page 56, Line 1 after Fig. 2.17, “that the device”

  Response:-Page 59, Line 1 after Fig. 2.17, “that device”changed to “that the device”

- Page 58, Line 4, “corrects”

  Response:-Page 60, Line 6, “correct”changed to “corrects”

- Page 58, Line 5, “the Dec axis”

  Response:-Page 61, Line 1, “Dec axis”changed to “the Dec axis”

- Page 58, Line 7, “the Dec axis drive unit, the telescope started giving satisfactory”

  Response:-Page 61, Line 3, Page 58, Line 7, “Dec axis drive unit and telescope started giving the satisfactory”changed to “the Dec axis drive unit, the telescope started giving satisfactory”

- Page 58, Line 14, “error is shown in Figure”

  Response:-Page 61, Line 10, “error is shown in the Figure”changed to “error is shown in Figure”

- Page 59, Line 1, “for the guiding, the AEM”

  Response:-Page 62, Line 1, “for the guiding, AEM”changed to“for the guiding, the AEM”

- Page 60, Line 1, “the tracking performance”

  Response:-Page 63, Line 1, “tracking performance”changed to “the tracking performance”

- Page 60, Line 2, “that the tracking error”

  Response:-Page 63, Line 2, “that tracking error”changed to “that the tracking error”

- Page 60, Line 3, “Whereas, the error”

  Response:-Page 63, Line 3, “Whereas, Error”changed to “Whereas, the error”

- Page 62, Line 7, “improvement to the Dec axis”

  Response:-Page 65, Line 7, “improvement in the Dec axis”changed to “improvement to the Dec axis”

- Page 62, Line 8, “the upgraded AEM housed inside a motorized”

  Response:-Page 65, Line 8, “upgraded AEM housed inside motorized”changed to “the upgraded AEM housed inside a motorized”

- Page 63, Line 3, “Since December 2015, the AEM has been in regular use”

  Response:-Page 66, Line 3, “since December 2015 AEM is in regular use”changed to “since December 2015, the AEM has been in regular use”

- Page 63, Line 7, “the initial instrument pointing was very poor, we”

  Response:-Page 66, Line 7, “initial instrument pointing was very poor, therefore we”changed to “the initial instrument pointing was very poor, we”

- Page 63, Section 3.2, Line 1, “the AEM need to be processed before they can be used for the”

Response:-Page 66, Section 3.2, Line 1, "AEM needs to be processed before they can be used for"changed to "the AEM need to be processed before they can be used for the"

- Page 63, Section 3.2, Line 3, "bias, dark, and flat field corrections"
  Response:-Page 66, Section 3.2, Line 3, "bias, dark corrections, and flat field correction"changed to "bias, dark, and flat field corrections"

- Page 65, Line 9, "this temperature constant"
  Response:-Page 68, Line 9, "this temperature same"changed to "this temperature constant"

- Page 65, Line 11, "down to -110"
  Response:-Page 68, Line 11, "up to -110"changed to"down to -110"

- Page 65, 3 lines from the bottom, "Like bias frames"
  Response:-Page 68, 3 lines from the bottom, "Likewise bias frames"changed to"Like bias frames"

- Page 68, Line 1, "the expectation was that it would"
  Response:-Page 71, Line 1, "then expectation was that it would"changed to "the expectation was that it would"

- Page 68, Section 3.2.4, Line 1, "flat, they are"
  Response:-Page 71, Section 3.2.4, Line 1, "flat then they are"changed to "flat, they are"

- Page 70, Line 2, "the AEM shutter opens, the telescope initializes and seeks"
  Response:-Page 73, Line 2, "then AEM shutter opens, telescope initializes and seeks"changed to "the AEM shutter opens, the telescope initializes and seeks"

- Page 70, Line 3, "the telescope"
  Response:- Page 73, Line 3, "telescope"changed to "the telescope"

- Page 70, Line 6, “the meridian”

  Response:-Page 73, Line 6, “meridian”changed to “the meridian”

- Page 70, Line 11, “gives a more precise”

  Response:-Page 73, Line 11, “gives much precise”changed to “gives a more precise”

- Page 71, Line 1, “gives a slope”

  Response:-Page 74, Line 1, “gives slope”changed to “gives a slope”

- Page 71, Line 2, “is quite large, at higher zenith angle, an airmass within”

  Response:-Page 74, Line 2, “is quite large, therefore at higher zenith angle air-mass within”changed to “is quite large, at higher zenith angle, an airmass within”

- Page 71, Line 7, “the average extinction”

  Response:-Page 74, Line 7, “average extinction”changed to “the average extinction”

- Page 71, Section 3.3.2, Line 2, “the atmospheric extinction...method, tis technique has hardly been used”

  Response:-Page 74, Section 3.3.2, Line 2, “atmospheric extinction...method, hardly this technique has been used”changed to “the atmospheric extinction...method, this technique has hardly been used”

- Page 71, Section 3.3.2, Line 5, “However, now that”

  Response:-Page 74, Section 3.3.2, Line 5, “However, now when”changed to“However, now that”

- Page 71, Section 3.3.2, Line 6, “simple to adopt”

  Response:-Page 74, Section 3.3.2, Line 6, “simpler to adopt”changed to “simple

to adopt"

- Page 71, Section 3.3.2, Line 7, "15 nights, it gives"
  Response:-Page 74, Section 3.3.2, Line 7, "15 nights so it gives"changed to "15 nights, it gives"

- Page 71, Section 3.3.2, Line 8, "measurements are possible"
  Response:-Page 74, Section 3.3.2, Line 8, "measurement is possible"changed to "measurements are possible"

- Page 71, 6 lines from the bottom, "stars are identified, we choose"
  Response:-Page 74, 3 lines from the bottom, "stars are identified then, we choose"changed to "stars are identified, we choose"

- Page 71, 5 lines from the bottom, "in which the sky"
  Response:-Page 74, 2 lines from the bottom, "in which the sky"changed to"in which the sky"

- Page 71, 4 lines from the bottom, "using the technique described earlier. Then the extinction-corrected"
  Response:-Page 74, last line, "using technique described earlier. Then after extinction corrected"changed to "using the technique described earlier. Then the extinction-corrected"

- Page 71, 2 lines from the bottom, "After that, the average"
  Response:-Page 75, Line 2, "After that the average"changed to "After that, the average"

- Page 71, last line, "in Equation"
  Response:-Page 75, Line 2, "in the Equation"changed to"in Equation"

- Page 72, Section 3.4.1, Line 1, "very few extinction measurement"

Response:-Page 75, Section 3.4.1, Line 1, “very few extinction measurement”changed to “very few extinction measurements”

- Page 72, Section 3.4.1, Line 4, “not spread over all season”

  Response:-Page 75, Section 3.4.1, Line 4, “not spread all over the seasons”changed to “not spread over all season”

- Page 73, Line 1, “either sky transparency was found to be unstable”

  Response:-Page 76, Line 4, “either sky transparency was found to be not stable”changed to “either sky transparency was found to be unstable”

- Page 73, Line 6, “to be Gaussian”

  Response:-Page 76, Line 9, “with Gaussian”changed to “to be Gaussian”

- Page 73, Section 3.4.2, last line, “having slightly higher”

  Response:-Page 76, Section 3.4.2, last line, “having little higher”changed to “having slightly higher”

- Page 77, Line 7, “we find the scatter to be very small”

  Response:-Page 80, Line 9, “we find this scatter very small”changed to “we find the scatter to be very small”

- Page 78, Line 1, “the AEM can also be”

  Response:-Page 81, Line 1, “AEM is also be”changed to “the AEM can also be”

- Page 80, last line, “a large number”

  Response:-Page 84, last line, “large number”changed to “a large number”

- Page 81, Line 15, “then the ensemble magnitude ”

  Response:-Page 81, Line 3 from bottom, “then after, the ensemble magnitude ”changed to “then the ensemble magnitude ”

- Page 81, 2 lines from bottom, “with an aperture”

  Response:-Page 84, Line 8, “close the aperture”changed to “with an aperture”

- Page 87, Section 4.1.3,last line “for cloud monitoring”

  Response:-Page 91, Section 4.1.3,last line “for the cloud monitoring”changed to “for cloud monitoring”

- Page 90, Title, “Operating principle of the Scanning Cloud Monitor ”

  Response:-Page 94, Title, “Operating principle of Scanning Cloud Monitor ”changed to “Operating principle of the Scanning Cloud Monitor ”

- Page 90, Line 1, “The scanning”

  Response:-Page 94, Line 1, “Scanning”changed to “The scanning”

- Page 90, Line 12, “we find a thermopile”

  Response:-Page 94, Line 12, “we find Thermopile sensor”changed to “we find a thermopile sensor”

- Page 90, Line 14, “A thermopile”

  Response:-Page 94, Line 14, “Thermopile”changed to “A thermopile”

- Page 91, Line 4, “The reference junction”

  Response:-Page 95, Line 4, “Reference junction”changed to“The reference junction”

- Page 91, Section 4.6, Line 1, “The thermopile”

  Response:-Page 95, Section 4.6, Line 1, “Thermopile”changed to “The thermopile”

- Page 92, Line 3, “We can modify Equation”

  Response:-Page 96, Line 3, “We can modify the Equation”changed to “We can modify Equation”

- Page 93, Line 1, “The voltage”

  Response:-Page 97, Line 1, “Voltage”changed to “The voltage”

- Page 94, Section 4.6, Line 4, “using a NI-6008”

  Response:-Page 98, Section 4.6, Line 4, “using NI-6008”changed to “using a NI-6008”

- Page 95, Line 7, “Both sensors”

  Response:-Page 99, Line 7, “Both the sensors”changed to “Both sensors”

- Page 95, Line 10, “that the thermopile sensor has indeed enough”

  Response:-Page 99, Line 10, “that indeed thermopile sensor has enough”changed to “that the thermopile sensor has indeed enough”

- Page 96, Line 2, “The TPS334”

  Response:-Page 100, Line 2, “TPS334”changed to “The TPS334”

- Page 98, Line 10, “A Hall effect based”

  Response:-Page 102, Line 10, “Hall effect based”changed to “A Hall effect based”

- Page 99, Line 5 from end, “The thermopile sensor”

  Response:-Page 103, Line 5 from end, “Thermopile sensor”changed to “The thermopile sensor”

- Page 100, Line 1, “the thermopile”

  Response:-Page 104, Line 2, “thermopile”changed to “the thermopile”

- Page 100, Section 4.8.2, Line 1, “the thermopile”

  Response:-Page 104, Section 4.8.2, Line 1, “thermopile”“the thermopile”

- Page 101, Section 4.8.2.1, Line 1 “A PIC18F97J60”

  Response:-Page 105, Section 4.8.2.1, Line 1 “PIC18F97J60”changed to “A PIC18F97J60”

- Page 102, Section 4.8.2.3, Line 1, “The ADC”

  Response:-Page 106, Section 4.8.2.3, Line 1, “ADC”changed to “The ADC”

- Page 102, Section 4.8.2.4, Line 1 “The availability”

  Response:-Page 106, Section 4.8.2.4, Line 1 “Availability”changed to “The availability”

- Page 103, Section 4.8.2.5, Line 1 “A DS12887”

  Response:-Page 107, Section 4.8.2.5, Line 1 “DS12887”changed to “A DS12887”

- Page 103, Section 4.8.3, Line 1 “the cloud monitor”

  Response:- Page 107, Section 4.8.3, Line 1 “Cloud monitor”changed to “The cloud monitor”

- Page 106, Line 1, “at any given”

  Response:-Page 110, Line 1, “at a given”changed to “at any given”

- Page 106, Line 6, “at a minimum. The voltage”

  Response:-Page 110, Line 6, “at the minimum. Voltage”changed to “at a minimum. The voltage”

- Page 106, Section 4.9.2, Line 3, “the thermopile”

  Response:- Page 110, Section 4.9.2, Line 3, “thermopile”changed to “the thermopile”

- Page 107, 2 lines from bottom, “A data acquisition”

  Response:-Page 112, Line 1, “Data acquisition”changed to “A data acquisition”

- Page 108, Line 1, “for the instrument”

  Response:-Page 112, Line 3, “for instrument”changed to “for the instrument”

- Page 109, Line 3, “The relationship”

  Response:-Page 113, Line 3, “Relationship”changed to “The relationship”

- Page 109, Line 6, “The calibration”

  Response:-Page 113, Line 6, “Calibration”changed to “The calibration”

- Page 110, Line 1, “the thermopile”

  Response:-Page 114, Section 4.9.3, Line 1, “Thermopile”changed to “the thermopile”

- Page 110, 4 lines from bottom, “where the size of the instrument”

  Response:-Page 115, Line 10, “where most of the time size of the instrument”changed to “where the size of the instrument”

- Page 111, add “The”at the beginning of the each bullet point

  Response:-Page 115, added “The”at the beginning of the each bullet point

- Page 113, Line 1, “near zenith”

  Response:-Page 117, Line 3, “near to zenith”changed to “near zenith”

- Page 113, Line 2, “were recorded”

  Response:-Page 117, Line 4, “was recorded”changed to “were recorded”

- Page 113, Line 9, “this made us extrapolate Equation 4.11”

  Response:-Page 117, Line 11, “this made us to extrapolate Equation 4.11”changed to“this made us extrapolate Equation 4.11”

- Page 115, Section4.10.2, Line 5 “has two windows”

  Response:-Page 119, Section4.10.2, Line 5 “has got two windows”changed to “has two windows”

- Page 116, 5 lines from the bottom, “then the software”

  Response:-Page 121, 6 lines from the bottom, “then software”changed to “then the software”

- Page 117, bullet point 2, “Out of four, the user”

  Response:-Page 122, bullet point 2, “Out of four, user”changed to “Out of four, the user”

- Page 117, bullet point 5, “The software”

  Response:-Page 122, bullet point 5, “Software”changed to “The software”

- Page 119, Line 2, “The cloud monitor is a fully automatic device”

  Response:-Page 124, Line 1, “Cloud Monitor instrument is fully automatic device”changed to “The cloud monitor is a fully automatic device”

- Page 121, Line 2, “Then after better understanding”

  Response:-Page 126, Line 3, “Then after to better understand”changed to“Then after better understanding”

- Page 121, Line 3, “we removed data”

  Response:-Page 126, Line 4, “we have removed data”changed to “we removed data”

- Page 125, Section 4.12.2, “The larger the zenith distance, the higher”

  Response:- Page 131, Section 4.12.2, “Larger the zenith distance, higher”changed to “The larger the zenith distance, the higher”

- Page 138, Line 6, “we planned to”

  Response:-Page 144, Line 6, “we plan to”changed to “we planned to”

- Page 139, Line 5, “The photon”

  Response:-Page 145, Line 5, “The Photon”changed to “The photon”

- Page 139, Line 8, “six turbulent layers”

  Response:-Page 145, Line 8, “six thin turbulent layers”changed to “six turbulent layers”

- Page 139, Line 15, “The first one being that”

  Response:-Page 145, Line 15, “The first one being it”changed to “The first one being that it”

- Page 139, 6 lines from the bottom, “resolution, knowing the seeing is not enough”

  Response:-Page 145, 6 lines from the bottom, “resolution, only knowledge of seeing is not enough”changed to“resolution, knowing the seeing is not enough”

- Page 140, Line 1, “The MASS-DIMM”

  Response:-Page 146, Line 1, “MASS-DIMM”changed to“The MASS-DIMM”

- Page 141, Line 1, “IAO Hanle, is subject to very high wind speed”

  Response:-Page 147, Line 1, “IAO Hanle is subjected to very high wind speed”changed to “IAO Hanle, is subject to very high wind speed”

- Page 141, Line 6, “The Meade telescope also uses”

  Response:-Page 147, Line 6, “Also, the Meade telescope uses”changed to “The Meade telescope also uses”

- Page 141, Line 7, “Hence, the wind loading is large”

  Response:-Page 147, Line 7, “Hence, wind loading is more”changed to “Hence, the wind loading is large”

- Page 141, Line 9, “the DIMM”

  Response:-Page 147, Line 9, “DIMM”changed to “the DIMM”

- Page 142, Line 4, “the telescope”

  Response:-Page 148, Line 4, “telescope”changed to“the telescope”

- Page 142, Line 6, “the backlash”

  Response:-Page 148, Line 6, “backlash”changed to “the backlash”

- Page 142, Section 5.3, Line 1, “provide a few”

  Response:-Page 148, Section 5.3, Line 1, “provide few”changed to “provide a few”

- Page 143, bullet point 9, “a provision”

  Response:-Page 149, bullet point 9, “provision”changed to “a provision”

- Page 144, 2 lines from the bottom, “The MASS-DIMM”

  Response:-Page 150, 2 lines from the bottom, “MASS-DIMM”changed to “The MASS-DIMM”

- Page 145, 4 lines from the bottom, “the cross section”

  Response:-Page 151, 4 lines from the bottom, “cross section”changed to “the cross section”

- Page 146, Line 8, “The telescope”

  Response:-Page 152, Line 8, “Telescope”changed to “The telescope”

- Page 147, Line 1, “The immediate”

  Response:-Page 153, Line 1, “Immediate”changed to “The immediate”

- Page 147, Line 4, “the existing”

  Response:-Page 153, Line 4, “existing”changed to“the existing”

- Page 147, Line 7, “the telescope...the only difference”

  Response:-Page 153, Line 7, “telescope...only difference”changed to “the telescope...the only difference”

- Page 147, Line 11, “the RA axis is aligned to the polar”

  Response:-Page 153, Line 11, “RA axis is aligned to polar”changed to “the RA axis is aligned to the polar”

- Page 147, Section 5.5.1, Line 1, “The TPO”

  Response:-Page 153, Section 5.5.1, Line 1, “TPO”changed to “The TPO”

- Page 147, Section 5.5.1, Line 4, “expansion, hence”

  Response:-Page 153, Section 5.5.1, Line 4, “expansion. Hence”changed to “expansion, hence”

- Page 147, 3 lines from the bottom, “The OTA”

  Response:-Page 153, 2 lines from the bottom, “OTA”changed to “The OTA”

- Page 147, last line, “is fixed, hence, there”

  Response:-Page 154, Line 2, “is fixed. Hence, there”changed to “is fixed, hence, there”

- Page 148, 2 lines from bottom, “A mechanical model and drawing of the OTA were”

  Response:- Page 155, Line 1, “Mechanical model and the drawings of the OTA was”changed to “A mechanical model and drawing of the OTA were”

- Page 148, last line, “telescope mount and for carrying”

  Response:-Page 155, Line 2, “the telescope mount as well for carrying”changed to “telescope mount and for carrying”

- Page 149, Line 1, “A mechanical”

  Response:-Page 155, Line 2, “Mechanical”changed to “A mechanical”

- Page 149, Line 3, “The manufacturer of the OTA”

  Response:-Page 155, Line 4, “Manufacturer of OTA”changed to “The manufacturer of the OTA”

- Page 149, Line 4, “information, so we decided to make a 3-D model of the OTA”

  Response:-Page 155, Line 5, “information. Therefore, we decided to make our

3-D model of OTA”changed to“information, so we decided to make a 3-D model of the OTA”

- Page 149, Section 5.5.2, Line 1, “A direct drive”

  Response:-Page 155, Section 5.5.2, Line 1, “Direct drive”changed to “A direct drive”

- Page 150, Line 3, “the magnets”

  Response:-Page 156, Line 5, “magnets”changed to “the magnets”

- Page 150, Line 4, “The azimuth”

  Response:-Page 156, Line 6, “Azimuth”changed to “The azimuth”

- Page 150, Line 5, “the motor”

  Response:-Page 156, Line 7, “motor”changed to “the motor”

- Page 151, Line 4, “unit which is shown in”

  Response:- Page 157, Line 7, “unit. IMTHP unit is shown in”changed to “unit which is shown in”

- Page 151, Section 5.5.4, Line 3, “A ring type”

  Response:-Page 157, Section 5.5.4, Line 3, “Ring type”changed to “A ring type”

- Page 151, 2 lines from bottom, “resolution it corresponds to 0.0027”

  Response:-Page 158, Line 4, “resolution, it is 0.0027”changed to “resolution it corresponds to 0.0027”

- Page 152, Section 5.5.5, “The use”

  Response:-Page 158, Section 5.5.5, “The use”changed to “Use”

- Page 152, Section 5.5.5, Line 3 “A VAR02 series rake from Warner Electric is used on both axes”

  Response:-Page 158, Section 5.5.5, Line 3 “VAR02 series brake from Warner

Electric is used on both the axes"changed to "A VAR02 series rake from Warner Electric is used on both axes"

- Page 152, Section 5.5.5, Line 8, "The brakes"
  Response:-Page 152, Section 5.5.5, Line 8, "Brakes"changed to "The brakes"

- Page 152, 2 lines from bottom, "a mathematical model"
  Response:-Page 159, Line 1, "mathematical model"changed to "a mathematical model"

- Page 154, Line 1 after the bullet points, "The above mentioned requirements"
  Response:-Page 160, Line 1 after the bullet points, "Above mentioned requirements"changed to "The above mentioned requirements"

- Page 154, Line 2 after the bullet points, "for both conditions. The telescope"
  Response:-Page 160, Line 2 after the bullet points, "for both of the conditions. Telescope"changed to "for both conditions. The telescope"

- Page 154, Line 4 in FEM section, "A finite element"
  Response:-Page 160, Line 4 in FEM section, "Finite element"changed to "A finite element"

- Page 154, Line 7 in FEM section, "The origin"
  Response:-Page 160, Line 7 in FEM section, "Origin"changed to "The origin"

- Page 154, 3 lines from the bottom, "In the present"
  Response:-Page 161, Line 1, "In present"changed to "In the present"

- Page 154, last line, "maximum safety factor"
  Response:-Page 161, Line 3, "maximum factor of safety"changed to "maximum safety factor"

- Page 155, last line, “The telescope”

  Response:-Page 162, Line 1, “Telescope”changed to “The telescope”

- Page 156, last line, “The telescope”

  Response:-Page 163, 2 line from bottom, “Telescope”changed to “The telescope”

- Page 157, caption of Fig. 5.14, “Stress”

  Response:-Page 164, caption of Fig. 5.14, “Sterss”changed to “Stress”

- Page 158, caption of Table 5.5, “conditions”

  Response:-Page 164, caption of Table 5.5, “condition”changed to “conditions”

- Page 159, Line 2, “manifest themselves”

  Response:-Page 165, Line 13, “manifests themselves”changed to “manifest themselves”

- Page 159, Line 4, “balanced on both axis”

  Response:-Page 165, Line 15, “balanced in both the axis”changed to “balanced on both axis”

- Page 159, 2 lines from the bottom, “will be the same”

  Response:-Page 166, Line 8, “will be same”changed to “will be the same”

- Page 159, last line, “torques”

  Response:-Page 166, Line 10, “torque”changed to “torques”

- Page 160, first line in the conclusion, “The following”

  Response:-Page 166, first line in the conclusion, “Following”changed to “The following”

- Page 162-63, each bullet point, “The drag”

  Response:-Page 169-70, each bullet point, “Drag”changed to “The drag”

- Page 163, title of section 5.8, “the telescope control”

  Response:-Page 170, title of section 5.8, “telescope control”changed to “the telescope control”

- Page 163, Section 5.8, Line 1, “being for the first time”

  Response:- Page 170, Section 5.8, Line 1, “being first time”changed to “being for the first time”

- Page 163, Section 5.8, Line 3, “the telescope”

  Response:-Page 170, Section 5.8, Line 3, “telescope”changed to “the telescope”

- Page 163, last line , “The larger”

  Response:-Page 171, Line 1 , “Larger”changed to “The larger”

- Page 164, Line 3, “encoders are similar to Renishaw encoders”

  Response:-Page 171, Line 4, “encoder is similar to Renishaw encoder”changed to “encoders are similar to Renishaw encoders”

- Page 164, Line 5, “The encoder”

  Response:-Page 171, Line 6, “Encoder”changed to “The encoder”

- Page 164, Line 8, “by a factor”

  Response:-Page 171, Line 89, “by factor”changed to “by a factor”

- Page 164, Line 10, “The encoder”

  Response:- Page 171, Line 11, “Encoder”changed to “The encoder”

- Page 165, bullet point 1, Line 1, “for a 3 minutes duration”

  Response:-Page 172, bullet point 1, Line 1, “or 3 minutes of duration”changed to “for a 3 minutes duration”

- Page 166, Line 4, “The proportional”

  Response:-Page 171, Line 4, “proportional”changed to “The proportional”

- Page 168, Line 5, “achieve a much-improved”

  Response:-Page 176, Line 2, “achieve much-improved”changed to “achieve a much-improved”

- Page 168, Section 5.9, Line 6, “the azimuth”

  Response:-Page 176, Section 5.9, Line 6, “azimuth”changed to “the azimuth”

- Page 170, Line 1, “In the past, various”

  Response:-Page 178, Line 1, “In the past various”changed to“In the past, various”

- Page 170, Line 5, “large telescopes (such as NLOT) require a very customized motors”

  Response:-Page 178, Line 5, “large telescope (such as NLOT) requires a very customized motor”changed to “large telescopes (such as NLOT) require a very customized motors”

- Page 182, Line 2, “The nature”

  Response:-Page 190, Line 5, “Nature”changed to “The nature”

- Page 185, Line 2, “magnets”

  Response:-Page 194, Line 2, “magnates”changed to “magnets”

- Page 187, Line 3, “These are the Automated”

  Response:-Page 196, Line 3, “These are Automated”changed to “These are the Automated”

- Page 187, Line 7, “The TMT project”

  Response:-Page 196, Line 7, “TMT project”changed to “the TMT project”

- Page 190, Line 7, “The telescope”

  Response:-Page 199, Line 14, “Telescope”changed to “The telescope”